SYNTHESIS, CHARACTERIZATION AND ANTI-CANCER ACTIVITY OF NEW RUTHENIUM MALTOLATO AND IMIDAZOLE COMPLEXES

by

DAVID CHARLES KENNEDY

B. Sc., The University of British Columbia, 1998

A THESIS SUBMITTED IN PARTIAL FULFILMENT
OF THE REQUIREMENTS FOR THE DEGREE OF

DOCTOR OF PHILOSOPHY

in

THE FACULTY OF GRADUATE STUDIES
(Department of Chemistry)

We accept this thesis as conforming to the required standard

THE UNIVERSITY OF BRITISH COLUMBIA

December 2003

© 2003 David Kennedy

Abstract

Several new Ru(III) maltolato (ma) and ethylmaltolato (Ema) complexes have been synthesized, characterized, and tested for biological activity *in vitro* against MDA-MB-435S cells, a human breast cancer cell line. $Ru(ma)_3$ (**1**) and $Ru(Ema)_3$ (**2**) were studied in detail using a number of spectroscopic techniques. In particular, the solution ^1H NMR spectra of these paramagnetic solids were investigated and, through the use of

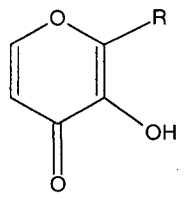

Maltol (R = Me) (Hma) and
Ethylmaltol (HEma) (R = Et)

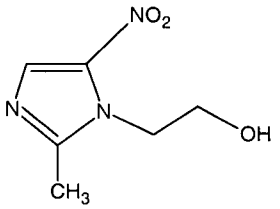

Metronidazole

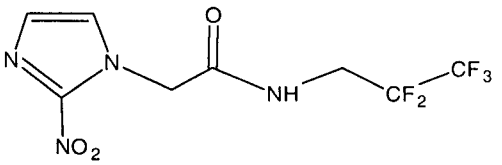

EF5

2D NMR techniques, structural information about the complexes was determined. These two complexes were then used to synthesize bis-imidazole complexes via removal of one ma or Ema ligand with triflic acid. *Trans*-$[Ru(ma)_2(2MeIm)_2]CF_3SO_3$ (**10**), -$[Ru(ma)_2(1MeIm)_2]CF_3SO_3 \cdot CH_2Cl_2$ (**8**), and -$[Ru(Ema)_2(metro)_2]CF_3SO_3$ (**11**), where 2MeIm = 2-methylimidazole, 1MeIm = 1-methylimidazole, and metro = metronidazole, were synthesized and characterized by X-ray crystallography, while *trans*-$[Ru(ma)_2(metro)_2]CF_3SO_3$ (**4**) was also synthesized and subsequently characterized by X-ray crystallography by another member of our group. Comparison of the ^1H NMR data of **8**, **10**, and **11** with those for the analogous complexes $[Ru(ma)_2(4MeIm)_2]CF_3SO_3 \cdot CH_2Cl_2$ (**6**), $[Ru(Ema)_2(4MeIm)_2]CF_3SO_3$ (**12**), and $[Ru(Ema)_2(2MeIm)_2]CF_3SO_3$ (**13**), where 4MeIm = 4-methylimidazole, implies that these last three complexes also have trans-configurations. By a similar comparison, $[Ru(ma)_2(Im)_2]CF_3SO_3$ (**7**), where Im = imidazole, was found to be a mixture of cis- and trans-isomers that could not be separated.

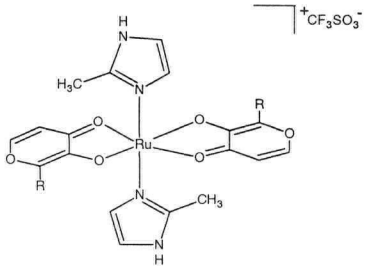

10 (R = Me), **13** (R = Et)

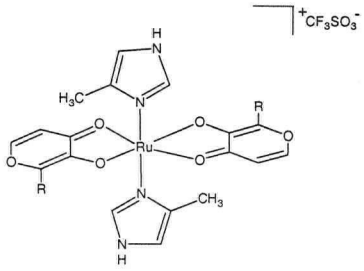

6 (R = Me), **12** (R = Et)

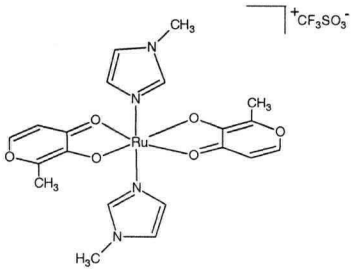

8

The ma and Ema complexes were then tested *in vitro* using a so-called MTT assay against human breast cancer cells to evaluate their antiproliferatory activity. This assay determines cell viability as a measure of the cell's ability to reduce the yellow MTT (3-(4,5-dimethylthiazol-2-yl)-2,5-diphenyltetrazolium bromide) to the purple formazan in the mitochondria. Complexes containing Ema exhibited lower IC_{50} values (complex concentration at which cell proliferation has been reduced by 50 % after 3 days), than the corresponding ma complexes, and **13** exhibited the lowest value of 500 nM, compared to that for cisplatin (IC_{50} = 40 μM). Ru-uptake data showed that Ema complexes were taken into Chinese Hamster Ovarian (CHO) cells at levels 4-5 times greater than those for corresponding ma complexes. No significant difference in Ru-uptake was observed between ma complexes with different imidazole ligands when these lacked a nitro group. $[Ru(ma)_2(EF5)_2]CF_3SO_3 \cdot EtOH$ (**14**), where EF5 = 2-(2-nitro-1-H-imidazol-1-yl)-N-(2,2,3,3,3-pentafluoropropyl)acetamide, exhibited the highest Ru-uptake of the complexes tested, and was the only complex to exhibit DNA-binding in CHO cells over a 3h incubation period, although it exhibited very low activity in the MTT assay (IC_{50} value > 500 μM).

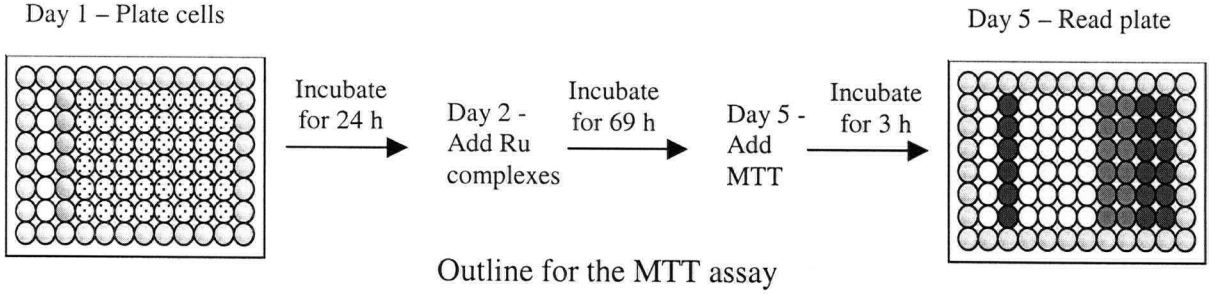

Outline for the MTT assay

Complexes containing the bidentate ligands 4,4'-biimidazole (biim) and 2,2'-dimethyl-4,4'-biimidazole (Me_2biim) were also synthesized, characterized and tested by the MTT assay. The Ru(III) complexes $[Ru(ma)_2(L)]CF_3SO_3 \cdot 2H_2O$, where L = biim (**24**) or Me_2biim (**25**), were synthesized from **1**. The Ru(II) complexes $[Ru(L)_3][CF_3SO_3]_2$ (L = biim (**26**) and L = Me_2biim (**27**)) were synthesized from $[Ru(DMF)_6][CF_3SO_3]_3$, while the complexes $RuCl_2(DMSO)_2(L)$ (L = biim (**20**) and L = Me_2biim (**22**)) and $Ru_2Cl_4(DMSO)_4(L)$ (L = biim (**21**) and L = Me_2biim (**23**)) were synthesized from *cis*-$RuCl_2(DMSO)_4$. **24** – **27** all exhibited significant activity in the MTT assay (IC_{50} values 15-50 μM), but **20** and **22** were essentially inactive. The Ru-uptake values of **24** – **27** in CHO cells were comparable to those observed for the Ru-ma bis-imidazole complexes (**4**, **6**, **7**, **8** and **10**).

The new Ru complexes $[Ru_2(pic)_4(EtOH)Cl] \cdot H_2O$ (**31**) and $Ru(Im\text{-}CO_2)(Im\text{-}CO_2H)_2Cl_2 \cdot H_2O \cdot EtOH$ (**33**), synthesized using the N-heterocyclic carboxylic acid ligands pyridine-2-carboxylic acid (Hpic) and imidazole-4-carboxylic acid (Im-CO_2H), were also tested using the MTT assay, but were considerably less active than either the biimidazole or bis-imidazole complexes (IC_{50} values = 100 and 400 μM for **31** and **33**, respectively).

Table of Contents

Abstract ii

Table of Contents v

List of Figures xiii

List of Tables xix

List of Symbols and Abbreviations xxi

Key to Numbered Complexes xxiv

Acknowledgements xxvi

Chapter 1 Introduction 1

1.1 Introduction 1

1.2 Nitroimidazoles and Hypoxia 2

1.3 *In Vitro* Bioassays 4

1.4 Platinum Anti-Cancer Drugs 5

1.4.1 Cisplatin and Other Pt(II) Anti-Cancer Drugs 5

1.4.2 Platinum(IV) as a Pro-drug 7

1.5 Ruthenium Complexes and Their Potential as Anti-Cancer Drugs 8

1.5.1 Activation by Reduction 8

1.5.2 *cis*-$RuCl_2(DMSO)_3(DMSO)$ 9

1.5.3 Ru-imidazole Complexes 9

1.5.3.1 NAMI and NAMI-A 10

1.5.4 Ru-arene Complexes 11

1.5.5 Ru-azopyridine Complexes 13

1.5.6 Ru Intercalators 14

1.6 Maltolato (ma) Chemistry 15

1.6.1 Maltolato Complexes with Ru 15

1.6.2 Maltolato Complexes with other Transition Metals 16

1.7 Goals of this Thesis 17

1.8 References 18

Chapter 2 General Experimental Procedures, and Syntheses of Ruthenium Precursor Complexes 23
2.1 Chemicals 23
2.1.1 Ligand Precursors 23
2.1.2 Solvents 23
2.1.3 Gases 24
2.1.4 Biological Reagents 24
2.1.5 Other reagents 24
2.2 Analytical Techniques and Instrumentation 24
2.2.1 Nuclear Magnetic Resonance Spectroscopy 24
2.2.2 Infrared Spectroscopy 26
2.2.3 Mass Spectrometry 27
2.2.4 UV-Visible Spectroscopy 27
2.2.5 Cyclic Voltammetry 27
2.2.6 Conductivity 28
2.2.7 X-Ray Analysis 28
2.2.8 Elemental Analysis 29
2.2.9 Biological Analysis 29
2.3 Chromatographic Techniques 29
2.4 Ruthenium Precursors 31
2.4.1 $RuCl_3 \cdot 3H_2O$ 31
2.4.2 $[Ru(DMF)_6][CF_3SO_3]_3$ 31
2.4.3 *cis*-$RuCl_2(DMSO)_3(DMSO)$ 31
2.4.4 $K_3[RuCl_6]$ 32
2.4.5 $Ru_2(CH_3COO)_4Cl$ 32
2.5 References 33

Chapter 3 Synthesis and Characterization of Ruthenium(III) Maltolato and Imidazole Complexes 35
3.1 Introduction 35
3.2 Investigation of $Ru(ma)_3$ and $Ru(Ema)_3$ 36

3.2.1 Characterization and Solution NMR Data for $Ru(ma)_3$ (**1**) 36
3.2.2 Characterization and Solution NMR Data for $Ru(Ema)_3$ (**2**) 43
3.2.3 "Activation" of $Ru(ma)_3$ with CF_3SO_3H – Synthesis of $[Ru(ma)_2(EtOH)_2]CF_3SO_3$ (**3**) 47
3.3 Reactions of $Ru(ma)_3$ (**1**) and $Ru(Ema)_3$ (**2**) with Imidazoles and Triazoles 49
3.3.1 Synthesis and Characterization of Imidazole and Triazole Complexes 49
3.3.2 Solution ^1H NMR Spectroscopy of the Im, 2MeIm, 4MeIm and 1MeIm Complexes 55
3.3.3 Solution ^1H NMR Spectroscopy of metro, $2NO_2Im$, $4NO_2Im$ and $3NO_2tri$ Complexes 61
3.3.4 Compounds Synthesized Using 2,2,3,3,3-Pentafluoropropylamine (F5) 62
3.3.5 Synthesis, Characterization, and Solution ^1H NMR Spectroscopy of $[Ru(ma)_2(EF5)_2]CF_3SO_3 \cdot EtOH$ (**14**) and $[Ru(ma)_2(triF5)_2]CF_3SO_3$ (**18**) 64
3.4 Synthesis of $[Ru(HMepyr)_3]Cl_3$ (**19**) 65
3.5 Cyclic Voltammetry of Complexes 66
3.6 Experimental Procedures for the Syntheses of Compounds Derived from F5 68
3.6.1 N-(2,2,3,3,3-pentafluoropropyl) chloroacetamide (ClF5) 68
3.6.2 2-(2-Nitro-1-H-imidazol-1-yl)-N-(2,2,3,3,3-pentafluoropropyl)-acetamide (EF5) 68
3.6.3 2-(3-Nitro-1-H-triazol-1-yl)-N-(2,2,3,3,3-pentafluoropropyl)-acetamide (triF5) 69
3.6.4 IMF10 69
3.7 Experimental Procedures for the Syntheses of Ru(III) Complexes 70
3.7.1 $Ru(ma)_3$ (**1**) 70
3.7.2 $Ru(Ema)_3$ (**2**) 70
3.7.3 $[Ru(ma)_2(EtOH)_2]CF_3SO_3$ (**3**) 71

3.7.4 $[Ru(ma)_2(metro)_2]CF_3SO_3$ (**4**) and $[Ru(ma)_2(metro)(EtOH)]CF_3SO_3$ (**5**) 71
3.7.5 $[Ru(ma)_2(4MeIm)_2]CF_3SO_3 \cdot CH_2Cl_2$ (**6**) 72
3.7.6 $[Ru(ma)_2(Im)_2]CF_3SO_3$ (**7**) 73
3.7.7 $[Ru(ma)_2(1MeIm)_2]CF_3SO_3 \cdot CH_2Cl_2$ (**8**) 73
3.7.8 $[Ru(ma)(1MeIm)_4][CF_3SO_3]_2$ (**9**) 74
3.7.9 $[Ru(ma)_2(2MeIm)_2]CF_3SO_3$ (**10**) 75
3.7.10 $[Ru(Ema)_2(metro)_2]CF_3SO_3$ (**11**) 75
3.7.11 $[Ru(Ema)_2(4MeIm)_2]CF_3SO_3$ (**12**) 76
3.7.12 $[Ru(Ema)_2(2MeIm)_2]CF_3SO_3$ (**13**) 76
3.7.13 $[Ru(ma)_2(EF5)_2]CF_3SO_3 \cdot EtOH$ (**14**) 77
3.7.14 $[Ru(ma)_2(2NO_2Im)_2]CF_3SO_3$ (**15**) 77
3.7.15 $[Ru(ma)_2(4NO_2Im)_2]CF_3SO_3$ (**16**) 78
3.7.16 $[Ru(ma)_2(3NO_2tri)_2]CF_3SO_3$ (**17**) 78
3.7.17 $[Ru(ma)_2(triF5)_2]CF_3SO_3$ (**18**) 78
3.7.18 $[Ru(HMepyr)_3]Cl_3$ (**19**) 78
3.8 References 79

Chapter 4 Synthesis and Characterization of Ru Complexes with 4,4'-Biimidazoles 81
4.1 Introduction 81
4.2 Synthesis and Reactions of 4,4'-Biimidazoles 82
4.2.1 Synthesis of 4,4'-Biimidazoles 82
4.2.2 Attempted Nitration of H_2biim 85
4.3 Attempted Synthesis of 5,5'-Dinitro-3,3'-bi(1,2,4-triazole) 86
4.4 Ru-biim Complexes Synthesized from *cis*-$RuCl_2(DMSO)_4$ 87
4.5 Complexes Synthesized from $Ru(ma)_3$ 95
4.6 Complexes Synthesized from $[Ru(DMF)_6](CF_3SO_3)_3$ 97
4.7 Complexes Synthesized from $RuCl_3 \cdot 3H_2O$ 99
4.8 Experimental Preparation of Biimidazoles 100
4.8.1 Sources of Materials 100

4.8.2 2,4,5-Triiodoimidazole 100
4.8.3 4(5)-Iodoimidazole 101
4.8.4 4-Iodo-1-(triphenylmethyl)imidazole 101
4.8.5 1,1'-Bis(triphenylmethyl)-4,4'-biimidazole 101
4.8.6 4,4'-Biimidazolium trifluoroacetate (H_2biim) 102
4.8.7 4,5,-Diiodo-2-methylimidazole 102
4.8.8 4(5)-Iodo-2-methylimidazole 103
4.8.9 4-Iodo-2-methyl-1-(triphenylmethyl)imidazole 103
4.8.10 2,2'-Dimethyl -1,1'-bis(triphenylmethyl)-4,4'-biimidazole 103
4.8.11 2,2'-Dimethyl-4,4'-biimidazolium trifluoroacetate (H_2Me_2biim) 104
4.9 Experimental Syntheses of Complexes 104
4.9.1 *cis*-$RuCl_2(DMSO)_2$(biim) (**20**) 104
4.9.2 $Ru_2Cl_4(DMSO)_4$(biim) (**21**) 104
4.9.3 $RuCl_2(DMSO)_2(Me_2biim)$ (**22**) 105
4.9.4 $Ru_2Cl_4(DMSO)_4(Me_2biim)$ (**23**) 105
4.9.5 [Ru(maltolato)$_2$(biim)]$CF_3SO_3 \cdot 2H_2O$ (**24**) 105
4.9.6 [Ru(maltolato)$_2$(Me_2biim)]$CF_3SO_3 \cdot 2H_2O$ (**25**) 106
4.9.7 $[Ru(biim)_3][CF_3SO_3]_2$ (**26**) 106
4.9.8 $[Ru(Me_2biim)_3][CF_3SO_3]_2$ (**27**) 107
4.9.9 $[Ru(Hbiim)_2Cl_2]Cl_2$ (**28**) 107
4.9.10 $[Ru((HMe_2biim)Me_2biim)_2(HMe_2biim)]Cl_3$ (**29**) 107
4.10 References 108

Chapter 5 Synthesis and Characterization of Ru Complexes with Chelating N-Heterocyclic Carboxylates 110
5.1 Introduction 110
5.2 Synthesis and Characterization of $[Ru_2(pic)_4(EtOH)Cl] \cdot H_2O$ (**31**) 112
5.3 Complexes of Ru with Imidazole-4-carboxylic Acid 115
5.3.1 Synthesis and Characterization of $Ru(Im\text{-}CO_2)_3 \cdot 2H_2O$ (**32**) 115

5.3.2 Synthesis and Characterization of $Ru(Im\text{-}CO_2)(Im\text{-}CO_2H)_2Cl_2 \cdot EtOH \cdot H_2O$ (**33**) 116
5.4 Synthesis of Nitroimidazole and Nitrotriazole Carboxylic Acids 119
5.4.1 Synthesis of 3-Nitro-1,2,4-triazole-5-carboxylic Acid (HCANT) 119
5.4.2 Attempted Synthesis of 2-Nitroimidazole-4-carboxylic Acid 119
5.4.3 Attempted Synthesis of 2-Nitroimidazole-4,5-dicarboxylic Acid 120
5.5 Attempted Reactions of HCANT with Ru Precursors 121
5.6 Experimental Procedures 122
5.6.1 3-Nitro-1,2,4-triazole-5-carboxylic Acid (HCANT) 122
5.6.2 Methyl imidazole-4-carboxylate 122
5.6.3 Methyl 1-tritylimidazole-4-carboxylate 123
5.6.4 4-Hydroxymethyl-1-tritylimidazole 123
5.6.5 4-Hydroxymethyl-2-nitroimidazole 124
5.6.6 Dimethyl imidazole-4,5-dicarboxylate 125
5.6.7 Dimethyl 1-tritylimidazole-4,5-dicarboxylate 125
5.6.8 4,5-Dihydroxymethyl-1-tritylimidazole 126
5.6.9 $Ru(pic)_3 \cdot H_2O$ (**30**) 126
5.6.10 $[Ru_2(pic)_4(EtOH)Cl] \cdot H_2O$ (**31**) 127
5.6.11 $Ru(Im\text{-}CO_2)_3 \cdot 2H_2O$ (**32**) 127
5.6.12 $Ru(Im\text{-}CO_2)(Im\text{-}CO_2H)_2Cl_2 \cdot EtOH \cdot H_2O$ (**33**) 128
5.7 References 128

Chapter 6 Antiproliferatory Activity of Ruthenium Complexes Using the MTT Assay 130
6.1 Introduction 130
6.2 General Experimental Procedures 132
6.2.1 Experimental Media, Solutions, and Materials 132
6.2.2 Cell Preparation 133
6.2.3 Preparation of Ru Complexes 133

6.2.4 Preparation of Ligand Precursor Solutions 134
6.3 MTT Assay Procedure 134
6.3.1 Day 1 - Plating Cells 134
6.3.2 Day 2 – Addition of Ru Complexes and Ligand Precursors 135
6.3.3 Day 5 – Addition of MTT and Plate Reading 136
6.3.4 Data Analysis 137
6.4 Results and Discussion 138
6.4.1 Ligand Precursors 138
6.4.2 Ru Maltolato and Imidazole Complexes 139
6.4.3 Ru 4,4'-Biimidazole Complexes 145
6.4.4 Ru Carboxylate complexes 149
6.5 Summary 150
6.6 References 151

Chapter 7 ***In Vitro*** **Toxicity, Ru-Uptake and Ru-DNA Binding Studies of Ru Complexes, and Antibody Recognition Studies of a New Nitrotriazole in Chinese Hamster Ovarian (CHO) Cells** 153
7.1 Introduction 153
7.2 General Experimental 154
7.2.1 Materials, Media, and Prepared Solutions 154
7.2.2 Cell Preparation 155
7.2.3 Stock Solutions of Ru Complexes 156
7.3 Hypoxia Selectivity Assays 156
7.3.1 Incubation of Complexes and Plating Efficiency 156
7.3.2 Ru-Uptake Determination 158
7.3.3 DNA Isolation 159
7.3.4 Monoclonal Antibody Binding Assay 160
7.4 Results and Discussion 162
7.4.1 Plating Efficiency of CHO Cells 162
7.4.2 Ru-Uptake 164
7.4.3 Ru-DNA Binding 167

7.4.4 The Monoclonal Antibody Binding Assay 168
7.4.5 Reaction of $[Ru(ma)_2(2MeIm)_2]CF_3SO_3$ (**10**) with L-cysteine ... 169
7.5 References 171

Chapter 8 Conclusions, and Direction of Future Work 173
8.1 Conclusions 173
8.2 New Complexes to Synthesize and Test 174
8.3 New Directions for Hypoxia Markers 175
8.4 Future Biotests 176
8.5 References 177

Structural Appendices

Appendix A1 Experimental Details for the X-ray Crystallographic Study of *mer*-$Ru(ma)_3$ (**1**) 179
Appendix A2 Experimental Details for the X-ray Crystallographic Study of *trans*-$[Ru(ma)_2(1MeIm)_2]CF_3SO_3 \cdot CH_2Cl_2$ (**8**) 185
Appendix A3 Experimental Details for the X-ray Crystallographic Study of *trans*-$[Ru(ma)_2(2MeIm)_2]CF_3SO_3$ (**10**) 193
Appendix A4 Experimental Details for the X-ray Crystallographic Study of *trans*-$[Ru(Ema)_2(metro)_2]CF_3SO_3$ (**11**) 201
Appendix A5 Experimental Details for the X-ray Crystallographic Study of 1,1'-Bis(triphenylmethyl)-4,4'-biimidazole 209

List of Figures

Figure 1.1 Gradient of oxygen concentration in cancerous tumours (adapted from ref. 6). 3

Figure 1.2 Molecular structures of metronidazole, EF5 and triF5. 3

Figure 1.3 Proposed reduction pathway of nitroimidazoles (adapted from ref. 12). 4

Figure 1.4 Molecular structures of Pt(II) anti-cancer complexes. 6

Figure 1.5 Pt-DNA adduct formed from a d(GpG) intrastrand cross-link. 7

Figure 1.6 Molecular structures of Pt(IV) anti-cancer complexes. 8

Figure 1.7 Molecular structures of Ru(III) anti-cancer complexes. 10

Figure 1.8 Molecular structure of NAMI-A. 11

Figure 1.9 Molecular structure of [RuCl(*p*-cymene)(en)]PF_6. 12

Figure 1.10 Molecular structure of RuCl(*p*-cymene)(BESE)]PF_6. 12

Figure 1.11 Molecular structure of [Ru(*p*-cymene)Cl_2(pta)]. 13

Figure 1.12 Molecular structure of α-dichlorobis(2-phenylazopyridine)-ruthenium(II). 13

Figure 1.13 Molecular structure of [Ru(phen)$_2$dppz]$(PF_6)_2$. 14

Figure 1.14 Molecular structures of maltol (R = Me) and ethylmaltol (R = Et). 15

Figure 1.15 Molecular structures of tropolone and catechol. 15

Figure 1.16 Molecular structure of Ru(ma)$_2$(DMSO)$_2$ (R = Me) and Ru(Ema)$_2$-(DMSO)$_2$ (R = Et). 16

Figure 2.1 NMR set-up for performing the Evans method determination of μ_{eff}. 25

Figure 2.2 Cyclic Voltammetry cell used with Pt wire counter and working electrodes, and an Ag wire reference electrode. 28

Figure 2.3 Preparative TLC chamber with silica gel plate. 30

Figure 3.1 Numbered molecular structures of imidazole and 3-nitro-1,2,4-triazole. 36

Figure 3.2 Molecular structure of Ru(ma)$_3$ (**1**). 36

Figure 3.3 ORTEP diagram of *mer*-Ru(ma)$_3$ (**1**) with 33 % probability thermal ellipsoids (see Appendix A1 for details). 37

Figure 3.4 ^{1}H NMR spectrum (300 MHz, 298 K) of Ru(ma)$_3$ (**1**) in CD_2Cl_2. 38

Figure 3.5 ^{1}H-^{1}H COSY spectrum (300 MHz, 298 K) of $Ru(ma)_3$ (**1**) in CD_2Cl_2. 39

Figure 3.6 ^{1}H-^{13}C HMQC spectrum (300 MHz, 298 K) of $Ru(ma)_3$ (**1**) in CD_2Cl_2 with the ^{13}C spectrum on the left-hand side and the ^{1}H spectrum at the top. 40

Figure 3.7 Partial ^{13}C NMR spectrum of **1** (300 MHz, 298 K) in CD_2Cl_2 generated as a positive projection of the y-axis from the ^{1}H-^{13}C HMQC spectrum of **1**. 41

Figure 3.8 Plot of the chemical shift (ppm) vs. 1/T (K^{-1}) for the H(5) and H(6) protons on each ma ring of $Ru(ma)_3$ (**1**), here labelled H(a)-(f). 42

Figure 3.9 Plot of the chemical shift (ppm) vs. 1/T (K^{-1}) for the Me groups of $Ru(ma)_3$ (**1**). 43

Figure 3.10 ^{1}H NMR spectrum of $Ru(Ema)_3$ (**2**) (300 MHz, 298 K) in CD_2Cl_2. 44

Figure 3.11 ^{1}H-^{1}H COSY spectrum of **2** (300 MHz, 298 K) in CD_2Cl_2. 45

Figure 3.12 ^{1}H-^{13}C HMQC spectrum (300 MHz, 298 K) of $Ru(Ema)_3$ (**2**) in CD_2Cl_2 with the ^{13}C spectrum on the left-hand side and the ^{1}H spectrum at the top. 46

Figure 3.13 *In situ* formation of $[Ru(ma)_2(CD_3OD)_2]CF_3SO_3$ as shown by ^{1}H NMR spectroscopy, the broad downfield signal being characteristic of a trans-geometry for the maltolato ligands (see text). 48

Figure 3.14 Molecular structures for the *trans*-isomers of **4**, **6** – **8** and **10**. 49

Figure 3.15 Molecular structure of $[Ru(ma)(1MeIm)_4][CF_3SO_3]_2$ (**9**). 50

Figure 3.16 ORTEP diagram of the cation of *trans*-$[Ru(ma)_2(1MeIm)_2]CF_3SO_3 \cdot CH_2Cl_2$ (**8**) with 50 % probability thermal ellipsoids (see Appendix A2 for details). 51

Figure 3.17 ORTEP diagram of the cation of *trans*-$[Ru(ma)_2(2MeIm)_2]CF_3SO_3$ (**10**) with 50 % probability thermal ellipsoids (see Appendix A3 for details).. 52

Figure 3.18 Diagram depicting the potential steric interaction between an Im-Me group and the ma plane for **10**. 53

Figure 3.19 Template with numbering scheme for crystal structure information displayed in Table 3.2. 53

Figure 3.20 ORTEP diagram of the cation of *trans*-$[Ru(Ema)_2(metro)_2]CF_3SO_3$ (**11**) with 50 % probability thermal ellipsoids (see Appendix A4 for details).. 54

Figure 3.21 ^1H NMR spectrum of $[Ru(ma)_2(1MeIm)_2]CF_3SO_3$ (**8**) in a) acetone-d_6 (300 MHz, 298 K) and b) $CDCl_3$ (300 MHz, 298 K). 56

Figure 3.22 The effect of varying the temperature when reacting **1** with 1MeIm..... 57

Figure 3.23 ^1H NMR spectrum (300 MHz, 298 K) of $[Ru(ma)(1MeIm)_4][CF_3SO_3]_2$ (**9**) in acetone-d_6 showing the ma-Me at δ 81.6 and 1MeIm H(2) protons at δ –19.4 and -24.0. 58

Figure 3.24 ^1H NMR spectrum (300 MHz, 298 K) of $[Ru(ma)_2(2MeIm)_2]CF_3SO_3$ (**10**) in $CDCl_3$. 58

Figure 3.25 ^1H NMR spectra (300 MHz, 298 K) of a) $[Ru(Ema)_2(2MeIm)_2]CF_3SO_3$ (**13**) in $CDCl_3$ and b) $[Ru(Ema)_2(4MeIm)_2]CF_3SO_3$ (**12**) in $_{CDCl3}$..... 61

Figure 3.26 Molecular structures of three compounds synthesized from F5. 62

Figure 3.27 Synthesis of 2,2,3,3,3-pentrafluoropropylamine (F5) from 2,2,3,3,3-pentafluoroproprionic acid. 63

Figure 3.28 Molecular structure of IMF10. 64

Figure 3.29 ^{19}F NMR spectrum (300 MHz, 298 K) of $[Ru(ma)_2(EF5)_2]CF_3SO_3 \cdot EtOH$ (**14**). 65

Figure 3.30 Cyclic voltammogram of $[Ru(metro)_2(ma)_2]CF_3SO_3$ (**4**) in MeCN containing ferrocene. 67

Figure 4.1 Molecular structure of 2,2'-biimidazole. 81

Figure 4.2 Synthesis for H_2biim and H_2Me_2biim. 82

Figure 4.3 ORTEP diagram of 1,1'-bis(triphenylmethyl)-4,4'-biimidazole with 50 % probability thermal ellipsoids (see Appendix A5 for details). 84

Figure 4.4 Molecular structure of 5,5'-diamino-3,3'-bi(1,2,4-triazole). 86

Figure 4.5 ^1H NMR spectra (300 MHz, 298 K) in CD_3OD showing the imidazole protons of a) free H_2biim in CD_3OD, b) 1:2 H_2biim:$RuCl_2(DMSO)_4$ after 4 h at 65 °C in CD_3OD, and c) 1:1 H_2biim:$RuCl_2(DMSO)_4$ after 4 h at 65 °C in CD_3OD. 88

Figure 4.6 Proposed solid state structure for $RuCl_2(DMSO)_2(biim)$. 88

Figure 4.7 ^1H-^1H COSY NMR spectrum (300 MHz, 298 K) of **20** in CD_3OD..... 89

Figure 4.8 Mass spectrum of $RuCl_2(DMSO)_2(biim)$ (**20**): the most intense group of signals is for (M^+ – Cl – DMSO). 90

Figure 4.9 Structures (a) and (b) represent possible solution structures for **21**, where all DMSO ligands are S-bound and S = CD_3OD. 92

Figure 4.10 ^1H NMR data (300 MHz, 298 K) for Me_2biim complexes. 93

Figure 4.11 Mass spectrum for $Ru_2Cl_4(DMSO)_4(Me_2biim)$ (**23**); the most intense group of signals is for [M^+ - Cl – 3 DMSO], centred at 551. 94

Figure 4.12 ^1H NMR spectra of **24** and **25**. 96

Figure 4.13 Proposed structure for the cation of **24**. 96

Figure 4.14 Three possible structures for the cation of **25**. 97

Figure 4.15 Possible structure for a bis-biimidazole species, from reduction of the Ru centre. 98

Figure 4.16 Molecular structure for **28**. 99

Figure 5.1 Binding modes of carboxylate groups with transition metal complexes; a) Monodentate, b) Chelating, and c) Bridging. 110

Figure 5.2 Molecular structure of pyridine-2-carboxylic acid, Hpic. 111

Figure 5.3 ESI-MS spectrum (in MeOH) of $[Ru_2(pic)_4(EtOH)Cl]\cdot H_2O$ (**31**) clearly showing the [M^+ - EtOH] fragment centered at 727. 112

Figure 5.4 Theoretical isotopic distribution for the [M^+] peak of $Ru(Im\text{-}CO_2)(Im\text{-}CO_2H)_2Cl_2\cdot EtOH\cdot H_2O$ (**33**, left) (Section 5.3), and for the [M^+ - EtOH] peak of $[Ru_2(pic)_4(EtOH)Cl]\cdot H_2O$ (**31**, right). 113

Figure 5.5 ^1H NMR spectrum (300 MHz, 298 K) of $[Ru_2(pic)_4(EtOH)Cl]\cdot H_2O$ (**31**) in D_2O. 114

Figure 5.6 Proposed solid state structures for **31** where N-O ≡ pic^-. 115

Figure 5.7 Molecular structure of $Im\text{-}CO_2H$. 116

Figure 5.8 One possible isomer for the proposed structure for $Ru(Im\text{-}CO_2)(Im\text{-}CO_2H)_2Cl_2\cdot EtOH\cdot H_2O$ (**33**) (solvent molecules not shown). 117

Figure 5.9 Molecular structure of $[Ru(PPh_3)_2(L\text{-}H)_2]$ ($L\text{-}H_2$ = imidazole 4,5-dicarboxylic acid). 117

Figure 5.10 Mass spectrum of $Ru(Im\text{-}CO_2)(Im\text{-}CO_2H)_2Cl_2\cdot EtOH\cdot H_2O$, showing M^+ at 508. 118

Figure 5.11 Molecular structure of HCANT. 119
Figure 6.1 Mitochondrial reduction of MTT to Formazan. 130
Figure 6.2 Pictures of cells on Day 5 of MTT assay before adding MTT in a control experiment with no complex (left), and in an experiment incubated for 69 h in 2 mM $Ru(ma)_3$ (right). 131
Figure 6.3 Outline of MTT assay from Day 1 - Day 5; see Section 6.3. 131
Figure 6.4 Experimental 96-well plate set-up showing the control column (dark grey), the blank (white), the wells with water (light grey) and those containing the complex solutions (speckled). 135
Figure 6.5 Image of plate after MTT treatment. 137
Figure 6.6 Cell viability vs. concentration for $[Ru(ma)_2(2MeIm)_2]CF_3SO_3$ (**10**), with error bars representing 95% confidence limit. 140
Figure 6.7 Cell viability vs. concentration for $Ru(ma)_3$ (**1**), with error bars representing 95% confidence limit. 142
Figure 6.8 Cell viability vs. concentration for $Ru(Ema)_3$ (**2**), with error bars representing 95% confidence limit. 142
Figure 6.9 Cell viability vs. concentration for $[Ru(Ema)_2(2MeIm)_2]CF_3SO_3$ (**13**), with error bars representing 95% confidence limit. 144
Figure 6.10 Cell viability vs. concentration for cisplatin, with error bars representing 95% confidence limit. 145
Figure 6.11 Cell viability vs. concentration for $[Ru(ma)_2(Me_2biim)]CF_3SO_3 \cdot 2H_2O$ (**25**), with error bars representing 95% confidence limit. 147
Figure 6.12 Cell viability vs. concentration for $[Ru(ma)_2(biim)]CF_3SO_3 \cdot 2H_2O$ (**24**), with error bars representing 95% confidence limit. 147
Figure 6.13 Cell viability vs. concentration for $[Ru(Me_2biim)_3][CF_3SO_3]_2$ (**27**), with error bars representing 95% confidence limit. 148
Figure 6.14 Cell viability vs. concentration for $[Ru(biim)_3][CF_3SO_3]_2$ (**26**), with error bars representing 95% confidence limit. 149
Figure 6.15 Cell viability vs. concentration for $[Ru_2(pic)_4(EtOH)Cl] \cdot H_2O$ (**31**), with error bars representing 95% confidence limit. 150
Figure 7.1 CHO cells in α+/+ medium (~10^6 cells/mL) 156

Figure 7.2 Conical tube set-up used for CHO experiments (gas = air or N_2)..... 157

Figure 7.3 Colony of CHO cells after 7 days, following staining with methylene blue. 158

Figure 7.4 Structure of the indocarbocyanine fluorescent dye, Cy3, used to label the ELK3-51 MoAb. 161

Figure 7.5 Large cell colony formations resulting from clumped cells (A and B) compared with a colony grown from a single cell over the same time period, C. 163

Figure 7.6 Median fluorescence intensity of CHO cells incubated with EF5 or triF5 under N_2 or air and then treated with the ELK3-51/Cy3 antibody..... 169

Figure 7.7 Molecular structure of L-cysteine. 170

List of Tables

Table 3.1 Variable temperature chemical shifts of $Ru(ma)_3$ (300 MHz) in CD_2Cl_2 including values at $T = \infty$, as determined by linear regression. 42

Table 3.2 Selected X-ray data from bis-imidazole derivative structures. 53

Table 3.3 ^1H NMR data of Ru(III) maltolato-imidazole complexes in $CDCl_3$ at r.t. 55

Table 3.4 ^1H NMR data for the Ema-Im complexes **12** and **13**, compared with those for the ma-Im complexes **6** and **10**. 60

Table 3.5 Ru(III/II) reduction potentials of ma and Ema-containing complexes..... 66

Table 4.1 Ru (III/II) reduction potentials for the biimidazole complexes **24** and **25**, compared with those for **7** and **10**. 97

Table 5.1 Selected IR spectral data for Ru carboxylate complexes. 113

Table 6.1 Dilution table for the addition of complexes using a 4 mM stock solution. 136

Table 6.2 IC_{50} values for the ligand precursors against MDA-MB-435S cells in L-15 medium after incubation at 37 °C for 69 h. 138

Table 6.3 IC_{50} values for Ru-maltolato complexes against MDA-MB-435S cells in L-15 medium and against MDA435/LCC6-WT cells in DMEM after incubation at 37 °C for 69 h..... 140

Table 6.4 IC_{50} values for cisplatin, and three Ru complexes against MDA-MB-435S cells in L-15 medium after incubation at 37 °C for 69 h. 143

Table 6.5 IC_{50} values for ethylmaltolato complexes against MDA-MB-435S cells in L-15 medium after incubation at 37 °C for 69 h. 143

Table 6.6 IC_{50} values for biim and Me_2biim complexes against MDA-MB-435S cells in L-15 medium after incubation at 37 °C for 69 h; data for new Ru complexes containing picolinic acid (Hpic) or imidazole-4-carboxylic acid (Im-CO_2H) against the same cell line under the same conditions are also shown..... 146

Table 7.1 Plating efficiency of CHO cells after a 3 h incubation period under both aerobic and anaerobic conditions with several Ru(III) complexes at 100 μM. 164

Table 7.2 Uptake of Ru by CHO cells after a 3 h incubation period under both aerobic and anaerobic conditions with several Ru complexes at 100 μM. 166

Table 7.3 Amount of Ru associated with DNA isolated from CHO cells after a 3 h incubation period under both aerobic and anaerobic conditions with several Ru(III) complexes at 100 μM. 168

List of Symbols and Abbreviations

acac	acetylacetonate
Anal.	analysis
Ar	argon, or aryl
atm	atmosphere
biim	4,4'-biimidazole
br	broad
Calcd	calculated
cat.	catalyst
CHO	Chinese Hamster Ovarian (cell line)
COSY	homonuclear correlation spectroscopy (NMR)
cymene	isopropyltoluene
d	doublet, deoxy
dd	doubly distilled
DMEM	Dubelco's modified essential medium
DMSO	S-bound DMSO ligand
DMSO	O-bound DMSO ligand
e	electron
$E_{1/2}$	electrochemical half-wave potential
EDTA	ethylenediaminetetraacetato
EF5	2-(2-nitro-1-H-imidazol-1-yl)-N-(2,2,3,3,3-pentafluoropropyl) acetamide
Ema	ethylmaltolato, 2-ethyl-3-hydroxy-4-pyronate
equiv.	equivalent(s)
ESI	electrospray ionization
FBS	fetal bovine serum
$FeCp_2$	ferrocene
$FeCp^*_2$	bis(pentamethylcyclopentadienyl)iron(II)
G	guanosine
H_2biim	4,4'-biimidazolium trifluoroacetate
H_2Me_2biim	2,2'-dimethyl-4,4'-biimidazolium trifluoroacetate

HCANT	3-nitro-1,2,4-triazole-5-carboxylic acid
HMepyr	3-hydroxy-1,2-dimethyl-4-pyridone
HMQC	heteronuclear multiple quantum coherence
Hpic	pyridine-2-carboxylic acid, picolinic acid
IC_{50}	concentration at which 50 % inhibition of cell proliferation is observed
Im	imidazole
Im-CO_2H	imidazole-4-carboxylic acid
K	Kelvin (T)
LR	low resolution
LSIMS	liquid secondary ion mass spectrometry
m	multiplet, or medium intensity or milli
M	molar (mol L^{-1})
ma	maltolato, 3-hydroxy-2-methyl-4-pyronate
Me_2biim	2,2'-dimethyl-4,4'-biimidazole
1MeIm	1-methylimidazole
2MeIm	2-methylimidazole
4MeIm	4(5)-methylimidazole
metro	metronidazole
MoAb	monoclonal antibody
mol	mole
MS	mass spectrometry
MTT	3-(4,5-dimethylthiazol-2-yl)-2,5-diphenyltetrazolium
NMM	N-methylmorpholine
$2NO_2$Im	2-nitroimidazole
$4NO_2$Im	4-nitroimidazole
$3NO_2$tri	3-nitro-1,2,4-triazole
ORTEP	Oakridge Thermal Ellipsoid Program
p	phosphodiester linkage in a DNA backbone
PBS	phosphate-buffered saline solution
PE	plating efficiency
pF	paraformaldehyde

q	quartet
r.t.	room temperature
s	singlet
solv	solvent
T	Thymidine
TBAP	tetrabutylammonium hexafluorophosphate
TOF	time of flight
t	triplet
triF5	2-(3-nitro-1-H-triazol-1-yl)-N-(2,2,3,3,3-pentafluoropropyl) acetamide
δ	chemical shift (ppm)
λ	wavelength (nm)
ν	wavenumber (cm^{-1})
μ	micro, or bridging coordination mode
η	hapticity
[ ]	concentration (mol L^{-1})
{ }	broadband decoupled (NMR)

Key to Numbered Complexes

1 $Ru(ma)_3$

2 $Ru(Ema)_3$

3 $[Ru(ma)_2(EtOH)_2]CF_3SO_3$

4 $[Ru(ma)_2(metro)_2]CF_3SO_3$

5 $[Ru(ma)_2(metro)(EtOH)]CF_3SO_3$

6 $[Ru(ma)_2(4MeIm)_2]CF_3SO_3 \cdot CH_2Cl_2$

7 $[Ru(ma)_2(Im)_2]CF_3SO_3$

8 $[Ru(ma)_2(1MeIm)_2]CF_3SO_3 \cdot CH_2Cl_2$

9 $[Ru(ma)(1MeIm)_4][CF_3SO_3]_2$

10 $[Ru(ma)_2(2MeIm)_2]CF_3SO_3$

11 $[Ru(Ema)_2(metro)_2]CF_3SO_3$

12 $[Ru(Ema)_2(4MeIm)_2]CF_3SO_3$

13 $[Ru(Ema)_2(2MeIm)_2]CF_3SO_3$

14 $[Ru(ma)_2(EF5)_2]CF_3SO_3 \cdot EtOH$

15 $[Ru(ma)_2(2NO_2Im)_2]CF_3SO_3$

16 $[Ru(ma)_2(4NO_2Im)_2]CF_3SO_3$

17 $[Ru(ma)_2(3NO_2tri)_2]CF_3SO_3$

18 $[Ru(ma)_2(triF5)_2]CF_3SO_3$

19 $[Ru(HMepyr)_3]Cl_3$

20 $RuCl_2DMSO_2(biim)$

21 $Ru_2Cl_4DMSO_4(biim)$

22 $RuCl_2DMSO_2(Me_2biim)$

23 $Ru_2Cl_4DMSO_4(Me_2biim)$

24 $[Ru(ma)_2(biim)]CF_3SO_3 \cdot 2H_2O$

25 $[Ru(ma)_2(Me_2biim)]CF_3SO_3 \cdot 2H_2O$

26 $[Ru(biim)_3][CF_3SO_3]_2$

27 $[Ru(Me_2biim)_3][CF_3SO_3]_2$

28 $[Ru(Hbiim)_2Cl_2]Cl_2$

29 $[Ru(HMe_2biim)(Me_2biim)_2]Cl_3$

30 $Ru(pic)_3 \cdot H_2O$

31 $[Ru_2(pic)_4(EtOH)Cl] \cdot H_2O$

32 $Ru(Im\text{-}CO_2)_3 \cdot 2H_2O$

33 $Ru(Im\text{-}CO_2)(Im\text{-}CO_2H)_2Cl_2 \cdot H_2O \cdot EtOH$

Acknowledgements

I would like to thank my supervisor Prof. Brian James for his help and guidance during the past five years, and for his encouragement in my development as a scientist. I would also like to thank Dr. Jörn Müller for allowing me the opportunity of coming to working with his research group for a year at the Technisches Universität (TU) in Berlin towards the completion of my degree here at UBC.

I thank the remaining group members, Maria, Julio and Paolo, as well as the many past members I have had the honour of working with, particularly Jo Ling, Craig, Nathan, Paul, Cristina, Adam, Ian, Matt, Guibin, Hossein, Erin and Marcio.

Without the assistance and helpful insight of my workmates in Berlin, the year I spent could not have been nearly as productive as it was, and so I would like to thank Mattel, Tews, Andy 'Mahlzeit' Hejl, Petra, Captain Schiller, and Speedy Kempf for all their help and the Polisches Frau for keeping me posted on travel deals and always reminding me that the end would eventually arrive.

I would also like to acknowledge the work of Dr. Brian Patrick of this department in solving the X-ray crystal structures in this thesis work. Thank you as well to Marietta and Liane for all of their help with the NMR spectroscopy work I performed. I thank too all the other members of the UBC Chemistry Department with whom I have had the pleasure of working.

Special thanks to the GSP: Gord, Pav, Joe and Pete for supporting me in all my endeavours and to Mark for nighttime blading and a friendship that has stood the test of time, some 22 odd years now.

Finally I would like to thank my family who have supported me in so many ways and have never failed to be a guiding light in my life. My parents who have always encouraged me in everything I have done and my brothers, Chris and Jon, who through friendly competition and brotherly understanding have helped me strive to do my best.

As a great French-Canadian once said...

"when you have snow and ice for 6 months of the year,

you might as well skate."

Chapter 1

Introduction

1.1 Introduction

Although often thought of as a single condition, cancer actually consists of more than 100 diseases, all of which result from the uncontrolled growth of abnormal cells. Such cell growth is the result of genetic mutations that disrupt the normal function of the cell, and disable the cell's own internal repair pathways. This, in turn, leads to uncontrolled growth and spread of these abnormal cells.[1] Cancer can be divided into five major subclasses; carcinomas (cancer of the epithelial cells), sarcomas (cancer of the muscle, bone, fat, or tendons), myelomas (cancer of the plasma cells of bone marrow), leukemias (cancer of the bone marrow), and lymphomas (cancer of the lymphatic system) with carcinomas accounting for 80-90 % of total cases. The Canadian Cancer Society estimates that in 2003 almost 140,000 new cases of cancer will be diagnosed in Canada and over 67,000 Canadians will die from the disease.[2] Based on current trends it is estimated that approximately 38 % of men and 41 % of women will be diagnosed with some form of cancer in their lifetime.[2]

Although the death rate of cancer patients has been steadily decreasing over the last ten years, there is still a great demand for new drug treatments, particularly in light of the fact that some cancer tumours develop resistance to drug treatment over time, while other types of cancer have only a very limited response to chemotherapy and can only prolong the life of the patient at best.[3] One major goal in cancer research is to develop new drugs that can selectively target cancer tumours and trigger apoptosis, cell death, while exhibiting only limited side-effects to normal healthy tissue. Research directed at understanding tumour biology now makes it possible to specifically target tumour cells.[4]

Some of the differences between normal tissue and cancerous tumours result from the rapid growth and division often characteristic of malignant tumour cells. This can lead to poor vasculature forming around the tissue, generating a local region of low extra-

cellular pH and low oxygen concentration (hypoxia).[5] Local regions of hypoxia have been exploited in the search of new cancer treatments (Section 1.6.1) and new cancer imaging agents (Section 1.2). The use of hypoxia selective imaging agents is important not only for the detection of tumours, but also to quantify the extent of hypoxia in a given tumour. The presence of hypoxic cells is a major limiting factor in the efficacy of radiotherapy and thus the diagnosis of such cells prior to prescribing a treatment is of the utmost importance.[5]

In this chapter the concept of hypoxia detection will be briefly introduced, followed by an introduction to the development of Pt anti-cancer compounds and a review of the rapidly evolving field of Ru anti-cancer compounds.

1.2 Nitroimidazoles and Hypoxia

Hypoxia is defined as a condition in which a tissue receives a reduced supply of oxygen. As stated in Section 1.1, hypoxic regions often occur in tumours due to poor vasculature resulting from rapid growth of the tumour. Although cells deprived of an adequate oxygen supply will ultimately die, a tumour at any given time, may possess a region of viable, hypoxic cells that will be resistant to radiation treatment. O_2 diffuses from the capillaries through tissues, and in tumours containing hypoxic cells, a gradient of $[O_2]$ is established with healthy cells nearest the capillary, then a region of viable hypoxic cells as the $[O_2]$ decreases, with necrotic cells being those farthest from the capillary (Figure 1.1)[6]. Regions of hypoxia in a tumour can cause problems in treatment, as hypoxic cells are considerably less responsive than normal tissue to radiation therapy. The effectiveness of radiation therapy is dependent on the partial pressure of oxygen inside the cell. This ratio of hypoxic to oxic doses of radiation required to produce the same biological effect is known as the oxygen enhancement ratio (OER). For sparsely ionizing radiation such as γ-rays or X-rays, OER values are typically between 2.5 and 3.[6]

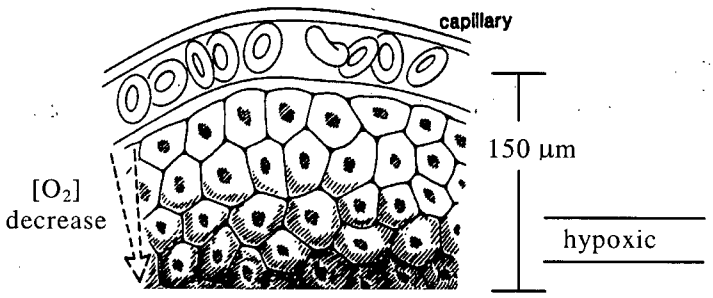

Figure 1.1 Gradient of oxygen concentration in cancerous tumours (adapted from ref. 6).

Since the early 1970s, nitroimidazoles have been investigated as potential radiosensitizers. Radiosensitizers enhance the effectiveness of radiation therapy by binding to the damaged DNA caused by the free radicals that result from irradiation of the cell. In the case of nitroimidazoles, the nitro group is thought to react with damaged DNA under hypoxic conditions in a manner similar to that of oxygen under normal oxic conditions, making the DNA irreparable and thus leading to cell death. Metronidazole (Figure 1.2) was one of the first nitroimidazoles investigated as a potential radiosensitizer but was found to cause extreme gastrointestinal toxicity at biologically active doses.[7] Since then, research has focused on the more electron affinic 2-nitroimdiazoles[5] ($E_{1/2}$ values typically between –360 and –400 mV for $2NO_2Im$ systems vs. –510 to –545 mV for $5NO_2Im$ and –540 to –685 mV for $4NO_2Im$ systems).[8]

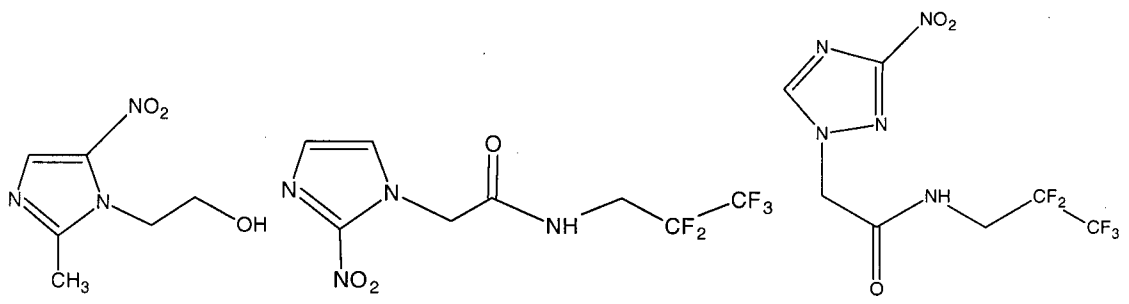

metronidazole EF5 triF5

Figure 1.2 Molecular structures of metronidazole, EF5 and triF5.

Some nitroimidazoles are also known to preferentially accumulate in hypoxic cells. 2-(2-Nitro-1-H-imidazol-1-yl)-N-(2,2,3,3,3-pentafluoropropyl)acetamide (EF5) (Figure 1.2) is currently undergoing clinical trials as a potential hypoxia imaging agent.[9] Labelled with radioactive ^{19}F, this compound can be traced using positron emission topography (PET).[10] EF5 accumulation can also be monitored using invasive techniques by detection of adducts formed with a fluorescent antibody (ELK3-51) that is specific for EF5.[11]

Both the detection and treatment of hypoxic cells by nitroimidazoles result from the reducibility of the nitro group under physiological conditions. The higher activity of 2-nitroimidazoles over other nitroimidazoles is likely a result of their more positive reduction potentials. It has been proposed that nitroreductase enzymes inside the cell carry out the reduction, and that the selectivity for hypoxic cells is a result of a lack of oxygen to carry out the reverse oxidation (Figure 1.3).[12,13] The radical anion formed as a result of the one-electron reduction can then undergo further reductions or react with other components inside the cell. In the presence of oxygen, the radical anion is reoxidized rapidly to the nitro group, and the compound can then diffuse back out of the cell.[13] The further reduction or other reactivity of the radical anion traps it inside the hypoxic cells and results in the accumulation of the reduced nitroimidazole species.

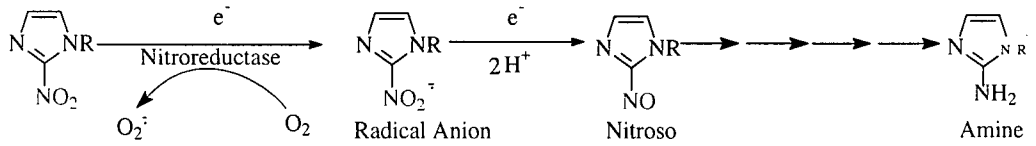

Figure 1.3 Proposed reduction pathway of nitroimidazoles (adapted from ref. 12).

1.3 *In Vitro* Bioassays

A detailed introduction to the bioassays used in this thesis work will be presented at the beginning of both Chapters 6 and 7. The MTT assay, used here as a preliminary screening assay for antiproliferatory activity and cytotoxicity of some newly synthesized Ru complexes, has been used similarly by several groups with other Ru complexes before proceeding with *in vivo* experiments.[14-20] Ru-uptake and Ru-DNA binding assays are

also performed to quantify the amount of metal accumulated in cells or in DNA, respectively.[21,22] These assays can be modified to place the cells under anaerobic conditions, and thus can be used to investigate the uptake of Ru under both normal and hypoxic conditions.

A monoclonal antibody specific for the side-chain of EF5 has been developed[11] and is used in Chapter 7 to determine the hypoxic selectivity of 2-(3-nitro-1-H-triazol-1-yl)-N-(2,2,3,3,3-pentafluoropropyl)acetamide (triF5, Figure 1.2) for comparison with that of EF5 under the same conditions (medium, cell line, concentration).

1.4 Platinum Anti-Cancer Drugs

1.4.1 Cisplatin and Other Pt(II) Anti-Cancer Drugs

The first metal anti-cancer drug to be developed was cisplatin, discovered by Rosenberg *et al.* in 1965 after noting that the cell division of *Escherichia coli* bacteria in their reaction medium was being inhibited by an electrolysis product formed *in situ* from a Pt electrode.[23,24] This product, identified as $[NH_4]_2[PtCl_6]$, was then converted to *cis*-$PtCl_4(NH_3)_2$ via a photochemical process, while subsequent reduction gave the biologically active complex, *cis*-$PtCl_2(NH_3)_2$ (cisplatin, Figure 1.4).[25] Cisplatin, the most active of a series of cis-amine Pt species against sarcoma 180 and leukemia L1210 tumour models in mice, entered clinical trials in 1971 and was approved for the treatment of testicular and ovarian cancer in 1978.[26] Unfortunately, there are drawbacks to cisplatin therapy: action against a limited range of tumours, poor solubility (thus the drug requires intravenous administration), and several toxic side-effects. The high incidence of nausea, vomiting, neuropathy, ototoxicity and nephrotoxicity has led to the search for new metal complexes having similar activity but with fewer side-effects.

Carboplatin (Figure 1.4), a less toxic analogue of cisplatin, was introduced into clinical trials in 1981, and is the only other Pt complex that has received worldwide approval and regular clinical use.[26] The major drawbacks of carboplatin therapy are that it is only applicable to the same narrow range of tumours as that of cisplatin and still must be administered intravenously.

Two other Pt(II)-amine complexes have received limited approval for use in some countries. Oxaliplatin ((*trans*-L-diaminocyclohexane)oxalatoplatinum(II)) has been approved in France for the secondary treatment of metastatic colorectal cancer, while nedaplatin (*cis*-diammine-glycolato-O,O'-platinum(II)) has received approval in Japan for the treatment of some cancers.[26]

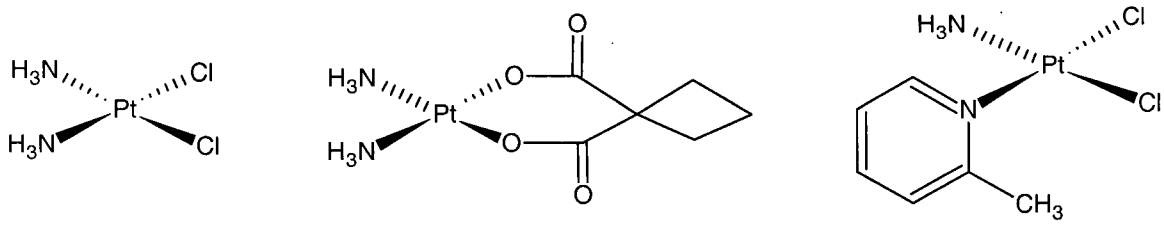

cisplatin carboplatin AMD473

Figure 1.4 Molecular structures of Pt(II) anti-cancer complexes.

More recently, the rational design of Pt(II) complexes with a greater steric bulk in the amine ligands in order to limit deactivation of the complex by glutathione has led to the development of AMD473, *cis*-(ammine)dichloro(2-methylpyridine)platinum(II) (Figure 1.4). AMD473 entered clinical trials after exhibiting improved activity over that of cisplatin against cisplatin-sensitive and -resistant cell lines; this complex is also sufficiently water-soluble that it can be administered orally,[26] and is currently in Phase II clinical trials for treatment of hormone resistant prostate cancer (HRPC).[27]

The mechanism by which cisplatin arrests cell division is well understood. In aqueous solution, cisplatin undergoes chloride dissociation to give both mono- and diaqua species. In the presence of DNA, these species react with the N(7) position on guanine bases, and give rise to either d(GpG) (Figure 1.5) or d(GpTpG) intrastrand cross-links (d = deoxy, G = guanosine, p = phosphodiester linkage and T = thymidine).[28] The resulting intrastrand adduct can be removed and repaired by the cell; however, the intrastrand cross-link also results in a kink in the DNA that can then be recognized by damage-recognition proteins[29] that may then block the repair enzymes from accessing the damaged DNA.[30]

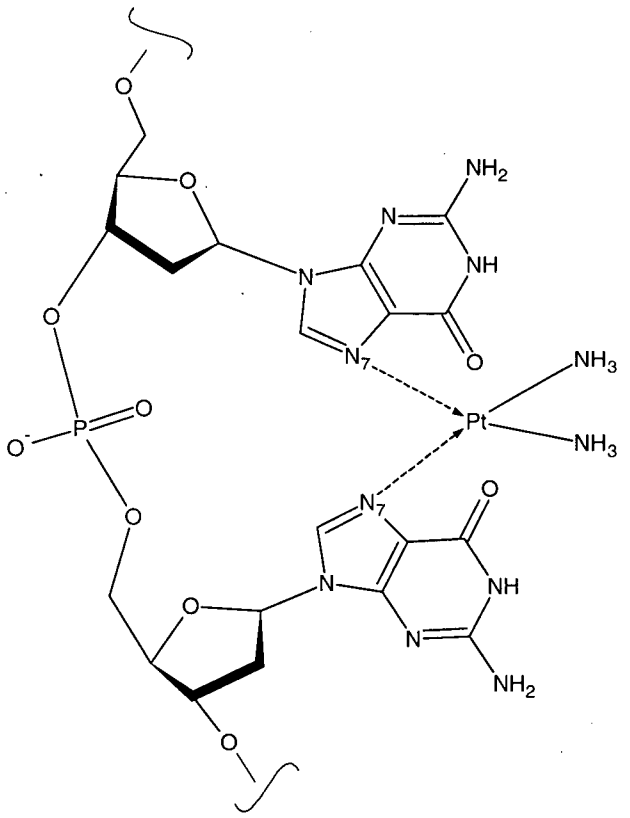

Figure 1.5 Pt-DNA adduct formed from a d(GpG) intrastrand cross-link.

1.4.2 Platinum(IV) as a Pro-Drug

The anti-cancer activity of Pt(IV) complexes such as *cis*-$PtCl_4(NH_3)_2$ has been known since the discovery of cisplatin.[23,25] Several Pt(IV) compounds have since been made in the hope that they might be activated by an *in vivo* reduction of the metal centre. At least three of these compounds (iproplatin,[31] tetraplatin,[32] and JM216,[33-35] Figure 1.6) have entered clinical trials, but have ultimately failed to produce results better than those of cisplatin; trials with iproplatin and JM216 failed to produce significant *in vivo* effects, while treatment with tetraplatin gave acute toxic side-effects. Complexes that remain in the higher Pt(IV) oxidation state in the bloodstream have the potential advantage over Pt(II) complexes of undergoing fewer, unwanted side-reactions. This can result in fewer, toxic side-effects and thus a greater amount of the active drug arriving in the target cells.[36] The higher lipophilicity of some Pt(IV) complexes can also lead to better cellular uptake.[36]

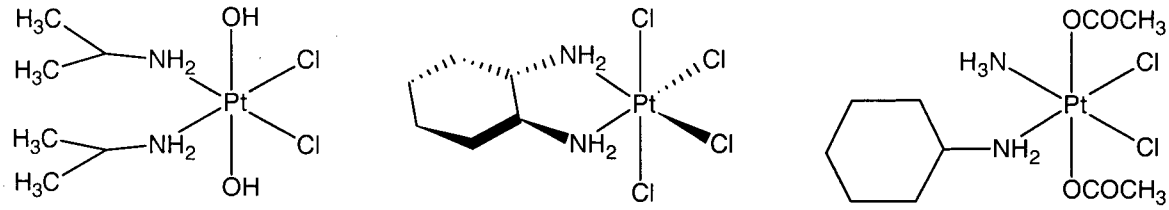

Iproplatin Tetraplatin JM216

Figure 1.6 Molecular structures of Pt(IV) anti-cancer complexes.

The rate of *in situ* reduction of Pt(IV) to Pt(II) varies greatly depending on the ligands bound to the metal, and the ease at which the metal centre is reduced may greatly influence its biological activity.[36] Direct correlations between the activity of a complex and its Pt(IV/II) reduction potential cannot always be made; the reduction potential of tetraplatin is about 300 mV more positive than that of JM216, yet both are highly active *in vitro*.[36] It may be possible, though, to tune the reduction potential of complexes already known to be active, to try and slow the *in vivo* reduction so that the more active complex reaches and is taken up into the cells.[36]

1.5 Ruthenium Complexes and Their Potential as Anti-Cancer Drugs

Since the discovery of cisplatin, complexes with other transition metals have been investigated, and Ru complexes have emerged as strong candidates for potential therapeutic use. Some proposed mechanisms of action and potential anti-cancer drugs will be discussed in the following sections.

1.5.1 Activation by Reduction

Ru(III) complexes have been investigated as pro-drugs for potentially more active Ru(II) species, and a mechanism of activation by reduction may be the reason that several Ru(III) complexes have shown high levels of *in vivo* activity against various types of cancerous tumours.[37] The concept is the same as the use of Pt(IV) as a pro-drug, to

deliver a greater percentage of active complex to the cancerous cells by starting with a less reactive species that then becomes activated by reduction in the hypoxic regions of tumours. Ru(II) complexes are generally more substitutionally labile than those of Ru(III)[37] and are thus more likely to lose ligands *in vitro*, opening coordination sites for DNA or other cellular targets.

1.5.2 *cis*-$RuCl_2(DMSO)_3(DMSO)$

cis-$RuCl_2(DMSO)_3(DMSO)$ (*cis*-DMSO) was first reported by our group in 1971.[38] Studies suggesting that this complex could interact *in vitro* with DNA were reported in 1975,[39] and this resulted in further studies comparing its antimutagenic properties with those of cisplatin.[40] *cis*-DMSO, tested *in vivo* in mice implanted with Lewis lung carcinoma-, B16 melanoma-, and Mca mammary carcinoma tumour models, was as effective as cisplatin against primary tumour growth and lung metastases and significantly less toxic.[40,41] Coluccia *et al.* have reported *in vivo* testing of *cis*-DMSO in mice bearing P388 and the cisplatin-resistant P388/DDP leukemia tumour models, and in the latter, *cis*-DMSO was more effective than cisplatin at reducing primary tumour growth.[42]

cis-DMSO likely acts via a DNA-binding mechanism, and several groups have reported its interactions with purines.[43-45] Although the O-bound DMSO ligand of *cis*-DMSO rapidly dissociates in aqueous solution, followed by the slow loss of one Cl^- ligand,[46] Farrell and De Oliveira have reported a dicationic Ru-bis(adenine) complex in which the O-bound DMSO is retained and the two Cl^- ligands are replaced by adenine.[43]

1.5.3 Ru-imidazole Complexes

Keppler *et al.* first reported on the synthesis and biological activity of imidazolium [*trans*-tetrachlorobis(imidazole)ruthenate(III)] (ICR) in 1987 (Figure 1.7).[15] Since then, numerous studies on analogues of this complex using other N-heterocyclic ligands in place of imidazole have been reported.[14,16-18] Preliminary studies of ICR against P388 leukemia-, Walker 256 carcinosarcoma-, and sarcoma 180 tumour-infected mice resulted in increased survival times (T/C values of up to 194 vs. 175 % for cisplatin,[15] where T/C values are calculated as the survival time of mice treated with the

complex divided by the survival time of mice to which no complex was administered). The methylimidazole derivatives were less active than ICR against P388 leukemia (T/C values of 130 - 150 %), while (Htri)[*trans*-$Ru(tri)_2Cl_4$] (tri = 1,2,4-triazole) also exhibited weaker activity (T/C = 138 %).[14] (HInd)[*trans*-$Ru(Ind)_2Cl_4$] (Ind = indazole) (Figure 1.7) was as effective as ICR in reducing colorectal tumour growth (typically 50 - 80 % reduction in growth) and was devoid of any side-effects at active dosages.[41,47]

Imidazolium pentachloro(imidazole)ruthenate(III) ($(HIm)_2[Ru(Im)Cl_5]$)[16] and the analogous triazole complex, $(Htri)_2[Ru(tri)Cl_5]$,[14] exhibit survival rates in P388 tumour-bearing mice that are lower than those for cisplatin and ICR (T/C = 150-162 % for $(HIm)_2[Ru(Im)Cl_5]$[16] and 150 % for $(Htri)_2[Ru(tri)Cl_5]$).[14]

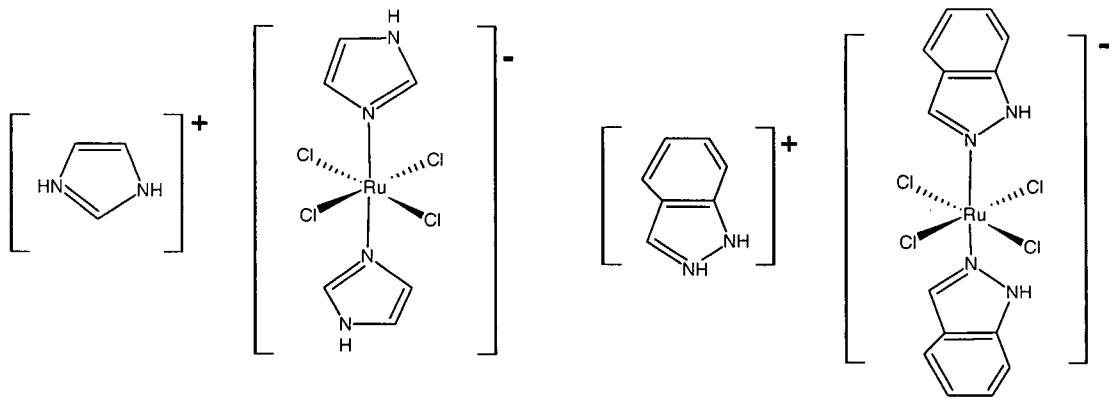

(HIm)[*trans*-$Ru(Im)_2Cl_4$] (HInd)[*trans*-$Ru(Ind)_2Cl_4$]

Figure 1.7 Molecular structures of Ru(III) anti-cancer complexes.

1.5.3.1 NAMI and NAMI-A

(HIm)[*trans*-Ru(Im)(DMSO)Cl_4] (NAMI-A) (Figure 1.8) exhibits an anti-metastatic effect on several tumour models and is the only Ru complex to date to enter into clinical trials.[41] *In vivo* studies show that both NAMI-A and NAMI (Na[*trans*-Ru(Im)(DMSO)Cl_4]), like cisplatin, are capable of reducing primary tumour growth in Lewis lung carcinoma-, B16 melanoma-, Mca mammary carcinoma tumour-models by up to 40 %.[48,49] Unlike cisplatin, however, treatment with NAMI or NAMI-A also increased the life-span of the hosts, independent of the tumour model used, and reduced the

formation of lung metastases even when the inhibition of primary tumour growth was negligible.[41] NAMI and NAMI-A are thought to arrest cells in the G2/M phase of the cell cycle, and do not appear to act via a DNA-binding mechanism, although they do bind DNA *in vitro*.[50] The complexes may be activated by an *in situ* reduction to a Ru(II) species.[51] The major advantage of NAMI-A over NAMI is that it is a more stable solid.[51]

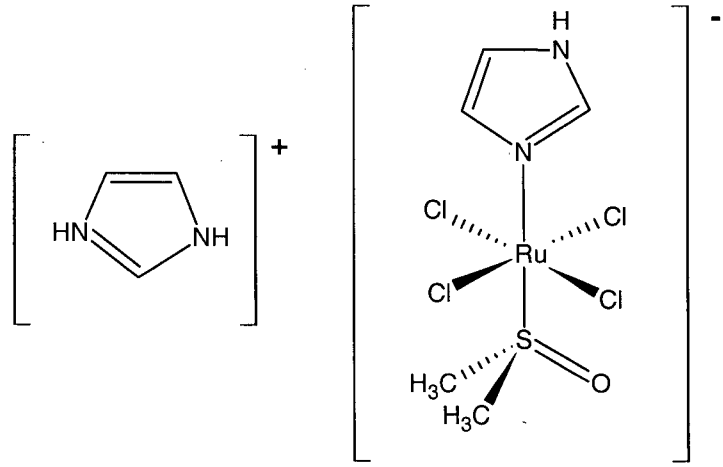

Figure 1.8 Molecular structure of NAMI-A.

1.5.4 Ru-arene Complexes

Morris *et al.* have reported the synthesis and *in vitro* testing of Ru(II)-arene complexes against A2780 human ovarian cancer cells.[19] Complexes such as [RuX(*p*-cymene)(en)]PF_6, where X = Cl or I (Figure 1.9), exhibited IC_{50} values (9 and 8 μM for Cl and I, respectively) similar to that of carboplatin (6 μM) against the same cell line, but more than an order of magnitude higher than that of cisplatin (0.5 μM).[19] These complexes bind strongly to the guanine bases of DNA.[19] It is thought that the arene group not only stabilizes the Ru(II) metal centre but may also help in cellular uptake by increasing the hydrophobicity of the complex.[19] The range of Ru-arene complexes studied was then expanded by the same group who then reported that [RuCl-(tetrahydroanthracene)(en)]PF_6 exhibited the lowest IC_{50} value, 0.5 μM, of a range of complexes tested, equal to that observed for cisplatin.[52]

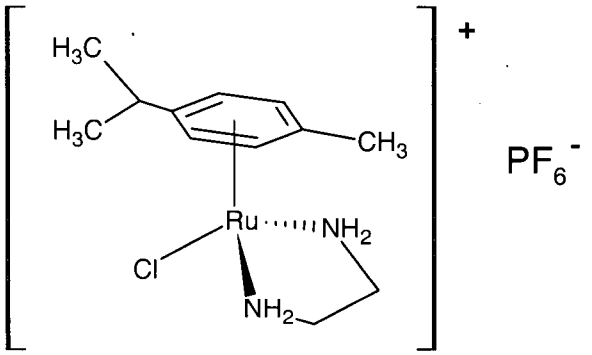

Figure 1.9 Molecular structure of [RuCl(*p*-cymene)(en)]PF_6.

Ru-arene complexes have also been synthesized in our group and tested for anti-cancer activity against MDA-MB-435S cells, a human breast cancer cell line.[53] The complex, [RuCl(*p*-cymene)(BESE)]PF_6 (Figure 1.10), where BESE = 1,2-bis(ethylsulfinyl)ethane, and the dimeric complex, [$RuCl_2$(*p*-cymene)]$_2$(μ-BESE), have been tested for activity using the MTT assay to determine their IC_{50} values. RuCl(*p*-cymene)(BESE)]PF_6 exhibited significant activity (IC_{50} = 55 μM) when compared with data for cisplatin (IC_{50} = 10 μM).[53]

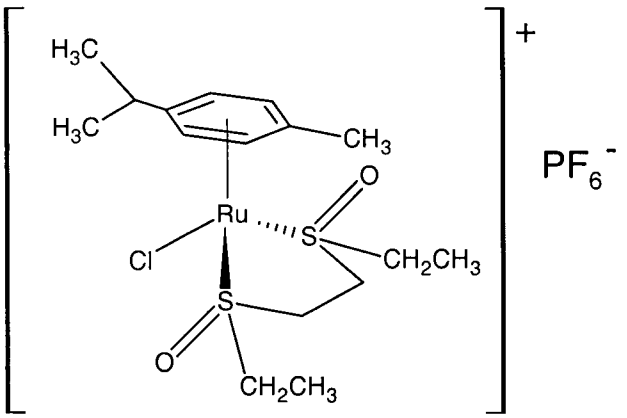

Figure 1.10 Molecular structure of RuCl(*p*-cymene)(BESE)]PF_6.

A third group has reported on the pH dependent cytotoxicity of Ru(*p*-cymene)Cl_2(pta) (Figure 1.11), where pta = 1,3,5-triaza-7-phosphatricyclo-[3.3.1.1]decane, which may also prove useful as an anti-cancer agent.[54]

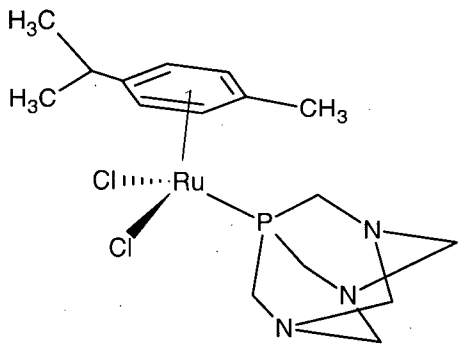

Figure 1.11 Molecular structure of Ru(*p*-cymene)Cl_2(pta).

1.5.5 Ru-azopyridine Complexes

Velders *et al.* have reported on the activity of the so-called α-isomer of dichlorobis(2-phenylazopyridine)ruthenium(II) (Figure 1.12) against 7 different tumour cell lines;[20] the activity was invariably equal to or better than that of cisplatin, with IC_{50}

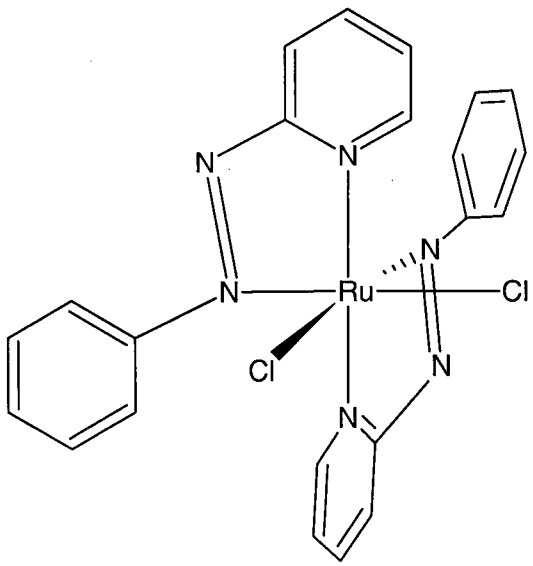

Figure 1.12 Molecular structure of α-dichlorobis(2-phenylazopyridine)ruthenium(II).

values being an order of magnitude lower than that of cisplatin in both the EVSA-T (a human breast cancer cell line) and M19 (a Chinese hamster ovarian cell line) cell lines.[20] Two geometric isomers, the so-called β- (containing cis-pyridine and cis-Cl ligands) and γ- (containing cis-pyridine and trans-Cl) isomers were considerably less active. Believing that the α-isomer acts in a manner similar to that of cisplatin by binding to the guanine bases of DNA, the same group later showed that this complex reacts with 9-ethylguanine[55] to form α-[Ru(2-phenylazopyridine)$_2$(9-ethylguanine)(H_2O)](PF_6)$_2$, with the guanine bound through the N(7) position; 3-methyladenine, correspondingly formed α-[Ru(2-phenylazopyridine)$_2$(3-methyl-adenine)](PF_6)$_2$, in which the adenine is chelated through the N(6) and N(7) positions.[55] It was thought that such Ru-adducts might form in the presence of DNA and be responsible for the anti-tumour activity of α-dichlorobis(2-phenylazopyridine)ruthenium(II).

1.5.6 Ru Intercalators

Ru complexes with large conjugated ligands can also interact with the purine bases of DNA via π-stacking interactions. Such Ru intercalators are of particular interest in photodynamic therapy in which they can be activated to cause local damage to the surrounding DNA.[37] Both enantiomers of [Ru(phen)$_2$dppz](PF_6)$_2$, where phen = 1,10-phenanthroline and dppz = 2,2'-dipyrido-3,3'-phenazine (Figure 1.13), exhibit a high affinity for DNA without loss of any chelating ligand.[56]

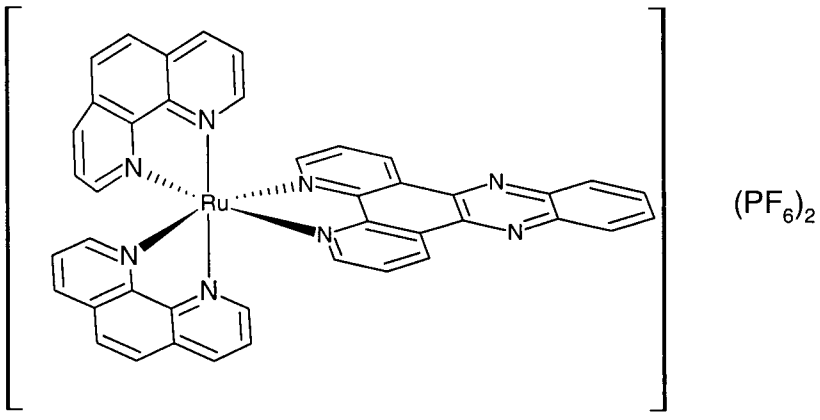

Figure 1.13 Molecular structure of [Ru(phen)$_2$dppz](PF_6)$_2$.

1.6 Maltolato (ma) Chemistry

Maltol (3-hydroxy-2-methyl-4-pyranone, Figure 1.14), is a water-soluble food additive with a pK_a of 8.67 for the hydroxy group;[57] the anionic form, maltolato (ma), can then chelate to transition metal centres. This is an attractive ligand to use in biological inorganic chemistry as complexes that contain one or more maltolato ligands are often water-soluble and the free ligand, if dissociated *in vivo*, is non-toxic.[58]

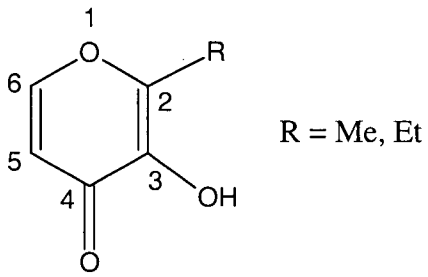

Figure 1.14 Molecular structures of maltol (R = Me) and ethylmaltol (R = Et).

1.6.1 Maltolato Complexes with Ru

$Ru(ma)_3$, first reported by Griffith and Greaves in 1988,[59] was synthesized as part of a research project investigating the transition metal complexes of tropolone and catechol (Figure 1.15). Indeed, the assignment of the ^1H NMR spectrum of

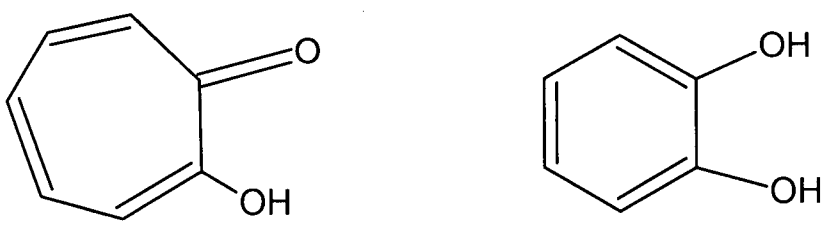

tropolone catechol

Figure 1.15 Molecular structures of tropolone and catechol.

Ru(tropolonato)$_3$, first discussed by Eaton *et al.*,[60] shows similarities to that of Ru(ma)$_3$ which will be discussed in Chapter 3. El-Hendawy and El-Shahawi reported later the synthesis of another Ru(III) maltolato species, $RuCl_2(ma)(PPh_3)_2$,[61] while other groups have reported Ru(II) complexes containing one or more maltolato ligands. Fryzuk *et al.* have reported on *cis*-Ru(ma)$_2$(PPh$_3$)$_2$, *cis*-Ru(ma)$_2$(DMSO)$_2$, and *cis*-Ru(ma)$_2$(COD)$_2$,[62] while Capper *et al.* have characterized Ru(mes)Cl(L) and [Ru(mes)(CO)(L)](BF$_4$) where L = maltolato (ma) or ethylmaltolato (Ema) and mes = 1,3,5-trimethylbenzene.[63]

Our group has recently reported on the anti-cancer activity of Ru-maltolato-sulfoxide complexes of the type Ru(L)$_2$(DMSO)$_2$ where L = maltolato (ma) or ethylmaltolato (Ema) (Figure 1.16).[64,65] These complexes were tested against the human breast cancer cell line MDA-MB-435S and exhibited IC_{50} values of 190 (L = Ema) and 220 μM (L = ma), these data being taken from Wu's M.Sc. thesis.[65] Replacement of the DMSO ligands by BESE (see Section 1.6.4) led to less active complexes.[64,65] The higher stability of the chelated-BESE complexes in solution may limit the potential *in vitro* for the Ru to bind DNA or other cellular targets.[64,65]

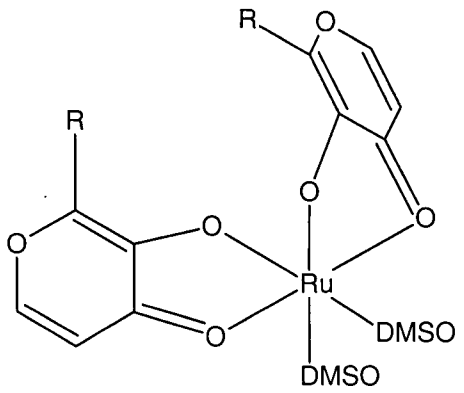

Figure 1.16 Molecular structure of Ru(ma)$_2$(DMSO)$_2$ (R = Me) and Ru(Ema)$_2$(DMSO)$_2$ (R = Et).

1.6.2 Maltolato Complexes with Other Transition Metals

Fe(ma)$_3$ has been structurally characterized and proposed as a potential drug for iron-deficiency anaemia,[66] while trivalent complexes of Cr, Mn, Rh, Ga, In, V and Al

have also been reported.[67,68] $VO(ma)_2$ and $VO(Ema)_2$ are being studied as potential insulin mimetic drugs.[69,70] Greaves and Griffith have also reported the syntheses of *trans*-$Os(O)_2(ma)_2$, *trans*-$U(O)_2(ma)_2$ and *cis*-$Mo(O)_2(ma)_2$.[59] $Sn(ma)_2Cl_2$[71] and $Sn(ma)_2$[72] have been synthesized, and other divalent maltolato complexes of Co, Ni, Cu, and Zn have been reported.[67] Numerous trivalent lanthanide complexes of the form $M(ma)_3 \cdot H_2O$ have also been synthesized (M = La, Pr, Nd, Sm, Gd, Dy, and Yb).[57]

1.7 Goals of this Thesis

The goals at the onset of this thesis work were to synthesize and characterize new Ru-maltolato-imidazole and -nitroimidazoles complexes, and to investigate their toxicity, cellular uptake and interactions with DNA in cells using standard *in vitro* bioassays. Previous work in our group had shown that Ru-EF5 complexes could be used as potential radiosensitizers[73] while other groups have shown that Ru(III) imidazole complexes may be good anti-metastasis drugs[50] or intercalators.[52] A 3-nitro-1,2,4-triazole analogue of EF5 was proposed as a possible new hypoxia selective agent, and was thus synthesized, characterized and tested; this compound was examined *in vitro* for hypoxia selective activity but proved to be not as effective as EF5. Of the Ru(III)-maltolato-imidazole complexes tested, several exhibited interesting biological activity, and as the biological testing proceeded, it became apparent that these complexes might also produce an antiproliferatory effect similar to that of NAMI-A, and thus the MTT assay was used as a general screening assay to probe complexes for anti-cancer activity.

The range of Ru complexes synthesized and characterized was then expanded to investigate complexes of several, bidentate ligands, especially imidazole-4-carboxylic acid, 4,4'-biimidazole and 2,2'-dimethyl-4,4'-biimidazole. Complexes of these ligands with $Ru(ma)_3$ and several other Ru starting materials afforded several new complexes that were characterized and tested in preliminary *in vitro* bio-assays.

This thesis consists of 8 chapters, and appendices containing data for the 5 crystal structures presented. In Chapter 2, general experimental procedures and methods are discussed. The syntheses and characterization data of new Ru(III)-maltolato-imidazole

complexes are described in Chapter 3. The syntheses of 4,4'-biimidazole ligands, and the reactions of these ligands with both Ru(II) and Ru(III) precursors to afford new Ru-biimidazole complexes, are described in Chapter 4. These ligands were designed initially to synthesize a bidentate biimidazole analog of EF5. Ultimately, the complexes with the biimidazole ligands were themselves found to be worthy of study even without nitration to form the intended 2,2'-dintrobiimidazole species. The successful results from biotests with Ru-bis(2MeIm) complexes (Chapter 3), led to the development of the analgous 2,2'-dimethyl-4,4'-biimidazole complexes for study. In Chapter 5, the reactions of imidazole-4-carboxylic acid and other N-heterocyclic carboxylic acids with Ru(III) precursors are described, as are the attempted syntheses of new 2-nitroimidazole-4-carboxylic acid derivatives. In Chapter 6, the results from the MTT assay for many of the complexes described in Chapters 3-5 will be discussed, while in Chapter 7, the results of Ru-uptake and –DNA binding experiments for several Ru complexes are reported and discussed. A monoclonal antibody binding assay is also discussed and the results of this assay with both EF5 and triF5 are presented. Although general conclusions will be included at the end of each individual chapter, in Chapter 8 some general conclusions about this thesis work will be presented. Directions for future research on this topic will also be discussed.

1.8 References

(1) Griffiths, A. J.; Miller, J. H.; Suzuki, D. T.; Lewontin, R. C.; Gelbart, W. M. *An Introduction to Genetic Analysis 6th Ed.;* , W. H. Freeman and Company: New York, 1996, p. 736.

(2) National Cancer Institute of Canada *Canadian Cancer Statistics 2003*: Toronto, 2003.

(3) Fricker, S. P. *Metal Compounds in Therapy*; Fricker, S. P. ed.; Chapman and Hall: London, 1994.

(4) Ruddon, R. W. *Cancer Biology* , Oxford University Press: New York, 1995, p.3.

(5) Hodgkiss, R. J. *Anti-Cancer Drug Des.* **1998**, *13*, 687.

(6) Farrell, N. *Transition Metal Complexes as Drugs and Chemotherapeutic Agents*; Kluwer Acadewmic: Dordrecht, 1989.

(7) Fowler, J. F.; Denekamp, J. *J. Pharmacol. Therapeut.* **1979**, *7*, 413.

(8) Adams, G. E.; Flockhart, I. R.; Smither, C. E.; Stratford, I. J.; Wardman, P.; Watts, M. E. *Radiat. Res.* **1976**, *67*, 9.

(9) Evans, S. M.; Hahn, S.; Pook, D. R.; Jenkins, W. T.; Chalian, A. A.; Zhang, P.; Stevens, C.; Weber, R.; Weinstein, G.; Benjamin, I.; Mirza, N.; Morgan, M.; Rubin, S.; Gilles, W.; Lord, E. M.; Koch, C. J. *Cancer Res.* **2000**, *60*, 2018.

(10) Bruelmeier, M.; Achermann, R.; Kaser-Hotz, B.; Blagoev, M.; Evans, S. M.; Koch, C. J.; Rohrer, B. C.; Gardelle, O.; Keller, C.; Schubiger, P. A.; Ametamey, S. M. *J. Radiat. Oncology Biol. Phys.* **2003**, *55*, 468.

(11) Cohen-Jonathan, E.; Evans, S. M.; Koch, C. J.; Muschel, R. J.; McKenna, W. G.; Wu, J.; Bernhard, E. J. *Cancer Res.* **2001**, *61*, 2289.

(12) Chapmann, J. D.; Meeker, B. E. *Selective Activation of Drugs by Redox Processes*; Adams, G. E., Breccia, A., Fielden, E. M., Wardman, P. ed.; Plenum Press: New York, 1990.

(13) Wardman, P. *Environ. Health Perspect.* **1985**, *64*, 309.

(14) Keppler, B. K.; Balzer, W.; Seifried, V. *Drug. Res.* **1987**, *37*, 770.

(15) Keppler, B. K.; Rupp, W.; Juhl, U. M.; Endres, H.; Niebl, R.; Balzer, W. *Inorg. Chem.* **1987**, *26*, 4366.

(16) Keppler, B. K.; Wehe, D.; Endres, H.; Rupp, W. *Inorg. Chem.* **1987**, *26*, 844.

(17) Keppler, B. K.; Galeano, A.; Berger, M. R. *Drug Res.* **1992**, *42*, 821.

(18) Nikolova, A.; Ivanov, D.; Buyukliev, R.; Konstantinov, S.; Karaivanova, M. *Drug Res.* **2001**, *51*, 758.

(19) Morris, R. E.; Arid, R. E.; Murdoch, P. S.; Chen, H.; Cummings, J.; Hughes, N. D.; Parsons, S.; Parkin, A.; Boyd, G.; Jodrell, D. I.; Sadler, P. J. *J. Med. Chem.* **2001**, *44*, 3616.

(20) Velders, A. H.; Kooijman, H.; Spek, A. L.; Haasnoot, J. G.; de Vos, D.; Reedijk, J. *Inorg. Chem.* **2000**, *39*, 2966.

(21) Frausin, F.; Cocchietto, M.; Bergamo, A.; Scarcia, V.; Furlani, A.; Sava, G. *Cancer Chemother. Pharmacol.* **2002**, *50*, 405.

(22) Bergamo, A.; Stocco, G.; Gava, B.; Cocchietto, M.; Alessio, E.; Serli, B.; Iengo, E.; Sava, G. *J. Pharmacol. Exp. Ther.* **2003**, *305*, 725.

(23) Rosenberg, B.; Van Camp, L.; Krigas, T. *Nature* **1965**, *205*, 698.

(24) Rosenberg, B.; Van Camp, L.; Grimely, E. B.; Thomson, A. J. *J. Biol. Chem.* **1967**, *242*, 1347.

(25) Rosenberg, B.; Van Camp, L.; Trosko, J. E.; Mansour, V. H. *Nature* **1969**, *222*, 385.

(26) Wong, E.; Giandomenico, C. M. *Chem. Rev.* **1999**, *99*, 2451.

(27) Beale, P.; Judson, I.; O'Donnell, A.; Trigo, J.; Rees, C.; Raynaud, F.; Turner, A.; Simmons, L.; Etterley, L. *Br. J. Cancer* **2003**, *88*, 1128.

(28) Beck, D. J.; Popoff, S.; Sancar, A.; Rupp, W. D. *Nucleic Acid Res.* **1985**, *13*, 7395.

(29) Hughes, E. N.; Engelsberg, B. N.; Billings, P. C. *J Biol. Chem.* **1992**, *267*, 13520.

(30) Donahue, B. A.; Augot, M.; Bellon, S. F.; Treiber, D. K.; Toney, J. H.; Lippard, S. J.; Essigmann, J. M. *Biochem.* **1990**, *29*, 5872.

(31) Braddock, P. D.; Connors, T. A.; Jones, M.; Khokhar, A. R.; Melzack, D. H.; Toobe, M. L. *Chem.-Biol. Interact.* **1975**, *11*, 145.

(32) Christian, M. C. *7th Intl. Symp. on Pt and other Metal Coord. Cpds. in Chemotherapy, Abstract* **1995**, S128.

(33) McKeage, M. J.; Raynaud, F.; Ward, J.; Berry, C.; O'Dell, D.; Kelland, L. R.; Murrer, B.; Santabarabara, P.; Harrap, K. R.; Judson, I. R. *J. Clin. Oncol.* **1997**, *15*, 2691.

(34) Kelland, L. R.; Jones, M.; Abel, G.; Harrap, K. R. *Cancer Chemother. Pharmacol.* **1992**, *30*, 43.

(35) Kelland, L. R.; Mistry, P.; Abel, G.; Freidlos, F.; Loh, S. Y.; Roberts, J.; Harrap, K. R. *Cancer Res.* **1992**, *52*, 1710.

(36) Hall, M. D.; Hambley, T. W. *Coord. Chem. Rev.* **2002**, *232*, 49.

(37) Clarke, M. J. *Coord. Chem. Rev.* **2002**, *232*, 69.

(38) James, B. R.; Ochiai, E.; Rempel, G. L. *Inorg. Nucl. Chem. Lett.* **1971**, *7*, 781.

(39) Monti-Bragadin, C.; Ramani, L.; Samer, L.; Mestroni, G.; Zassinovich, G. *Antimicrob. Agents Chemother.* **1975**, *7*, 825.

(40) Giraldi, T.; Sava, G.; Bertoli, G.; Mestroni, G.; Zassinovich, G. *Cancer Res.* **1977**, *37*, 1662.

(41) Sava, G.; Bergamo, A. *Int. J. Oncol.* **2000**, *17*, 353.

(42) Coluccia, M.; Sava, G.; Pacor, S.; Mestroni, G.; Alessio, E. *Eur. J. Cancer* **1993**, *29A*, 1873.

(43) Farrell, N.; De Oliveira, N. G. *Inorg. Chim. Acta* **1982**, *66*, L61.

(44) Cauci, S.; Alessio, E.; Mestroni, G.; Quadrifoglio, F. *Inorg. Chim. Acta* **1987**, *137*, 19.

(45) Tian, Y.; Yang, P.; Li, Q.; Guo, M.; Zhao, M. *Polyhedron* **1997**, *16*, 1993.

(46) Alessio, E.; Mestroni, G.; Nardin, G.; Attia, W. M.; Calligaris, M.; Sava, G.; Zorzet, S. *Inorg. Chem.* **1988**, *27*, 4099.

(47) Berger, M. R.; Garzon, F. T.; Keppler, B. K.; Schmahl, D. *Anticancer Res.* **1989**, *9*, 761.

(48) Sava, G.; Capozi, I.; Clerici, K.; Gagliardi, G.; Alessio, E.; Mestroni, G. *Exp. Metastasis* **1998**, *16*, 371.

(49) Sava, G.; Pacor, S.; Coluccia, M.; Mariggio, M.; Cocchietto, M.; Alessio, E.; Mestroni, G. *Drug Invest.* **1994**, *8*, 150.

(50) Gagliardi, R.; Sava, G.; Pacor, S.; Mestroni, G.; Alessio, E. *Clin. Exp. Metastasis* **1994**, *12*, 93.

(51) Clarke, M. J.; Zhu, F.; Frasca, D. R. *Chem. Rev.* **1999**, *99*, 2511.

(52) Aird, R. E.; Cummings, J.; Ritchie, A. A.; Muir, M.; Morris, R. E.; Chen, H.; Sadler, P. J.; Jodrell, D. I. *Br. J. Cancer* **2002**, *86*, 1652.

(53) Huxham, L. A.; Cheu, E. L. S.; Patrick, B. O.; James, B. R. *Inorg. Chim. Acta* **2003**, *352*, 238.

(54) Allardyce, C. S.; Dyson, P. J.; Ellis, D. J.; Heath, S. L. *Chem. Comm.* **2001**, 1396.

(55) Hotze, A. C. G.; Broekhuisen, M. E. T.; Velders, A. H.; Kooijman, H.; Spek, A. L.; Haasnoot, J. G.; Reedijk, J. *J. Chem. Soc., Dalton Trans.* **2002**, 2809.

(56) Hiort, C.; Lincoln, P.; Norden, B. *J. Am. Chem. Soc.* **1993**, *115*, 3448.

(57) Dutt, N. K.; Sarma, U. U. M. *J. Inorg. Nucl. Chem.* **1975**, *37*, 1801.

(58) Sun, Y.; James, B. R.; Rettig, S. J.; Orvig, C. *Inorg. Chem.* **1996**, *35*, 1667.

(59) Greaves, S. J.; Griffith, W. P. *Polyhedron* **1988**, *7*, 1973.

(60) Eaton, S. S.; Eaton, G. R.; Holm, R. H.; Muetterties, E. L. *J. Am. Chem. Soc.* **1973**, *95*, 1116.

(61) El-Hendawy, A. M.; El-Shahawi, M. S. *Polyhedron* **1989**, *8*, 2813.

(62) Fryzuk, M. D.; Jonker, M. J.; Rettig, S. J. *Chem. Commun.* **1997**, 377.

(63) Capper, G.; Carter, L. C.; Davies, D. L.; Fawcett, J.; Russell, D. R. *J. Chem. Soc., Dalton Trans.* **1996**, 1399.

(64) Wu, A.; Kennedy, D. C.; Patrick, B. O.; James, B. R. *Inorg. Chem.* **2003**, *42*, 7579.

(65) Wu, A. *Synthesis and Characterization of Ruthenium Maltolato, Sulfoxide, and Nitroimidazole Complexes as Potential Anticancer Agents* , M. Sc. Dissertation, University of British Columbia: Vancouver, 2002.

(66) Ahmet, M. T.; Frampton, C. S.; Silver, J. *J. Chem. Soc., Dalton Trans.* **1988**, 1159.

(67) Morita, H.; Hayashi, Y.; Shimomura, S.; Kawaguchi, S. *Chem. Lett.* **1975**, 339.

(68) Melchior, M.; Rettig, S. J.; Liboiron, B. D.; Thompson, K. H.; Yuen, V. G.; McNeill, J. H.; Orvig, C. *Inorg. Chem.* **2001**, *40*, 4686.

(69) Song, B.; Aebischer, N.; Orvig, C. *Inorg. Chem.* **2002**, *41*, 1357.

(70) Caravan, P.; Gelmini, L.; Glover, N.; Herring, F. G.; Li, H.; McNeill, J. H.; Rettig, S. J.; Setyawati, I. A.; Shuter, E.; Sun, Y.; Tracey, A. S.; Yuen, V. G.; Orvig, C. *J. Am. Chem. Soc.* **1995**, *117*, 12759.

(71) Burgess, J.; Parsons, S. A. *Polyhedron* **1993**, *12*, 1959.

(72) Ahmed, S. I.; Burgess, J.; Fawcett, J.; Parsons, S. A.; Russell, D. R.; Laurie, S. H. *Polyhedron* **2000**, *19*, 129.

(73) Baird, I. R. *Fluorinated Nitroimidazoles and Their Complexes: Potential Hypoxia-Imaging Agents* , Ph. D. Dissertation, University of British Columbia: Vancouver, 1999.

Chapter 2

General Experimental Procedures, and Syntheses of Ruthenium Precursor Complexes

2.1 Chemicals

2.1.1 Ligand Precursors

Imidazole (Im), 1-methylimidazole (1MeIm), 2-methylimidazole (2MeIm), 4-methylimidazole (4MeIm), metronidazole (metro), 2-nitroimidazole ($2NO_2Im$), 4-nitroimidazole ($4NO_2Im$), 3-nitro-1,2,4-triazole ($3NO_2tri$), 4-(hydroxymethyl)imidazole, imidazole-4-carboxylic acid (Im-CO_2H), pyridine-2-carboxylic acid (Hpic), 3-hydroxy-1,2-dimethyl-4-pyridone (HMepyr) and imidazole-4,5-dicarboxylic acid were purchased from Aldrich and used as received. 4,4'-Biimidazolium trifluoroacetate (H_2biim) and 2,2'-dimethyl-4,4'-biimidazolium trifluoroacetate (H_2Me_2biim) were synthesized using modified literature procedures[1] (Sections 4.8.2 - 4.8.11). 2-(2-Nitro-1-H-imidazol-1-yl)-N-(2,2,3,3,3-pentafluoropropyl) acetamide (EF5) and 2-(3-nitro-1-H-triazol-1-yl)-N-(2,2,3,3,3-pentafluoropropyl) acetamide (triF5) were synthesized using a modified literature procedure[2] (Sections 3.6.2 and 3.6.3, respectively). 3-Nitro-1,2,4-triazole-5-carboxylic acid (HCANT) was also synthesized using a modified literature procedure[3] (Section 5.6.1). 3-Hydroxy-2-methyl-4-pyrone (maltol) (Cultor Food Science) and 2-ethyl-3-hydroxy-4-pyrone (ethylmaltol) (Pfizer Food Science) were donated by Dr. C. Orvig.

2.1.2 Solvents

Reagent grade DMF, DMSO, MeCN, $CHCl_3$, and EtOAc were purchased from Fisher Scientific and used as received. Other solvents (also purchased form Fisher) were dried and distilled prior to use: EtOH (distilled from Mg), MeOH (distilled from Mg), CH_2Cl_2 (distilled from CaH_2), Et_2O (distilled from Na), hexanes (distilled from Na), THF (distilled from Na), and acetone (distilled from K_2CO_3). Deuterated solvents $CDCl_3$,

CD_2Cl_2, CD_3OD, D_2O, acetone-d_6, and dmso-d_6 were purchased form Cambridge Isotope Laboratories and used without further drying or purification.

2.1.3 Gases

N_2 (medical grade), Ar, compressed air, and H_2 (extra dry) were purchased from Praxair and used as received.

2.1.4 Biological Reagents

Materials used in the biological experiments are listed in Sections 6.2.1 and 7.2.1.

2.1.5 Other reagents

2,2,3,3,3-Pentafluoropropylamine was purchased from Interchim and Lancaster Synthesis. It was also prepared in small amounts according to a literature procedure.[4,5] Trifluoromethane sulphonic acid (triflic acid), ferrocene ($FeCp_2$), bis(pentamethylcyclopentadienyl)iron(II) ($FeCp^*_2$), tetrabutylammonium hexafluorophosphate (TBAP), potassium *tert*-butoxide, chlorotriphenylmethane (trityl chloride), N-methylmorpholine (NMM) and chloroacetyl chloride were purchased from Aldrich and used as received. $RuCl_3 \cdot 3H_2O$ was kindly donated by Colonial Metals Inc., and had a Ru composition of 39 %. All other chemicals were used as received unless otherwise stated.

2.2 Analytical Techniques and Instrumentation

2.2.1 Nuclear Magnetic Resonance Spectroscopy

1D NMR spectra were recorded on Bruker AV300 (^1H, ^{19}F, ^{13}C), Bruker AV400 (^1H, ^{13}C), Bruker ARX200 (^1H,^{19}F), Bruker ARX400 (^1H,^{19}F) and Bruker AC200F (^1H, ^{19}F, ^{13}C) spectrometers. The AC200F spectrometer was typically used for testing ligand samples as many of the complexes were paramagnetic and required a wider sweep width to record their NMR spectra, typically 150 ppm for ^1H spectra, than the AC200F could provide, and therefore their spectra were recorded on the AV300 and 400 spectrometers. All ^1H NMR and ^{19}F NMR spectra performed during my stay at the TU Berlin were

recorded on the ARX200 or ARX400 spectrometers. ^{1}H-^{1}H COSY and ^{1}H-^{13}C HMQC experiments were performed on the Bruker AV300 and AV400 spectrometers. Low temperature ^{1}H NMR spectra were all recorded on the AV300 spectrometer. The peaks are described in this thesis as observed in the spectra: s = singlet, d = doublet, t = triplet, q = quartet, br = broad, and m = multiplet. ^{1}H NMR spectra were referenced using the residual protonated solvent signals: 7.24 ($CDCl_3$), 5.32 (CD_2Cl_2), 4.65 (D_2O), 3.30 (CD_3OD), 2.49 (dmso-d_6) and 2.04 (acetone-d_6). ^{13}C NMR spectra were referenced to the ^{13}C solvent signal: 77.0 ($CDCl_3$) and 53.8 (CD_2Cl_2).

MestRe-C (Magnetic Resonance Companion, Version 1.5.0) was used to process the raw data for spectra obtained on the AC200F NMR spectrometer. For all other spectrometers, Win-NMR was used to analyze and process the spectral data.

Determination of μ_{eff} for Ru(III) paramagnetic complexes and the corresponding number of unpaired electrons for these complexes was performed using the Evans method at r.t.[6] This technique measures the shift of the residual solvent signal due to the presence of the paramagnetic complex. The signal is typically shifted downfield. The complex solution was placed inside a melting point capillary that was subsequently flame-sealed and suspended inside a standard NMR tube containing only the deuterated solvent (Figure 2.1). Typically, the complex is in the NMR tube and the pure solvent

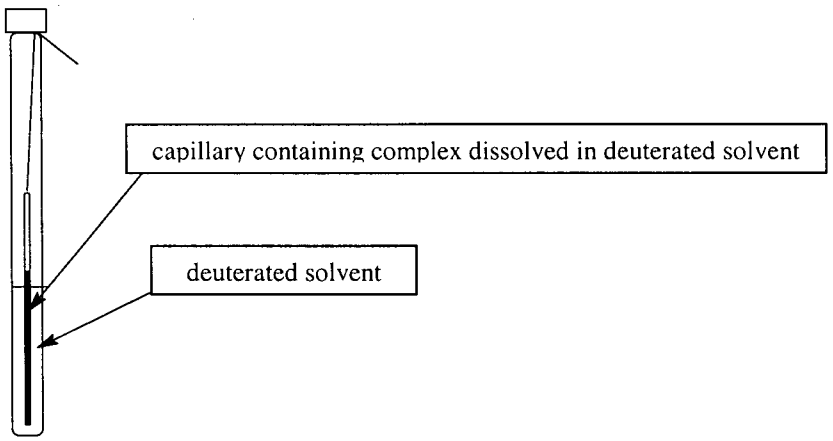

Figure 2.1 NMR set-up for performing the Evans method[6] determination of μ_{eff}. The capillary is flame-sealed after being filled with a solution of known complex concentration, and lowered into an NMR tube using Teflon tape that allows for easy retrieval of the sample.

in the capillary; however, because of limited quantities of some samples and overlapping signals in the solvent region from the complex, it was decided to place the complex solution in the capillary. Because of paramagnetic broadening of multiplet solvent signals, only solvents with sharp residual singlet signals were used for these measurements, i.e. $CDCl_3$ or CD_2Cl_2. The values for $\Delta\nu$ were determined using the AV300 spectrometer and, from these values, μ_{eff} was calculated using the following equations (Equations 2.1-2.4).[6,7] The diamagnetic correction value, χ_L, was calculated from literature values for each ligand.[8]

$$\chi_g = \frac{3\Delta\nu}{4\pi\nu_o m} + \chi_o$$

m = concentration of sample (g/mL)
$\Delta\nu$ = peak separation (Hz)
ν_o = frequency of spectrometer (Hz)
χ_o = mass susceptibility of solvent

(Eq. 2.1)

$$\chi_M = \chi_g M$$

M = compound molecular weight (g/mol)

(Eq. 2.2)

$$\chi_M' = \chi_M - \sum\chi_L$$

χ_M' = mass susceptibility of metal ion
χ_L = diamagnetic correction for ligands

(Eq. 2.3)

$$\mu_{eff} = 2.84\sqrt{\chi_M' T} = \sqrt{n(n+2)}$$

T = absolute temperature (K)
n = number of unpaired e^- on metal ion

(Eq. 2.4)

2.2.2 Infrared Spectroscopy

Infrared spectra were recorded at UBC on an ATI Matson Genesis or Bomem-Michelson MB-100 FT-IR spectrometer. At the TU Berlin, spectra were recorded by Nicolet on a Typ Magna-IR 750 spectrometer. Spectra were recorded as KBr pellets and are reported in wavenumbers ($\pm$ 4 cm^{-1}) with selected functional groups assigned based on data for similar, previously reported complexes (see, for example, Section 5.3.2),[9] and on references from standard IR textbooks.[10,11]

2.2.3 Mass Spectrometry

Mass spectral data were collected in the Mass Spectrometry laboratory at UBC under the supervision of Dr. G. Eigendorf and Dr. Y. Ling. The spectra were measured on a Kratos Concept IIHQ liquid secondary ion mass spectrometer, a Bruker Esquire electrospray (ESI ion trap) spectrometer and a Micromass LCT electrospray time of flight (ESI TOF) spectrometer. At the TU Berlin, mass spectra were collected on a Varian double focussed MS - Typ 311 A/AMD. M^+ is defined as the positive molecular ion of a given species and does not include the mass of solvated molecules or counter anions (e.g. for $[Ru(ma)_2(1MeIm)_2]CF_3SO_3 \cdot CH_2Cl_2$, $M^+ = [Ru(ma)_2(1MeIm)_2]^+$).

2.2.4 UV-Visible Spectroscopy

UV-Vis spectra were recorded on an HP 8452A diode array spectrophotometer and are reported as λ_{max} ($\pm$ 3 nm) (ε_{max} x 10^{-3}, $M^{-1}cm^{-1}$).

2.2.5 Cyclic Voltammetry

Cyclic Voltammetry was performed on selected compounds in solutions of 0.1 M TBAP in degassed MeCN under a flow of N_2. Voltammograms were recorded on a Pine Biopotentiostat, model AFCBP1, and processed using the accompanying software Pinechem v2.00. Compounds were scanned at 100 mV/s between –2 V and +2 V. The home-made cell used to perform these measurements (Figure 2.2) contained a Pt wire working electrode, a Pt wire counter electrode, and a silver wire reference electrode. $FeCp_2$ and $FeCp^*_2$ were used as internal standards ($E_{1/2}$ ($Fe^{III/II}$) = 0.40 and –0.19 V vs. SCE in MeCN, respectively).[12] The electrodes were cleaned with conc. HNO_3 before use, then rinsed with water and acetone, and dried at 100 °C. A voltammogram was then recorded with just solvent and electrolyte to ensure a flat baseline before repeating the CV measurement with the sample. The sample solution was scanned once without $FeCp_2$, then again after $FeCp_2$ had been added, this procedure being repeated to ensure values for the reduction potentials, $E_{1/2}$, were reproducible. The $E_{1/2}$ values are calculated as the average of the oxidation and reduction peaks ($E_{1/2} = (E_{p.c.} + E_{a.c.})/2$), and are reported as the average of two or more values for each compound ($\pm$ 4mV). The

reported values are calculated as follows: $E_{1/2}$(compound) in mV vs. SCE in MeCN = 400 - $E_{1/2}(FeCp_2)$ + $E_{1/2}$(observed).

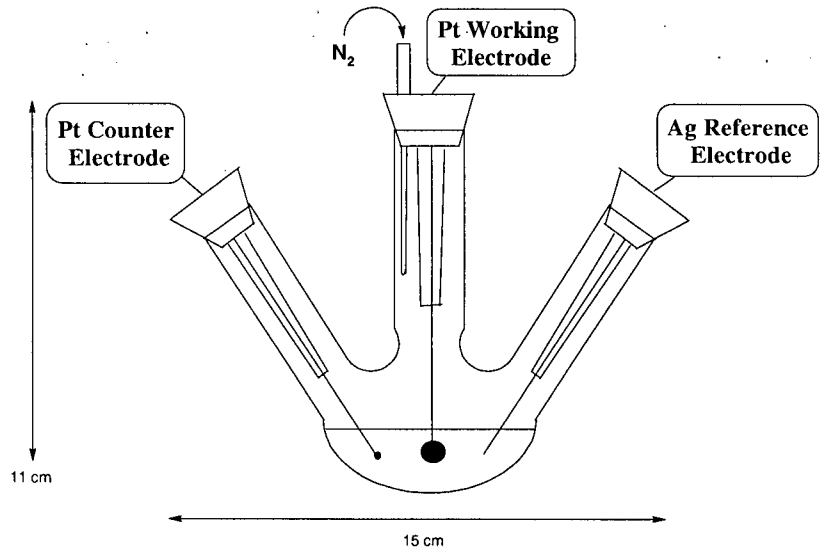

Figure 2.2 Cyclic Voltammetry cell used with Pt wire counter and working electrodes, and an Ag wire reference electrode.

2.2.6 Conductivity

Conductivity measurements were performed using a Serfass conductance bridge model RCM151B (Arthur H. Thomas Co. Ltd.) connected to a 3403 cell (Yellow Springs Instrument Co.). The cell was calibrated using a 0.0100 M KCl solution with a molar conductance (Λ_M) of 141.3 $\Omega^{-1}cm^2mol^{-1}$ at 25 °C and a cell constant of 1.016 cm^{-1} (measurement of the cell constant was performed by another group member).[13,14] Solutions to be tested were prepared at 10^{-3} M. Values in this thesis are reported as Λ_M ($\Omega^{-1}cm^2mol^{-1}$).[14]

2.2.7 X-Ray Analysis

Four X-ray crystal structures were determined by Dr. B. O. Patrick in the X-ray crystallographic laboratory at UBC on a Rigaku/ADSC CCD area detector with graphite

monochromated MoKα radiation (see Appendices 1-4). One X-ray crystal structure was determined by Dr. P. Escarpa at the TU Berlin on a Siemens Smart CCD area detector with graphite monochromated MoKα radiation (see Appendix 5).

2.2.8 Elemental Analysis

Elemental analyses were performed at UBC by Dr. P. Borda and M. Lakha on a Carlo Erba Instruments EA 1106 CHN-O elemental analyzer. Some samples were also analyzed by Mr. M. K. Yang of the SFU Chemistry Department and by Canadian Microanalytical Services Ltd.

2.2.9 Biological Analysis

Biological assays were performed in the biological services laboratory of the chemistry department at UBC under the supervision of Dr. E. Polishchuk, with the exception of the antibody binding assay which was performed at the BC Cancer Research Centre in the laboratory of Dr. K Skov. A discussion of biological techniques will be reserved for Chapters 6 and 7, at which point the techniques used will be discussed in detail along with the general experimental procedures for the biological assays.

2.3 Chromatographic Techniques

Reactions for the syntheses of both ligands and metal complexes were monitored by TLC. The reaction mixtures were typically viewed under a UV lamp (Mineralight® Lamp Model UVG-54 short-wave UV-254 nm). For imidazoles and other compounds that could not be seen under the UV lamp, the developed TLC strips were exposed to I_2 to visualize the remaining bands. Solvent combinations, including volume ratios, are listed in brackets as follows: e.g. (CH_2Cl_2:MeOH, 10:1).

Many samples were purified using column chromatography or, more commonly, preparative thin layer chromatography. For columns, silica gel (230-400 mesh, Silicycle) was added to the eluent, the mixture stirred for ~30 seconds, and then slowly poured into the glass column (plugged with glass wool just above the stopcock to prevent silica from

pouring out the bottom) to avoid forming air bubbles. The column was then eluted under a positive pressure of N_2 until the solvent level reached the top of the silica gel. The compound to be purified was then dissolved in a minimum amount of eluent and the solution then added to the top of the column with care taken not to disturb the top of the column. The solvent level was again lowered to the top of the silica gel. A layer of approximately 5 mm of silica gel was then added to the top of the column to prevent the compound from migrating back up into the solvent reservoir before the eluent was added and the column eluted.

For preparative TLC, a complex was dissolved in a minimum amount of eluent and the solution then loaded onto the TLC plate (20 cm x 20 cm x 1000 μm thick, Uniplate from Analtech). Loading consisted of slowly streaking the solution across the plate forming a line about 1 cm in height centred approximately 1 inch from the bottom of the plate, and leaving approximately 2-3 cm between the line edge and the plate edge on either side of plate. The compounds were loaded slowly to prevent broadening of the line of streaked solution, using up to 150 mg of sample on a single plate. The plates were dried in air for 30 min before being developed to prevent streaking and improve separation (Figure 2.3).

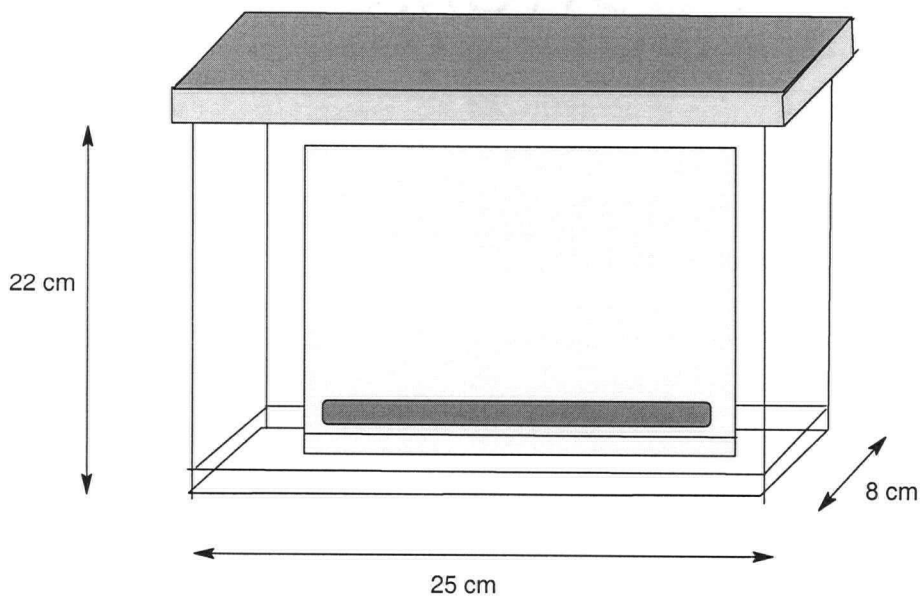

Figure 2.3 Preparative TLC chamber with silica gel plate.

2.4 Ruthenium Precursors

2.4.1 $RuCl_3 \cdot 3H_2O$

This starting material, as stated in Section 2.1.5, was generously donated by Colonial Metals Inc. The actual oxidation state of the metal is likely a mixture of Ru^{III} and Ru^{IV}.[15,16] The material comes with a certificate of authenticity stating a Ru content of 39 % which agrees with the formulation of $RuCl_3 \cdot 3H_2O$; however, the sample is highly hygroscopic and readily absorbs water if left exposed to air.

2.4.2 $[Ru(DMF)_6][CF_3SO_3]_3$

This complex was synthesized using a modified version of the procedure published by Judd *et al.*[17] A solution of $RuCl_3 \cdot 3H_2O$ (0.50 g, 1.9 mmol) in DMF (40 mL) was refluxed under a flow of H_2 for 3 h. The initially brown solution eventually became blue. To the blue solution was added $AgCF_3SO_3$ (2.20 g, 8.6 mmol), and the resulting solution was then refluxed for 1 h under 1 atm N_2. The mixture was then cooled in an ice-bath and then filtered to remove AgCl. The resulting filtrate was reduced in volume under vacuum at 80 °C to ~10 mL, when 100 mL of EtOAc was added. The resulting yellow precipitate was then collected by filtration, washed with Et_2O (3 x 5 mL), and then dried under vacuum for 24 h at 78 °C . Yield: 1.60 g (85 %). ^1H NMR (dmso-d_6): δ 22.46, 19.73 (s, CH_3). IR (KBr): 1650 (C=O). Anal. Calcd for $C_{21}H_{42}F_9N_6O_{15}S_3Ru$: C, 25.56; H, 4.26; N, 8.52. Found: C, 25.22; H, 4.24; N, 8.46. The ^1H NMR and IR data agree with those previously reported.[17,18]

2.4.3 *cis*-$RuCl_2(DMSO)_3(DMSO)$

This complex was synthesized according to the procedure of Evans *et al.*[19] A brown solution of $RuCl_3 \cdot 3H_2O$ (0.80 g, 3.1 mmol) in DMSO (10 mL) was stirred and refluxed at 180 °C for 10 min, during which time the solution became red and then yellow. The yellow solution was then cooled to r.t., and acetone (50 mL) was added with continued stirring. Over 20 min a yellow precipitate formed. The mixture was filtered

and the yellow solid washed with acetone (3 x 10 mL), and then dried under vacuum at 78 °C for 48 h. Yield: 0.92 g (62 %). ^{1}H NMR ($CDCl_3$): δ 2.70 (s, 6H, C*H*$_3$S<u>O</u>); 3.30, 3.41, 3.47, 3.50 (s, 18H, C*H*$_3$S<u>O</u>). LR-MS (+LSIMS, thioglycerol): 485 (M^+), 449 (M^+ - Cl), 371 (M^+ - Cl - DMSO). IR (KBr): 916 (<u>O</u>=S); 1096, 1120 (<u>S</u>=O). Anal. Calcd for $C_8H_{24}O_4S_4Cl_2Ru$: C, 19.83; H, 4.99. Found: C, 20.04; H, 4.96. The ^{1}H NMR and IR data are in agreement with those in the literature.[19]

2.4.4 $K_3[RuCl_6]$

This compound was synthesized from a literature procedure.[20] A solution of $RuCl_3 \cdot 3H_2O$ (1.00 g, 3.82 mmol) in MeOH (50 mL) was refluxed under a stream of H_2. After 3 h the brown solution became green. KCl (0.90 g, 12 mmol) was then added and the mixture was refluxed in air for 3 h. As the KCl dissolved, a brown precipitate formed, and this was collected by filtration and recrystalized from 12 M HCl. The product was then washed with MeOH (2 x 10 mL) and dried under vacuum for 24 h at 78 °C . Yield 1.22 g (74 %). UV-Vis (12 M HCl) 348 (3.41), 311 (3.31), 229 (4.38). The UV-Vis data agree with the literature values.[20]

2.4.5 $Ru_2(CH_3COO)_4Cl$

The complex was synthesized via a modified version of the procedure by Stephenson and Wilkinson.[21] A brown solution of $RuCl_3 \cdot 3H_2O$ (1.00 g, 3.82 mmol) in glacial acetic acid (30 mL) and acetic anhydride (5 mL) was refluxed in air for 2 h. The solution slowly developed a dark green colour and after 2 h was cooled to r.t. and filtered to remove a black precipitate. The solution was then refluxed for an additional 6 h at which time the green solution was cooled to r.t. and left standing in air for 16 h. Brown crystals were then removed from the solution by filtration, washed with cold acetic acid (2 x 5 mL, 0 °C) and Et_2O (2 x 5 mL) and then dried for 24 h at 78 °C . Yield: 0.65 g (72 %). LR-MS (+ESI): 440 (M^+ - Cl). IR (KBr): 1445, 1401 (μ-$MeCO_2^-$). Anal. Calcd for $C_8H_{12}O_8ClRu_2$: C, 20.27; H, 2.53. Found: C, 20.43; H, 2.62.

2.5 References

(1) Cliff, M.; Pyne, S. *Synthesis* **1994**, 681.

(2) Baird, I. R.; Skov, K. A.; James, B. R.; Rettig, S. J.; Koch, C. J. *Synth. Commun.* **1998**, *28*, 3701.

(3) Bagal, L. I.; Pevzner, M. S.; Frolov, A. N.; Sheludyakova, N. I. *Khim. Geterotsikl. Soedin. [English Translation]* **1970**, *2*, 240.

(4) Haszeldine, R. N. *J. Chem. Soc.* **1953**, 1548.

(5) Husted, D. R.; Ahlbrecht, A. H. *J. Am. Chem. Soc.* **1953**, *75*, 1605.

(6) Evans, D. F. *J. Chem. Soc.* **1959**, 2003.

(7) Crawford, T. H.; Swanson, J. *J. Chem. Educ.* **1971**, *48*, 382.

(8) Figgis, B. N. *Modern Coordination Chemistry*; Lewis, J., Wilkins, R. G. ed.; Interscience Publishers, Inc.: London, 1960.

(9) Sengupta, P.; Dinda, R.; Ghosh, S.; Sheldrick, W. *Polyhedron* **2001**, *20*, 3349.

(10) Nakamoto, K.; McCarthy, P. J. *Spectroscopy and Structure of Metal Chelate Compounds*; John Wiley and Sons, Inc.: New York, 1968.

(11) Pavia, D. L.; Lampman, G. M.; Kriz, G. S. *Introduction to Spectroscopy 2nd ed.*; Harcourt Brace & Company: Orlando, 1996.

(12) Connelly, N. G.; Geiger, W. E. *Chem. Rev.* **1996**, *96*, 877.

(13) Geary, W. J. *Coord. Chem. Rev.* **1971**, *7*, 81.

(14) Huheey, J. E. *Inorganic Chemistry: Principles of Structure and Reactivity, third ed.*; Harper Collins Publishers: New York, 1983.

(15) Hui, B. C.; James, B. R. *Can. J. Chem.* **1974**, *52*, 348.

(16) Seddon, E. A.; Seddon, K. R. *The Chemistry of Ruthenium*; Elsevier: Amsterdam, 1984.

(17) Judd, R. J.; Cao, R.; Biner, M.; Armbruster, T.; Buergi, H.; Merbach, A. E.; Ludi, A. *Inorg. Chem.* **1995**, *34*, 5080.

(18) Baird, I. R. *Fluorinated Nitroimidazoles and Their Complexes: Potential Hypoxia-Imaging Agents* , Ph. D. Dissertation, University of British Columbia: Vancouver, 1999.

(19) Evans, I. P.; Spencer, A.; Wilkinson, G. J. *J. Chem. Soc. Dalton Trans.* **1973**, 204.

(20) James, B. R.; McMillan, R. S. *Inorg. Nucl. Chem. Lett.* **1975**, *11*, 837.

(21) Stephenson, T. A.; Wilkinson, G. *J. Inorg. Nucl. Chem.* **1966**, *28*, 2285.

Chapter 3

Synthesis and Characterization of Ruthenium(III) Maltolato and Imidazole Complexes

3.1 Introduction

This chapter examines the synthesis and characterization of several new Ru(III) maltolato and imidazole complexes. $Ru(ma)_3$ was first synthesized by Greaves and Griffith in 1988,[1] but the ^1H NMR spectrum for this paramagnetic complex was not reported; such data are quite useful in determining structural information about this complex and its derivatives. The ^1H NMR spectra of paramagnetic complexes can exhibit chemical shifts far removed from the "expected" diamagnetic ones.[2] Paramagnetic shifts can range from a few Hz to > 100 ppm, and the signals are often broad and of relatively low intensity. Their appearance varies greatly depending on the geometry and nature of the ligands present.[3,4] For these reasons, ^1H NMR spectra of paramagnetic complexes can be difficult to interpret. In this Chapter, the 1D ^1H NMR and 2D ^1H-^1H COSY and ^1H-^{13}C HMQC spectra of some Ru(III) complexes are examined in order to elucidate structural information of the species in solution.

Anderson and Beauchamp have studied the paramagnetic ^1H NMR spectra of Ru(III) complexes of imidazole and methyl-imidazoles,[5-7] where 2-deuteroimidazole was used to make spectral assignments.[8] A general trend was observed in the shift of the imidazole protons with H(5) < H(4) < H(2), the H(2) signal being shifted the farthest upfield. As will be discussed in Section 3.3, methyl signals on both maltolato and imidazole ligands shift downfield, while imidazole proton signals shift upfield.

Eaton *et al.* have performed in depth studies of paramagnetic tropolonato species,[9] and the ^1H NMR data for $Ru(tropolonato)_3$ have been used in assigning the maltolato and ethylmaltolato spectra presented in Section 3.2. In this thesis work, no distinct pattern has been observed for the chemical shifts of the maltolato ring protons; in fact, these proton signals are generally not observed in the spectra of the mixed maltolato imidazole complexes.

In addition to maltolato complexes with ancillary imidazole and nitroimidazole ligands, this work was expanded to investigate 3-nitro-1,2,4-triazoles (Figure 3.1) as well because nitrotriazoles, like nitroimidazoles, can be effective radiosensitizers.[10] A triazole analogue of EF5 was synthesized and will be discussed in more detail in Section 3.3 and Chapter 7.

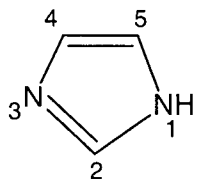

Imidazole

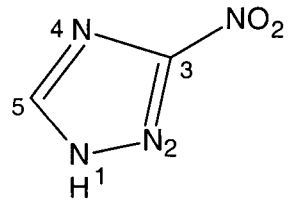

3-Nitro-1,2,4-triazole

Figure 3.1 Numbered molecular structures of imidazole and 3-nitro-1,2,4-triazole.

3.2 Investigation of $Ru(ma)_3$ and $Ru(Ema)_3$

3.2.1 Characterization and Solution NMR Data for $Ru(ma)_3$ (1)

The synthesis of $Ru(ma)_3$ (Figure 3.2) has been previously reported[1] but, in this thesis work, its purification was modified to remove impurities (observed by TLC), thus improving the elemental analysis from that reported (Section 3.6.1). The IR data agreed with those reported[1] and the mass spectrum showed the parent peak at 477. The

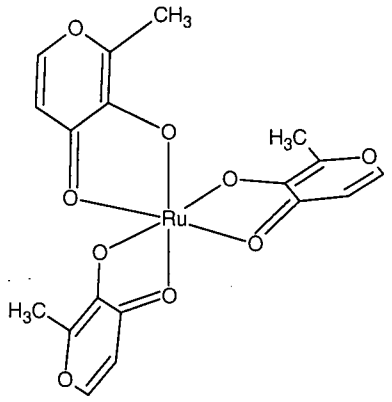

Figure 3.2 Molecular structure of *mer*-$Ru(ma)_3$ (**1**).

conductivity of an aqueous solution of **1** was 25 $\Omega^{-1}cm^2mol^{-1}$, at the upper limit for a non-electrolyte,[11] suggesting that a small amount of the maltolato ligand may be dissociating in solution. The structure of the red complex was determined in this department by X-ray crystallography (Figure 3.3), but disorder in the crystal (grown from slow evaporation of a CH_2Cl_2:acetone, 1:1 solution) prevented full refinement of the structure (see Appendix A1 for structure details). Nevertheless, the complex crystallizes in the mer-configuration, and the solution ^1H NMR spectrum at r.t. in CD_2Cl_2 also shows the mer-configuration as the primary isomer.

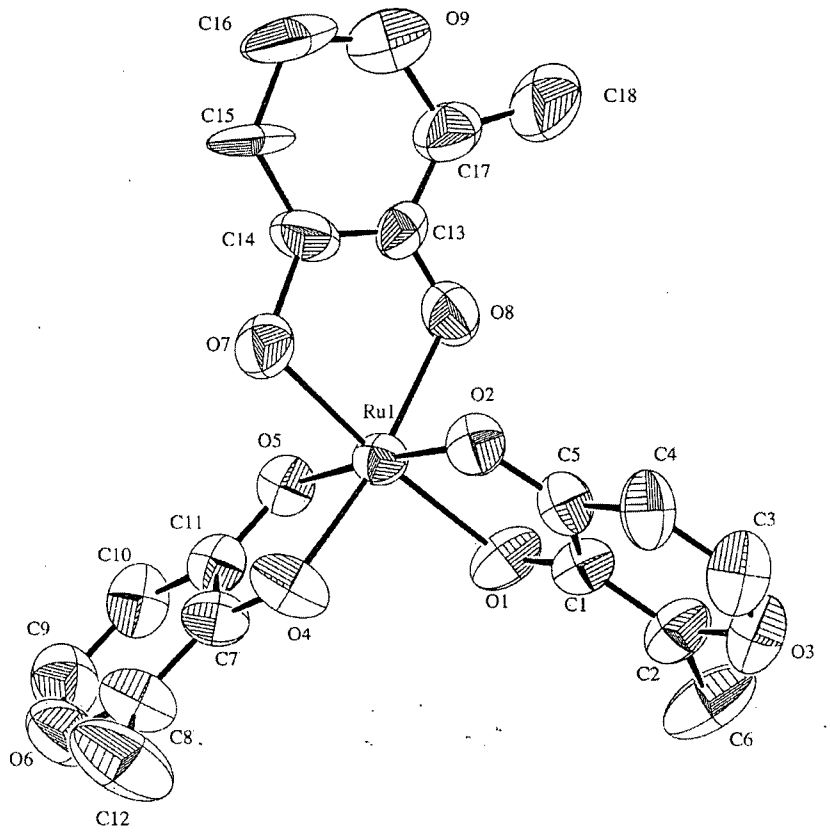

Figure 3.3 ORTEP diagram of *mer*-Ru(ma)$_3$ (**1**) with 33 % probability thermal ellipsoids (see Appendix A1 for details).

The ^{1}H NMR spectrum (Figure 3.4) clearly shows nine singlets assigned to *mer*-**1** and an additional 3 trace singlets that are assigned to the fac-isomer (δ 33.8, 1.6, 1.0). ^{1}H NMR was performed in $CDCl_3$, CD_2Cl_2, CD_3OD, D_2O and acetone-d_6 and in each case the mer-isomer was observed. The three resonances assigned to the fac-isomer are only observed in $CDCl_3$ and CD_2Cl_2 in which **1** is more soluble, and varied proportionally in intensity between different samples, giving further evidence that their assignment to a single species is correct.

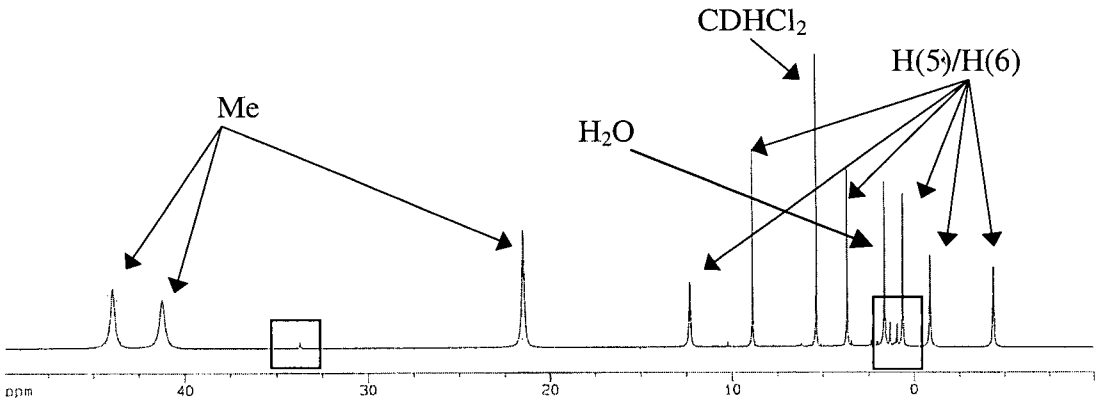

Figure 3.4 ^{1}H NMR spectrum (300 MHz, 298 K) of Ru(ma)$_3$ (**1**) in CD_2Cl_2. Resonances for the mer-isomer have been labelled and those for the fac-isomer have been identified with boxes.

The signals shifted the farthest downfield, δ 43.2, 41.0 and 21.1, are for the Me groups on the maltolato ring, and this was confirmed by the ^{1}H-^{1}H COSY spectrum (Figure 3.5); these 3 signals showed no crosspeaks as expected for the Me groups, while the remaining 6 resonances each showed a mutual correlation to one of the other resonances, giving 3 pairs of singlets (δ 11.8 and 9.2, 3.1 and –4.6, 0.8 and –0.9), one pair for the H(5) and H(6) protons for each maltolato ring. The resonances assigned to the solvent, $CDHCl_2$, and to H_2O also gave no crosspeaks, suggesting that these assignments are correct.

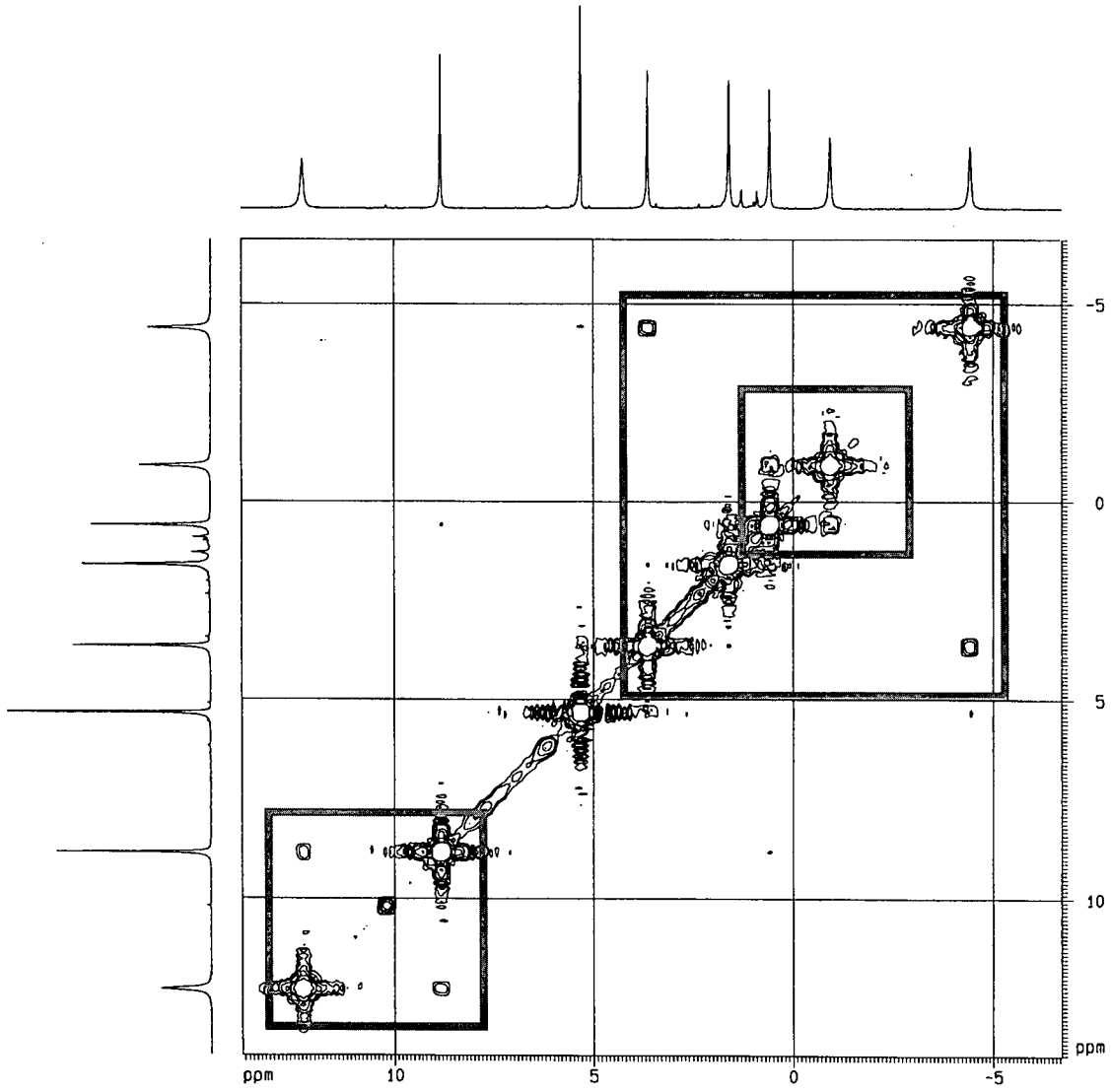

Figure 3.5 ^{1}H-^{1}H COSY spectrum (300 MHz, 298 K) of $Ru(ma)_3$ (**1**) in CD_2Cl_2. The signals downfield of δ 20 are omitted as they showed no crosspeaks. The coupled pairs for H(5) and H(6) are highlighted with boxes.

The ^{1}H-^{13}C HMQC spectrum (Figure 3.6) provides further evidence for the ^{1}H assignments, as the 6 maltolato ring proton signals each give a crosspeak between δ 75 and 175 in the ^{13}C NMR spectrum as expected for protons on an sp^2-hybridized carbon.[12] Two crosspeaks for the Me groups are also observed, that for the ^{1}H signal at δ 21.1, giving a ^{13}C crosspeak at δ –7, the other for the trace fac-signal at δ 33.8 giving rise

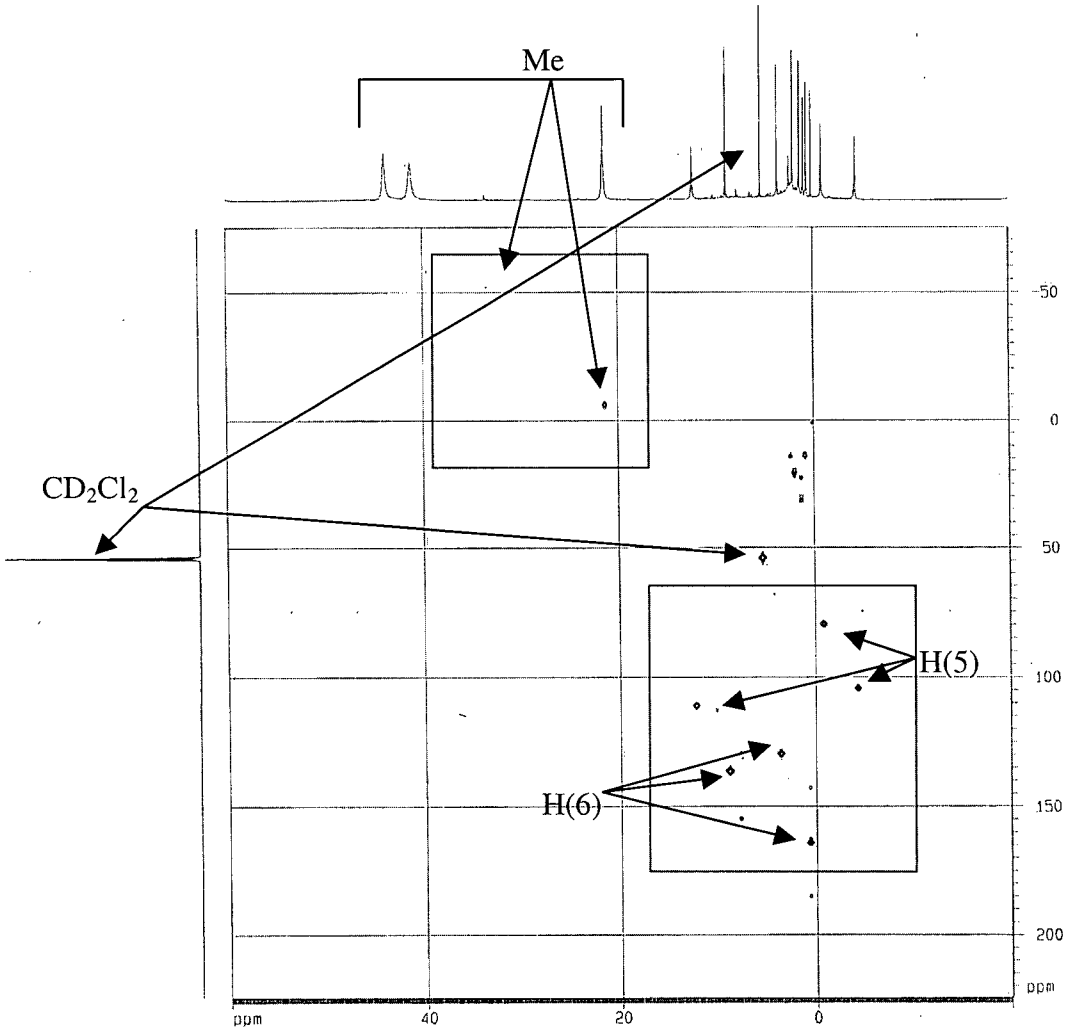

Figure 3.6 ^{1}H-^{13}C HMQC spectrum (300 MHz, 298 K) of Ru(ma)$_3$ (**1**) in CD_2Cl_2 with the ^{13}C spectrum on the left-hand side and the ^{1}H spectrum at the top. Some decomposition occurred in this sample leading to additional crosspeaks. The H(5) and H(6) protons, the solvent and two Me groups, which all show crosspeaks, are indicated with arrows.

to a ^{13}C crosspeak at δ –52. Crosspeaks for the remaining two Me groups (δ 41.0 and 43.2) may be shifted too far upfield in the ^{13}C NMR spectrum, beyond δ –75, to be detected. Additional signals in the ^{1}H NMR spectrum between δ 0-5 result from slow decomposition of the sample *in situ* as the acquisition of the HMQC spectrum takes several hours. Although the decomposition products may be present in very small amounts, they can still give rise to relatively intense signals compared to those observed

for the paramagnetic complex. ^{13}C signals for these decomposition products are also not observed, but crosspeaks are seen between δ 0-40 with the ^{13}C NMR spectrum. Only a signal (δ 54) for CD_2Cl_2 is observed in the ^{13}C NMR spectrum after 12 h; however, a partial spectrum can be generated from the crosspeaks of the ^{1}H-^{13}C HMQC experiment, producing a spectrum that contains signals for those C-atoms that show correlation with signals in the ^{1}H NMR spectrum (Figure 3.7).

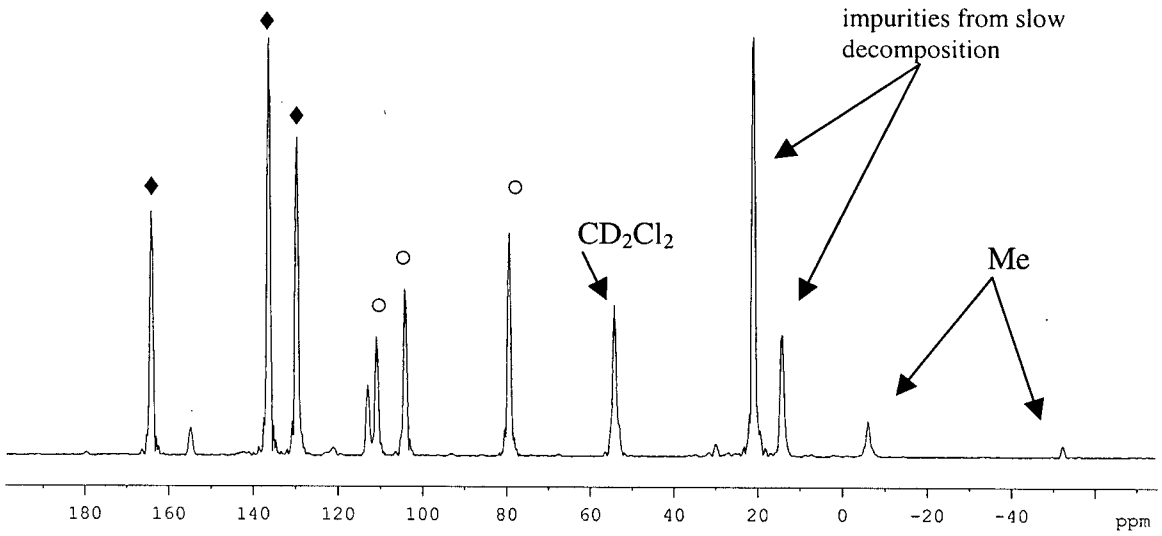

Figure 3.7 Partial ^{13}C NMR spectrum of **1** (300 MHz, 298 K) in CD_2Cl_2 generated as a positive projection of the y-axis from the ^{1}H-^{13}C HMQC spectrum of **1**. Only carbons that gave rise to crosspeaks in the 2D spectrum are observed (○ denotes carbons attached to H(6) protons and ♦ denote those attached to H(5) protons).

The ^{1}H NMR spectrum of $Ru(ma)_3$ was also recorded at lower temperatures (Table 3.1). These shifts can be plotted vs 1/T (Figures 3.8 and 3.9) and the intercept at 1/T = 0 should give the value expected for a corresponding diamagnetic species.[13] From the intercepts of Figure 3.7, it can be determined which of the six signals correspond to H(5) and H(6), because for free maltol, H(5) is observed at δ 6.4 and H(6) at δ 7.7. For each pair of singlets observed in the ^{1}H-^{1}H COSY spectrum of **1**, one can be assigned as H(5) and the other as H(6). H(a) and H(b) show correlation in Figure 3.5, and in Figure 3.8 give X-intercepts at δ 5.2 and 8.2, respectively; from these values, H(a) can be

assigned as an H(5) proton, and H(b) as an H(6) proton. Similarly, H(c) and H(d) can be assigned as H(6) protons, and H(e) and H(f) can be assigned as H(5) protons. The X-intercepts for the Me groups in Figure 3.9 (δ 14.3, 10.0 and 9.0) do not correlate well with the Me signal of free maltol (δ 2.4).

The ^{1}H NMR shift data were also used to determine μ_{eff} (1.52 BM at 22 °C) using Evan's method.[14]

Table 3.1 Variable temperature chemical shifts of $Ru(ma)_3$ (300 MHz) in CD_2Cl_2 including values at T = ∞, as determined by linear regression.

Temp (K)	δ Me1	δ Me2	δ Me3	δ H(a)	δ H(b)	δ H(c)	δ H(d)	δ H(e)	δ H(f)
∞	9.0	10.0	14.3	5.2	8.2	9.0	9.0	7.5	6.7
280	45.969	43.039	22.061	12.659	8.869	3.264	0.092	-1.368	-5.022
267	47.520	44.149	22.391	12.955	8.889	3.013	-0.327	-1.715	-5.488
256	49.163	45.936	22.807	13.269	8.932	2.722	-0.756	-2.080	-5.992
244	50.968	47.609	23.261	13.626	8.965	2.392	-1.223	-2.485	-6.546
233	52.986	49.384	23.719	14.023	9.002	2.044	-1.724	-2.930	-7.146
221	55.162	51.482	24.232	14.468	9.043	1.647	-2.312	-3.441	-7.837
212	57.6234	53.680	24.806	14.976	9.089	1.217	-2.953	-3.992	-8.574
200	60.351	56.057	25.379	15.521	9.134	0.702	-3.655	-4.632	-9.392

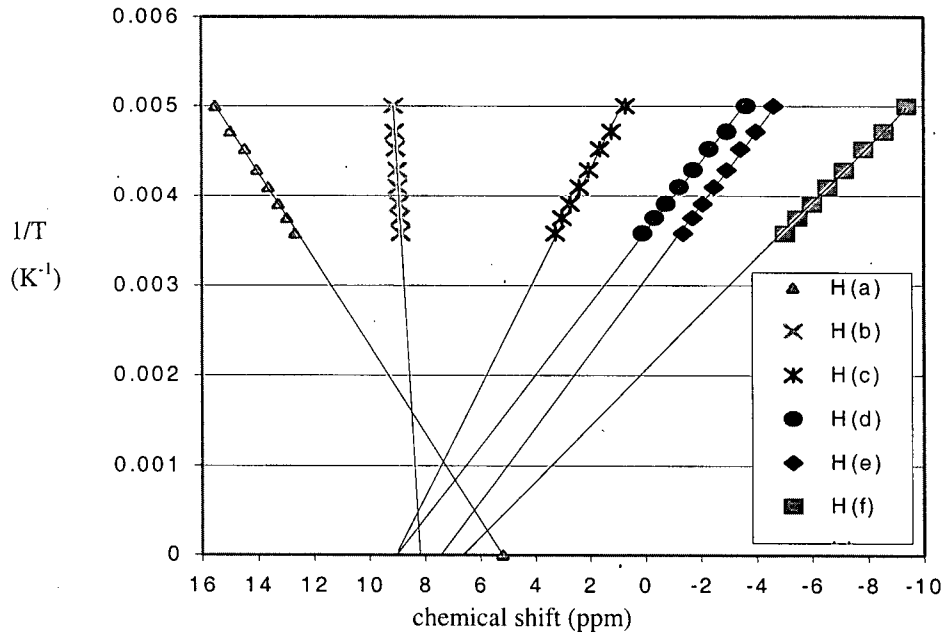

Figure 3.8 Plot of the chemical shift (ppm) vs. 1/T (K^{-1}) for the H(5) and H(6) protons on each ma ring of $Ru(ma)_3$ (**1**), here labelled H(a)-(f).

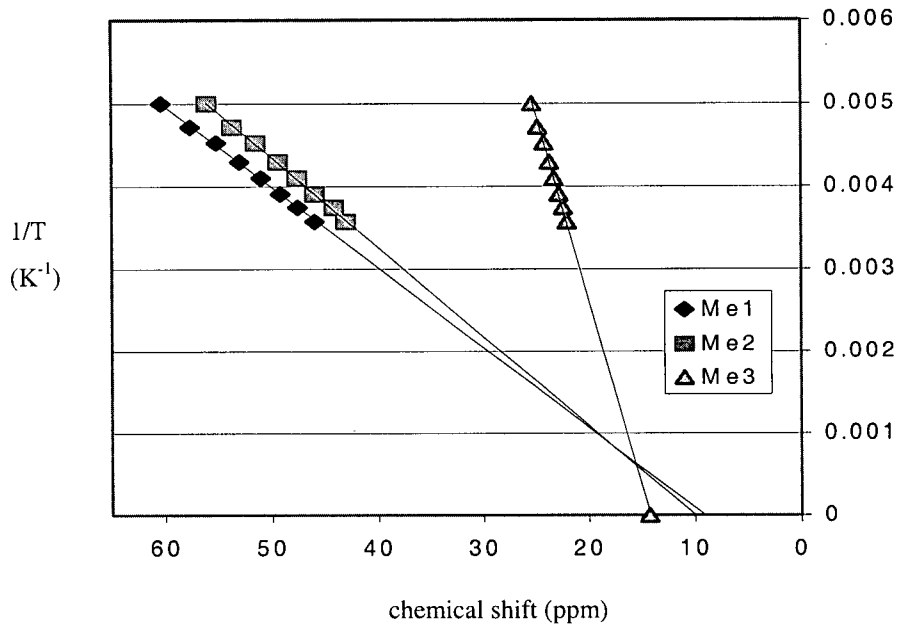

Figure 3.9 Plot of the chemical shift (ppm) vs. 1/T (K^{-1}) for the Me groups of $Ru(ma)_3$ (**1**).

3.2.2 Characterization and Solution NMR Data for $Ru(Ema)_3$ (2)

The general synthesis for $Ru(Ema)_3$ (**2**) is the same as for **1**, and **2** has also been characterized by elemental analysis, MS and IR spectroscopy. The 1D and 2D NMR spectra for **2** are more complicated than those for **1** because of the presence of an Et vs. Me group. $Ru(Ema)_3$ also exists predominantly as the mer-isomer in solution based on comparison with the ^1H NMR spectrum for **1**. The r.t. ^1H NMR spectrum for **2** (Figure 3.10) in CD_2Cl_2 shows 6 resonances of roughly equal intensity shifted downfield past δ 15, as opposed to the 3 seen in the ^1H NMR spectrum of **1** (Figure 3.4), and there are now two trace signals observed for the fac-isomer in the downfield region as opposed to the one seen for $Ru(ma)_3$. The three resonances for the Me, H(5) and H(6) protons for the fac-isomer of **2** are not observed, and presumably overlap with signals for the mer-isomer. The 6 major downfield signals are assigned to the 6 inequivalent protons of the three CH_2 groups.

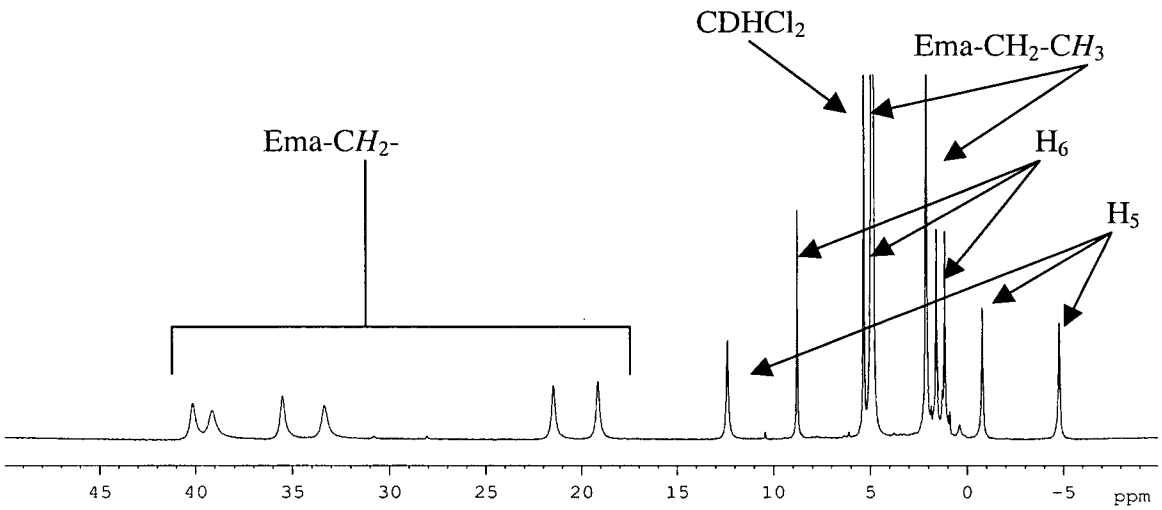

Figure 3.10 ^{1}H NMR spectrum of Ru(Ema)$_3$ (**2**) (300 MHz, 298 K) in CD_2Cl_2.

The resonances for the CH_3 of the Et groups are also shifted downfield (δ 4.9, 4.8, and 2.1 for **2** vs. δ 1.22 for free ethylmaltol in CD_2Cl_2), but by a considerably less amount than are the CH_2 signals. The Me signals are distinguished from those of the maltolato ring protons and from the residual solvent signal using 2D NMR spectroscopy. The ^{1}H-^{1}H COSY spectrum clearly shows that there are again 3 pairs of singlets for the maltolato ring protons (δ 12.5 with 9.0, 4.9 with -4.9, and 1.2 with -0.8) (Figure 3.11). The spectrum also shows pairs of signals for the CH_2 groups (those signals shifted downfield of δ 15) correlating with signals for the corresponding Me groups for each Ema ligand (δ 40.1 and 35.3 with δ 2.1, δ 38.8 and 33.4 with δ 4.9, and δ 21.7 and 18.9 with δ 4.8). The ^{1}H-^{1}H COSY spectrum also shows correlation between the two CH_2 protons, but only for the signals at δ 21.7 and 18.9. Although the resonances at δ 40.1 and 35.3 do not give rise to mutual crosspeaks, they can be still be assigned to one CH_2 group as they correlate with the same Me group (δ 2.1). The same holds true for the CH_2 resonances at δ 38.8 and 33.4 that give a crosspeak with the same Me resonance (δ 4.9).

As in the ^{13}C NMR spectrum of **1**, that of **2** shows no signals for the complex, only a single resonance for CD_2Cl_2 (δ 54). The ^{1}H-^{13}C HMQC spectrum, however,

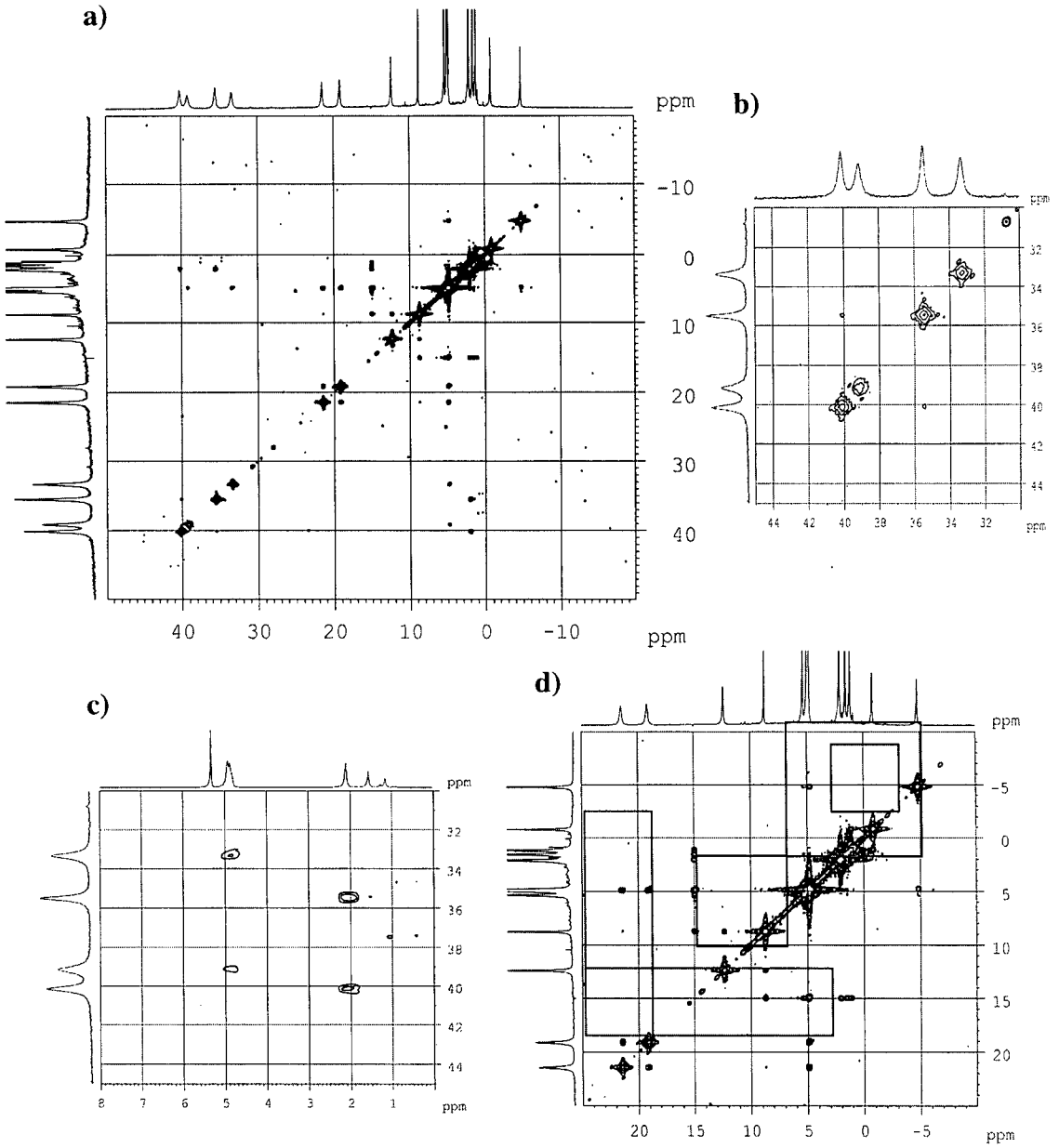

Figure 3.11 ^{1}H-^{1}H COSY spectrum of **2** (300 MHz, 298 K) in CD_2Cl_2. a) Complete spectrum. b) Expansion showing correlation between CH_2 protons shifted downfield for 2 of the ligands. c) Expansion showing correlation between CH_2 and Me protons for the same two CH_2 groups shown in (b). d) Expansion showing H(5) and H(6) correlations for all 3 ligands (blue boxes) as well as the CH_2/Me and CH_2 /CH_2 correlations for the third ligand not observed in (b) or (c) (purple boxes).

shows crosspeaks for many of the ^{1}H signals with the ^{13}C NMR spectrum of **2** (Figure 3.12). In particular, there are 6 signals observed between δ 75 and 175 for the H(5) and H(6) protons on the maltolato ring, as for $Ru(ma)_3$. No crosspeaks are observed for either the CH_2 or CH_3 of the ethyl groups. The partial ^{13}C NMR spectrum, as for **1**, can be generated for **2** from the HMQC spectrum.

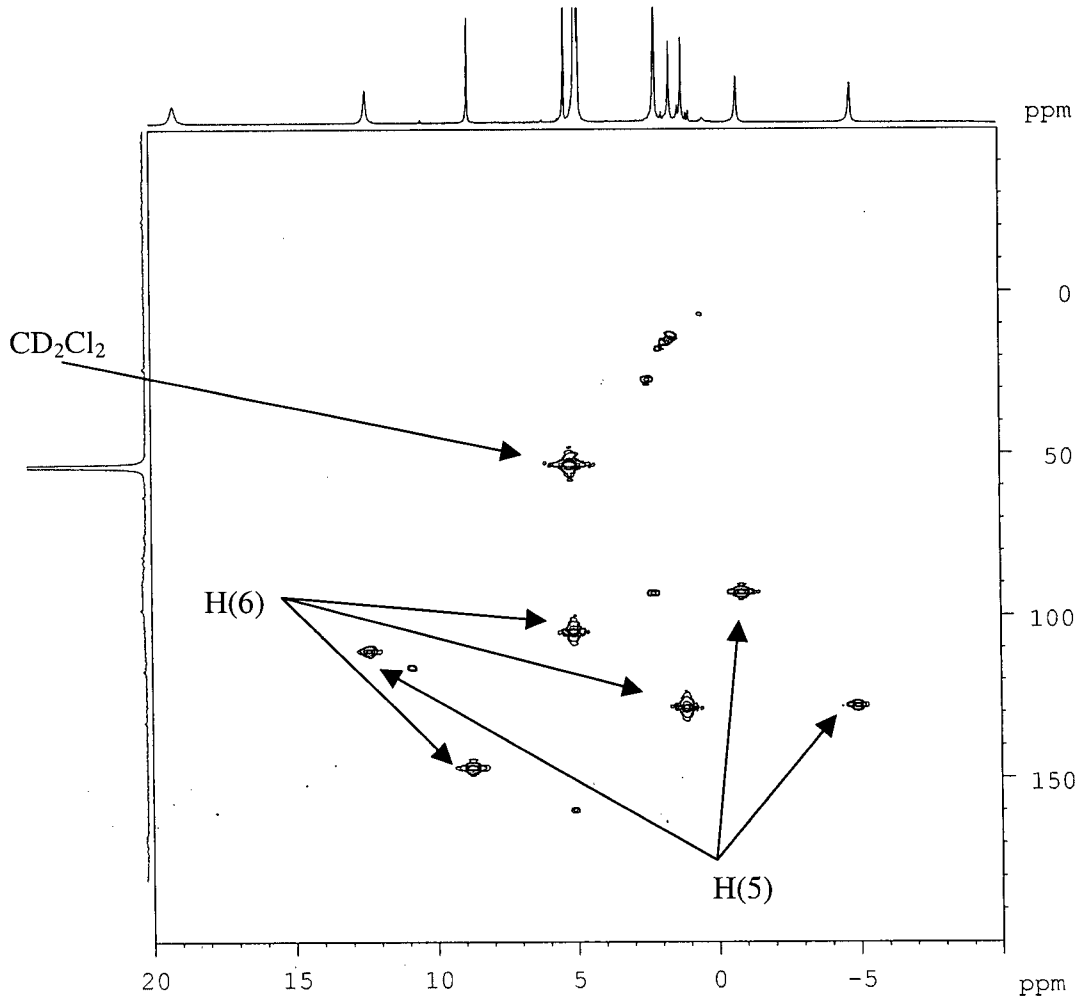

Figure 3.12 ^{1}H-^{13}C HMQC spectrum (300 MHz, 298 K) of $Ru(Ema)_3$ (**2**) in CD_2Cl_2 with the ^{13}C spectrum on the left-hand side and the ^{1}H spectrum at the top. Some decomposition occurred in this sample leading to additional crosspeaks. The H(5) and H(6) protons are indicated with arrows, as is the solvent. The ^{1}H NMR resonances downfield of δ 20 have been omitted as no crosspeaks were observed in this region of the spectrum.

3.2.3 "Activation" of $Ru(ma)_3$ with CF_3SO_3H – Synthesis of $[Ru(ma)_2(EtOH)_2]CF_3SO_3$ (3)

The reaction of $Ru(ma)_3$ (**1**) with triflic acid under N_2 was monitored in CD_3OD (Figure 3.13). The CD_3OD was degassed for one minute with N_2 in an NMR tube, to which was added 10 mg of **1**. The ^1H NMR spectrum of the sample was recorded (Figure 3.12a), then the NMR tube was removed from the spectrometer and 1 equivalent of CF_3SO_3H was added to the solution of **1**, still under N_2. This mixture was shaken vigorously for 2 min, and the spectrum of the mixture was then recorded (Figure 3.13b). The total time lapse between adding the triflic acid and recording the spectrum was 10 min. The sample was then left sitting at r.t. for an additional 50 min before recording the ^1H NMR spectrum of the solution mixture again (Figure 3.13c). In this reaction, loss of the signals for **1** was accompanied with generation of signals for a new Ru(III) complex, as well as signals for free maltol [δ 2.4 (s, Me), 6.4 (d, H(5)), and 7.7 (d, H(6))]. There is only one Ru(III) ma containing species present in solution after 1 h as evidenced by the single broad resonance at δ 45, likely for *trans*-$[Ru(ma)_2(CD_3OD)_2]CF_3SO_3$ (see below).

When **1** was treated with triflic acid in EtOH in a synthetic reaction, the initially red solution darkened and, after 1 h, TLC analysis revealed that **1** had been quantitatively converted to a new product. The volume of this solution was then reduced and the complex precipitated from the solution on addition of Et_2O. This complex has been characterized by elemental analysis, MS, IR and ^1H NMR spectroscopies as $[Ru(ma)_2(EtOH)_2]CF_3SO_3$ (**3**). The parent peak is found in the mass spectrum as are peaks for the subsequent fragmentation loss of one and two EtOH ligands. The IR spectrum shows strong bands for the C=O of ma and for O-H of EtOH. The conductivity of an EtOH solution of **3** (36 $\Omega^{-1}cm^2mol^{-1}$) was in the range for a 1:1 electrolyte.[15]

When **3** is dissolved in CD_3OD, the immediate ^1H NMR spectrum shows a single species (as evidenced by a single resonance for the ma-Me group); this then decomposes over 15 min to yield a spectrum for a complex identical to that formed from the *in situ* reaction (Figure 3.13c), with the exception that the free maltol signals are now absent and free EtOH signals are now present. The presence of only one Me signal for the maltolato ligand is consistent with a trans-isomer as observed with all the structurally characterized, Im-ma complexes described in the next section.

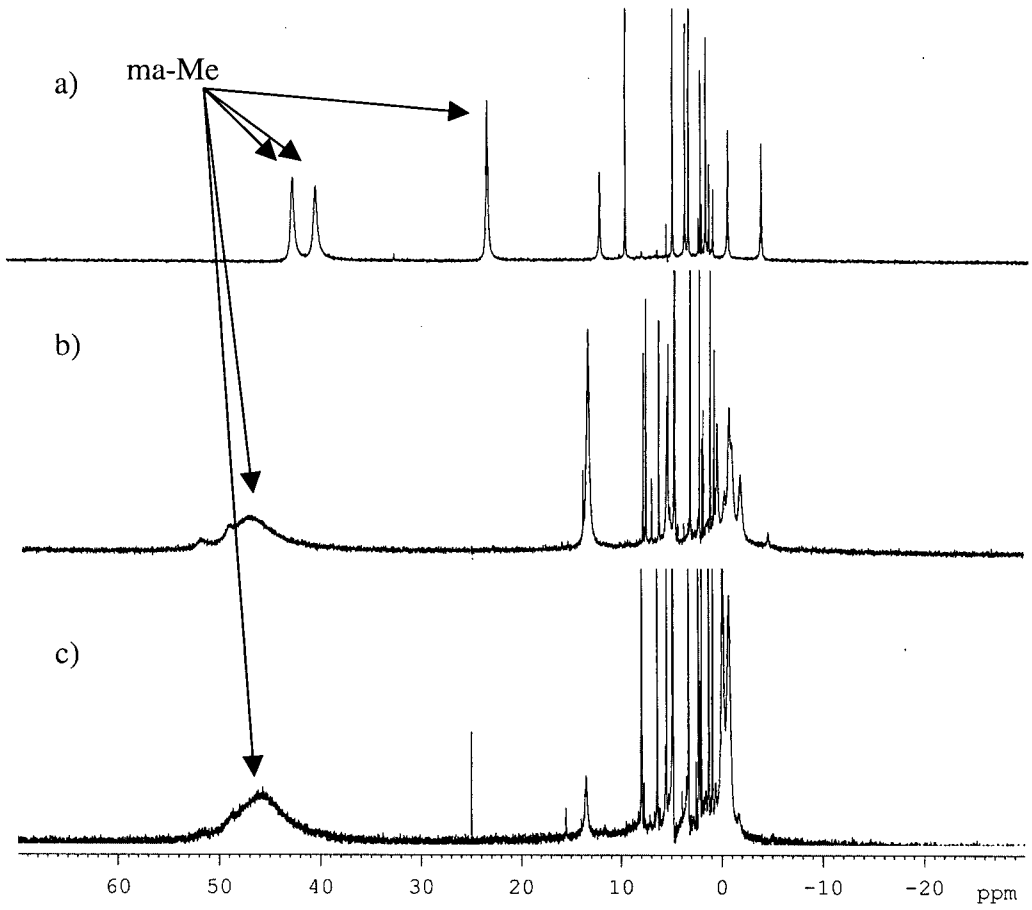

Figure 3.13 *In situ* formation of $[Ru(ma)_2(CD_3OD)_2]CF_3SO_3$ as shown by ^1H NMR spectroscopy, the broad downfield signal being characteristic of a trans-geometry for the maltolato ligands (see text). a) $Ru(ma)_3$ in CD_3OD b) $Ru(ma)_3$ in CD_3OD + CF_3COOH after ~10 min c) $Ru(ma)_3$ in CD_3OD + CF_3COOH after ~1 h.

3.3 Reactions of $Ru(ma)_3$ (1) and $Ru(Ema)_3$ (2) with Imidazoles and Triazoles

3.3.1 Synthesis and Characterization of Imidazole and Triazole Complexes

Complexes of the form $[Ru(ma)_2(L)_2]CF_3SO_3$ discussed in this section can be divided into two groups, those without nitro groups: L = 4MeIm (**6**), Im (**7**), 1MeIm (**8**), 2MeIm (**10**); and those with nitro groups: L = metro (**4**), EF5 (**14**), $2NO_2$Im (**15**), $4NO_2$Im (**16**), $3NO_2$tri (**17**) and triF5 (**18**). Two additional complexes, $[Ru(ma)(1MeIm)_4][CF_3SO_3]_2$ (**9**) and $[Ru(ma)_2(metro)(EtOH)]CF_3SO_3$ (**5**) were also isolated. These complexes have been characterized generally by elemental analysis, mass spectrometry, and NMR and IR spectroscopies. The complexes **15-18** were insoluble in all matrices for LSIMS, and lacked sufficient solubility in applicable solvents to examine them by ESI-MS. Solid state MS techniques were not available in the department MS facility. Complexes **6**, **7**, **8**, and **10** (Figure 3.14) were synthesized by reacting **1** with one equivalent of triflic acid in EtOH at r.t., and then adding excess of the imidazole to the reaction mixture. All four complexes were purified using preparative TLC and isolated as red solids. MeOH solutions of each gave conductivity values in the range for 1:1 electrolytes.[15] The elemental analyses for **6** and **8** indicate the presence of one CH_2Cl_2 solvate, and in the case of **8**, the solvated CH_2Cl_2 was detected by X-ray crystallography (Figure 3.16, Appendix A2).

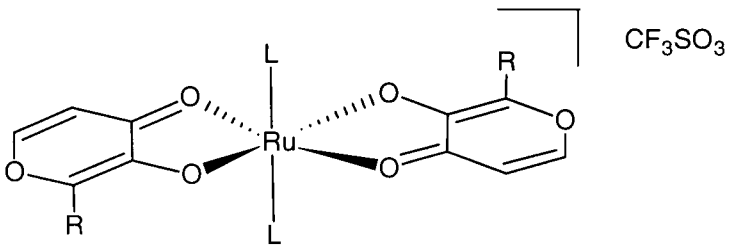

L = metro (**4**), 4MeIm (**6**), Im (**7**), 1MeIm (**8**), and 2MeIm (**10**).

Figure 3.14 Molecular structures for the trans-isomers of **4**, **6** – **8** and **10**.

The reaction between **1,** CF_3SO_3H and 4 equivalents of 1MeIm in refluxing EtOH was followed by TLC. A blue species that increased in intensity over time became the major product after 48 h, and was isolated by preparative TLC (18 % yield) and formulated as **9** (Figure 3.15). The reaction was repeated adding an 8-fold excess of 1MeIm and two equivalents of CF_3SO_3H instead of one; the percent yield of **9** after 48 h increased to 51 %. The conductivity of a MeOH solution of **9** (273 $\Omega^{-1}cm^2mol^{-1}$) is in the range for a 2:1 electrolyte.[15]

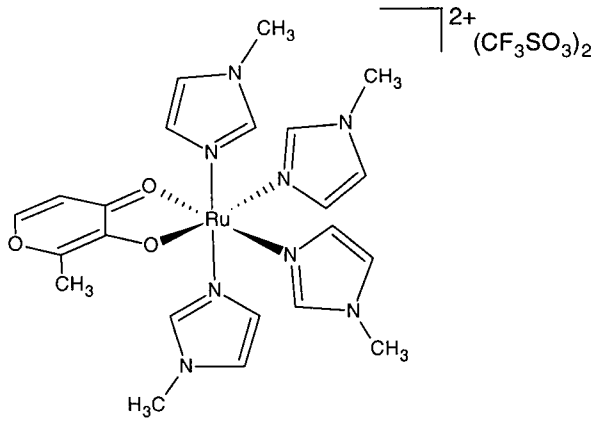

Figure 3.15 Molecular structure of $[Ru(ma)(1MeIm)_4][CF_3SO_3]_2$ (**9**).

4 (Figure 3.14) was synthesized by the same procedure as for **6**, **7**, **8**, and **10**, but with refluxing the reaction mixture for 6 h; the product then precipitated when the solution was cooled. Work-up of the filtrate led to the isolation of a second, green product in low yield, **5**. Elemental analysis and MS confirmed the formulations of **4** and **5**. **4** was then subsequently crystallized by another member of our group, and the X-ray structure determined that it was of a trans-configuration.[16]

Complexes **8** and **10** have also been characterized by X-ray crystallography (Figures 3.16 and 3.17, respectively), and all three structures show trans-imidazole ligands and a centre of inversion at the Ru.

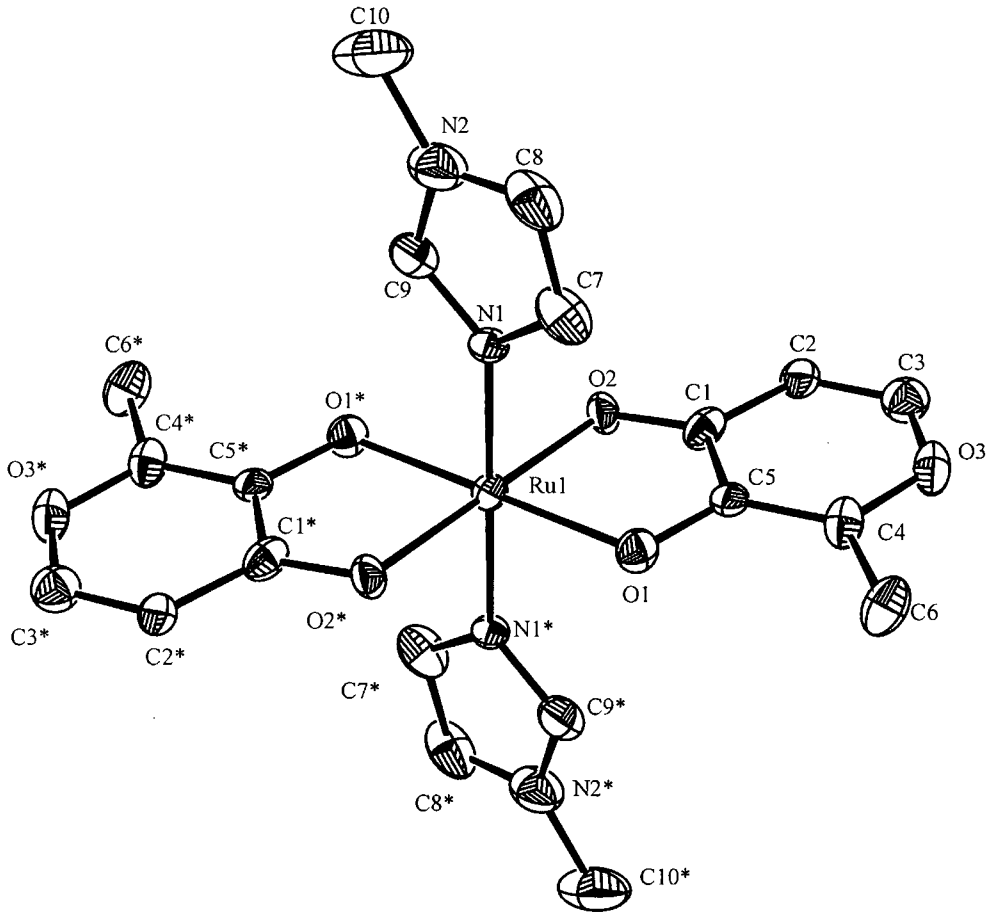

Figure 3.16 ORTEP diagram of the cation of *trans*-$[Ru(ma)_2(1MeIm)_2]CF_3SO_3 \cdot CH_2Cl_2$ (**8**) with 50 % probability thermal ellipsoids (see Appendix A2 for details).

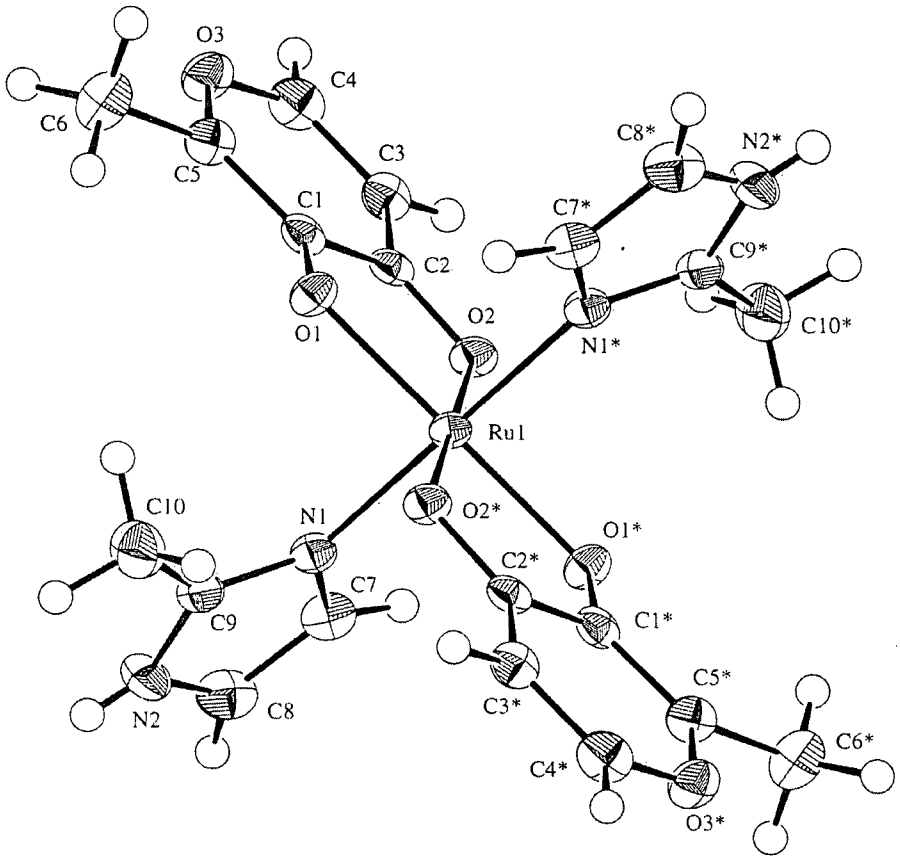

Figure 3.17 ORTEP diagram of the cation of *trans*-$[Ru(ma)_2(2MeIm)_2]CF_3SO_3$ (**10**) with 50 % probability thermal ellipsoids (see Appendix A3 for details).

The Ru-N bond lengths for **10** might be expected to be longer than those for **8** as the 2-Me group could give rise to steric interactions with the ma ligands: in **8**, a 1-Me derivative, the imidazole Me groups point away from the ma ligands and in **10** they point towards the ma ligands. However, there are no differences in the Ru-N bond lengths. Instead, the imidazole rings in **10** tilt to move the Me group away from the plane of the maltolato ligands (Figure 3.18). This can be seen by looking at the Ru-N(3)-C(2) and Ru-N(3)-C(4) angles (see Figure 3.19 for the atomic numbering scheme) in the structures of **8** and **10**. For **8**, these angles differ by less than one degree (Table 3.2), while for **10** these angles differ by 6.2 degrees.

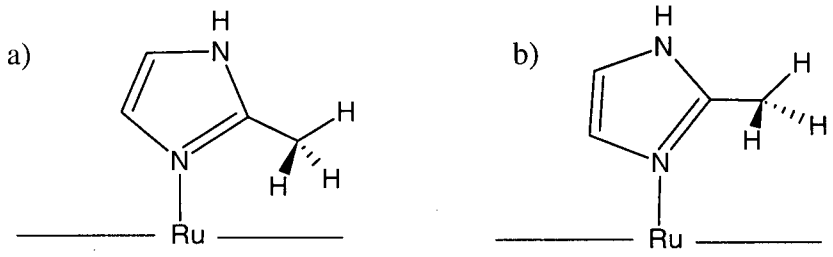

Figure 3.18 Diagram depicting the potential steric interaction between an Im-Me group and the ma plane for **10**. a) Steric interaction when coordinated symmetrically about N(3). b) Shows how tilting at the coordinated nitrogen removes this steric interaction by increasing the Ru-N(3)-C(2) bond angle and decreasing the Ru-N(3)-C(4) bond angle.

Table 3.2 Selected X-ray data from bis-imidazole derivative structures. The numbering used is shown in Figure 3.16.[a]

Complex	Ru-N(3) bond length	Ru-O(1) bond length	Ru-O(2) bond length	Ru-N(3)-C(2) bond angle	Ru-N(3)-C(4) bond angle
trans-[Ru(ma)$_2$(1MeIm)$_2$]CF_3SO_3 (**8**)	2.072(5)	2.012(4)	2.065(4)	126.7(4)	127.6(4)
trans-[Ru(ma)$_2$(2MeIm)$_2$]CF_3SO_3 (**10**)	2.078(2)	2.006(2)	2.061(2)	129.7(2)	123.5(2)
trans-[Ru(Ema)$_2$(metro)$_2$]CF_3SO_3 (**11**)	2.080(3)	1.998(3)	2.051(3)	130.6(3)	122.0(3)
trans-[Ru(ma)$_2$(metro)$_2$]CF_3SO_3 (**4**)	2.069(3)	2.010(3)	2.063(3)	130.1(3)	122.8(3)

a – the data for **4** are taken from reference 15.

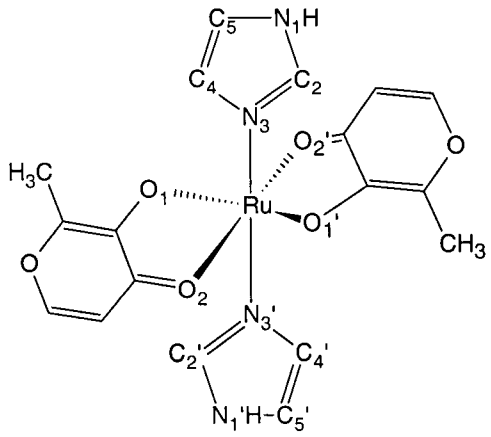

Figure 3.19 Template with numbering scheme for crystal structure information displayed in Table 3.2.

Complexes of the form $[Ru(Ema)_2(L)_2]CF_3SO_3$ were also synthesized from $Ru(Ema)_3$ with L = metro (**11**), 4MeIm (**12**) and 2MeIm (**13**). Again, complexes were characterized by elemental analysis, MS, and NMR and IR spectroscopies, while **11** was also characterized by X-ray crystallography (Figure 3.20). **11** was synthesized in the same manner as was **4**; however, the observed green TLC band, likely containing $[Ru(Ema)_2(metro)(EtOH)]CF_3SO_3$ (analogous to **5**), did not generate an isolable solid. The structure of **11**, like those for **4**,[16] **8** and **10**, shows trans-imidazole ligands with a centre of inversion at Ru, and the distortion of bond angles at N(3), to relieve the steric interaction between the 2-Me group and the ma-type ligands, is observed in the structures of **4**[16] and **11**, as was observed for **10** (Table 3.2).

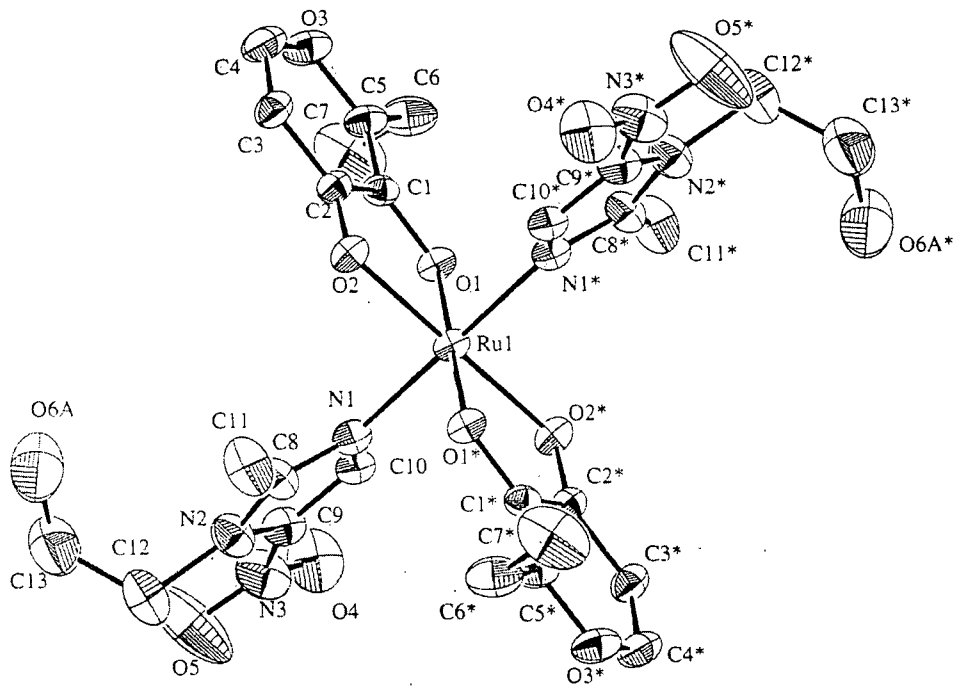

Figure 3.20 ORTEP diagram of the cation of *trans*-$[Ru(Ema)_2(metro)_2]CF_3SO_3$ (**11**) with 50 % probability thermal ellipsoids (see Appendix A4 for details).

$[Ru(ma)_2(L)_2]CF_3SO_3$ (L = $2NO_2Im$ (**15**), $4NO_2Im$ (**16**), $3NO_2tri$ (**17**)) were synthesized by adding an excess of the appropriate nitroimidazole or nitrotriazole to a solution of **1** and triflic acid in EtOH under N_2 and then refluxing the mixture for 24 h. Corresponding reactions at r.t. showed $[Ru(ma)_2(EtOH)_2]CF_3SO_3$ as the major species present in solution after 24 h, as analyzed by TLC. The elemental analyses for **15** - **17** were consistently high in C, H and N and, as the ^1H NMR spectra of suspensions of **15** and **16** in D_2O gave weak signals for free $2NO_2Im$ and $4NO_2Im$, respectively, some free ligand might be present in these complexes.

3.3.2 Solution ^1H NMR Spectroscopy of the Im, 2MeIm, 4MeIm and 1MeIm Complexes

The ^1H NMR spectra of **6** - **10** were examined in $CDCl_3$; the data for the structurally characterized complexes **8** and **10** are consistent with the primary isomer in solution being the trans-isomer (Table 3.3).

Table 3.3 ^1H NMR data of Ru(III) maltolato-imidazole complexes in $CDCl_3$ at r.t.

Complex	δ ma-Me	δ Im-Me	δ Im H(5)	δ Im H(4)	δ Im H(2)
trans-$[Ru(ma)_2(4MeIm)_2]CF_3SO_3$ (**6**)	60.0	16.3	-4.5	-	-20.0
trans-$[Ru(ma)_2(Im)_2]CF_3SO_3$ (**7**)	62.2	-	-3.7	a	-19.6
cis-$[Ru(ma)_2(Im)_2]CF_3SO_3$ (**7**)	60.0, 44.6		-1.5, -5.6		-15.5, -24.7
trans-$[Ru(ma)_2(1MeIm)_2]CF_3SO_3$ (**8**)	62.6	13.4	-3.8	a	-19.0
$[Ru(ma)(1MeIm)_4][CF_3SO_3]_2$ (**9**)	81.6	25.6, 20.4	-0.5, 5.7	a	-18.4, 24.0
trans-$[Ru(ma)_2(2MeIm)_2]CF_3SO_3$ (**10**)	67.0	42.0	-1.6	-4.7	-

a -signals for these protons were not observed.

For $[Ru(ma)_2(1MeIm)_2]CF_3SO_3$ (**8**), the ma-Me resonance is shifted downfield to δ 62.6 with respect to that of the Hma-Me (δ 2.37), and the Im-Me resonance at δ 13.41 (Table 3.3) also shows a downfield shift with respect to that of free 1MeIm (δ 3.64). The shift for the Im-Me resonance is consistent with data for other Ru(III)-1MeIm complexes,[5] and that for the ma-Me resonance is considered consistent with that observed for Ru(III)-ma (Table 3.1). The ^1H NMR spectrum of **8** was first studied in acetone-d_6

(Figure 3.21a), following purification of the complex by preparative TLC: the data suggest the presence of a mixture of isomers. An *in situ* synthesis in CD_3OD showed the formation of only the trans-isomer. When MeOH was used to extract the complex from the TLC plate, the ^1H NMR spectrum of the isolated solid in $CDCl_3$ showed numerous peaks between δ 1-5 that were not present in the ^1H NMR of the original crude mixture before purification; these can likely be assigned to the binder and other components of the TLC plate that may be soluble in MeOH. The workup procedure was then modified to use 1-2% MeOH in CH_2Cl_2 to remove the complex from the silica scraped from the plate. The ^1H NMR spectrum of **8** was then recorded in $CDCl_3$ and showed the trans-isomer in almost 100% purity (Figure 3.21b). Extraction of the other TLC-isolated imidazole complexes (**6**, **7**, **9**, **10**, **12** and **13**) from the silica was subsequently performed using either neat CH_2Cl_2 or a mixture of MeOH (< 5%) and CH_2Cl_2.

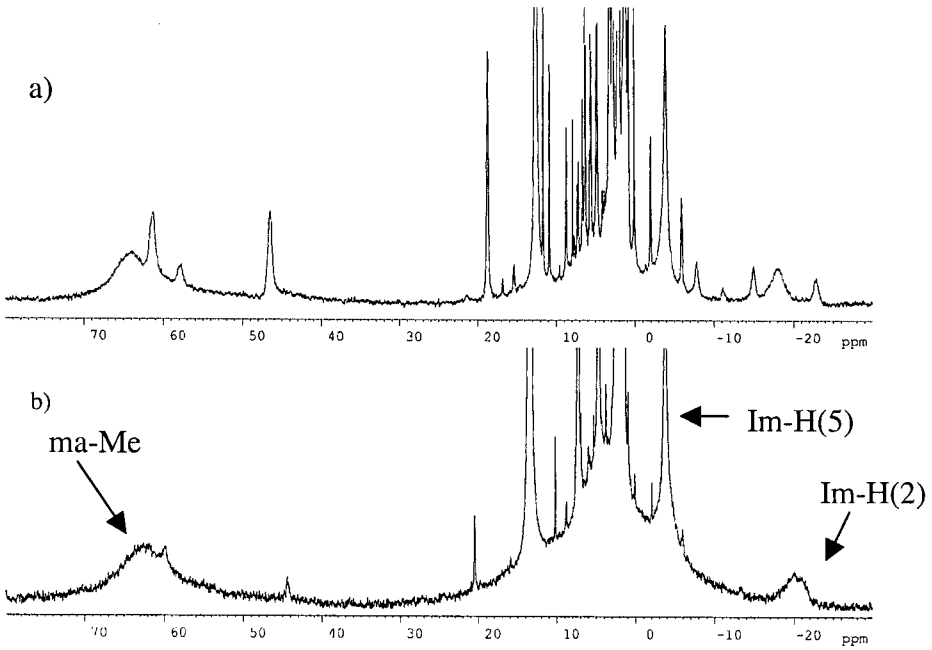

Figure 3.21 ^1H NMR spectrum of $[Ru(ma)_2(1MeIm)_2]CF_3SO_3$ (**8**) in a) acetone-d_6 (300 MHz, 298 K) and b) $CDCl_3$ (300 MHz, 298 K).

As discussed in Section 3.3.1, the complexes $[Ru(ma)_2(L)_2]CF_3SO_3$, where L = Im, 2MeIm, 4MeIm and 1MeIm, were all synthesized via reactions at r.t. Heating the reaction mixtures led to the formation of numerous side-products. In the case of 1MeIm

(Figure 3.22), at least 11 signals for the ma-Me group were observed in the ^{1}H NMR spectrum in $CDCl_3$ of a solid isolated after a reaction mixture of **1** in EtOH with four equivalents of 1MeIm and one equivalent of triflic acid had been refluxed for 6 h. Numerous additional signals were also observed in the regions where the imidazole methyl (δ 21 to 12) and H(5) (δ 2 to –8) proton resonances occur. After this reaction mixture was refluxed for 48 h, $[Ru(ma)(1MeIm)_4][CF_3SO_3]_2$ (**9**) was isolated. The signal for the ma-Me of **9** (δ 81.6, Figure 3.23) is shifted farther downfield than for the bis-imidazole complexes (Table 3.3). Two sharp resonances at δ 25.6 and 20.4, assigned as Im-Me groups, are shifted farther downfield than are those observed for the Im-Me groups of **8** (δ 13.4).

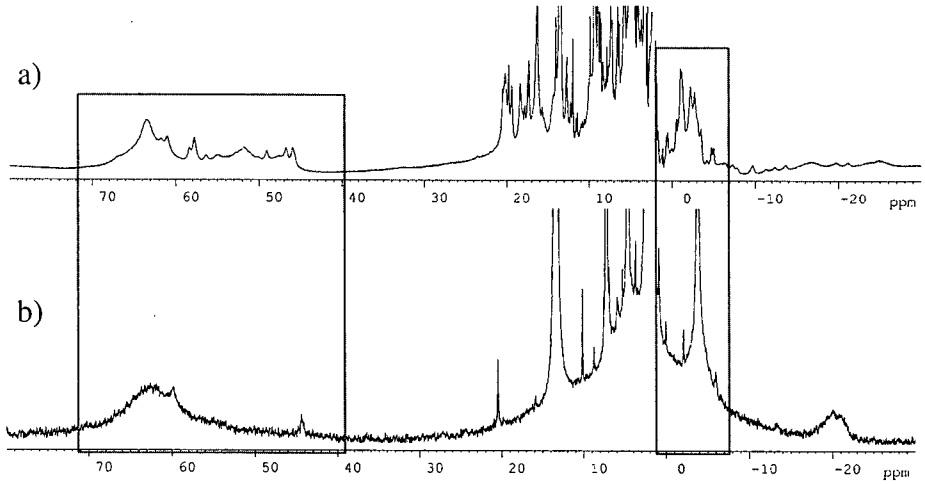

Figure 3.22 The effect of varying the temperature when reacting **1** with 1MeIm. a) ^{1}H NMR spectrum in $CDCl_3$ (300 MHz, 298 K) of the crude reaction mixture isolated after refluxing $Ru(ma)_3$ with 4 equiv. of 1MeIm and 1 equiv. of triflic acid in EtOH under N_2 for 6 h. b) ^{1}H NMR spectrum (300 MHz, 298 K) of $[Ru(ma)_2(1MeIm)_2]CF_3SO_3$ (**8**) in $CDCl_3$.

Attempts to form similar tetrakis(imidazole) complexes with Im, 2MeIm, and 4MeIm were unsuccessful. Attempts to form a mixed tetrakis(imidazole) complex by refluxing 6 equivalents of 1MeIm with one equivalent of $[Ru(ma)_2(2MeIm)_2]CF_3SO_3$ (**10**) and one equivalent of CF_3SO_3H in EtOH were also unsuccessful.

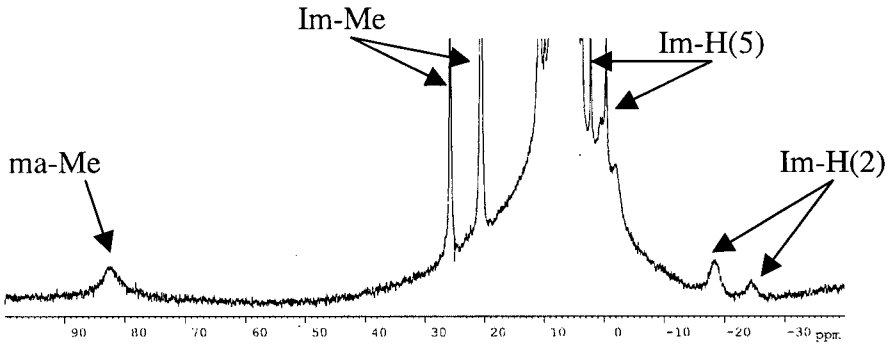

Figure 3.23 ^{1}H NMR spectrum (300 MHz, 298 K) of $[Ru(ma)(1MeIm)_4][CF_3SO_3]_2$ (**9**) in acetone-d_6 showing the ma-Me at δ 81.6 and 1MeIm H(2) protons at δ –19.4 and -24.0. Two sharp resonances at δ 25.6 and 20.4 are assigned as Im-Me groups.

The ^{1}H NMR spectrum of *trans*-$[Ru(ma)_2(2MeIm)_2]CF_3SO_3$ (**10**) shows a single resonance at δ 67.0 for the ma-Me groups (Figure 3.24); resonances for the H(4) (δ -4.7), H(5) (δ -1.6), and Im-Me (δ 42.0) protons are also observed.

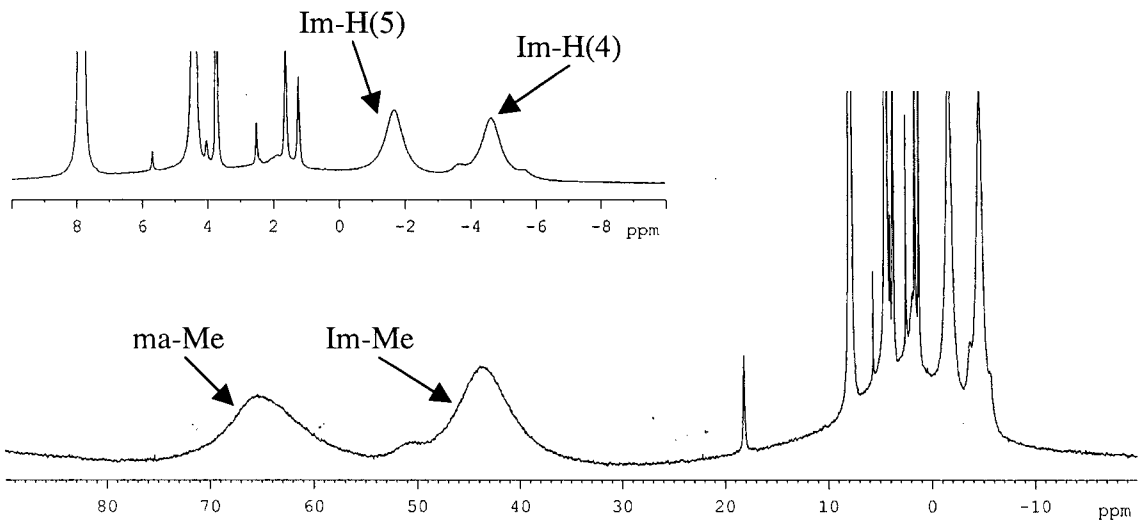

Figure 3.24 ^{1}H NMR spectrum (300 MHz, 298 K) of $[Ru(ma)_2(2MeIm)_2]CF_3SO_3$ (**10**) in $CDCl_3$.

The ^{1}H NMR spectrum of $[Ru(ma)_2(4MeIm)_2]CF_3SO_3$ (**6**) also shows only a single broad resonance for the ma-Me protons. Even though this complex has not been characterized crystallographically, it can be inferred from similarities between its ^{1}H NMR spectrum and those of *trans*-**8** and *trans*-**10,** that **6** is also in a trans-configuration. The resonance for the Im-Me group is shifted less downfield for **6** (δ 16.3) than is observed for **10** (δ 42.0). In some Ru(III) complexes formed from 4MeIm, the 4MeIm isomerizes to 5MeIm upon coordination,[5] to relieve steric interactions between the Me group and other coordinated ligands. Anderson and Beauchamp have reported the ^{1}H NMR spectrum for the anion $[RuCl_4(5MeIm)_2]^-$ in D_2O, attributing signals between δ –0.2 and 2.3 to the Me group of coordinated 5MeIm.[5] Previous work in our group has described the chemical shifts of the Im-Me groups of a mixed 4-Me/5-Me Ru(III) cation, $[Ru(acac)_2(4MeIm)(5MeIm)]^+$, assigning a signal for the 4-Me group at δ 14.7 and one for the 5-Me group at δ 7.5.[17] This suggests that $[Ru(ma)_2(4MeIm)_2]CF_3SO_3$ (**6**) likely exists as the 4-Me species as its structure is analogous to that of the acac complex, and the chemical shift of the Im-Me falls close to that reported for the 4-Me group of the mixed-acac complex. It is difficult to determine if the chemical shift of the imidazole proton of **6** is definitive of either an H(4) or an H(5). Although the relative chemical shifts of the Im protons remain constant, H(5) < H(4) < H(2), H(2) being the farthest upfield, the absolute regions in which these resonances are found varies considerably and are dependent on the nature of the other coordinated ligands. Steric interactions between the Im-Me and the ma ligands of **10** are overcome as the 2MeIm tilts to move the Me away from the ma plane (Table 3.1, Section 3.3.1). The 4MeIm of **6** could tilt in a similar manner to remove steric interactions without isomerizing to 5MeIm. Without an X-ray structure, it is not possible to define this complex as the 4MeIm species, but this would agree with the literature observations and the data collected for this complex.

The ^{1}H NMR spectrum of $[Ru(ma)_2(Im)_2]CF_3SO_3$ (**7**) showed both the cis- and trans-isomers in solution, despite using the modified isolation technique that succeeded in removing the cis-isomers for **6**, **8**, and **10**. Attempts to separate the two isomers of **7** by chromatography were unsuccessful. The intensities of the ^{1}H NMR signals for the cis-isomer varied between samples suggesting the absence of a solution equilibrium, and that two overlapping TLC bands may be the source of the two isomers. When silica taken

from the lower part of the red band was not included in the isolation, weaker signals for the cis-isomer were observed in the ^{1}H NMR spectrum, but the ^{1}H NMR spectrum taken from a sample isolated from a thin section (~1 mm in width) cut from the top of the red band still revealed the presence of two isomers in solution.

Table 3.4 summarizes some ^{1}H NMR signals for *trans*-[Ru(Ema)$_2$(4MeIm)$_2$]CF_3SO_3 (**12**) and *trans*-[Ru(Ema)$_2$(2MeIm)$_2$]CF_3SO_3 (**13**), both synthesized from Ru(Ema)$_3$, and the data for the corresponding ma complexes, **6** and **10**; the chemical shifts for the Im-protons and -Me groups of **12** and **13** are almost identical to those of **6** and **10**, respectively, while the Ema-CH_2 resonances are shifted upfield from those of the ma-Me resonances for **6** and **10**, respectively. As only one resonance is observed for the Ema-CH_2 group, the Im-Me group, and each of the Im protons for both **12** and **13** (Figure 3.25), these complexes are likely trans-isomers. The chemical shift of the Im-Me group for **12** is almost identical to that of **6**, and therefore, by the same reasoning discussed previously in this Section for **6**, **12** also likely exists as a 4MeIm complex and not a 5MeIm one. The resonances for the Ema-CH_2-CH_3 is not observed and likely overlaps with the δ 0-10 region in the spectrum where the solvent signals likely overwhelm any paramagnetic resonances.

Table 3.4 ^{1}H NMR data for the Ema-Im complexes **12** and **13**, compared with those for the ma-Im complexes **6** and **10**.

Complex	δ Ema-CH_2	δ ma-CH_3	δ Im-CH_3	δ Im-H(5)	δ Im-H(4)	δ Im-H(2)
trans-[Ru(Ema)$_2$(4MeIm)$_2$]CF_3SO_3 (**12**)	49.1	-	16.5	-4.6	-	-19.0
trans-[Ru(Ema)$_2$(2MeIm)$_2$]CF_3SO_3 (**13**)	51.7	-	43.7	-1.9	-5.2	-
trans-[Ru(ma)$_2$(4MeIm)$_2$]CF_3SO_3 (**6**)	-	60.0	16.3	-4.5	-	-20.0
trans-[Ru(ma)$_2$(2MeIm)$_2$]CF_3SO_3 (**10**)	-	67.0	42.0	-1.6	-4.7	-

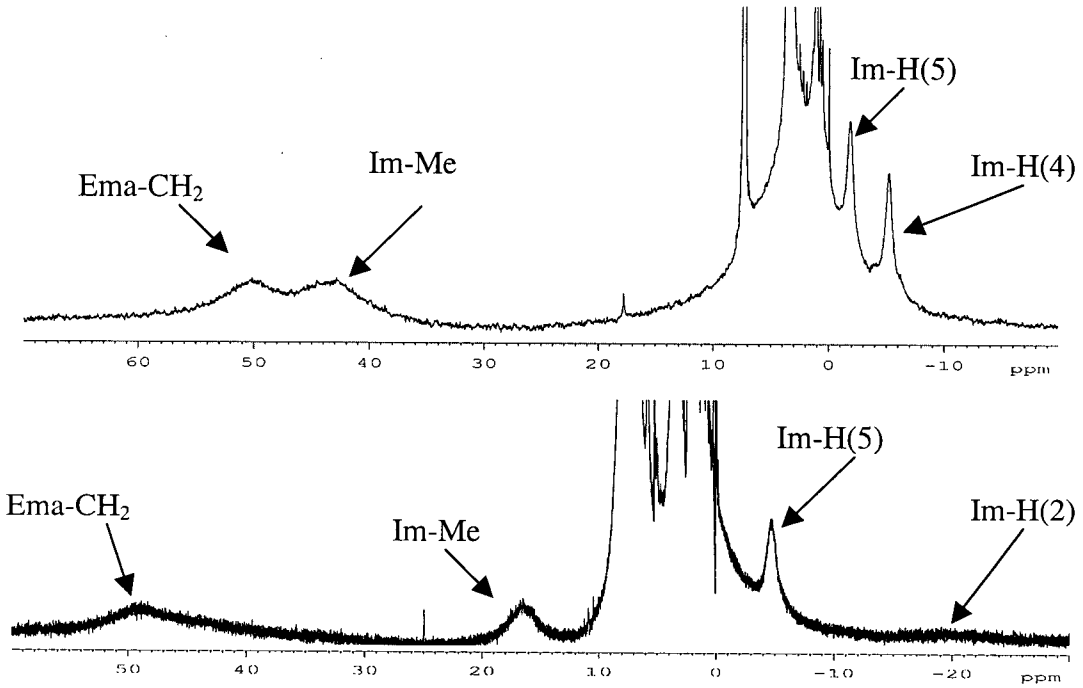

Figure 3.25 ^{1}H NMR spectra (300 MHz, 298 K) of a) $[Ru(Ema)_2(2MeIm)_2]CF_3SO_3$ (**13**) in $CDCl_3$ and b) $[Ru(Ema)_2(4MeIm)_2]CF_3SO_3$ (**12**) in $CDCl_3$. The H(2) signal in (b) is very broad and can only be observed when the y-axis is expanded.

3.3.3 Solution ^{1}H NMR Spectroscopy of the metro, $2NO_2$Im, $4NO_2$Im and $3NO_2$tri Complexes

Of the complexes with metro (**4**, **5**, and **11**), $2NO_2$Im (**15**), $4NO_2$Im (**16**) and $3NO_2$tri (**17**), only those with metro were soluble in aqueous solution. Unlike the ^{1}H NMR spectra for **6**-**10**, **12** and **13**, which were measured in $CDCl_3$ (Section 3.3.2), the ^{1}H NMR spectrum of $[Ru(ma)_2(metro)_2]CF_3SO_3$ (**4**) was measured in acetone-d_6 because of its insolubility in $CDCl_3$; observed were a broad resonance for the ma-Me group (δ 70.0) and another for the Im-Me group (δ 34.0), consistent with a trans-geometry (as discussed in Section 3.3.2 for **6**, **8** and **10**) and the solid state structure.[16]

Similarly, in the ^{1}H NMR spectrum of $[Ru(Ema)_2(metro)_2]CF_3SO_3$ (**11**), broad signals for each of the ma-Me protons (δ 65.3), the Im-Me protons (δ 32.2), and the H(5) of metronidazole (δ -4.8) are consistent with the trans-geometry determined by X-ray crystallography (Section 3.3.1, Figure 3.20).

The ^{1}H NMR spectrum of $[Ru(ma)_2(metro)(EtOH)]CF_3SO_3$ (**5**) in acetone-d_6 shows 4 signals in the region where the ma-Me group is typically observed. Five singlets between δ 21 and 8, which are not present in the spectrum for **4**, were also observed. These signals could be due to the H(5) or H(6) protons of ma, the metro-Me group, the metro 1-hydroxyethyl group, or bound EtOH; signals for free EtOH were not observed even after 1 h showing that the acetone-d_6 was not displacing the coordinated EtOH.

The $[Ru(ma)_2(L)_2]CF_3SO_3$ complexes, where L = $2NO_2Im$ (**15**), $4NO_2Im$ (**16**) and $3NO_2tri$ (**17**) were only readily soluble in dmso-d_6 for ^{1}H NMR investigation. For each of these three complexes, no paramagnetic signals were detected; however, intense signals were observed for the free heterocyclic ligands, implying that the complexes dissociate the (N)-bound ligands in dmso-d_6. Weak signals were also observed for free ma, suggesting further decomposition of the complexes. The ^{1}H NMR spectrum of a suspension of **16** in acetone-d_6 was recorded (4096 scans over 2h) and a trace resonance was observed for the coordinated ma-Me group at δ 63.8. Attempts to study **15** and **17** in a similar manner were unsuccessful. Further study of **15** - **17** is needed to better understand their structures.

3.3.4 Compounds Synthesized Using 2,2,3,3,3-Pentafluoropropylamine (F5)

Three heterocyclic compounds were prepared via reaction with 2,2,3,3,3-pentafluoropropylamine (F5). An improved synthesis of EF5 (Figure 3.26) has been published

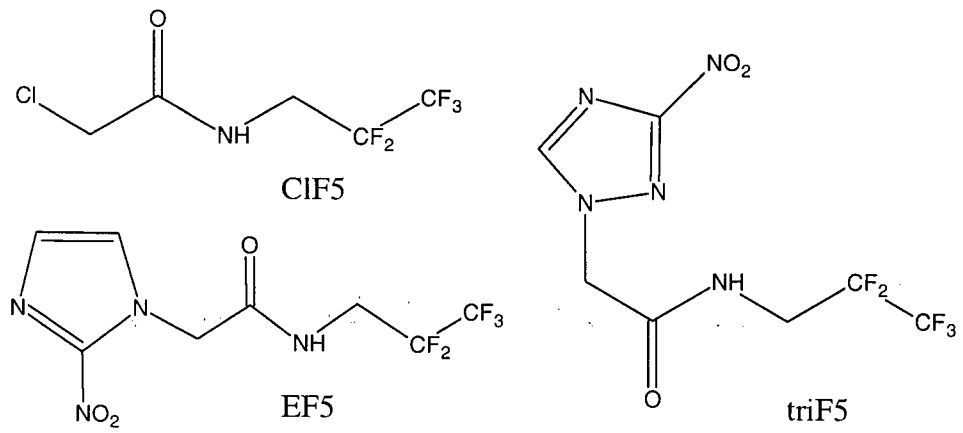

Figure 3.26 Molecular structures of three compounds synthesized from F5.

by our group,[18] but was further modified in this thesis work to limit the number of reagents required to convert F5 into EF5 and conserve the amount of F5 required because of the rapidly rising cost of this amine. In this work, F5 was purchased from Lancaster or Interchim or was prepared according to a published procedure (Figure 3.27).[19,20]

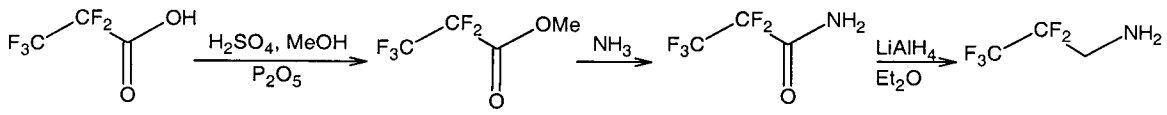

Figure 3.27 Synthesis of 2,2,3,3,3-pentrafluoropropylamine (F5) from 2,2,3,3,3-pentafluoroproprionic acid.

The procedure for synthesizing EF5 used chloroacetyl chloride to form the precursor N-(2,2,3,3,3-pentafluoropropyl)chloroacetamide (ClF5, Figure 3.26) instead of the previously used iodoacetic acid to form N-(2,2,3,3,3-pentafluoropropyl)-iodoacetamide (IF5).[18] The chloroacetyl chloride reaction proceeded more quickly and gave a higher yield (91 for ClF5 vs. 53 % for IF5) than the corresponding reaction in which iodoacetic acid is first activated with isobutyl chloroformate before being reacted with F5.[18] The reaction of ClF5 with $2NO_2Im$ to afford EF5 proceeded identically to that reported for the corresponding reaction with IF5.[18]

The procedure used to prepare EF5 was also used to synthesize the new ligand 2-(3-nitro-1-H-triazol-1-yl)-N-(2,2,3,3,3-pentafluoropropyl)acetamide (triF5, Figure 3.26), but with use of $3NO_2tri$ instead of $2NO_2Im$. Elemental analysis agreed with the formulation for triF5 that was further characterized by NMR and IR spectroscopies. A report investigating nitrotriazoles as potential anticancer agents[10] led to the interest in developing this triazole analogue of EF5. Although complexes of this ligand were not tested for bioactivity in this work, preliminary biological results for triF5 itself will be discussed in Chapter 7.

The compound 1H-imidazole-4,5-N,N'-bis(2,2,3,3,3-pentafluoropropyl)-dicarboxamide, (IMF10, Figure 3.28), was synthesized by reacting imidazole-4,5-dicarboxylic acid with two equivalents of isobutyl chloroformate and then adding two

equivalents of F5; IMF10 was characterized by MS and NMR spectroscopy. Elemental analysis indicates the presence of a 0.5 H_2O solvate. The two IR bands between 3200-3400 cm^{-1} presumably arise from ν(NH) and ν(OH).

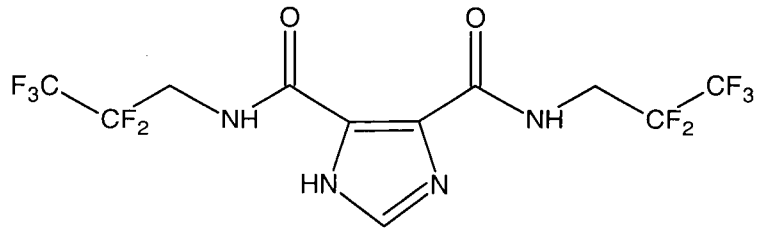

Figure 3.28 Molecular structure of IMF10.

3.3.5 Synthesis, Characterization, and Solution ^1H NMR Spectroscopy of $[Ru(ma)_2(EF5)_2]CF_3SO_3 \cdot EtOH$ (14) and $[Ru(ma)_2(triF5)_2]CF_3SO_3$ (18)

Complexes **14** and **18** were synthesized from $[Ru(ma)_2(EtOH)_2]CF_3SO_3$ (**3**) instead of $Ru(ma)_3$ (**1**), because (in the absence of excess ma) this allowed for the use of stoichiometric amounts of EF5. The reactions proceeded quantitatively, and purification of the complexes was simpler than when using **1** as a precursor. **18** was insoluble in all solvents tested and thus was only characterized by IR spectroscopy and elemental analysis that agrees well with the proposed formulation. **14**, on the other hand, was soluble in both EtOH and H_2O and was therefore characterized by MS and NMR spectroscopy as well as IR spectroscopy and elemental analysis.

The ^1H NMR spectrum (r.t., CD_3OD) of $[Ru(ma)_2(EF5)_2]CF_3SO_3 \cdot EtOH$ (**14**) showed a broad resonance for the ma-Me group (δ 59.2) and two broad singlets at δ –4.8 and -16.1 for the H(5) and H(4) protons, respectively. Resonances for the EF5 side-chain, and H(5) and H(6) of ma, are likely hidden in the δ 0-10 region where trace signals for diamagnetic impurities and residual solvents overwhelm any 'paramagnetic' signals. Although the solid was dried for 24 h under vacuum at 78 °C before the ^1H NMR spectrum was taken, signals for free EtOH are observed. The addition of one EtOH to the molecular formula fits well the elemental analysis. In the ^{19}F NMR spectrum, two broad signals for the bound EF5 (δ -8.9 and –46.1) (Figure 3.29) overlap with a triplet (δ -46.5)

and a multiplet (δ -9.4) that are for either free EF5 in solution or a diamagnetic impurity, although TLC analysis of the NMR sample showed no evidence of the free ligand. A singlet for the triflate counterion is also observed at δ –3.52.

The mass spectrum gives peaks for [M^+ -16] and [M^+ - 16 – EF5], consistent with the commonly observed loss of an O-atom from a nitroaromatic group.[21,22]

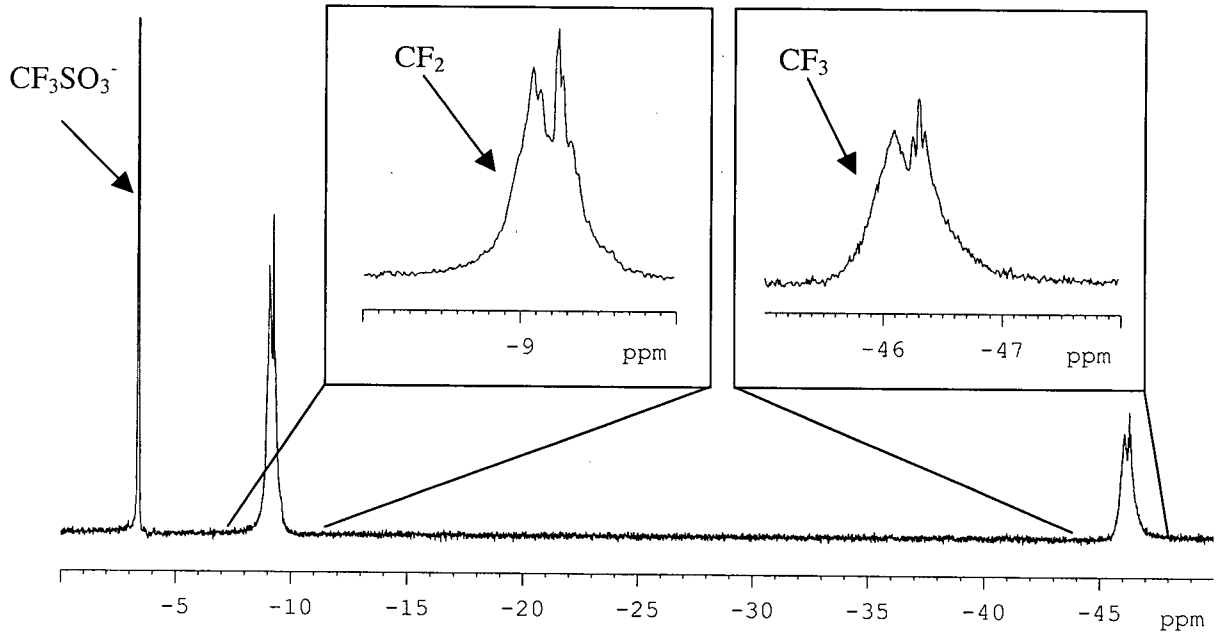

Figure 3.29 ^{19}F NMR spectrum (300 MHz, 298 K) of $[Ru(ma)_2(EF5)_2]CF_3SO_3 \cdot EtOH$ (**14**). Both signals for bound EF5 are broadened, while the sharper, diamagnetic signals likely correspond to those of free EF5.

3.4 Synthesis of $[Ru(HMepyr)_3]Cl_3$ (19)

Preliminary attempts to synthesize a complex analogous to **1** but with 3-hydroxy-1,2-dimethyl-4-pyridone led instead to the synthesis of **19** that was characterized by IR spectroscopy and the elemental analysis. The conductivity of an aqueous solution of **19** (451 $\Omega^{-1}cm^2mol^{-1}$) is in the range for a 3:1 electrolyte.[11] Attempts to deprotonate this complex and isolate a neutral species were unsuccessful.

3.5 Cyclic Voltammetry of Complexes

The Ru(III/II) one-electron reduction potentials were determined for the complexes that were soluble in either MeCN or CH_2Cl_2. The potentials determined for $Ru(ma)_3$ in CH_2Cl_2 agree with those reported in the literature,[1] and those in MeCN are reported in Table 3.5. Of the mixed Im-ma complexes tested, **10** had the lowest reduction potential, and is also the most active ma complex from the MTT biological studies (Section 6.4.2). This observation counters the theory that to be biologically active, Ru(III) complexes should have a more positive reduction potential to facilitate *in situ* reduction to potentially more labile Ru(II) species.[23] There does not appear, however, to be any direct link between the reduction potential and the *in vitro* activity, as will be discussed in more detail in Section 6.4.2.

Table 3.5 Ru(III/II) reduction potentials of ma and Ema-containing complexes.

Complex	Ru (III/II) Reduction Potential in MeCN vs SCE (mV)
$Ru(ma)_3$ (**1**)	-1132
$Ru(Ema)_3$ (**2**)	-1176
$[Ru(Ema)_2(2MeIm)_2]CF_3SO_3$ (**13**)	-889
$[Ru(Ema)_2(4MeIm)_2]CF_3SO_3$ (**12**)	-829
$[Ru(Ema)_2(metro)_2]CF_3SO_3$ (**11**)	-568
$[Ru(ma)_2(2MeIm)_2]CF_3SO_3$ (**10**)	-844
$[Ru(ma)_2(1MeIm)_2]CF_3SO_3 \cdot CH_2Cl_2$ (**8**)	-765
$[Ru(ma)_2(4MeIm)_2]CF_3SO_3 \cdot CH_2Cl_2$ (**6**)	-738
$[Ru(ma)_2(Im)_2]CF_3SO_3$ (**7**)	-705
$[Ru(ma)_2(metro)_2]CF_3SO_3$ (**4**)	-554
$[Ru(ma)_2(metro)(EtOH)]CF_3SO_3$ (**5**)	-496
$[Ru(ma)(1MeIm)_4][CF_3SO_3]_2$ (**9**)	-442

The Ru(III/II) reduction potentials of the Ema complexes were some 14 - 90 mV more negative than those for the corresponding ma complexes. **13**, the complex with the lowest IC_{50} of all those tested for bioactivity (Section 6.4.2), had the lowest Ru(III/II) reduction potential of the all the bis-imidazole complexes.

The voltammograms of the metro complexes were the only ones obtained for complexes with ligands containing a nitro group. With the exception of **14**, the other nitro containing complexes were insoluble in 0.100 M TBAP solutions in either CH_2Cl_2 or MeCN. The CV of $[Ru(ma)_2(metro)_2]CF_3SO_3$ (**4**) shows three reversible waves for $Ru^{III/II}$ (-554 mV), $Ru^{IV/III}$ (1085 mV), and NO_2/NO_2^- (–1111 mV) (Figure 3.30). Free metronidazole was found to undergo a 1-electron reduction for the nitro group at –1154 mV, 43 mV more negative than for the coordinated ligand, and 17 mV more negative than for $[Ru(Ema)_2(metro)_2]CF_3SO_3$ (**11**) ($E_{1/2}$ (NO_2/NO_2^-) = -1137 mV). From these data it can be concluded (as expected) that coordination of metronidazole to Ru(III) makes the reduction of the nitro group easier (i.e. gives a more positive potential). **14** was soluble in MeCN but no signals were observed in the voltammogram between –2 and 2 V.

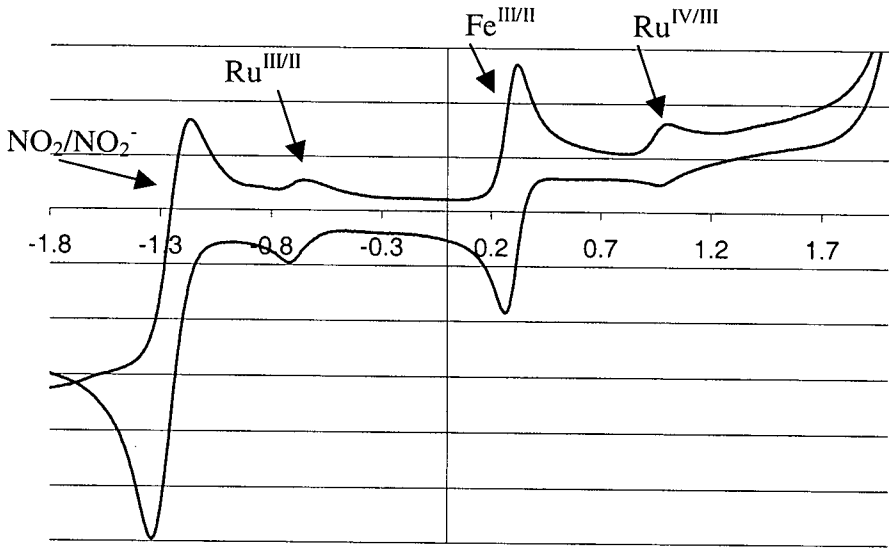

Figure 3.30 Cyclic voltammogram of $[Ru(metro)_2(ma)_2]CF_3SO_3$ (**4**) in MeCN containing ferrocene.

3.6 Experimental Procedures for the Syntheses of Compounds Derived from F5

3.6.1 N-(2,2,3,3,3-pentafluoropropyl)chloroacetamide (ClF5)

This compound was prepared via a modified reported procedure.[17] Chloroacetyl chloride (0.375 mL, 4.71 mmol) was dissolved in THF at 0 °C under N_2. To this solution was added 2,2,3,3,3-pentafluoropropylamine (F5) (0.500 mL, 4.70 mmol) and N-methylmorpholine (NMM) (0.410 mL, 4.70 mmol). The mixture was stirred at 0 °C for 30 min, at which time the ice-bath was removed and stirring was continued for an additional 30 min. The solution was filtered to remove a white precipitate and the filtrate was then evaporated under vacuum to leave a yellow, crystalline solid. This solid was dried under vacuum at 0 °C for 24 h. Yield: 0.96 g (91 %). ^{1}H NMR (acetone-d_6): δ 8.16 (s, 1H, N*H*); 4.26 (s, 2H, ClCH_2); 4.15 (td, 2H CH_2CF$_2$). ^{19}F{^{1}H} NMR (acetone-d_6): δ -8.25 (t, CF_3); -45.27 (q, CF_2). IR (KBr pellet): ν 3320 (N-H, m), 1655 (C=O, s). ESI-MS (MeOH): 190 (M^+ - Cl). The spectroscopic data agree with those previously reported.[17]

3.6.2 2-(2-Nitro-1-H-imidazol-1-yl)-N-(2,2,3,3,3-pentafluoropropyl)acetamide (EF5)

This ligand was synthesized using a modified procedure from that published by Baird *et al.*[18] A solution of 2NO$_2$Im (0.10 g, 0.92 mmol) in DMF (5 mL) was degassed with N_2 for 10 min. To this solution was added Cs_2CO_3 (0.30 g, 0.93 mmol). Stirring of this mixture at 50 °C for 2 h yielded a yellow solution and a white precipitate. To this mixture was added ClF5, and the reaction mixture was then stirred for 3 h at 50 °C. The solution was filtered and the precipitate washed with dry THF (3 x 5 mL). The filtrate was reduced in volume to 1 mL and then loaded onto a silica gel column. Elution of the column (CH_2Cl_2:acetone, 10:1) removed unreacted starting materials. The concentration of acetone was then increased to 40 % to elute EF5. The fractions containing the product were combined and evaporated under vacuum to yield EF5 as a white solid. Yield: 0.23 g (82 %). ^{1}H NMR (CD_3OD): δ 7.48 (s, 1H, Im-H_5); 7.21 (s, 1H, Im-H_4); 5.29 (s, 2H CH_2CO); 4.08 (t, 2H CH_2CF$_2$). ^{19}F{^{1}H} NMR (CD_3OD): δ -10.58 (t, CF_3); -47.21 (q, CF_2). IR (KBr pellet): ν 3305 (N-H, m), 1686 (C=O, s), 1490 (N-O_{asym}, m), 1363 (N-O_{sym}, s). ESI-MS (MeOH): 303 (M^+). Anal. Calcd for $C_8H_7N_4O_3F_5$: C, 31.80; H, 2.34;

N, 18.54. Found: C, 31.62; H, 2.44; N, 18.25. The data agree with those reported in the literature.[18]

3.6.3 2-(3-Nitro-1-H-triazol-1-yl)-N-(2,2,3,3,3-pentafluoropropyl)acetamide (triF5)

This compound was prepared using the same procedure as that for EF5, but using 3-nitro-1,2,4-triazole (0.048 g, 0.42 mmol) in place of $2NO_2Im$, and Cs_2CO_3 (0.14 g, 0.43 mmol). The triF5 product was isolated as a pale yellow solid. Yield: 0.86 g (67 %). ^1H NMR (aceton-d_6): δ 8.61 (s, 1H, tri-H_5); 8.17 (s, 1H N-H); 5.24 (s, 2H –CH_2-CO-); 4.11 (td, 2H –CH_2-CF_2-). $^{19}F\{^1H\}$ NMR (acetone-d_6): δ -10.41 (t, -CF_3); -48.65 (q, -CF_2-). IR (KBr pellet): ν 3341 (N-H, m), 1701 (C=O, s), 1407 (N-O_{asym}, m), 1318 (N-O_{sym}, s). ESI-MS (MeOH): 304 (M^+). Anal. Calcd for $C_7H_6N_5O_3F_5$: C, 27.72; H, 1.98; N, 23.10. Found: C, 27.62; H, 2.14; N, 22.87.

3.6.4 IMF10

To a suspension of imidazole-4,5,-dicarboxylic acid (0.10 g, 0.65 mmol) in THF (5 mL) under an atmosphere of N_2 was added NMM (0.115 mL, 1.32 mmol). The mixture was stirred for 10 min at which time isobutyl chloroformate was added (0.175 mL, 1.34 mmol). The mixture was stirred at r.t. for 1 h. Pentafluoropropyl amine (0.140 mL, 1.31 mmol) was then added and the mixture stirred under N_2 for 12 h at r.t. The mixture was then filtered to remove the white precipitate and the yellow filtrate was collected, and evaporated to leave a yellow oil. TLC analysis (CH_2Cl_2:MeOH, 10:1) showed a single major product, R_f = 0.67. The oil was purified using column chromatography (CH_2Cl_2:MeOH, 10:1) and the combined fractions for this band were collected and evaporated under vacuum to yield a yellow solid. Yield 0.086 g (31 %). ^1H NMR (CD_3OD): δ 7.72 (s, 1H, Im-H_2); 4.12 (td, 4H –CH_2-CF_2-). $^{19}F\{^1H\}$ NMR (acetone-d_6): δ -8.20 (t, -CF_3); -45.07 (q, -CF_2-). IR (KBr pellet): ν 3322 (N-H, m), 3226 (N-H, br s), 1648 (C=O, s). LR-MS (+LSIMS, thioglycerol): 418 (M^+). Anal. Calcd for $C_{11}H_8N_4O_2F_{10}\cdot 0.5H_2O$: C, 30.91; H, 2.11; N, 13.11. Found: C, 30.86; H, 2.31; N, 12.47.

3.7 Experimental Procedures for the Syntheses of Ru(III) Complexes

3.7.1 $Ru(ma)_3$ (1)

This compound was synthesized by a literature procedure.[1] To a brown solution of $RuCl_3 \cdot 3H_2O$ (1.01 g , 3.86 mmol) in water (80 mL) and sodium acetate (4.0 g, 30 mmol), maltol was added (2.50 g, 19.2 mmol) under N_2, and the mixture refluxed for 6 h; a red precipitate was then collected by filtration. TLC analysis (CH_2Cl_2:MeOH, 20:1) revealed two spots; the product (R_f = 0.6) and an impurity (R_f = 0). The mixture was then dissolved in CH_2Cl_2 (40 mL) and filtered through Celite (2 g) to remove the black impurity. The filtrate was reduced in volume to ~5 mL at which time hexanes (30 mL) were added to yield a red precipitate. The product was isolated via filtration and dried at 78 °C under vacuum for 48 h. Yield: 0.95 g (52 %). ^{1}H NMR (CD_2Cl_2): δ 43.2, 41.0, 21.1 (s, -C*H*$_3$); 11.8 (s, *H*$_5$-ma), 9.2 (s, *H*$_6$-ma); 3.1 (s, *H*$_6$-ma), -4.6 (s, *H*$_5$-ma); 0.8 (s, *H*$_6$-ma), -0.9 (s, *H*$_5$-ma). IR (KBr pellet): ν 1600 (C=O, s), 1551 (s), 1466 (s), 1261 (s), 1199 (s). LR-MS (+LSIMS, thioglycerol): 477 (M^+), 352 (M^+ - ma). UV-vis (H_2O): 216 (45.4), 284 (14.1), 380 (10.2). CV (MeCN): $E_{1/2}$ ($Ru^{III/II}$) = -1.132 V, $E_{1/2}$ ($Ru^{IV/III}$) = 0.524 V vs. SCE. CV (CH_2Cl_2): $E_{1/2}$ ($Ru^{III/II}$) = -1.273 V, $E_{1/2}$ ($Ru^{IV/III}$) = 0.497 V vs. SCE. Λ_M (H_2O) = 25 $\Omega^{-1}cm^2mol^{-1}$. Anal. Calcd for $C_{18}H_{15}O_9Ru$: C, 45.38; H, 3.17. Found: C, 45.32; H, 3.19. The CV (in CH_2Cl_2) and IR data agree with those reported in the literature[1] The X-ray structure shows a *mer*-configuration (Section 3.2.1).

3.7.2 $Ru(Ema)_3$ (2)

This complex was synthesized following the procedure outlined in Section 3.6.1, but using ethylmaltol in lieu of maltol (2.80 g, 20 mmol). TLC analysis (CH_2Cl_2:MeOH, 20:1) revealed two spots; the product (R_f = 0.55) and an impurity (R_f = 0). The mixture was then dissolved in CH_2Cl_2 (50 mL) and filtered through Celite (3 g) to remove the impurity. The filtered solution was reduced in volume to ~5 mL at which time hexanes (20 mL) were slowly added to yield a red precipitate. The precipitate was collected, and dried at 78 °C under vacuum for 48 h. Yield: 0.83 g (45 %). ^{1}H NMR (CD_2Cl_2): δ 40.1, 38.8, 35.3, 33.4, 21.7, 18.9 (s, -C*H*$_2$CH$_3$); 4.9, 4.8, 2.1 (s, -CH$_2$C*H*$_3$); 12.5 (*H*$_5$-Ema), 9.0 (*H*$_6$-Ema); 4.9 (*H*$_6$-Ema), -4.9 (*H*$_5$-Ema); 1.2 (*H*$_6$-Ema), -0.8 (*H*$_5$-Ema). IR (KBr pellet): ν

1596 (C=O, s), 1550 (s), 1471 (s), 1258 (s), 1187 (s). LR-MS (+LSIMS, thioglycerol): 519 (M^+), 380 (M^+ - Ema). UV-vis (H_2O): 216 (45.1), 284 (14.4), 382 (10.6). CV (MeCN): $E_{1/2}$ ($Ru^{III/II}$) = -1.176 V, $E_{1/2}$ ($Ru^{IV/III}$) = 0.540 V vs. SCE. CV (CH_2Cl_2): $E_{1/2}$ ($Ru^{III/II}$) = -1.292 V, $E_{1/2}$ ($Ru^{IV/III}$) = 0.493 V vs. SCE. Λ_M (H_2O) = 36 $\Omega^{-1}cm^2mol^{-1}$. Anal. Calcd for $C_{21}H_{21}O_9Ru$: C, 48.65; H, 4.08. Found: C, 48.64; H, 4.09.

3.7.3 $[Ru(ma)_2(EtOH)_2]CF_3SO_3$ (3)

To a red solution of **1** (0.090 g, 0.19 mmol) in EtOH (5 mL), triflic acid was added (0.030 g, 0.20 mmol) under N_2 and the solution refluxed for 1 h. The solvent was reduced to ~1 mL under vacuum to which Et_2O (20 mL) was added. A red precipitate, which contained only one band by TLC analysis (CH_2Cl_2:MeOH, 20:1; R_f = 0.45), was collected and washed with Et_2O (2 x 5 mL) before being dried at r.t. under vacuum for 24 h. Yield: 0.048 g (43 %). ^1H NMR (CD_3OD): δ 48.0 (br s, C*H*$_3$-ma); 28.0, 26.0 (br s, C*H*$_3$C*H*$_2$OH). IR (KBr pellet): ν 3427 (O-H, m), 1608 (C=O, s), 1471 (s), 1261 (s). LR-MS (+LSIMS, thioglycerol): 444 (M^+), 398 (M^+ - EtOH), 352 (M^+ - 2 EtOH). Λ_M (EtOH) = 36 $\Omega^{-1}cm^2mol^{-1}$. Anal. Calcd for $C_{17}H_{22}F_3O_{11}Ru$: C, 34.46; H, 3.72. Found: C, 34.53; H, 3.75.

3.7.4 $[Ru(ma)_2(metro)_2]CF_3SO_3$ (4) and $[Ru(ma)_2(metro)(EtOH)]CF_3SO_3$ (5)

To a red solution of **1** (0.090 g, 0.19 mmol) in EtOH (5 mL), triflic acid was added (0.030 g, 0.20 mmol) under N_2 and the solution was refluxed for 1 h. Metronidazole was then added (0.13 g, 0.76 mmol) and the solution was refluxed for an additional 6 h. After 2 h the solution was green and slowly turned blue over the next 4 h. The solvent was removed under vacuum and CH_2Cl_2 (10mL) was added. The mixture was shaken vigorously to leave a blue solid suspended in a green solution. The solid (**4**) was removed by filtration and washed with CH_2Cl_2 (2 x 5 mL) before being dried at 78 °C under vacuum for 48 h. Yield: 0.080 g (50 %). ^1H NMR (acetone-d_6): δ 70.0 (br s, C*H*$_3$-ma); 34.0 (br s, C*H*$_3$-metro); -6.3 (br s, *H*$_5$-metro). IR (KBr pellet): ν 3420 (O-H, m), 1604 (C=O, s), 1561 (N-O_{asym}, m), 1367 (N-O_{sym}, m), 1446 (s), 1263 (s). LR-MS (+LSIMS, thioglycerol): 694 (M^+), 523 (M^+ - metro), 352 (M^+ - 2 metro). CV (MeCN): $E_{1/2}$ (NO_2/NO_2^-) = -1.111 V, $E_{1/2}$ ($Ru^{III/II}$) = -0.554 V, $E_{1/2}$ ($Ru^{IV/III}$) = 1.085 V vs. SCE.

Anal. Calcd for $C_{25}H_{28}F_3N_6O_{15}SRu$ (**4**): C, 35.63; H, 3.33; N, 9.98. Found: C, 35.68; H, 3.41; N, 9.76.

After **4** was removed by filtration, the green solution was reduced in volume to ~2 mL and mounted on a 20 x 20 cm silica preparative TLC plate. The plate was developed with CH_2Cl_2:MeOH, 25:1 (130 mL). A green band was cut from the silica plate, suspended in 20 mL of a solution of CH_2Cl_2:EtOH, 19:1, and the mixture was left stirring for 16 h. The green mixture was then filtered to remove the silica and the solvent was removed under vacuum. The green oil remaining was dissolved in ~3 mL CH_2Cl_2 and hexanes (10 mL) were then added. The resulting green product was collected, washed with hexanes (2 x 5 mL) and dried at 78 °C under vacuum for 24 h. Yield: 0.032 g (12 %). ^{1}H NMR (acetone-d_6): δ 70.4, 65.6, 61.7, 54.2 (br s, CH_3-ma); 41.3, 34.9 (br s, CH_3-metro); 24.97, 20.99, 19.01 (br s, CH_3CH_2OH); -3.13, -6.29 (br s, metro-H_5). IR (KBr pellet): ν 3443 (N-H, m), 1701 (C=O, s), 1559 (N-O_{asym}, m), 1363 (N-O_{sym}, s), 1446 (s), 1263 (s). LR-MS (+LSIMS, thioglycerol): 523 (M^+ - EtOH), 352 (M^+ - EtOH - metro). CV (MeCN): $E_{1/2}$ ($Ru^{III/II}$) = -0.496 V. Anal. Calcd for $C_{21}H_{25}F_3N_3O_{13}SRu$ (**5**): C, 35.15; H, 3.49; N, 5.86. Found: C, 34.87; H, 3.32; N, 6.09.

3.7.5 [Ru(ma)$_2$(4MeIm)$_2$]CF_3SO_3·CH_2Cl_2 (6)

To a red solution of **1** (0.050 g, 0.11 mmol) in EtOH (5 mL), triflic acid was added (0.020 g, 0.13 mmol) under N_2 and the solution stirred at r.t. for 1 h. After 1 h, 4MeIm was added (0.041 g, 0.50 mmol) and the solution was stirred for an additional 12 h. After 4 h the solution was checked by TLC (CH_2Cl_2:MeOH, 10:1). The band for complex **5** had disappeared and been replaced by 3 major red bands (R_f = 0.32, 0.44, 0.54). After 12 h, only one major red band was observed by TLC (R_f = 0.56). The solvent was removed under vacuum and the dark red residue was dissolved in CH_2Cl_2 (2 mL) and mounted on a 20 x 20 cm silica preparative TLC plate that was developed with CH_2Cl_2:MeOH, 20:1 (130 mL), when one major red band observed. This red band was cut out, added to 50 mL of CH_2Cl_2, and the mixture was left stirring for 16 h. This was then filtered to remove the silica and the volume was reduced to ~5 mL. Hexanes (30 mL) were then added and the resulting red precipitate was collected, washed with

hexanes (2 x 5 mL) and dried at 78 °C under vacuum for 48 h. Yield: 0.032 g (42 %). ^{1}H NMR ($CDCl_3$): δ 60.0 (br s, CH_3-ma); 16.3 (br s, CH_3-Im); -4.5 (br s, H_5-Im); -20.0 (br s, H_2-Im). IR (KBr pellet): ν 3224 (N-H, m), 1601 (C=O, s), 1446 (s), 1263 (s). LR-MS (+LSIMS, thioglycerol): 516 (M^+), 434 (M^+ - 4MeIm), 352 (M^+ - 2 (4MeIm)). CV (MeCN): $E_{1/2}$ ($Ru^{III/II}$) = -0.738 V. Λ_M (MeOH) = 107 $\Omega^{-1}cm^2mol^{-1}$. Anal. Calcd for $C_{21}H_{22}F_3N_4O_9SRu \cdot CH_2Cl_2$: C, 35.25; H, 3.20; N, 7.48. Found: C, 35.63; H, 3.26; N, 7.55.

3.7.6 $[Ru(ma)_2(Im)_2]CF_3SO_3$ (7)

To a red solution of **1** (0.055 g, 0.12 mmol) in EtOH (5 mL), triflic acid was added (0.022 g, 0.14 mmol) under N_2 and the solution stirred at r.t. for 1 h. After 1 h, Im was added (0.035 g, 0.51 mmol) and the solution was stirred for an additional 12 h. After 4 h the solution was checked by TLC (CH_2Cl_2:MeOH, 10:1). The band for complex **5** had disappeared and been replaced by 11 minor bands. After 12 h, a single major band was observed with 5 minor bands of lower R_f. The solvent was removed under vacuum and the dark red residue was dissolved in CH_2Cl_2 (2 mL) and mounted on a 20 x 20 cm silica preparative TLC plate that plate was developed with CH_2Cl_2:MeOH, 15:1 (130 mL). When the major band had clearly separated, it was cut from the silica plate, and added to 50 mL of CH_2Cl_2 with 1 mL MeOH; this mixture was left stirring for 16 h. The red mixture was then filtered to remove the silica and the filtrate was reduced in volume to ~5 mL. Hexanes (30 mL) were then added and the resulting red precipitate was collected, washed with hexanes (2 x 5 mL) and dried at 78 °C under vacuum for 48 h. Yield: 0.038 g (51 %). ^{1}H NMR (*cis*-isomer, $CDCl_3$): δ 62.2, 44.6 (s, CH_3-ma); -1.5. -5.6 (s, H_5-Im); -15.5, -24.7 (s, H_2-Im). ^{1}H NMR (*trans*-isomer, $CDCl_3$): 60.0 (s, CH_3-ma); –3.7 (s, H_5-Im); -19.6 (s, H_2-Im). IR (KBr pellet): ν 3145 (N-H, m), 1603 (C=O, s), 1467 (s), 1263 (s). LR-MS (+LSIMS, thioglycerol): 488 (M^+), 420 (M^+ - Im), 352 (M^+ - 2 Im). CV (MeCN): $E_{1/2}$ ($Ru^{III/II}$) = -0.705 V. Λ_M (MeOH) = 119 $\Omega^{-1}cm^2mol^{-1}$. Anal. Calcd for $C_{19}H_{18}F_3N_4O_9SRu$: C, 35.85; H, 2.83; N, 8.81. Found: C, 35.92; H, 2.92; N, 8.73.

3.7.7 $[Ru(ma)_2(1MeIm)_2]CF_3SO_3 \cdot CH_2Cl_2$ (8)

To a red solution of **1** (0.080 g, 0.17 mmol) in EtOH (5 mL), triflic acid was added (0.028 g, 0.19 mmol) under N_2 and the solution stirred at r.t. for 1 h. After 1 h,

1MeIm was added (0.062 g, 0.76 mmol) and the solution was stirred for an additional 24 h. After 6 h the solution was checked by TLC (CH_2Cl_2:MeOH, 10:1): 6 bands were observed with the most intense being a red one at $R_f = 0.6$. After 18 h a similar analysis revealed two major bands, a red one at $R_f = 0.6$ and a less intense blue one at $R_f = 0.35$. After 24 h the solvent was removed under vacuum and the dark red residue was dissolved in CH_2Cl_2 (~2 mL) and mounted on a 20 x 20 cm silica preparative TLC plate that was developed with CH_2Cl_2:MeOH, 12:1 (130 mL). The red band was cut out, added to 50 mL of CH_2Cl_2 with 1 mL MeOH, and the mixture was left stirring for 16 h. Attempts to extract the blue band were unsuccessful. The red suspension was then filtered to remove the silica and the volume was reduced to ~3 mL. Hexanes (20 mL) were then added and the resulting red precipitate was collected, washed with hexanes (2 x 5 mL) and dried at 78 °C under vacuum for 48 h. Yield: 0.060 g (48 %). ^{1}H NMR ($CDCl_3$): δ 62.0 (br s, CH_3-ma); 13.4 (br s, CH_3-1MeIm); -3.8 br (s, H_5-1MeIm); -19.0 (br s, H_2-1MeIm). IR (KBr pellet): ν 3458 (m), 1601 (C=O, s), 1467 (s), 1263 (s), 1031 (s). LR-MS (+LSIMS, thioglycerol): 516 (M^+), 434 (M^+ - 1MeIm), 352 (M^+ - 2 (1MeIm)). CV (MeCN): $E_{1/2}$ ($Ru^{III/II}$) = -0.765 V. Λ_M (MeOH) = 109 $\Omega^{-1}cm^2mol^{-1}$. Anal. Calcd for $C_{21}H_{22}F_3N_4O_9SRu \cdot CH_2Cl_2$: C, 35.25; H, 3.20; N, 7.48. Found: C, 35.71; H, 3.22; N, 7.86.

3.7.8 [Ru(ma)(1MeIm)$_4$][CF_3SO_3]$_2$ (9)

To a red solution of **1** (0.067 g, 0.14 mmol) in EtOH (5 mL), triflic acid was added (0.054 g, 0.36 mmol) under N_2 and the solution stirred at r.t. for 1 h. After 1 h, 1MeIm was added (0.077 g, 1.1 mmol) and the solution was refluxed 48 h. After 24 h the solution was checked by TLC (CH_2Cl_2:MeOH, 10:1): 2 major bands were observed of approximately equal intensity; a red band at $R_f = 0.6$, and a blue band at $R_f = 0.35$. After 48 h, analysis revealed a major blue band ($R_f = 0.35$), several minor bands ($R_f = 0.2$ - 0.7), and a black spot ($R_f = 0$). The solvent was removed under vacuum and the dark blue residue was dissolved in CH_2Cl_2 (~1.5 mL) and mounted on a 20 x 20 cm silica preparative TLC plate that was developed with CH_2Cl_2:MeOH, 10:1 (130 mL). The blue band was cut out, added to 50 mL of CH_2Cl_2 with 2 mL MeOH, and the mixture was left stirring for 16 h. The blue mixture was then filtered to remove the silica and the volume was reduced to ~1 mL. Hexanes (10 mL) were then added and the resulting blue

precipitate was collected, washed with hexanes (2 x 5 mL) and dried at 78 °C under vacuum for 48 h. Yield: 0.055 g (46 %). ^{1}H NMR ($CDCl_3$): δ 81.6 (br s, C*H*$_3$-ma); 25.6, 20.4 (s, C*H*$_3$-1MeIm); -0.5, -5.7 (s, *H*$_5$-1MeIm); -18.4, -24.0 (s, *H*$_2$-1MeIm). IR (KBr pellet): ν 3137 (m), 1601 (C=O, s), 1546 (m), 1470 (m), 1265 (s), 1031 (s). LR-MS (+LSIMS, thioglycerol): 704 ($M^+ + CF_3SO_3$), 622 ($M^+ + CF_3SO_3$ - 1MeIm), 540 ($M^+ + CF_3SO_3$ - 2 1MeIm), 458 ($M^+ + CF_3SO_3$ - 3 1MeIm), 391 (M^+ - 2 1MeIm), 309 (M^+ - 3 1MeIm). CV (MeCN): $E_{1/2}$ ($Ru^{III/II}$) = -0.442 V. Λ_M (MeOH) = 273 $\Omega^{-1}cm^2mol^{-1}$. Anal. Calcd for $C_{24}H_{29}F_6N_8O_9S_2Ru$: C, 33.80; H, 3.40; N, 13.14. Found: C, 33.23; H, 3.34; N, 12.73.

3.7.9 [Ru(ma)$_2$(2MeIm)$_2$]CF$_3$SO$_3$ (10)

To a red solution of **1** (0.092 g, 0.193 mmol) in EtOH (5 mL), triflic acid was added (0.0320 g, 0.213 mmol) under N_2 and the solution stirred at r.t. for 1 h. After 1 h, 2MeIm was added (0.066 g, 0.805 mmol) and the solution was stirred for an additional 12 h. The solvent was then removed under vacuum and the dark red residue was dissolved in CH_2Cl_2 (~2 mL) and mounted on a 20 x 20 cm silica preparative TLC plate that was developed with CH_2Cl_2:MeOH, 20:1 (130 mL). The resulting single, red band was cut out, added to CH_2Cl_2 (50 mL), and the mixture was left stirring for 16 h. The red mixture was then filtered to remove the silica and the volume was reduced to ~2 mL. Hexanes (10 mL) were then added and the resulting red product was collected, washed with hexanes (2 x 5 mL) and dried at 78 °C under vacuum for 48 h. Yield: 0.063 g (56 %). ^{1}H NMR ($CDCl_3$): δ 67.0 (br s, C*H*$_3$-ma); 42.0 (br s C*H*$_3$-Im); -1.6 (br s, *H*$_5$-Im); -4.7 (br s, *H*$_4$-Im). IR (KBr pellet): ν 3216 (N-H, m), 1602 (C=O, s), 1447 (s), 1265 (s). LR-MS (+LSIMS, thioglycerol): 516 (M^+), 434 (M^+- 2MeIm), 352 (M^+-2 (2MeIm)). CV (MeCN): $E_{1/2}$ ($Ru^{III/II}$) = -0.844 V. Λ_M (MeOH) = 121 $\Omega^{-1}cm^2mol^{-1}$. Anal. Calcd for $C_{21}H_{22}F_3N_4O_9SRu$: C, 37.95; H, 3.31; N, 8.43. Found: C, 37.61; H, 3.38; N, 8.20.

3.7.10 [Ru(Ema)$_2$(metro)$_2$]CF$_3$SO$_3$ (11)

This complex was prepared using the same procedure as described for complex **3**, but using **2** instead of **1** (0.065 g, 0.125 mmol), triflic acid (0.0213 g, 0.141 mmol) and metro (0.094 g, 549 mmol). The green species for this reaction could not be isolated as

was the case with **4**. Yield: 0.0642 g (59 %). ^{1}H NMR (acetone-d_6): δ 65.3 (br s, CH_3CH_2-Ema); 32.2 (br s, CH_3-metro); -4.8 (br s, H_5-metro). IR (KBr pellet): ν 3439 (O-H, m), 1600 (C=O, s), 1560 ($N\text{-}O_{asym}$, m), 1367 ($N\text{-}O_{sym}$, m), 1265 (s). LR-MS (+LSIMS, thioglycerol): 722 (M^+), 551 (M^+ - metro), 380 (M^+ - 2 metro). CV (MeCN): $E_{1/2}$ (NO_2/NO_2^-) = -1.137 V, $E_{1/2}$ ($Ru^{III/II}$) = -0.568 V, $E_{1/2}$ ($Ru^{IV/III}$) = 0.967 V vs. SCE. Anal. Calcd for $C_{27}H_{32}F_3N_6O_{15}SRu$: C, 36.49; H, 3.86; N, 9.46. Found: C, 36.52; H, 3.72; N, 9.55.

3.7.11 $[Ru(Ema)_2(4MeIm)_2]CF_3SO_3$ (12)

To a red solution of **2** (0.060 g, 0.116 mmol) in EtOH (5 mL) was added triflic acid (0.0220 g, 0.146 mmol) under N_2 and the solution stirred at r.t. for 1 h. After 1 h, 4MeIm was added (0.038 g, 0.463 mmol) and the solution was stirred for an additional 16 h. After 3 h the solution was checked by TLC (CH_2Cl_2:MeOH, 10:1). A single major red band (R_f = 0.60) was present with a minor brown one (R_f = 0). After 16 h the solvent was removed under vacuum and the reddish-brown residue was dissolved in CH_2Cl_2 and mounted on a 20 x 20 cm silica preparative TLC plate that was developed with CH_2Cl_2:MeOH, 20:1 (130 mL). The major band was cut out, added to 50 mL of CH_2Cl_2:MeOH (49:1), and the mixture was stirred for 16 h. The red mixture was then filtered to remove the silica and the volume was reduced to ~1 mL. Hexanes (15 mL) were then added and the resulting dark red precipitate was collected, washed with hexanes (3 x 5 mL) and dried at 78 °C under vacuum for 48 h. Yield: 0.0449 g (56 %). ^{1}H NMR (CD_2Cl_2): δ 49.1 (br s, CH_3CH_2-Ema); 16.5 (br s, CH_3-4MeIm); -4.6 (br s, H_5-4MeIm); -19.0 (br s, H_2-4MeIm). IR (KBr pellet): ν 3439 (N-H, m), 1597 (C=O, s), 1547 (m), 1473 (m), 1259 (s), 1030 (s). LR-MS (+LSIMS, thioglycerol): 544 (M^+), 462 (M^+ - 4MeIm), 380 (M^+ - 2 (4MeIm)). CV (MeCN): $E_{1/2}$ ($Ru^{III/II}$) = -0.829 V. Anal. Calcd for $C_{23}H_{26}F_3N_4O_9SRu$: C, 39.88; H, 3.76; N, 8.09. Found: C, 39.48; H, 3.88; N, 7.93.

3.7.12 $[Ru(Ema)_2(2MeIm)_2]CF_3SO_3$ (13)

This complex was prepared using the same procedure as described for complex **12**, but using **2** (0.082 g, 0.158 mmol), triflic acid (0.0270 g, 0.179 mmol), and 2MeIm (0.051 g, 0.622 mmol). R_f = 0.55 for the major red band of **13**. Yield: 0.0629 g (58 %).

^{1}H NMR (CD_2Cl_2): δ 51.7 (br s, CH_3CH_2-Ema); 43.7 (br s, CH_3-2MeIm); -1.9 (br s, H_5-2MeIm); -5.2 (br s, H_4-2MeIm). IR (KBr pellet): ν 3463 (N-H, m), 1597 (C=O, s), 1548 (m), 1472 (m), 1260 (s), 1031 (s). LR-MS (+LSIMS, thioglycerol): 544 (M^+), 462 (M^+ - 2MeIm), 380 (M^+ - 2 (2MeIm)). CV (MeCN): $E_{1/2}$ ($Ru^{III/II}$) = -0.889 V. Anal. Calcd for $RuC_{23}H_{26}F_3N_4O_9S$: C, 39.88; H, 3.76; N, 8.09. Found: C, 39.71; H, 3.87; N, 7.82.

3.7.13 $[Ru(ma)_2(EF5)_2]CF_3SO_3 \cdot EtOH$ (14)

To a solution of **3** (0.104g, 0.175 mmol) in 5 mL EtOH under N_2 was added EF5 (0.106g, 0.351 mmol). This solution, on refluxing for 48 h, slowly became brown and finally blue. TLC showed that almost all of the EF5 had been consumed in the reaction and that there was one major blue band, R_f = 0 (CH_2Cl_2:MeOH, 10:1). A weak intensity pink band R_f = 0.6 was also observed. The solvent was reduced in volume to ~1 mL and CH_2Cl_2 was added (10 mL) to yield a blue precipitate that was collected, and dried at 78 °C under vacuum for 24 h. Yield: 0.098 g (51 %). ^{1}H NMR (CD_3OD): δ 59.2 (br s, CH_3-ma); -4.8 (br s, H_5-EF5); -16.1 (br s, H_4-EF5). ^{19}F NMR (CD_3OD): δ −3.52 (s, CF_3SO_3); -8.9 (br s, CF_2CF_3); -46.1 (br s, CF_2CF_3). IR (KBr pellet): ν 3423 (N-H, s), 2924 (C-H, m), 1686 (C=O, s), 1602 (C=O), 1548 (m), 1473 (m), 1264 (s), 1202 (s). LR-MS (+LSIMS, thioglycerol): 940 (M^+ - 16), 642 (M^+ - EF5 - 16), 352 (M^+ - 2 EF5). Anal. Calcd for $C_{29}H_{26}F_3N_4O_9SRu \cdot C_2H_6O$: C, 32.34; H, 2.61; N, 9.74. Found: C, 32.17; H, 2.52; N, 9.97.

3.7.14 $[Ru(ma)_2(2NO_2Im)_2]CF_3SO_3$ (15)

A solution of **1** (0.042 g, 0.088 mmol) in 5 mL EtOH and triflic acid (0.014 g, 0.093 mmol) was refluxed for 1 h under N_2; $2NO_2Im$ (0.040 g, 0.354 mmol) was then added and this solution was refluxed for 24 h. A blue precipitate that formed was then removed by filtration, washed with MeOH (2 x 5 mL) and dried under vacuum at 78 °C for 48 h. Yield: 0.017 g (27 %). IR (KBr pellet): ν 3431 (N-H, s), 2967 (C-H, m), 1653 (C=O, m), 1542 (m), 1491 ($N\text{-}O_{asym}$, s), 1367 ($N\text{-}O_{sym}$, s). Anal. Calcd for $C_{19}H_{16}F_3N_6O_{13}SRu$: C, 31.41; H, 2.20; N, 11.57. Found: C, 32.87; H, 2.32; N, 12.97.

3.7.15 $[Ru(ma)_2(4NO_2Im)_2]CF_3SO_3$ (16)

This complex was prepared using the same procedure as used for complex **15**, except using $4NO_2Im$ (0.041 g, 0.363 mmol) in place of $2NO_2Im$ with complex **1** (0.043 g, 0.090 mmol). Yield: 0.016 g (24 %). ^1H NMR (acetone-d_6): δ 63.8 (br s, CH_3-ma). IR (KBr pellet): ν 3471 (N-H, s), 2883, 2821 (C-H, m), 1556 (C=O, m), 1509 (m), 1496 ($N\text{-}O_{asym}$, s), 1380 ($N\text{-}O_{sym}$, s). Anal. Calcd for $C_{19}H_{16}F_3N_6O_{13}SRu$: C, 31.41; H, 2.20; N, 11.57. Found: C, 33.02; H, 2.37; N, 12.64.

3.7.16 $[Ru(ma)_2(3NO_2tri)_2]CF_3SO_3$ (17)

This complex was prepared using the same procedure as used for complex **15**, except using $3NO_2tri$ (0.044 g, 0.386 mmol) in place of $2NO_2Im$ with complex **1** (0.041 g, 0.086 mmol). Yield: 0.022 g (35 %). IR (KBr pellet): ν 3471 (N-H, m), 2883, 2821 (C-H, m), 1556 (C=O, m), 1509 (m), 1496 ($N\text{-}O_{asym}$, s), 1380 ($N\text{-}O_{sym}$, s). Anal. Calcd for $C_{19}H_{16}F_3N_6O_{13}SRu$: C, 28.02; H, 1.92; N, 15.38. Found: C, 30.06; H, 2.40; N, 16.47.

3.7.17 $[Ru(ma)_2(triF5)_2]CF_3SO_3$ (18)

This complex was prepared using the same procedure as used for complex **15**, except using triF5 (0.068 g, 0.224 mmol) in place of $2NO_2Im$ with complex **1** (0.041 g, 0.086 mmol). Yield: 0.032 g (34 %). IR (KBr pellet): ν 3435 (N-H, m), 2926 (C-H, m), 1601 (C=O, m), 1542 (m), 1466 ($N\text{-}O_{asym}$, m), 1371 ($N\text{-}O_{sym}$, w), 1264 (m). Anal. Calcd for $C_{27}H_{22}F_{13}N_{10}O_{15}SRu$: C, 29.29; H, 1.99; N, 12.66. Found: C, 29.43; H, 2.11; N, 12.24.

3.7.18 $[Ru(HMepyr)_3]Cl_3$ (19)

To a solution of $RuCl_3{\cdot}3H_2O$ (0.103 g, 0.394 mmol) in 10 mL H_2O was added HMepyr (0.164 g, 1.18 mmol). This solution was stirred for 15 min until it had turned dark purple in colour. The volume was reduced to ~2 mL and acetone (100 mL) was added. The resulting purple precipitate was collected, and dried under vacuum at 78 °C for 24 h. Yield: 0.227 g (92 %). IR (KBr pellet): ν 3419 (N-H, s), 1598 (C=O, m), 1497 (s), 1272 (s). Λ_M (H_2O) = 451 $\Omega^{-1}cm^2mol^{-1}$. Anal. Calcd for $C_{21}H_{27}N_3O_6Cl_3Ru$: C, 40.35; H, 4.32; N, 6.73. Found: C, 40.52; H, 4.47; N, 6.58.

3.8 References

(1) Greaves, S. J.; Griffith, W. P. *Polyhedron* **1988**, *7*, 1973.

(2) Nakamoto, K.; McCarthy, P. J. *Spectroscopy and Structure of Metal Chelate Compounds*; John Wiley & Sons, Inc.: New York, 1968.

(3) Harris, R. K.; Mann, B. E. *NMR and the Periodic Table*; Academic Press Inc.: New York, 1978.

(4) Lippard, S. J.; Berg, J. M. *Principles of Bioinorganic Chemistry*; University Science Books: Mill Valley, 1994.

(5) Anderson, C.; Beauchamp, A. *Can. J. Chem.* **1995**, *72*, 471.

(6) Anderson, C.; Beauchamp, A. *Inorg. Chim. Acta* **1995**, *233*, 33.

(7) Anderson, C. *Can. J. Chem.* **2001**, *79*, 1477.

(8) Anderson, C.; Beauchamp, A. *Inorg. Chem.* **1995**, *34*, 6065.

(9) Eaton, S. S.; Eaton, G. R.; Holm, R. H.; Muetterties, E. L. *J. Am. Chem. Soc.* **1973**, *95*, 1116.

(10) Nagao, Y.; Sano, S.; Ochiai, M. *Tetrahedron* **1990**, *46*, 3211.

(11) Huheey, J. E. *Inorganic Chemistry: Principles of Structure and Reactivity, third ed.*; Harper Collins Publishers: New York, 1983.

(12) Pavia, D. L.; Lampman, G. M.; Kriz, G. S. *Introduction to Spectroscopy*; Harcourt Brace College Publishers: Orlando, 1996.

(13) Banci, L.; Bertini, I.; Luchinat, C.; Pierattelli, R.; Shokhirev, N. V.; Walker, F. A. *J. Am. Chem. Soc.* **1998**, *120*, 8472.

(14) Evans, D. F. *J. Chem. Soc.* **1959**, 2003.

(15) Geary, W. J. *Coord. Chem. Rev.* **1971**, *7*, 81.

(16) Wu, A. *Synthesis and Characterization of Ruthenium Maltolato, Sulfoxide, and Nitroimidazole Complexes as Potential Anticancer Agents* , M. Sc. Dissertation, University of British Columbia: Vancouver, 2002.

(17) Baird, I. R. *Fluorinated Nitroimidazoles and Their Complexes: Potential Hypoxia-Imaging Agents* , Ph. D. Dissertation, University of British Columbia: Vancouver, 1999.

(18) Baird, I. R.; Skov, K. A.; James, B. R.; Rettig, S. J.; Koch, C. J. *Synth. Commun.* **1998**, *28*, 3701.

(19) Haszeldine, R. N. *J. Chem. Soc.* **1953**, 1548.

(20) Husted, D. R.; Ahlbrecht, A. H. *J. Am. Chem. Soc.* **1953**, *75*, 1605.

(21) McLafferty, F. W.; Turecek, F. *Mass Spectrometry*; University Science Books: Mill Valley, 1993.

(22) Domingues, M. R. M.; Marques, M. G. O. S.; Domingues, P.; Neves, M. G.; Cavaleiro, J. A. S.; Ferrer-Correia, A. J. *J. Am. Soc. Mass Spectrom.* **2001**, *12*, 381.

(23) Clarke, M. J. *Coord. Chem. Rev.* **2002**, *232*, 69.

Chapter 4

Synthesis and Characterization of Ru Complexes with 4,4'-Biimidazoles

4.1 Introduction

Although the coordination chemistry of 2,2'-biimidazole (Figure 4.1) with Ru and other transition metals has been extensively explored,[1-4] no complexes have been reported in the literature containing the analogous 4,4'-biimidazole ligand (biim). Since biim was first synthesized in 1994,[5] its only reported interaction with a transition metal ion was with Cu(II), to form *in situ* catalytic systems for making polymers from 2,6-dimethylphenol.[6] No complexes, however, were isolated or characterized *in situ*.

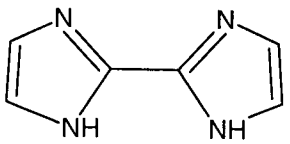

Figure 4.1 Molecular structure of 2,2'-biimidazole.

It has been suggested that some Ru complexes that show anticancer activity may act through a mechanism similar to that of cisplatin, in which dissociation of N-donor ligands such as imidazoles (instead of Cl^- as is the case for cisplatin), inside the cell, renders coordination sites available for DNA bases to bind the metal.[7] In such cases, however, any information contained in the imidazole ligand (e.g. radiolabels, fluorescent tags), is lost upon ligand dissociation. Bidentate imidazole ligands, with their ability to bind the metal centre more strongly through the chelate effect, could in principle remain bound *in situ* to a higher degree than their monodentate analogues and functional groups within the imidazole would then remain associated with the complex and could be targeted to the DNA. In this chapter, the synthesis and characterization of Ru complexes containing chelating 4,4'-biimidazole ligands will be discussed.

4.2 Synthesis and Reactions of 4,4'-Biimidazoles

4.2.1 Synthesis of 4,4'-Biimidazoles

These compounds were synthesized using modified procedures of those published by Cliff and Pyne.[5] The syntheses of both 4,4'-biimidazolium trifluoroacetate (H_2biim) and 2,2'-dimethyl-4,4'-biimidazolium trifluoroacetate (H_2Me_2biim) require 5 steps each, when conducted from the starting materials Im and 2MeIm, respectively (Figure 4.2). While the synthesis of H_2biim is straightforward, that of H_2Me_2biim required several modifications to the published procedure. Some of the refinements made for the

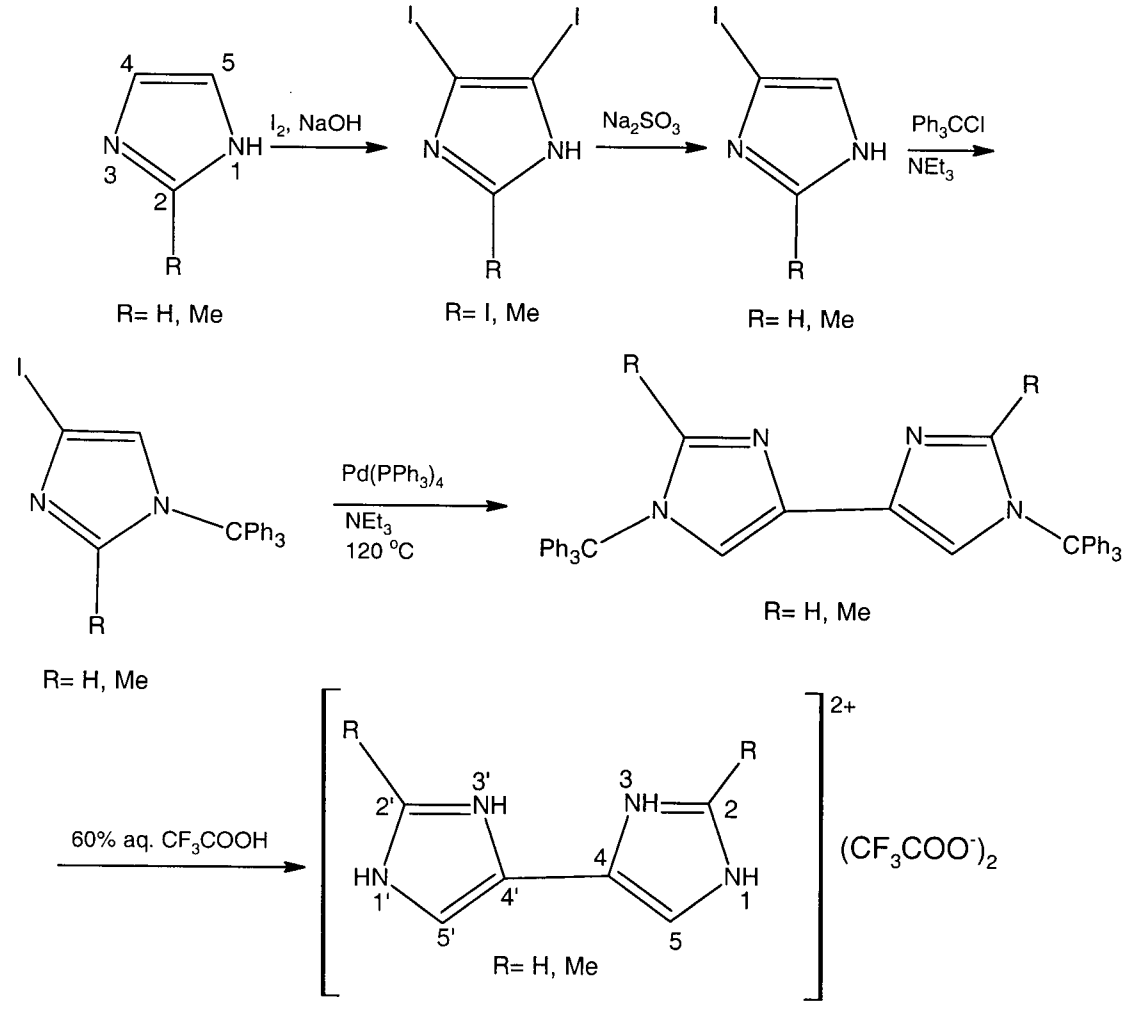

Figure 4.2 Synthesis for H_2biim and H_2Me_2biim.

synthesis of H_2Me_2biim were then applied to give a higher yield synthesis of H_2biim. In the first step of the H_2Me_2biim synthesis, formation of 4,5-diiodo-2-methylimidazole (Section 4.8.7), the reported rapid addition of I_2 to the biphasic $CHCl_3$/aq. NaOH system led to the formation of a brown emulsion that did not separate into two phases again over 24 h. To overcome this problem, the total amount of I_2 must be slowly added in 5 g increments over 20 min, allowing it to dissolve entirely after each addition. In the synthesis of H_2biim this modification was not required. A modified procedure was also adopted in the second step (Section 4.8.8), precipitation of the monoiodo-imidazole species, whereby addition of EtOH to the EtOH/water solution precipitated many of the Na salts which were then removed by filtration. The filtrate was then boiled to remove the EtOH and reduced in volume until the product, 4-iodo-2-methylimidazole, began to precipitate. This modification was also applied to give a higher yield synthesis of 4(5)-iodoimidazole (Section 4.8.3). As well, protection of the NH proton of 4-iodo-2-methylimidazole (third step), according to the literature that reported a 1:1, chlorotriphenylmethane:imidazole ratio, resulted in the isolation of a product containing a large excess of the trityl group (determined by ^1H NMR spectroscopy), presumably present as triphenylmethanol, which can form in H_2O under basic conditions.[8] Chromatographic separation of the product from this impurity could not be achieved because of their almost identical R_f values. By increasing the ratio of imidazole:trityl chloride to 1.5:1, it was found that 4-iodo-2-methyl-1-(triphenylmethyl)imidazole was isolable in pure form. The crude product containing the triphenylmethanol impurity does not undergo the next reaction step (Suzuki coupling); instead a black precipitate is formed which displays a single resonance for PPh_3 in the $^{31}P\{^1H\}$ NMR spectrum in $CDCl_3$ and no evidence for either the methyl or H(5) imidazole signals in the ^1H NMR spectrum.

It is important that the protected iodoimidazole species be pure before performing the coupling reaction. Purity was assessed by checking the relative integration values for the aromatic protons, Me protons, and H(5) proton of the imidazole species. As the residual $CHCl_3$ resonance in $CDCl_3$ overlaps with those of the aromatic signals, the ^1H NMR spectra were recorded in CD_2Cl_2 in order to avoid inaccurate integrations. The 15:3

aromatic region:methyl integration ratio for 4-iodo-2-methyl-1-(triphenylmethyl)-imidazole is consistent with the formulation.[5] A singlet at δ 6.72 (6.75 in $CDCl_3$, Section 4.8.9) integrating for one proton is observed for the imidazole H(5) proton. For 4-iodo-1-(triphenylmethyl)imidazole (Section 4.8.4), as the aromatic region overlaps the H(2) resonance of the imidazole, the aromatic region:H(5)-imidazole integration ratio is 16:1. The singlet for the H(5) proton at δ 6.87 (6.92 in $CDCl_3$, Section 4.8.4) is shifted out of the aromatic region.

The Suzuki coupling for preparing both 4,4'-biimidazoles was performed according to the published procedure;[5] however, considerably improved yield and purity in the desired product can be obtained (78 vs. 43% for 1,1'-bis(triphenylmethyl)-4,4'-biimidazole and 69 vs. 27% for 2,2'-dimethyl–1,1'-bis(triphenylmethyl)-4,4'-biimidazole) when the catalyst, $Pd(PPh_3)_4$, is freshly prepared[9] just prior to use. The protecting groups were removed in step 5 to afford H_2biim (Section 4.8.6) and H_2Me_2biim (Section 4.8.11) according to the reported procedures.[5]

X-ray quality crystals of 1,1'-bis(triphenylmethyl)-4,4'-biimidazole were grown from slow evaporation of a CH_2Cl_2 solution of the compound (Figure 4.3). The imidazole rings are essentially co-planar (the torsion angle between them is 0.8 degrees), and the molecule has a centre of inversion. The C4-C4' bond length is 1.448 Å, intermediate between that observed for the C4=C5 double bond (1.353 Å) and the single bond between C-Ph (1.544 Å) in the protecting group.

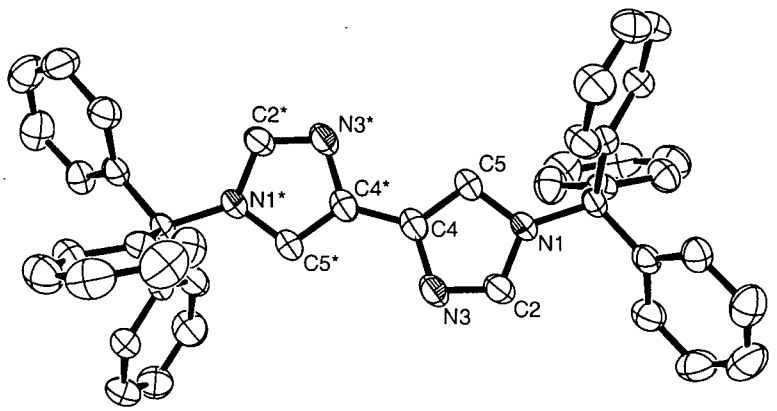

Figure 4.3 ORTEP diagram of 1,1'-bis(triphenylmethyl)-4,4'-biimidazole with 50 % probability thermal ellipsoids (see Appendix A5 for details).

4.2.2 Attempted Nitration of H_2biim

2-Nitroimidazoles are known to accumulate in hypoxic cells, and by nitrating H_2biim, one could potentially synthesize new hypoxic markers.[10] Such bidentate nitrobiimidazole ligands might also bind more strongly to metal centres than do nitroimidazoles, thus leading to increased stability of the nitroimidazole-type complexes *in situ*.

Nitration at the 4,4' and 5,5' positions of 2,2'-biimidazole using conc. HNO_3 has been reported, and 4,4',5,5'-tetranitro-2,2'-biimidazole has been characterized by X-ray diffraction.[11,12] The di-substituted derivative, 4,4'-dinitro-2,2'-biimidazole, has also been synthesized, again using conc. HNO_3 as the nitrating agent; however, its characterization solely by elemental analysis leaves some ambiguity as to the actual position of the nitro groups.[13] In this thesis work, attempts were made to nitrate H_2biim selectively at the 2,2' positions, to obtain a bidentate analogue of $2NO_2$Im. In the case of imidazole itself, nitration with conc. HNO_3 takes place preferentially at the H(4) position, and in the case of 4MeIm, the H(5) position is nitrated preferentially over the H(2) position.[14,15] In this thesis work, nitration of 1,1'-bis(triphenylmethyl)-4,4'-biimidazole at the 2,2'-positions was attempted following the procedure described by Davis *et al.* for the nitration of 1-(triphenylmethyl)imidazole at the 2-position using *n*-propyl nitrate.[16] 1,1'-Bis(triphenylmethyl)-4,4'-biimidazole, however, is insoluble in non-chlorinated solvents and no reaction was observed upon treatment of a suspension of this biimidazole in THF, dioxane or hexanes, with n-BuLi, even at refluxing temperatures. Attempts to synthesize the desired 2,2'-dinitro-4,4'-biimidazole via an alternate route, namely Suzuki coupling of two $2NO_2$Im derivatives, were also unsuccessful. 4-Bromo-1-methyl-2-nitroimidazole has been reported[17,18] but the described syntheses proceed in low yield (< 40 %). 4-Bromo-2-nitroimidazole has also been reported, but the pure compound could not be isolated from the reaction mixture.[17] It was also determined (Section 4.3) that the Suzuki coupling step does not tolerate a nitro functional group on the reactant.

4.3 Attempted Synthesis of 5,5'-Dinitro-3,3'-bi(1,2,4-triazole)

Work with 3-nitro-1,2,4-triazoles as potential anticancer agents suggests that nitrotriazoles can act in a manner similar to that of nitroimidazoles.[19] The synthesis of 5,5'-diamino-3,3'-bi(1,2,4-triazole) (bisAT) (Figure 4.4) has been reported in a patent,[20] and an improved procedure subsequently established by a member of our group led to bisAT being obtained in 76 % yield.[21] The synthesis of the corresponding 5,5'-dinitro-3,3'-bi(1,2,4-triazole) from bisAT using a described literature procedure[22] was unsuccessful. The procedure involved reacting the amino groups with conc. H_2SO_4 and $NaNO_2$ to form diazonium salts that can then undergo substitution reactions with $NaNO_2$ to form the dinitro species. Even after several extractions of the aqueous reaction mixture with ethyl acetate, no product was observed. Attempts to isolate the bitriazole from the aqueous mixture by neutralizing the solution, removing the solvent, and triturating the residue with ethyl acetate, yielded a solid which showed no evidence of any nitro groups by IR spectroscopy and no evidence for the bitriazole unit by ESI-MS. Conversely, the same procedure was successfully employed in the nitration of 3-amino-1,2,4-triazole-5-carboxylic acid (see Section 5.4) to yield the corresponding 3-nitro compound. Suzuki coupling of 3-iodo-5-nitrotriazole to afford the desired dinitro-bitriazole was also unsuccessful; the $Pd(PPh_3)_4$ catalyst may react with the nitro group itself, thus decomposing both reactant and catalyst.

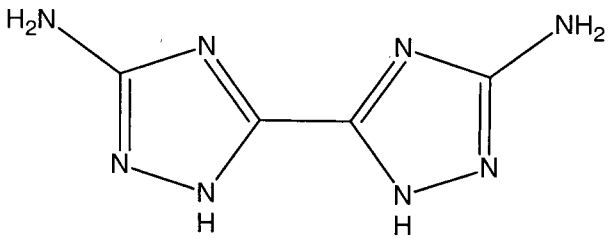

Figure 4.4 Molecular structure of 5,5'-diamino-3,3'-bi(1,2,4-triazole).

4.4 Ru-biim Complexes Synthesized from *cis*-$RuCl_2(DMSO)_4$

Complexes of the type $RuCl_2(DMSO)_2L_2$ (L = imidazole or nitroimidazole) have been synthesized from the precursor *cis*-$RuCl_2(DMSO)_4$ by our group,[23] although no crystal structures were performed to determine unambiguously the geometries of the complexes.[23] Similarly, the addition of one equiv. of a biimidazole to the same precursor was expected to lead to the displacement of 2 DMSO ligands with formation of the analogous complex containing one bidentate biimidazole in place of 2 monodentate imidazole ligands, and indeed a 1:1 reaction of H_2biim with $RuCl_2(DMSO)_4$ gives the monomeric $RuCl_2(DMSO)_2$(biim) species (**20**).

The ^1H NMR spectrum of a solution species formed from **20** in CD_3OD displays 4 resonances for the biimidazole protons indicating that each of the two rings inhabits a different chemical environment (Figure 4.5c, this region of the spectrum is identical for isolated and *in situ* formed **20**); four different resonances are also detected for the DMSO methyl groups, indicating that each of them is inequivalent in solution. Only the all cis-isomer (Figure 4.6) in the solid state (as precursor of the solution species), perhaps accounts for these observations. Figure 4.5a shows the resonances for the free ligand, H_2biim, in CD_3OD to show how the spectrum of the ligand changes upon coordination to the metal centre (Figure 4.5c). The conductivity of **20** in MeOH (127 $\Omega^{-1}cm^2mol^{-1}$), is in the range for a 1:1 electrolyte[24] thus showing that one Cl^- ligand is dissociated in solution. An all cis structure has been demonstrated crystallographically for the similar complex $RuCl_2(DMSO)_2$(1,2-dimethylimidazole)$_2$,[25] this finding contrasts, however, with those from our group for a related compound containing a chelating sulfoxide, *trans*-$RuCl_2$[*R,R*-1,2-bis(ethylsulfinyl)ethane](metro)$_2$, in which the chloride ligands are mutually trans in the solid state structure as determined by X-ray diffraction, although the solution ^1H NMR spectrum in D_2O shows a mixture of cis- and trans-isomers.[26]

The ^1H-^1H COSY NMR spectrum of **20** shows correlation between the two DMSO singlets at δ 2.29 and 3.01 and between those at δ 3.23 and 3.49 (Figure 4.7), each pair corresponding to the two Me groups within one DMSO ligand. Similarly, the resonances for the H(5) and H(2) imidazole protons on each ring also correlate with each

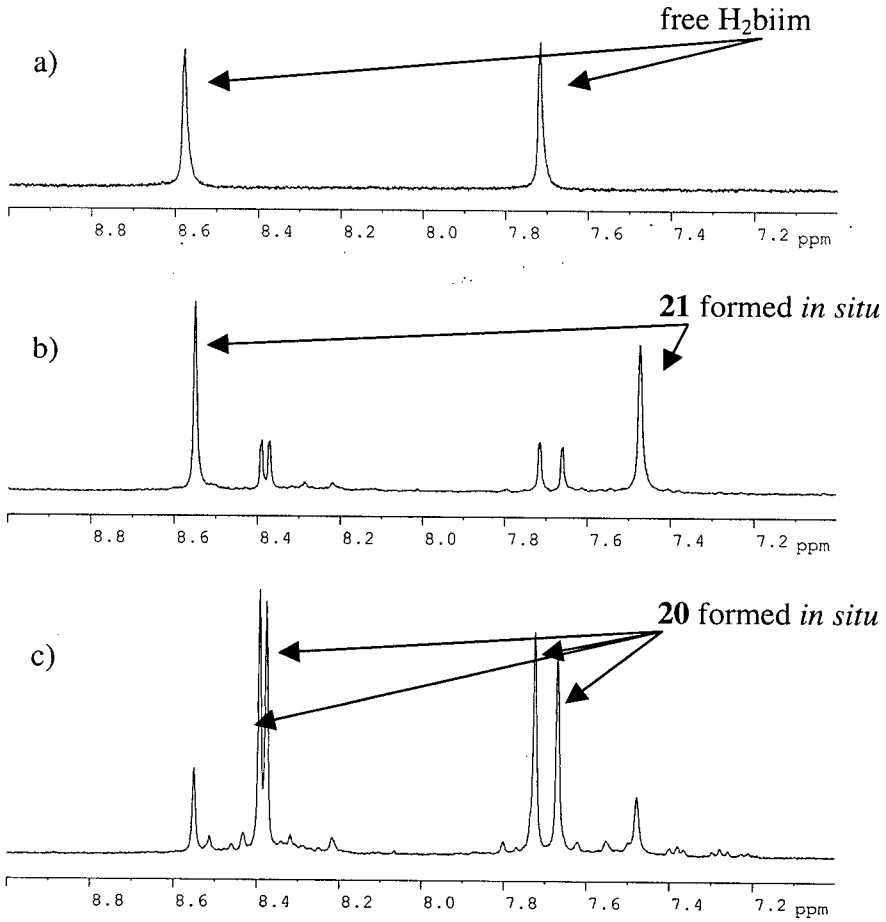

Figure 4.5 ^{1}H NMR spectra (300 MHz, 298 K) in CD_3OD showing the imidazole protons of a) free H_2biim in CD_3OD, b) 1:2 H_2biim:$RuCl_2(DMSO)_4$ after 4 h at 65 °C in CD_3OD, and c) 1:1 H_2biim:$RuCl_2(DMSO)_4$ after 4 h at 65 °C in CD_3OD. The spectra for isolated **21** and **20** in CD_3OD are identical to those in (b) and (c), respectively, in this region.

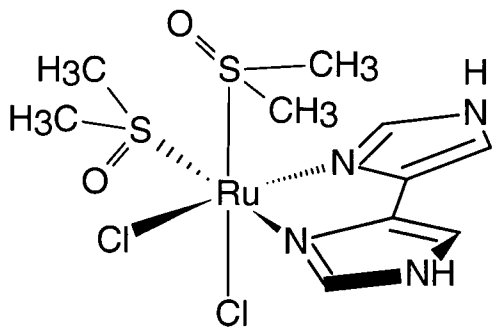

Figure 4.6 Proposed solid state structure for $RuCl_2(DMSO)_2$(biim).

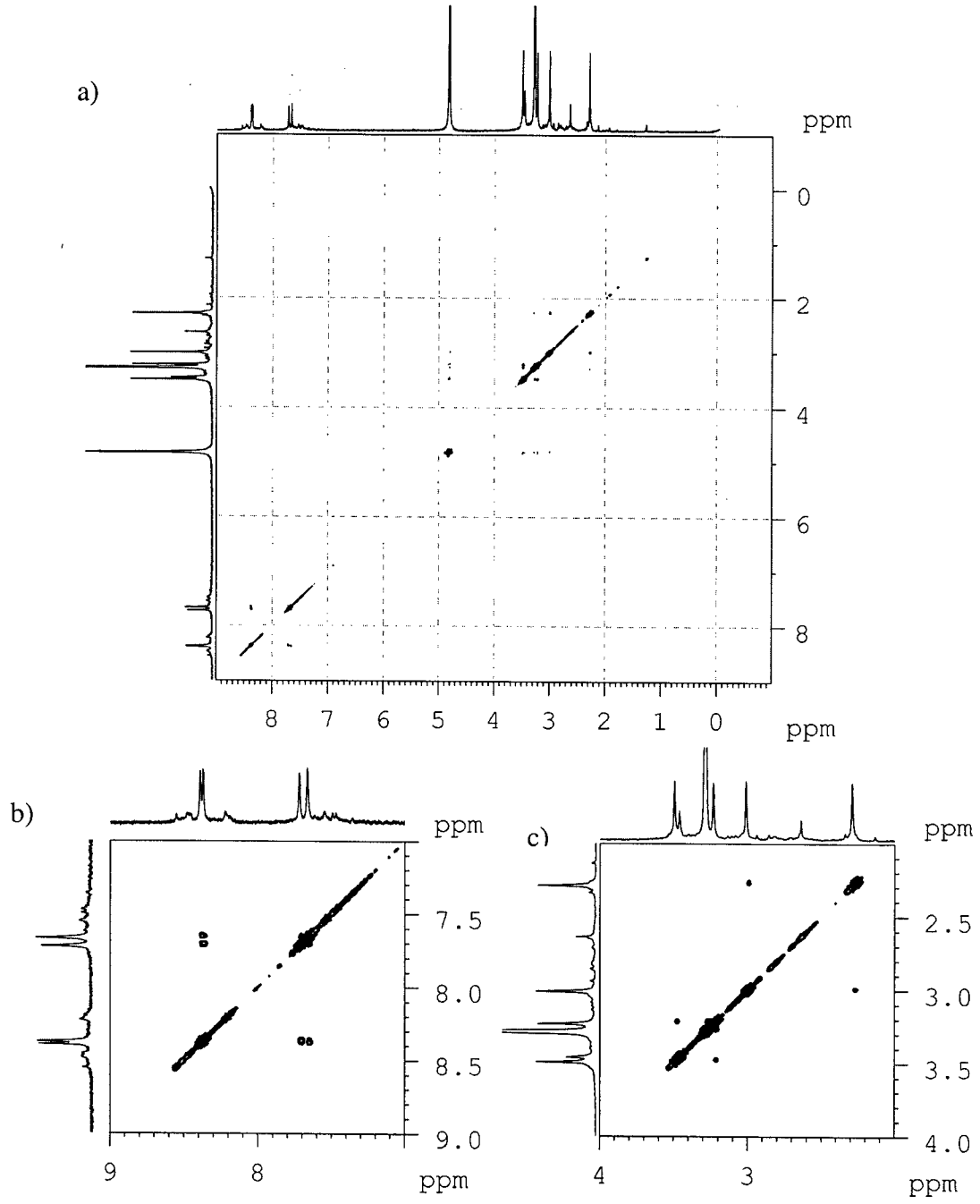

Figure 4.7 ^{1}H-^{1}H COSY NMR spectrum (300 MHz, 298 K) of **20** in CD_3OD. a) Complete spectrum. b) Expansion showing correlation of imidazole protons. c) Expansion showing correlation of DMSO protons. Small peaks at δ 3.38 and 2.65 are due to $Ru_2Cl_4(DMSO)_4$(biim) (**21**) (see text).

other, showing that the signals at δ 8.39 and 7.67 belong to the H(2) and H(5) of one ring and those at δ 8.37 and 7.72 to the H(2) and H(5) on the other ring, respectively.

From the ^{1}H NMR spectrum , it appears as if there is one S-bound DMSO (δ 3.23 and 3.49) and one O-bound DMSO (δ 2.29 and 3.01) present; however, the IR shows two strong S=O stretches at 1071 and 1067 cm^{-1}, both in the region for S-bound DMSO. No IR bands are observed for O-bound DMSO (typically 900 – 1000 cm^{-1} for Ru(II) complexes).[27a] The possible upfield shift of the resonances at δ 3.01 and 2.29 may arise from an interaction between the Me protons on the S-bound DMSO (cis to biim) and the π–system of biim.

The mass spectrum of this complex (Figure 4.8) is consistent with the proposed formulation, clearly showing the M^+ species, as well as fragments corresponding to the loss of one Cl^- and to the subsequent loss of one DMSO ligand. Elemental analysis was also consistent with the formulation. By increasing the H_2biim:Ru ratio to 2:1, it was expected that two biim ligands might displace all 4 DMSO ligands of the starting material as is the case when $RuCl_2(DMSO)_4$ is reacted with pyridine to afford *cis*-$Ru(pyridine)_4Cl_2$;[28] however, only **20** could be isolated from this reaction. Attempts to further substitute **20** with a 5-fold excess of H_2biim were also unsuccessful.

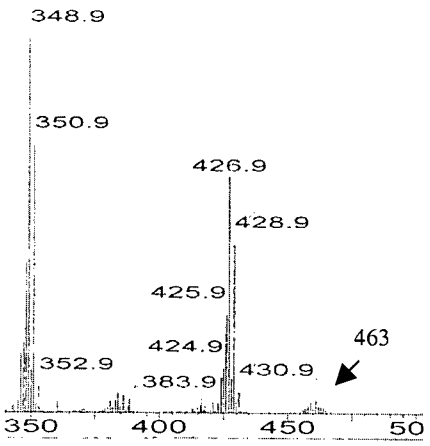

Figure 4.8 Mass spectrum of $RuCl_2(DMSO)_2$(biim) (**20**): the most intense group of signals is for (M^+ – Cl – DMSO). The parent peak is the small cluster centred at 463.

Reaction of H_2biim with $RuCl_2(DMSO)_4$ (H_2biim:Ru, 1:2) results in the formation of a bimetallic complex, $Ru_2Cl_4(DMSO)_4$(biim) (**21**). Elemental analysis supports this formulation and an [M^+ - Cl] fragmentation splitting pattern characteristic for this formulation is observed in the mass spectrum (see Figure 5.4 for description of splitting pattern differences between Ru and Ru_2). The splitting pattern differs from that of **20** as it clearly shows the isotopic distribution for a unit with two Ru atoms present. The ^{1}H NMR spectrum of a solution form of **21**, made *in situ* in CD_3OD, displays two major resonances for the H(2) and H(5) protons of the bound biim (Figure 4.4b). This indicates that each set of protons within the two rings is in an equivalent chemical environment, and is consistent with a solid-state formulation in which the biim ligand is situated trans to two bridging chlorides (Figure 4.9). In the region of the ^{1}H NMR spectrum corresponding to the DMSO protons, two major singlets are present, one for free DMSO at δ 2.65 and one at δ 3.38 for bound DMSO, integrating in a 1:1 ratio. A set of weaker intensity resonances is also detected in this region; however, they account for < 5 % of the total integration of the DMSO resonances. The presence of a resonance corresponding to free DMSO in a 1:1 ratio with that of bound DMSO indicates that two of the four DMSO ligands formulated for this species, are displaced in CD_3OD. The conductivity of a MeOH solution of isolated **21** (112 $\Omega^{-1}cm^2mol^{-1}$) is in the range for a 1:1 electrolyte, suggesting that one chloride is also dissociated in this solvent.[24] The IR data show two strong stretches for S=O at 1081 and 1086 cm^{-1}, in the region for S-bound DMSO.

From the ^{1}H NMR data, two possible solution structures (Figures 9a and b) can account for the resonances observed in CD_3OD; these two representations contain equivalent DMSO ligands and equivalent biim rings. Four possible solid state structures (Figure 9c-f) can give rise to the two solution structures (Figures 9a and b); 9e and 9f are preferred, as 9c and 9d are formally Ru(I/III) spceies. Bimetallic species containing a Ru(I) metal centre are uncommon and almost exclusively involve a metal-metal bond.[27b] Precedence for the loss of DMSO and Cl^- ligands in solution has been shown with $RuCl_2(DMSO)_4$ which rapidly loses one O-bound DMSO ligand upon dissolution in D_2O, and then slowly loses a Cl^-.[29]

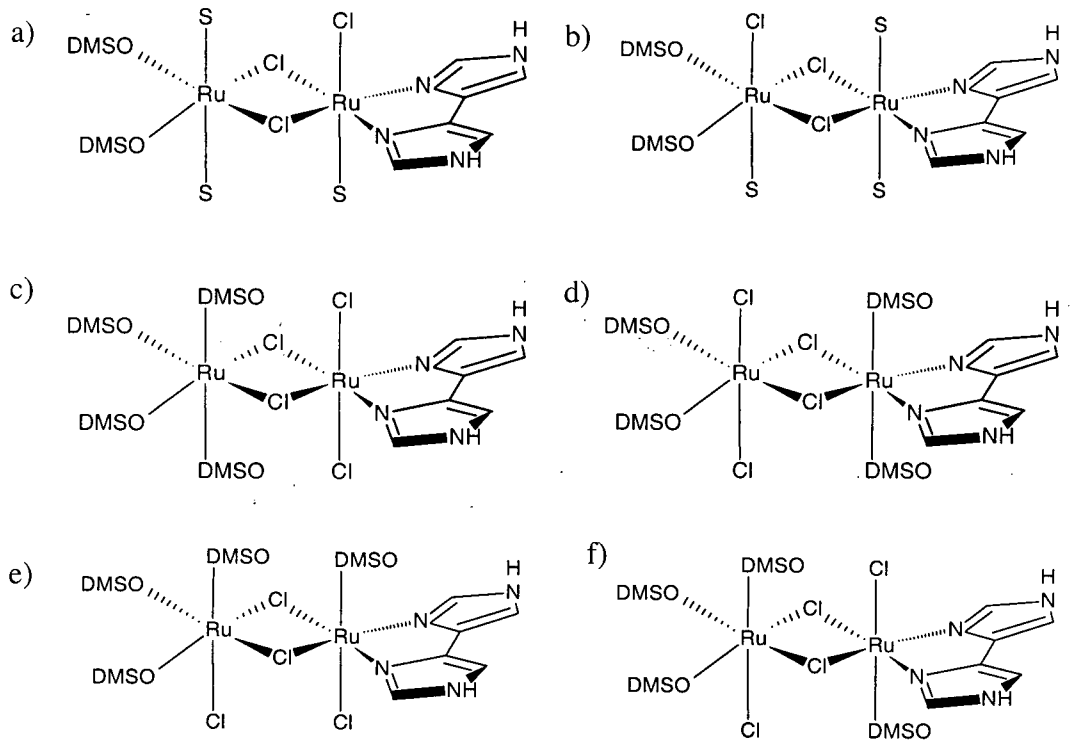

Figure 4.9 Structures (a) and (b) represent possible solution structures for **21**, where all DMSO ligands are S-bound and S = CD_3OD. Structures (c), (d), (e) and (f) represent the four corresponding solid state structures which could give rise to (a) and (b) in CD_3OD; again all DMSO ligands are S-bound.

Similar to the biim system, carrying out a 1:1 reaction with H_2Me_2biim and $RuCl_2(DMSO)_4$ gives formation of the monomeric $RuCl_2(DMSO)_2(Me_2biim)$ species (**22**). ESI-MS and elemental analysis agree with the proposed formulation, and the IR spectrum shows two distinct bands for S-bound DMSO (ν = 1091 and 1099 cm^{-1}).

The ^1H NMR spectrum of **22** in CD_3OD is more complicated than that for the corresponding biim complex, **20**, in that 3 resonances are observed for the H(5) protons of the Me_2biim ligand: δ 7.65, 7.46, and 7.25 (Figure 4.10b). The integrations at δ 7.65 and 7.25 are the same, while that at δ 7.47 is 1.4 times greater. Three resonances are also observed for the methyl protons of the Me_2biim ligand: δ 1.66, 1.59, and 1.58 (Figure 4.10c). The integration of the resonances at δ 1.58 and 1.59 are the same, and each of

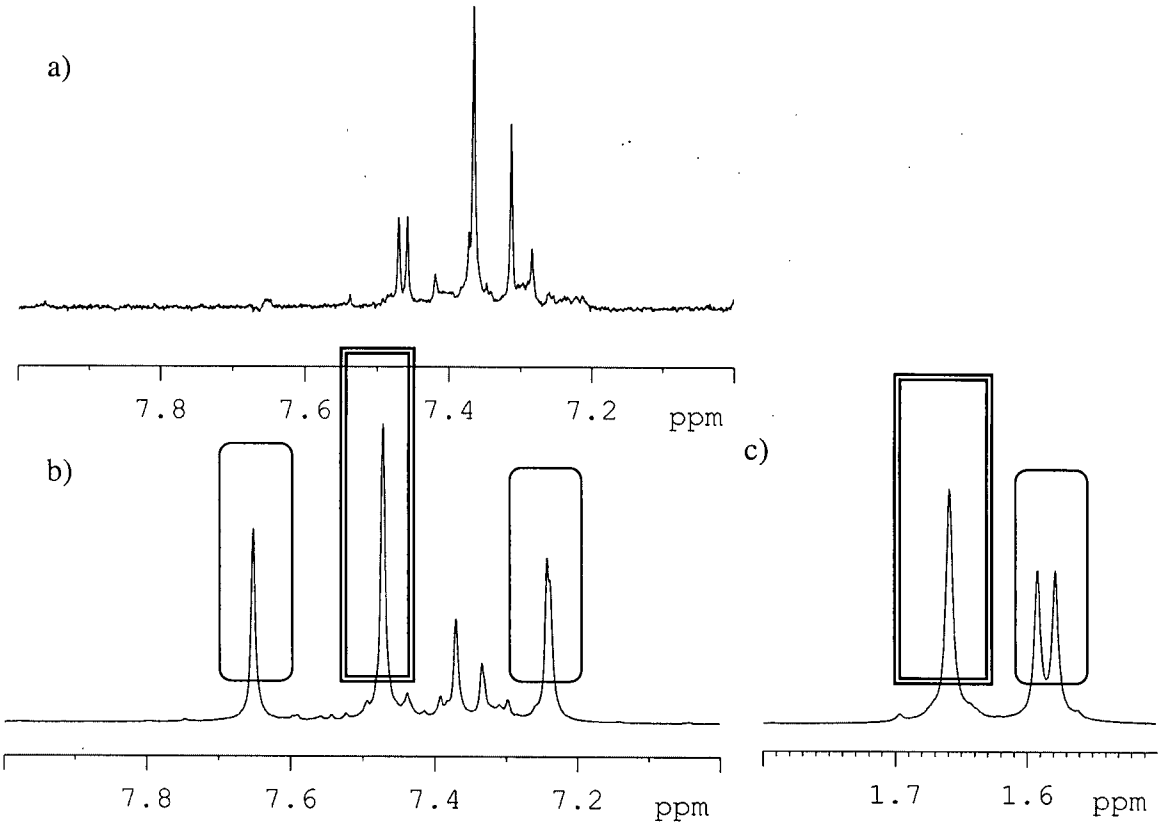

Figure 4.10 ^{1}H NMR data (300 MHz, 298 K) for Me_2biim complexes. a) H(5) protons of **23** (see text) in CD_3OD. b) H(5) protons for **22** in CD_3OD; weak resonances for **23** are observed as an impurity. c) Corresponding methyl signals for Me_2biim of **22** in CD_3OD. Resonances for single isomers are highlited in (b) and (c).

these integrates in a 3:1 ratio with those at δ 7.65 and 7.25, suggesting that these four resonances correspond to a single isomer in which the two rings of the Me_2biim ligand are inequivalent. The remaining two 1:3 resonances at δ 7.47 and 1.66 correspond to a second isomer in which the two Me_2biim rings are equivalent. In the ^{1}H NMR spectrum of **22** there are overlapping signals for bound DMSO between δ 3.51-2.23. The IR data suggest only S-bound DMSO is present; however, from the ^{1}H NMR spectrum, no interpretation of the DMSO proton resonances can be made, other than that there is no evidence for free DMSO.

The conductivity of **22** in MeOH solution (132 $\Omega^{-1}cm^2\ mol^{-1}$) is in the range for a 1:1 electrolyte,[24] suggesting that one Cl^- is dissociated, probably from each isomer. The

isomer with the equivalent Me_2biim rings must have trans-chloride and cis-DMSO ligands in the solid state structure, and when one Cl^- dissociates and is replaced by MeOH in solution, the equivalence of the two Me_2biim rings is preserved. Two solid state structures can be proposed for the other isomer with inequivalent Me_2biim rings. The first, a cis-Cl, trans-DMSO species, could produce the observed resonances in the ^1H NMR spectrum upon dissociating on chloride in CD_3OD; however, precedence in the literature for such a species with other N-donor ligands could not be found. It is more probable that this species is a cis-Cl, cis-DMSO species as is the case for the analogous biim complex, **20**. In the case of the reported $RuCl_2(DMSO)_2(2MeIm)_2$, the monodentate analogue of **22**, the ^1H NMR spectrum (in $CDCl_3$) is consistent with an all cis-structure.[30]

When H_2Me_2biim and $RuCl_2(DMSO)_4$ are reacted in a 1:2 ratio, a bimetallic species analogous to that seen with biim (**21**) is formed. Elemental analysis and mass spectral data of the isolated complex are consistent with the formulation $Ru_2Cl_4(DMSO)_4(Me_2biim)$ (**23**). Although the parent peak is not seen, as for **21**, intense signals for $[M^+ - Cl]$ (785), and then fragments for the subsequent loss of 1, 2, and 3

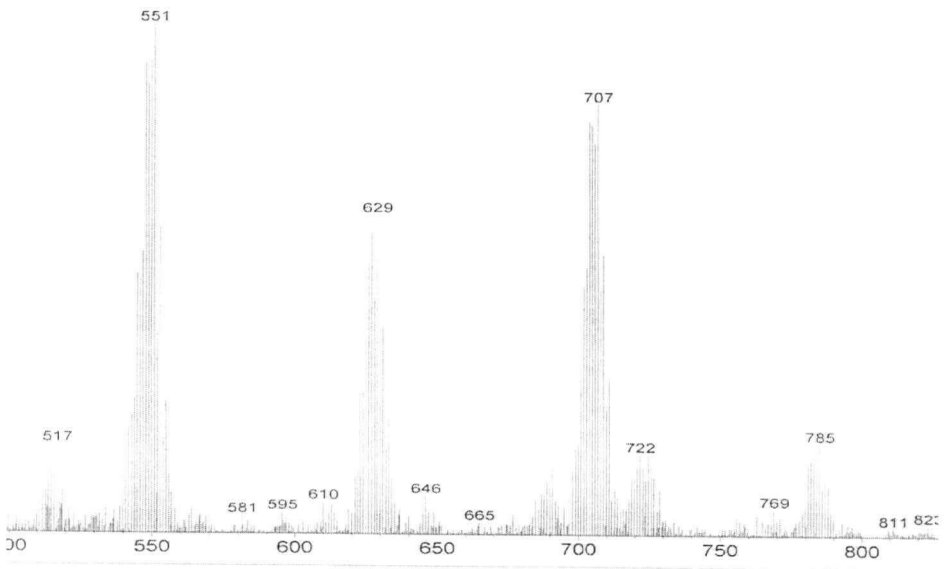

Figure 4.11 Mass spectrum for $Ru_2Cl_4(DMSO)_4(Me_2biim)$ (**23**); the most intense group of signals is for $[M^+ - Cl - 3\ DMSO]$, centred at 551.

DMSO ligands are observed (Figure 4.11), all exhibiting an isotopic splitting pattern consistent with the presence of two Ru atoms in the complex. In the ^{1}H NMR spectrum in CD_3OD, two major resonances are observed for the H(5) proton at δ 7.38 and 7.33 (Figure 4.10a), that at δ 7.38 being roughly twice the size of that at δ 7.33; this suggests the presence of two isomers with equivalent Me_2biim rings. There is also a pair of 1:1 singlets at δ 7.47 and 7.46, implying the presence of one isomer with inequivalent Me_2biim rings. Between δ 3.55 and 2.54, numerous overlapping and unresolved resonances are observed for the Me resonances of the DMSO and Me_2biim ligands, including an intense resonance for free DMSO. As for **21**, the conductivity of **23** in MeOH solution (97 $\Omega^{-1}cm^2\ mol^{-1}$) is in the range for a 1:1 electrolyte,[24] suggesting replacement of a terminal Cl ligand by MeOH.

4.5 Complexes Synthesized from $Ru(ma)_3$

In Chapter 3, the synthesis and characterization of Ru(III) complexes of the type $[Ru(ma)_2(L)_2]CF_3SO_3$, where L is an N-bound imidazole or triazole derivative, were presented. With the same experimental procedure used for **14** (Section 3.3.5), analogous complexes of the type $[Ru(ma)_2(L)]CF_3SO_3{\cdot}2H_2O$, where L = biim (**24**) or Me_2biim (**25**), were synthesized. These were characterized by elemental analysis, mass spectrometry, and IR and NMR spectroscopies. The ^{1}H NMR spectrum of **24** in $CDCl_3$ (Figure 4.12a) shows a single resonance for the maltolato Me groups. As the biim rings are "locked" in a cis-configuration, the maltolato ligands must be coordinated so that the "same type" oxygen from each maltolato is trans to biim (Figure 4.13).

In the corresponding ^{1}H NMR spectrum of **25**, two resonances are detected for the maltolato Me groups as well as two resonances for the Me_2biim Me groups. This is due either to inequivalent oxygen atoms bound trans to Me_2biim (Figure 4.14b), or to the complex existing in solution as a combination of two different isomers with equivalent oxygen atoms bound trans to Me_2biim (Figure 4.14b and c). Although the integrations of signals in paramagnetic ^{1}H NMR spectra are generally poor, the near equal intensities and

peak widths of the two maltolato Me signals might indicate that they are for a single species, thus favouring the structure in Figure 4.14a.

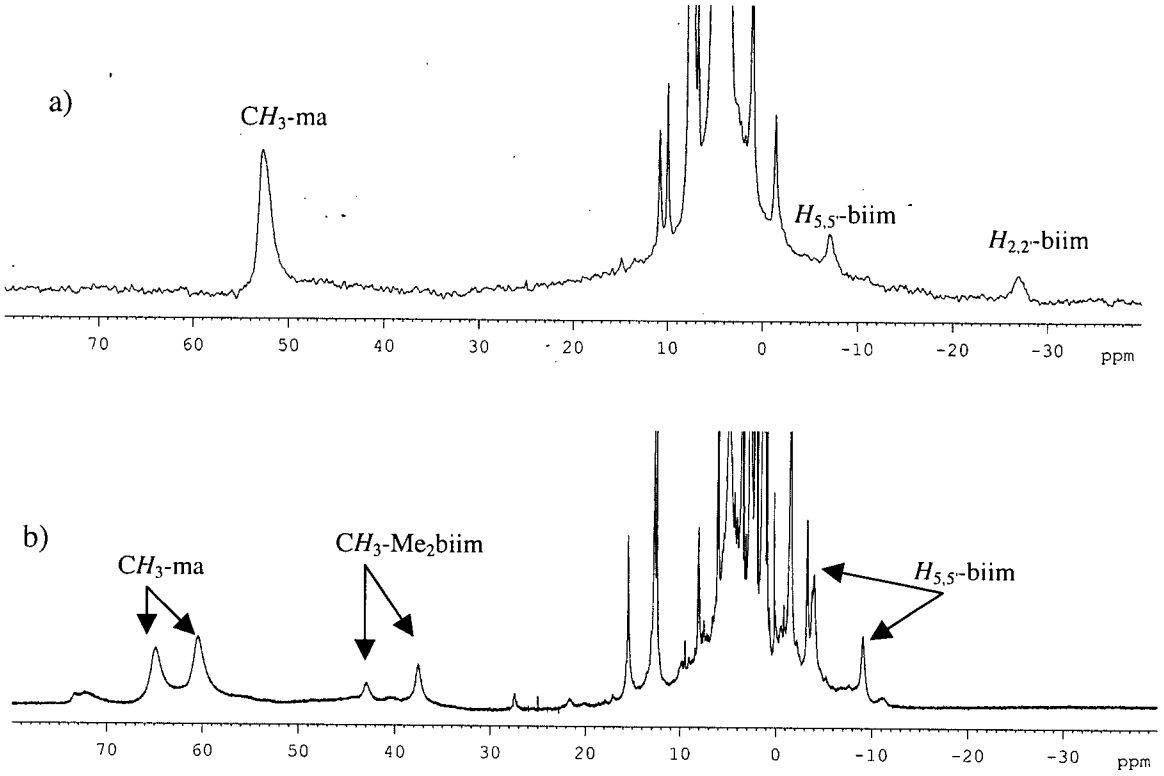

Figure 4.12 ^{1}H NMR spectra of **24** and **25**. a) ^{1}H NMR spectrum (300 MHz, 298 K) of **24** in $CDCl_3$. b) ^{1}H NMR spectrum (300 MHz, 298 K) of **25** in $CDCl_3$.

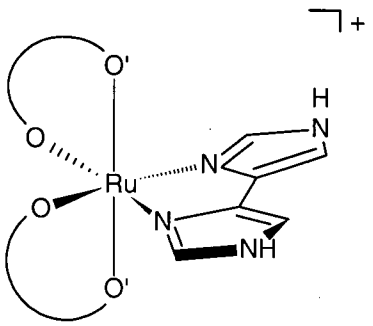

Figure 4.13 Proposed structure for the cation of **24**.

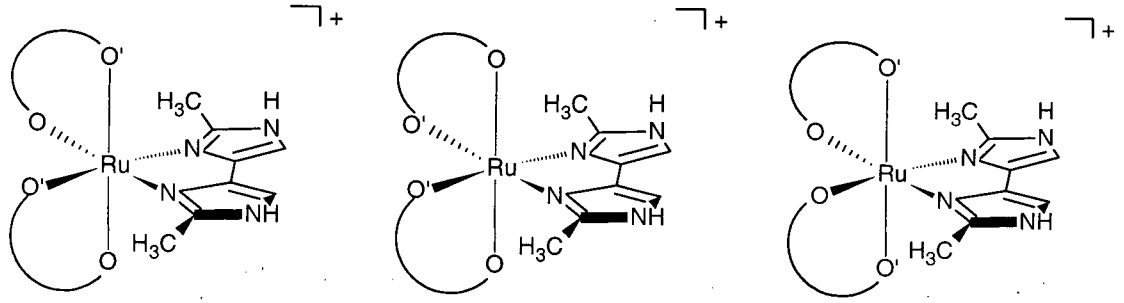

(a) (b) (c)

Figure 4.14 Three possible structures for the cation of **25**.

The elemental analyses for both complexes give formulations with two hydrated H_2O molecules. The IR spectra show strong, broad bands at 3514 and 3550 cm^{-1} for O-H for **24** and **25**, respectively, consistent with the presence of H_2O in the solids. The cyclic voltammograms of the complexes in MeCN reveal markedly more positive reduction potentials than for the analogous bis(imidazole) complexes (**7** and **10**, Table 4.1). The difference in cis/trans geometry of the bis(imidazole) and biimidazole complexes can not account for such a large difference in potential; however, the more conjugated π-system of the biimidazole ligands may make these ligands better π-acceptors and thus increase the reduction potentials for **24** and **25**.

Table 4.1 Ru (III/II) reduction potentials for the biimidazole complexes **24** and **25**, compared with those for **7** and **10**.

Complex	Ru (III/II) Reduction Potential in MeCN vs. SCE (mV)
cis-$[Ru(ma)_2(biim)][CF_3SO_3]$ (**24**)	-101
cis-$[Ru(ma)_2(Me_2biim)][CF_3SO_3]$ (**25**)	-35
$[Ru(ma)_2(Im)_2][CF_3SO_3]$ (**7**)	-705
trans-$[Ru(ma)_2(2MeIm)_2][CF_3SO_3]$	-844

4.6 Complexes Synthesized from $[Ru(DMF)_6](CF_3SO_3)_3$

$[Ru(DMF)_6](CF_3SO_3)_3$ has been previously used in this group as a precursor for the synthesis of Ru(II) hexakis(imidazole) complexes.[31] The same general synthetic

procedure with MeOH as solvent was employed in the synthesis of the analogous complexes $[Ru(L)_3](CF_3SO_3)_2$, where L = biim (**26**) and Me_2biim (**27**), which were isolated in 72 and 83 % yield, respectively. Four equivalents of ligand are required for the syntheses, whereby one equivalent of H_2biim or H_2Me_2biim reduces the Ru centre (III→II).[32] Although MeOH can also act as a reducing agent,[33] the same synthetic reaction with H_2biim performed *in situ* in CD_3OD showed no trace of free H_2biim after 12 h by ^{1}H NMR spectroscopy, but instead the spectrum of the product solution showed two singlets at δ 8.92 and 7.84, not present in the spectrum for the isolated complex, **26**. These resonances may be due to a bis-biimidazole species (such as that shown in Figure 4.15), resulting from one equivalent of H_2biim being oxidized by the Ru(III). This type of Ru(III)→Ru(II) reduction in the presence of excess Im has been reported to occur in water at r.t. over several days.[32] For both **26** and **27**, the mass spectra clearly show both the $Ru(L)_3^+$ peaks (M^+ for **26** and **27** is defined as $[Ru(L)_3][CF_3SO_3]_2$, see Sections 4.9.7 and 4.9.8) as well as the $[Ru(L)_3][CF_3SO_3]^+$ peaks (L = biim or Me_2biim, respectively). The ^{1}H NMR spectrum of the **26** displays 2 equal intensity singlets at δ 8.37 for H(2) and 7.62 for H(5). In the corresponding ^{1}H NMR spectrum of **27**, two resonances at δ 7.43 for H(5) and 2.54 for the Me-group, integrating for 1 and 3 protons, respectively, are detected.

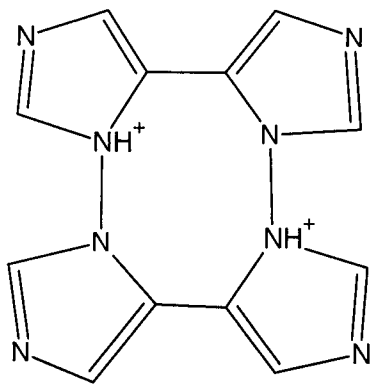

Figure 4.15 Possible structure for a bis-biimidazole species, from reduction of the Ru centre.

4.7 Complexes Synthesized from $RuCl_3 \cdot 3H_2O$

$RuCl_3 \cdot 3H_2O$ was also used as a precursor for the synthesis of Ru-biim and Ru-Me_2biim complexes; these were synthesized via the 'Ru blue' solution, formed upon reduction of $RuCl_3 \cdot 3H_2O$ by H_2 in MeOH.[34] Addition of 2 equivalents of H_2biim to such a solution gives a complex formulated as $[Ru(Hbiim)_2Cl_2]Cl_2$ (**28**), which was isolated as a brown precipitate from a MeOH/acetone solution and characterized by ^1H NMR spectroscopy and ESI-MS. Only two broad singlets at δ 8.59 and 7.52 are observed in

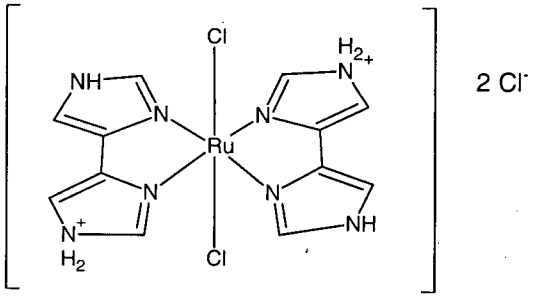

Figure 4.16 Molecular structure for **28**.

the ^1H NMR spectrum in D_2O, suggesting that the biim ligands are trans with 4 chemically equivalent heterocyclic rings. The two additional protons in the complex presumably exchange mutually in solution, thus broadening the proton resonances of H(2) and H(5). A potentiometric titration of a solution of **28** in H_2O at r.t. with 0.01 M $AgNO_3$ solution confirmed the presence of the two non-coordinated chlorides, the solution conductivity increased sharply after 2 equivalents of $AgNO_3$ had been added, suggesting that two equivalents of chloride had been titrated. MS on the resulting solution, after the titration was completed, revealed that the complex was still intact (M^+ at 440) with two Cl^- bound. Titration of a solution of **28** in H_2O with 0.01 M NaOH gave two equivalence points for the two titratable protons with pK_a values of 7.7 and 8.5. The conductivity of an aqueous solution of **28** was 265 Ω^{-1} cm^2 mol^{-1}, in the range for a 2:1 electrolyte.[35]

The corresponding "Ru blue" reaction with H_2Me_2biim in place of H_2biim gave a product consistent with the formulation for $[Ru(HMe_2biim)(Me_2biim)_2]Cl_3$ (**29**). Again, only two broad signals are observed in the ^1H NMR spectrum in D_2O, one for the H(5)

protons, and one for the Me protons, consistent with three equivalent Me_2biim ligands with the extra proton presumably exchanging between all 3 of them. Titration of a solution of **29** in H_2O with $AgNO_3$ confirmed the presence of 3 unbound Cl^- ions while titration with NaOH showed that there was one titratable proton with a pK_a of 8.8. The conductivity of **29** in H_2O (385 Ω^{-1} cm^2 mol^{-1}) is in the range for a 3:1 electrolyte.[35] Unlike **28** where two biim ligands can adopt a trans-configuration, 2 Me_2biim ligands are unlikely to be mutually trans due to the steric hindrance of the 2-methyl groups, and this results in the ready formation of the all-cis tris-substituted product.

4.8 Experimental Preparation of Biimidazoles

4.8.1 Sources of Materials

The sources of solvents, some reagents and Ru precursors are reported in Chapter 2. $Pd(PPh_3)_4$ was prepared according to a literature procedure.[9] $PdCl_2$ was obtained from Colonial Metals Inc. I_2, NEt_3, $Na_2S_2O_3$ and Na_2SO_3 (not listed in Chapter 2) were all purchased from Fisher Scientific.

4.8.2 2,4,5-Triiodoimidazole

This compound was synthesized according to literature procedures.[36-39] To a solution of I_2 (112.0 g, 441 mmol) in $CHCl_3$ (400 mL) was added Im (10.0 g, 147 mmol) and 2 M NaOH (400 mL). This mixture formed a two-phase system with the organic phase containing the I_2 on the bottom, and the top aqueous phase being colourless. The mixture was stirred for 3 h at r.t. after which time the bottom phase had become colourless and the top phase had turned pink. The phases were separated and the organic phase was discarded. To the aqueous phase was added $Na_2S_2O_3$ (50.0 g) to prevent colouration of the product, before the aqueous phase was neutralized to pH 7.0 with AcOH. The resulting white precipitate was collected, washed with cold water (2 x 10 mL) and dried at 80 °C for 16 h. Yield: 46.42 g (70 %). FAB-MS: 446 (M^+), 320 (M^+ - I), 193 (M^+ - 2 I).

4.8.3 4(5)-Iodoimidazole

This compound was synthesized from a modified literature procedure.[36] To a solution of Na_2SO_3 (70.0 g, 555 mmol) in 30 % aq. EtOH (1.0 L), 2,4,5-triiodoimidazole (30.0 g, 67.3 mmol) was added. The mixture was heated at 50 °C for 1 h at which time the solid had completely dissolved affording a yellow solution that was refluxed for 24 h. The condenser was then removed and the solution concentrated until a precipitate started to form. The flask was then immediately removed from the heating mantel and allowed to cool slowly to r.t. The resulting pale yellow crystals were removed by filtration and dried under vacuum for 24 h. Yield: 8.42 g (64 %). ^{1}H NMR (acetone-d_6): δ 10.20 (br s, 1H, Im-H_1), 7.80 (s, 1H, Im-H_2), 7.28 (s, 1H, Im-H_5). FAB-MS: 194 (M^+) , 67 (M^+ - I). Anal. Calcd for $C_3H_3N_2I$: C, 18.56; H, 1.55; N, 14.43. Found: C, 18.52; H, 1.61; N, 14.21.

4.8.4 4-Iodo-1-(triphenylmethyl)imidazole

This compound was synthesized from a literature procedure.[36] To a solution of 4-iodoimidazole (4.00 g, 20.6 mmol) in DMF (35 mL) was added chlorotriphenylmethane (5.75 g, 20.6 mmol). The solution was degassed for 10 min and then stirred at r.t. for 1 h under N_2. To this solution was then added NEt_3 (2.30 g, 22.7 mmol) and the resulting mixture was stirred for 24 h. The mixture was then poured into an ice slurry (150 mL) and the precipitate was collected via filtration. The solid was dried under vacuum at 78 °C for 24 h. Yield: 6.23 g (69 %). ^{1}H NMR ($CDCl_3$): δ 7.37-7.29 (m, 10H, Im-H_2 and Ar*H*), 7.14-7.09 (m, 6H, Ar*H*), 6.92 (d, 1H, Im-H_5). FAB-MS: 436 (M^+), 243 (CPh_3), 194 (M^+ - CPh_3). Anal. Calcd for $C_{22}H_{17}N_2I$: C, 60.55; H, 3.90; N, 6.42. Found: C, 60.69; H, 4.11; N, 6.18. The ^{1}H NMR data for this compound agree with those reported.[36]

4.8.5 1,1'-Bis(triphenylmethyl)-4,4'-biimidazole

This compound and the following six compounds were synthesized via modified literature procedures.[5] A solution of 4-iodo-1-(triphenylmethyl)imidazole (4.00 g, 9.17 mmol) in DMF (15 mL) was degassed with Ar for 10 min. To this solution was added $Pd(PPh_3)_4$ (450 mg, 0.39 mmol) and NEt_3 (1.96 g, 18.4 mmol). The flask was then

wrapped in foil and heated to 120 °C for 48 h in the dark. The solution was cooled to r.t., and the resulting precipitate was collected by filtration, rinsed with acetone (3 x 5 mL), and dried under vacuum for 24 h at 78 °C. Yield: 2.21 g (78 %). ^{1}H NMR ($CDCl_3$): δ 7.37 (d, 2H, $H_{2,2'}$-biim), 7.32-7.29 (m, 18H, Ar*H*), 7.27 (d, 2H, $H_{5,5'}$-biim), 7.20-7.17 (m, 12H, Ar*H*). FAB-MS: 618 (M^+), 243 (CPh_3). Anal. Calcd for $C_{44}H_{34}N_4$: C, 85.43; H, 5.50; N, 9.06. Found: C, 85.61; H, 5.43; N, 8.75. The ^{1}H NMR and MS characterization data for this compound and for the next six compounds agree with those reported.[5]

4.8.6 4,4'-Biimidazolium trifluoroacetate (H_2biim)

1,1'-Bis(triphenylmethyl)-4,4'-biimidazole (2.00 g, 3.23 mmol) was dissolved in 50% CF_3CO_2H/H_2O (50 mL) and the solution was stirred at r.t. for 12 h. The resulting white precipitate (CPh_3OH) was then removed by filtration and the yellow filtrate was evaporated under vacuum to yield a bright yellow oil. Addition of MeCN (2.0 mL) yielded a white solid that was collected, rinsed with acetone (3 x 5 mL) and dried under vacuum at 78 °C for 24 h. Yield: 0.96 g (82 %). ^{1}H NMR (CD_3OD): δ 8.74 (s, 2H, $H_{2,2'}$-biim), 7.79 (s, 2H, $H_{5,5'}$-biim). ESI-MS: 135 (M^+). Anal. Calcd for $C_{10}H_8N_4F_6O_4$: C, 33.15; H, 2.21; N, 15.47. Found: C, 33.24; H, 2.12; N, 15.68.

4.8.7 4,5,-Diiodo-2-methylimidazole

To a solution of 2MeIm (10.0 g, 122 mmol) in 2 M NaOH (300 mL) was added $CHCl_3$ (300 mL). I_2 (62.0 g, 244 mmol) was then added to this mixture slowly over 20 min, adding 5 g at a time and waiting until it had completely dissolved before adding more. Adding the I_2 too quickly led to the formation of a brown foam, from which the final product could not be separated. The two-phase system was then stirred for an additional 3 h at which time the lower phase had become colourless. The phases were separated and the aqueous phase neutralized according to the procedure described in Section 4.8.2. Yield: 28.10 g (69 %). ^{1}H NMR ($CDCl_3$): δ 10.72 (br s, Im-H_1), 2.48 (s, Im-CH_3). FAB: 335 (M^+), 209 (M^+ - I).

4.8.8 4(5)-Iodo-2-methylimidazole

4,5,-Diiodo-2-methylimidazole (20.0 g, 59.9 mmol) was dissolved in 700 mL H_2O. To this solution was added Na_2SO_3 (60.0 g, 476 mmol) and EtOH (300 mL). This mixture was heated for 1 h at 50 °C until the sulfite had completely dissolved. The yellow solution was then refluxed for 24 h, cooled to r.t., and 500 mL of EtOH were added. The resulting white precipitate (sodium salts) was removed by filtration and the filtrate was concentrated until a fine precipitate started to form. The filtrate was then cooled and the resulting yellow crystals were collected, washed with cold H_2O (2 x 5 mL) and dried at 78 °C for 24 h. Yield: 6.82 g (55 %). ^{1}H NMR ($CDCl_3$): δ 11.08 (br s, 1H, Im-H_1), δ 7.08 (s, 1H, Im-H_5), 2.44 (s, 3H, Im-CH_3). FAB: 209 (M^+).

4.8.9 4-Iodo-2-methyl-1-(triphenylmethyl)imidazole

4(5)-Iodo-2-methylimidazole (4.69 g, 22.5 mmol) was added to a solution of chlorotriphenylmethane (4.18 g, 15.0 mmol) in DMF (40.0 mL). Under 1 atm N_2, NEt_3 (1.95 g, 19.2 mmol) was added and the solution was stirred at r.t. for 24 h. The mixture was then poured onto an ice slurry (150 mL) and the resulting precipitate was collected and dried under vacuum for 24 h at 78 °C. Yield: 4.52 g (67 %). ^{1}H NMR ($CDCl_3$): δ 7.36-7.33 (m, 9H, Ar*H*), 7.14-7.09 (m, 6H, Ar*H*), 6.75 (s, 1H, Im-H_5), 1.58 (s, 3H, Im-CH_3). FAB: 450 (M^+), 243 (CPh_3), 209 (M^+ - CPh_3). Anal. Calcd for $C_{23}H_{19}N_2I$: C, 61.33; H, 4.22; N, 6.22. Found: C, 61.25; H, 4.17; N, 6.02.

4.8.10 2,2'-Dimethyl -1,1'-bis(triphenylmethyl)-4,4'-biimidazole

4-Iodo-2-methyl-1-triphenylmethylimidazole(4.00 g, 8.89 mmol) was dissolved in DMF (15 mL), and the solution was degassed with Ar for 10 min. To this was added $Pd(PPh_3)_4$ (550 mg, 0.440 mmol) and NEt_3 (1.80 g, 17.8 mmol). The flask was then sealed under N_2 and wrapped in foil to exclude all light, and the reaction mixture then heated at 120 °C for 48 h. The flask was then cooled to r.t. and the resulting precipitate was collected, washed with acetone (3 x 5 mL), and dried under vacuum at 78 °C for 24 h. Yield: 1.97 g (69 %). ^{1}H NMR ($CDCl_3$): δ 7.31-7.29 (m, 18H, Ar*H*), 7.22 (s, 2H, $H_{5,5'}$-Me_2biim), 7.17-7.15 (m, 12H, Ar*H*), 1.60 (s, 6H, CH_3-Me_2biim). LSIMS: 647 (M^+), 243

(CPh_3). Anal. Calcd for $C_{46}H_{38}N_4$: C, 85.45; H, 5.88; N, 8.67. Found: C, 85.34; H, 5.75; N, 8.48.

4.8.11 2,2'-Dimethyl-4,4'-biimidazolium trifluoroacetate (H_2Me_2biim)

2,2'-Dimethyl–1,1'-bis(triphenylmethyl)-4,4'-biimidazole (1.90 g, 2.94 mmol) was suspended in 60 % CF_3CO_2H/H_2O (50 mL), and the mixture was then refluxed for 6 h and cooled to r.t., when the resulting precipitate was removed by filtration. The filtrate was evaporated to give a yellow oil. MeCN (3 mL) was added affording a white precipitate that was collected, washed with acetone (3 x 5 mL), and dried under vacuum for 24 h at 78 °C. Yield: 0.89 g (78 %). ^{1}H NMR (CD_3OD): δ 7.65 (s, 2H, $H_{5,5'}$-Me_2biim), 2.72 (s, 6H, CH_3-Me_2biim). ESI-MS: 163 (M^+). Anal. Calcd for $C_{12}H_{12}N_4F_6O_4$: C, 36.92; H, 3.08; N, 14.36. Found: C, 37.19; H, 2.98; N, 14.38.

4.9 Experimental Syntheses of Complexes

4.9.1 *cis*-$RuCl_2(DMSO)_2$(biim) (20)

To a yellow solution of $RuCl_2(DMSO)_4$ (0.070 g, 0.15 mmol) in MeOH (10 mL), H_2biim was added (0.054 g, 0.15 mmol) under N_2 and the mixture refluxed for 4 h. The solvent was then reduced in volume to ~1 mL, followed by the addition of 10 mL of acetone that yielded a yellow precipitate that was collected, washed with acetone (2 × 5 mL), and dried in vacuo. Yield: 0.059 g (88 %). ^{1}H NMR (CD_3OD): δ 8.39, 8.37 (s, 2H, $H_{2,2'}$-biim), 7.72, 7.67 (s, 2H, $H_{5,5'}$-biim), 3.49 (s, 3H, CH_3SOCH_3), 3.23 (s, 3H, CH_3SOCH_3), 3.01 (s, 3H, CH_3SOCH_3), 2.29 (s, 3H, CH_3SOCH_3). IR (KBr pellet): ν 3451 (s, N-H), 1067 (s, S=O), 1020 (m). ESI-MS (MeOH): 463 (M^+), 427 (M^+ - Cl), 349 (M^+ - Cl - DMSO). Λ_M (MeOH) = 127 $\Omega^{-1}cm^2mol^{-1}$. Anal. Calcd for $C_{10}H_{18}Cl_2N_4O_2S_2Ru$: C, 25.87; H, 3.90; N, 12.12. Found: C, 25.67; H, 3.98; N, 11.99.

4.9.2 $Ru_2Cl_4(DMSO)_4$(biim) (21)

This complex was synthesized following the procedure outlined in Section 4.9.1, but using H_2biim (0.026 g, 0.074 mmol) and $RuCl_2(DMSO)_4$ (0.071 g, 0.15 mmol). Yield: 0.042 g (73 %). ^{1}H NMR (CD_3OD): δ 8.55 (s, 2H, $H_{2,2'}$-biim), 7.48 (s, 2H, $H_{5,5'}$-

biim), 3.46 (s, 6H, CH_3SOCH_3), 2.65 (s, 6H, free DMSO). IR (KBr pellet): ν 3449 (br s, N-H), 1086 (s, S=O), 1081 (s, S=O), 1013 (m). ESI-MS (MeOH): 757 (M^+ - Cl), 679 (M^+ - Cl - DMSO). Λ_M (MeOH) = 112 $\Omega^{-1}cm^2mol^{-1}$. Anal. Calcd for $C_{14}H_{30}Cl_4N_4O_4S_4Ru_2$: C, 21.27; H, 3.80; N, 7.09. Found: C, 21.36; H, 4.00; N, 7.51.

4.9.3 $RuCl_2(DMSO)_2(Me_2biim)$ (22)

This complex was synthesized following the procedure outlined in Section 4.9.1, but using H_2Me_2biim (0.058 g, 0.15 mmol) and $RuCl_2(DMSO)_4$ (0.072 g, 0.15 mmol). Yield: 0.064 g (90 %). ^1H NMR (CD_3OD): δ 7.65, 7.47, 7.25 (s, 2H, $H_{5,5'}$-Me_2biim), 3.54-3.32, 3.25-2.73, 2.32 (s, 12H, CH_3SOCH_3), 1.66, 1.59, 1.58 (s, 6H, CH_3-Me_2biim). IR (KBr pellet): ν 3455 (N-H), 1420 (s), 1091 (s, S=O), 1099 (s, S=O), 1014 (m). ESI-MS (MeOH): 491 (M^+), 455 (M^+ - Cl), 377 (M^+ - Cl - DMSO). Λ_M (MeOH) = 132 $\Omega^{-1}cm^2mol^{-1}$. Anal. Calcd for $C_{12}H_{22}Cl_2N_4O_2S_2Ru$: C, 29.39; H, 4.49; N, 11.43. Found: C, 29.58; H, 4.64; N, 11.82.

4.9.4 $Ru_2Cl_4(DMSO)_4(Me_2biim)$ (23)

This complex was synthesized following the procedure outlined in Section 4.9.1, but using H_2Me_2biim (0.029 g, 0.074 mmol) and $RuCl_2(DMSO)_4$ (0.070 g, 0.15 mmol). Yield: 0.049 g (81 %). ^1H NMR (CD_3OD): δ 7.47, 7.46, 7.38, 7.33 (s, $H_{5,5'}$-Me_2biim), 3.55-3.31, 3.05-2.75, 2.59, 2.54 (s, CH_3SOCH_3 and CH_3-Me_2biim), 2.65 (s, free DMSO). IR (KBr pellet): ν 3457 (s, N-H), 1086(s, S=O), 1081 (s, S=O). ESI-MS (MeOH): 785 (M^+ - Cl), 707 (M^+ - Cl - DMSO), 629 (M^+ - Cl – 2 DMSO), 551 (M^+ - Cl – 3 DMSO). Λ_M (MeOH) = 97 $\Omega^{-1}cm^2mol^{-1}$. Anal. Calcd for $C_{16}H_{34}Cl_4N_4O_4S_4Ru_2$: C, 23.47; H, 4.16; N, 6.85. Found: C, 23.58; H, 4.19; N, 6.65.

4.9.5 $[Ru(maltolato)_2(biim)]CF_3SO_3 \cdot 2H_2O$ (24)

To a solution of $[Ru(maltolato)_2(EtOH)_2]CF_3SO_3$ (**3**) (0.088g, 0.15 mmol) in 5 mL EtOH was added H_2biim (0.055g, 0.15 mmol), and the mixture was refluxed under N_2 for 24 h, when it slowly turned brown. After 24 h, the solvent was removed under vacuum and the brown residue was redissolved in acetone; this was cooled to 0 °C and then filtered through Celite (2g). The filtrate was warmed to r.t. and reduced in volume

to 2 mL. Hexanes (15 mL) were then added to yield a brown precipitate that was collected, washed with hexanes (2 x 5 mL) and dried at 78 °C under vacuum for 48 h. Yield 0.054 g (58 %). ^{1}H NMR ($CDCl_3$): δ 52.7 (br s, CH_3-ma), -7.0 (br s, $H_{5,5'}$-biim), -26.2 (br s, $H_{2,2'}$-biim). IR (KBr pellet): ν 3514 (O-H, s), 2899 (C-H, m), 1602 (C=O, m), 1548 (m), 1467 (m), 1264 (m), 1031 (s). LR-MS (+LSIMS, thioglycerol): 486 (M^+), 361 (M^+ - ma). Λ_M (MeOH) = 106 $\Omega^{-1}cm^2mol^{-1}$. CV (MeCN): $E_{1/2}$ ($Ru^{III/II}$) = -0.101 V. Anal. Calcd for $C_{19}H_{16}F_3N_4O_9SRu{\cdot}2H_2O$: C, 34.02; H, 2.99; N, 8.36. Found: C, 34.11; H, 2.89; N, 8.18.

4.9.6 [Ru(maltolato)$_2$(Me$_2$biim)]CF$_3$SO$_3$·2H$_2$O (25)

This complex was prepared using the same procedure of section 4.9.5 but using **3** (0.090 g, 0.15 mmol) and H_2Me_2biim (0.060 g, 0.15 mmol). Yield 0.061 g (61 %). ^{1}H NMR ($CDCl_3$): δ 64.8, 60.6 (br s, CH_3-ma), 42.1, 37.5 (br s, CH_3-Me_2biim), -9.1 br (s, $H_{5,5'}$-Me_2biim). IR (KBr pellet): ν 3550 (O-H, s), 2916 (C-H, m), 1602 (C=O, m), 1542 (m), 1468 (m), 1263 (m), 1030 (s). ESI-MS: 514 (M^+), 389 (M^+ - ma). Λ_M (MeOH) = 127 $\Omega^{-1}cm^2mol^{-1}$. CV (MeCN): $E_{1/2}$ ($Ru^{III/II}$) = -0.035 V vs. SCE. Anal. Calcd for $C_{21}H_{20}F_3N_4O_9SRu{\cdot}\ 2H_2O$: C, 36.00; H, 3.43; N, 8.00. Found: C, 35.92; H, 3.28; N, 8.17.

4.9.7 [Ru(biim)$_3$][CF$_3$SO$_3$]$_2$ (26)

To a solution of $[Ru(DMF)_6][CF_3SO_3]_3$ (0.083 g, 0.085 mmol) in MeOH (5 mL) was added H_2biim (0.12 g, 0.34 mmol). This yellow solution was refluxed; after 10 h, the solution had turned green and after 24 h had become very dark green. The solvent was removed under vacuum and the green residue was redissolved in acetone (10 mL); the mixture was filtered through Celite, and the filtrate was then reduced in volume to ~1 mL. To this was added hexanes (8 mL) to yield a green precipitate that was collected, washed with hexanes (2 x 5 mL), and dried under vacuum at 78 °C for 24 h. Yield: 0.034 g (60 %). ^{1}H NMR (CD_3OD): δ 8.37 (s, 6H, $H_{2,2'}$-biim), 7.62 (s, 6H, $H_{5,5'}$-biim). ESI-MS (MeOH): 652 (M^+ - CF_3SO_3), 502 (M^+ - 2 CF_3SO_3), 369 (M^+ - 2 CF_3SO_3 - biim). Λ_M (MeOH) = 243 $\Omega^{-1}cm^2mol^{-1}$. Anal. Calcd for $C_{20}H_{18}F_6N_{12}O_6S_2Ru$: C, 29.96; H, 2.25; N, 20.97. Found: C, 29.75; H, 2.31; N, 20.64.

4.9.8 $[Ru(Me_2biim)_3][CF_3SO_3]_2$ (27)

To a solution of $[Ru(DMF)_6][CF_3SO_3]$ (0.074 g, 0.075 mmol) in MeOH (5 mL) was added H_2Me_2biim (0.12 g, 0.30 mmol). This yellow solution was refluxed for 16 h; the solution turned brown after 2 h and slowly became dark blue in colour. After 16 h, the solvent was removed under vacuum and the black residue was redissolved in acetone (10 mL); this mixture was filtered through Celite, and the filtrate reduced in volume to ~1 mL. To this was added hexanes (8 mL) to yield a blue precipitate that was subsequently collected and dried under vacuum at 78 °C for 24 h. Yield: 0.042 g (63 %). ^{1}H NMR (CD_3OD): δ 7.43 (s, 6H, $H_{5,5'}$-Me_2biim), 2.54 (s, 18H, CH_3-Me_2biim). ESI-MS (MeOH): 736 (M^+ - CF_3SO_3), 587 (M^+ - 2 CF_3SO_3), 575 (M^+ - CF_3SO_3 – Me_2biim), 425 (M^+ - 2 CF_3SO_3 – Me_2biim). Anal. Calcd for $C_{26}H_{30}F_6N_{12}O_6S_2Ru$: C, 35.25; H, 3.39; N, 18.98. Found: C, 35.16; H, 3.32; N, 18.44.

4.9.9 $[Ru(Hbiim)_2Cl_2]Cl_2$ (28)

H_2 was bubbled through a solution of $RuCl_3 \cdot 3H_2O$ (0.054 g, 0.21 mmol) in refluxing MeOH for 3 h at which time the brown solution had become blue. To this solution was added H_2biim (0.15 g, 0.40 mmol). and the mixture was refluxed for 10 h under 1 atm H_2 when it slowly turned brown. The solvent was then reduced in volume under vacuum to ~1 mL and acetone (5 mL) was added to yield a brown precipitate that was collected, washed with acetone (2 x 5 mL), and dried under vacuum at 78 °C for 24 h. Yield: 0.042 g (42 %). ^{1}H NMR (D_2O): δ 8.59 (br s, $H_{2,2'}$-biim), 7.58 (br s, $H_{5,5'}$-biim). ESI-MS (H_2O): 440 (M^+ - 2H), 404 (M^+ - H - Cl). Λ_M (H_2O) = 265 $\Omega^{-1}cm^2mol^{-1}$. Anal. Calcd for $C_{12}H_{14}Cl_4N_8Ru$: C, 28.07; H, 2.73; N, 21.83. Found: C, 27.92; H, 2.79; N, 21.59.

4.9.10 $[Ru(HMe_2biim)(Me_2biim)_2]Cl_3$ (29)

The procedure of Section 4.9.9 was followed but using $RuCl_3 \cdot 3H_2O$ (0.042 g, 0.16 mmol) and H_2Me_2biim (0.13 g, 0.33 mmol); also Et_2O (5 mL) rather than acetone was added to give the brown product. Yield: 0.034 g (30 %). ^{1}H NMR (D_2O): δ 7.71 (br s, 1H, $H_{5,5'}$-Me_2biim), 1.68 (br s, 3H, CH_3-Me_2biim). ESI-MS (H_2O): 587 (M^+ - H), 425

(M^+ - HMe_2biim). Λ_M (H_2O) = 385 $\Omega^{-1}cm^2mol^{-1}$. Anal. Calcd for $C_{24}H_{31}Cl_3N_{12}Ru$: C, 41.47; H, 4.46; N, 24.19. Found: C, 41.25; H, 4.51; N, 23.93.

4.10 References

(1) Goulle, V.; Thummel, R. *Inorg. Chem.* **1990**, *29*, 1767.

(2) Rillema, D. P.; Sahai, R.; Matthews, P.; Edwards, A. K.; Shaver, R. J.; Morgan, L. *Inorg. Chem.* **1990**, *29*, 167.

(3) Rau, S.; Buettner, T.; Temme, C.; Ruben, M.; Goerls, H.; Walther, D.; Duati, M.; Fanni, S.; Vos, J. G. *Inorg. Chem.* **2000**, *39*, 1621.

(4) Elgafi, S.; Field, L. D.; Messerle, B. A.; Hambley, T. W.; Turner, P. *J. Chem. Soc., Dalton Trans.* **1997**, 2341.

(5) Cliff, M.; Pyne, S. *Synthesis* **1994**, 681.

(6) Gamez, P.; Simons, C.; Aromi, G.; Driessen, W.; Challa, G.; Reedijk, J. *Appl. Catal. A* **2001**, *214*, 187.

(7) Clarke, M. J.; Zhu, F.; Frasca, D. R. *Chem. Rev.* **1999**, *99*, 2511.

(8) McMurry, J. *Organic Chemistry, third ed.*; Brooks/Cole Publishing Co.: Pacific Grove, 1992.

(9) Coulson, D. R. *Inorg. Synth.* **1972**, *13*, 121.

(10) Hodgkiss, R. J. *Anti-Cancer Drug Des.* **1998**, *13*, 687.

(11) Cromer, D. T.; Storm, C. B. *Acta Cryst. C* **1990**, *46*, 1959.

(12) Cromer, D. T.; Storm, C. B. *Acta Cryst. C* **1990**, *46*, 1957.

(13) Melloni, P.; Dradi, E.; Logemann, W. *J. Med. Chem.* **1972**, *15*, 926.

(14) Novikov, S. S.; Khmel'nitskii, L. I.; Lebedev, O. V.; Sevast'yanova, V. V.; Epishina, L. V. *Khim. Geterotsikl. Soedin. [English Translation]* **1970**, *6*, 465.

(15) Novikov, S. S.; Khmel'nitskii, L. I.; Lebedev, O. V.; Sevast'yanova, V. V.; Epishina, L. V. *Khim. Geterotsikl. Soedin. [English Translation]* **1970**, *6*, 614.

(16) Davis, D. P.; Kirk, K. L.; Cohen, L. A. *J. Heterocycl. Chem.* **1982**, *19*, 253.

(17) Farah, S. F.; McClelland, R. A. *Can. J. Chem.* **1993**, *71*, 427.

(18) Palmer, B. D.; Denny, W. A. *J. Chem. Soc., Perkin Trans. I* **1989**, 95.

(19) Nagao, Y.; Sano, S.; Ochiai, M. *Tetrahedron* **1990**, *46*, 3211.

(20) Shreve, R. N.; Charlesworth, R. K. *U.S. Patent 2,744,116* **1956**.

(21) Tsang, J. Y. K. *Synthesis of Ruthenium(II) Complexes Containing Biheterocycles,* B.Sc. Dissertation, University of British Columbia: Vancouver, 2003.

(22) Bagal, L. I.; Pevzner, M. S.; Frolov, A. N.; Sheludyakova, N. I. *Khim. Geterotsikl. Soedin. [English Translation]* **1970**, *2*, 240.

(23) Chan, P. K. L.; Chan, P. K. H.; Frost, D. C.; James, B. R. *Can. J. Chem.* **1988**, *66*, 117.

(24) Geary, W. J. *Coord. Chem. Rev.* **1971**, *7*, 81.

(25) Iwamoto, M.; Alessio, E.; Marzilli, L. G. *Inorg. Chem.* **1996**, *35*, 2384.

(26) Wu, A.; Kennedy, D. C.; Patrick, B. O.; James, B. R. *Inorg. Chem.* **2003**, *42*, 7579.

(27) Seddon, E. A.; Seddon, K. R. *The Chemistry of Ruthenium*; Elsevier Sceince Publishers: New York, 1984. (a) p354, (b) p 891.

(28) Evans, I. P.; Spencer, A.; Wilkinson, G. *J. Chem. Soc., Dalton Trans.* **1972**, 204.

(29) Alessio, E.; Mestroni, G.; Nardin, G.; Attia, W. M.; Calligaris, M.; Sava, G.; Zorzet, S. *Inorg. Chem.* **1988**, *27*, 4099.

(30) Chan, P. K. L. *Ruthenium Nitroimidazole Complexes as Radiosensitizers*, Ph. D. Dissertation, University of British Columbia: Vancouver, 1988.

(31) Baird, I. R. *Fluorinated Nitroimidazoles and Their Complexes: Potential Hypoxia-Imaging Agents*, Ph. D. Dissertation, University of British Columbia: Vancouver, 1999.

(32) Anderson, C.; Beauchamp, A. *Inorg. Chem.* **1995**, *34*, 6065.

(33) Hallman, P. S.; Stephenson, T. A.; Wilkinson, G. *Inorg. Synth.* **1970**, *12*, 237.

(34) Rose, D.; Wilkinson, G. *J. Chem. Soc., Dalton Trans.* **1970**, 1791.

(35) Huheey, J. E. *Inorganic Chemistry: Principles of Structure and Reactivity, third ed.*; Harper Collins Publishers: New York, 1983.

(36) Kirk, K. L. *J. Heterocycl. Chem.* **1985**, *22*, 57.

(37) Iddon, B.; Lim, B. L. *J. Chem. Soc., Perkin Trans. 1* **1983**, 735.

(38) Brunings, K. J. *J. Am. Chem. Soc.* **1947**, *69*, 205.

(39) Pauly, H.; Arauner, E. *J. Prakt. Chem.* **1928**, *118*, 33.

Chapter 5

Synthesis and Characterization of Ru Complexes with Chelating N-Heterocyclic Carboxylates

5.1 Introduction

The coordination of carboxylate groups to transition metals is typically investigated using IR spectroscopy, the difference in the symmetric and asymmetric stretching frequencies being used to determine the coordination mode when X-ray structural data are not available (Figure 5.1).[1,2]

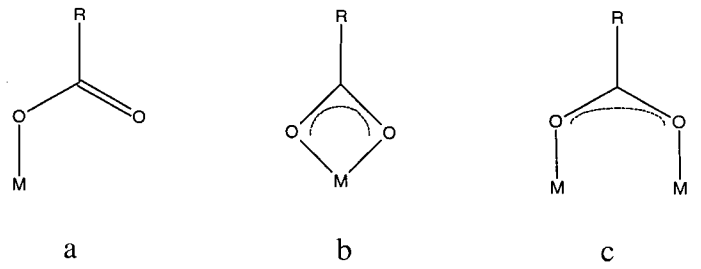

Figure 5.1 Binding modes of carboxylate groups with transition metal complexes; a) Monodentate, b) Chelating, and c) Bridging.

The coordination chemistry of pyridine-2-carboxylic acid, more commonly referred to as picolinic acid (Hpic) (Figure 5.2), has been widely studied.[3-9] Hpic is a tryptophan metabolite, and its transition metal complexes may have biological implications.[10] For example, $Cr(pic)_3$ is currently marketed as a nutritional supplement and weight-loss agent.[8,11] Trace Cr is essential in the body, while $Cr(pic)_3$ is readily absorbed by the body and shows a lack of toxicity at doses as high as 30 mg Cr per kg body weight in rats.[12] The fate of the complex and nature of the absorbed active species, however, remain unknown.[8] At a concentration of 120 μM, $Cr(pic)_3$ on reduction can react with O_2 to form hydroxyl radicals that possibly cleave DNA.[11] At pH < 1, aqueous

solutions of $Cr(pic)_3$ form $[Cr(pic)_2(H_2O)]^+$, which may be the active species absorbed by the body.[8]

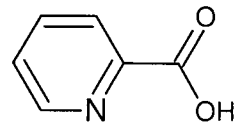

Figure 5.2 Molecular structure of pyridine-2-carboxylic acid, Hpic.

Ru readily forms bridged-carboxylate bimetallic complexes when reacted with carboxylic acids,[13] for example, the Ru(III/II) bimetallic precursor used in the work discussed in this chapter, $[Ru_2(\mu\text{-}CH_3COO)_4Cl]$. Related oxo-centered Ru trimetallic carboxylate complexes have also been reported.[13,14] More recently there have been reports of N-heterocyclic carboxylates chelating via N- and O-atoms to Ru to form monomeric complexes. For example, *mer*-$Ru(pic)_3 \cdot H_2O$ has been synthesized from $K_2[RuCl_5(H_2O)]$,[3] $[Ru_2(\mu\text{-}CH_3COO)_4Cl]$,[4] and $RuCl_3 \cdot 3H_2O$;[5] however, this complex is only sparingly soluble in aqueous solution thus limiting its potential for biological applications. In Section 5.2, a new Ru(III/II) bimetallic picolinate complex is described; this complex is highly water-soluble, and may have useful biological applications. Reactions analogous to those reported in the literature with Ru and Hpic, but using instead imidazole-4-carboxylic acid (Im-CO_2H), will then be discussed in Section 5.3. Finally, some preliminary work with a third ligand, 3-nitro-1,2,4-triazole-5-carboxylic acid (HCANT), will be presented. In Section 3.3.3, it was noted that Ru-maltolato complexes containing $2NO_2$Im, $4NO_2$Im or $3NO_2$tri ligands were not stable in DMSO solution and were insoluble in other solvents. It was thought, therefore, that as two of the carboxylate complexes discussed in this chapter ($[Ru_2(pic)_4(EtOH)Cl] \cdot H_2O$ (**31**) and Ru(Im-CO_2)(Im-$CO_2H)_2Cl_2 \cdot EtOH \cdot H_2O$ (**33**)) exhibited high water-solubility, that Ru complexes with HCANT might also be water-soluble and thus have potential for further biological testing.

5.2 Synthesis and Characterization of $[Ru_2(pic)_4(EtOH)Cl]\cdot H_2O$ (31)

mer-$Ru(pic)_3\cdot H_2O$ (**30**) is a yellow solid, sparingly soluble in water and DMSO, and completely insoluble in other solvents tested.[4] The synthesis of **30** was carried out using a modification of procedures reported by Ellis *et al.*[3] and Barral *et al.*[4] Both groups used base to deprotonate Hpic in solution; however, base was found to be unnecessary and yields obtained were similar to those reported. The reaction of Hpic with $RuCl_3\cdot 3H_2O$, reported by Ghatak *et al.*,[5] was also repeated. Again, the procedure was modified to omit base; however, this time **30** was not formed, and an orange solid (**31**) was isolated. The $RuCl_3\cdot 3H_2O$ reaction was also repeated with base as reported,[5] but neither **30** nor any other identifiable species could be isolated. A precipitated black solid had very low C (6.2 %) and N (1.4 %) content and thus contained minimal picolinate.

Elemental analysis of **31** supports the formulation $[Ru_2(pic)_4(EtOH)Cl]\cdot H_2O$. The MS data (in MeOH), showing a Ru dinuclear splitting pattern with a parent peak for $[M^+ - EtOH]$ at 727 (Figure 5.3), also support this formulation. This pattern is easily identified compared to that of a mononuclear species because of the distinct isotopic splitting for a Ru_2 species vs. that for one Ru atom (Figure 5.4).

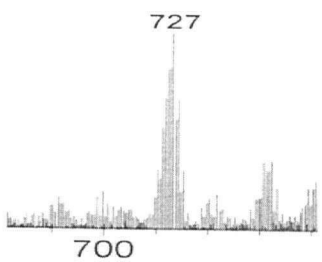

Figure 5.3 ESI-MS spectrum (in MeOH) of $[Ru_2(pic)_4(EtOH)Cl]\cdot H_2O$ (**31**) clearly showing the $[M^+ - EtOH]$ fragment centered at 727.

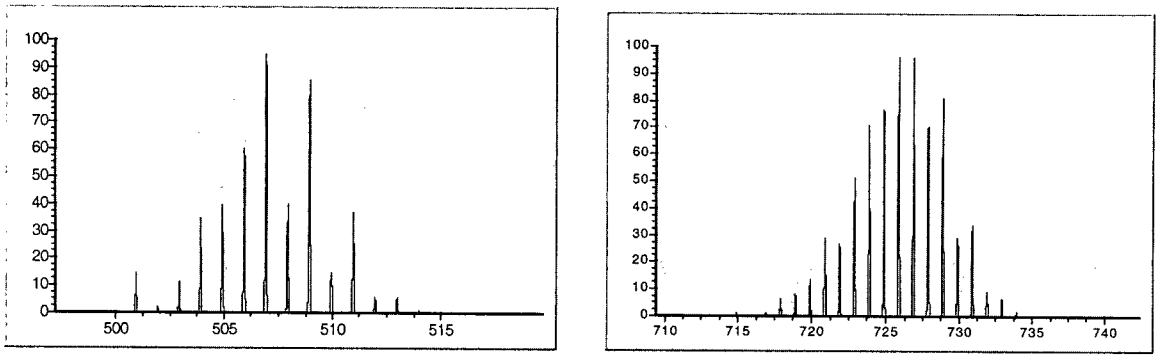

Figure 5.4 Theoretical isotopic distribution for the $[M^+]$ peak of $Ru(Im\text{-}CO_2)(Im\text{-}CO_2H)_2Cl_2 \cdot EtOH \cdot H_2O$ (**33**, left) (Section 5.3), and for the $[M^+ - EtOH]$ peak of $[Ru_2(pic)_4(EtOH)Cl] \cdot H_2O$ (**31**, right), clearly showing the difference in isotopic splitting patterns between a Ru and a Ru_2 species.

The IR data for **31** (Table 5.1) show that the carboxylate groups are not bridging, and that the bridging is likely via one O-atom and the pyridine-N. For bridging carboxylate groups, the difference between ν_{sym} and ν_{asym} is typically < 150 cm^{-1} for Ru_2 complexes;[1] for **31** $\Delta\nu$ is ~300 cm^{-1}, suggesting that the carboxylate group is binding in a monodentate fashion, similar to that observed for **30**.

Table 5.1 Selected IR spectral data for Ru carboxylate complexes.

Complex	ν_{asym} (cm^{-1})	ν_{sym} (cm^{-1})
mer-$Ru(pic)_3 \cdot H_2O$ (**30**)	1661	1315
$[Ru_2(pic)_4(EtOH)Cl] \cdot H_2O$ (**31**)	1672, 1639	1396, 1316
$Ru(Im\text{-}CO_2)_3 \cdot 2H_2O$ (**32**)	1642	1324
$Ru(Im\text{-}CO_2)(Im\text{-}CO_2H)_2Cl_2 \cdot EtOH \cdot H_2O$ (**33**)	1718, 1706, 1570	1384, 1350, 1313

The strong IR band at 3468 cm^{-1} is assigned to ν_{OH} and could be for either coordinated EtOH or the H_2O solvate. The bound EtOH is more easily identified by the ^1H NMR data (Figure 5.5): two broadened resonances (the Me-triplet at δ 1.45, and the CH_2 quartet at δ 4.53) are shifted downfield from those of free EtOH (with the Me-triplet at δ 1.12, and the CH_2 quartet at δ 3.55). The relative intensities of the free and bound EtOH resonances in D_2O imply that in this solvent, ~ 40 % of **31** is converted to a species with coordinated D_2O.

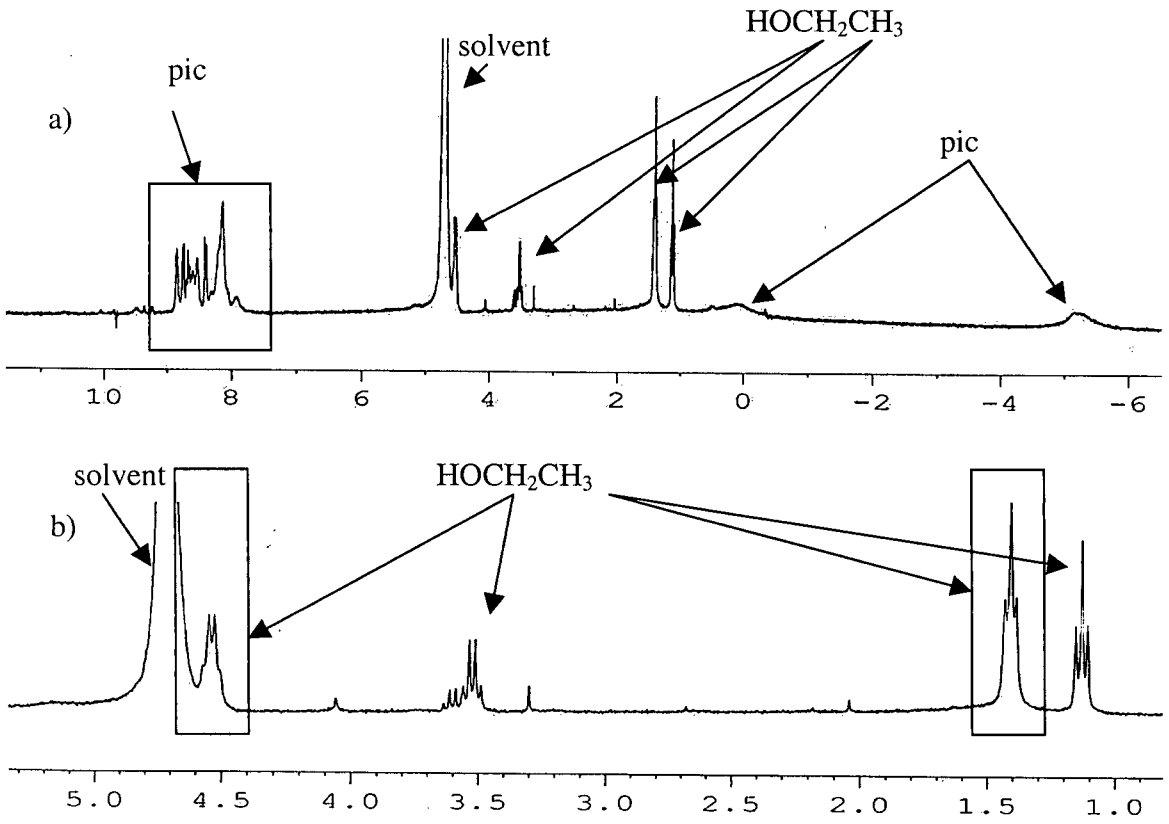

Figure 5.5 ^1H NMR spectrum (300 MHz, 298 K) of $[Ru_2(pic)_4(EtOH)Cl]\cdot H_2O$ (**31**) in D_2O. a) Complete spectrum. b) Expansion showing signals of the bound EtOH at δ 4.53 and 1.45 highlighted with boxes.

Barral *et al.*[4] have reported the synthesis of $[Ru_2(pic)_4]$, with a proposed structure containing either four bridging N,O-pic ligands or two bridging N,O-pic ligands and two

non-bridging η^2-pic ligands. Similar structures with four bridging pic ligands, each Ru having a terminal EtOH or Cl (Figure 5.6a), or two μ-pic ligands and two, non-bridging η^2-pic ligands, one on each Ru (Figure 5.6b), are plausible for **31**. The conductivity for **31** in MeOH is 112 $\Omega^{-1}cm^2mol^{-1}$, in the range for a 1:1 electrolyte,[15,16] suggesting Cl^- dissociation. If the Cl^- was bridging, its dissociation in solution would likely lead to decomposition of the bimetallic unit; however, ESI-MS data in MeOH show it to be still intact.

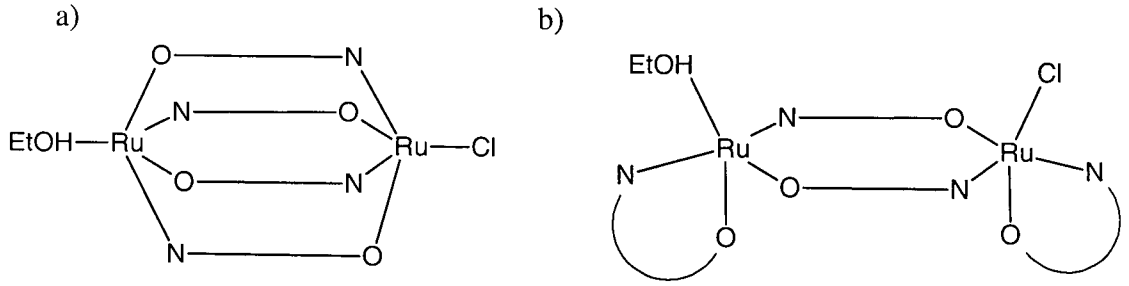

Figure 5.6 Proposed solid state structures for **31** where N-O ≡ pic$^-$. a) unit with four bridging pic$^-$ ligands. b) unit with two bridging and two non-bridging pic$^-$ ligands.

5.3 Complexes of Ru with Imidazole-4-carboxylic Acid

5.3.1 Synthesis and Characterization of $Ru(Im\text{-}CO_2)_3 \cdot 2H_2O$ (32)

In reactions similar to those reported for the synthesis of $Ru(pic)_3 \cdot H_2O$ (**30**) (Section 5.2), $Ru(Im\text{-}CO_2)_3$ was synthesized from both K_3RuCl_6 and $Ru_2(acetate)_4Cl$, using Im-CO_2H (Figure 5.7) in place of Hpic.[3,4] The isolated, pale yellow product, was characterized by elemental analysis, MS, and IR and NMR spectroscopies. Elemental analysis was consistent with the formulation of $Ru(Im\text{-}CO_2)_3 \cdot 2H_2O$. The $\Delta\nu$ value of 318 cm^{-1} for ν_{asym} - ν_{sym} (Table 5.1) is consistent with a chelated structure with binding via the imidazole-N(3) and one carboxylate-O atom as for $Ru(pic)_3 \cdot H_2O$; the presence of water is indicated by a ν_{OH} at 3423 cm^{-1}, and by an increase in intensity of the residual

water signal in dmso-d_6 in the spectrum of the complex compared with that of a blank of the solvent containing no complex.

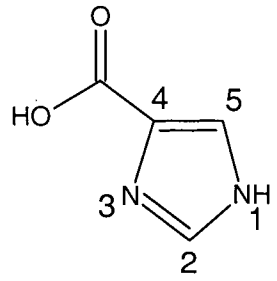

Figure 5.7 Molecular structure of Im-CO_2H.

32 is only sparingly soluble in DMSO, and is insoluble in other solvents. The ^1H NMR spectrum in dmso-d_6 (recorded over 6 h, ~20,000 scans) shows 6 very weak resonances for the bound imidazoles at δ 0.31, 0.09 and –0.09 for H(5) and δ –2.67, -13.55 and –17.87 for H(2), the assignments being based on those observed for monodentate imidazole ligands with Ru(III) (Section 3.3.2).

As for the synthesis of $Ru(pic)_3 \cdot H_2O$ (**30**), no base was used in the synthesis of **32**. With the use of 3 equivalents of base to reproduce the reaction conditions reported for the synthesis of **30**,[3-5] **32** was not formed; the isolated products using Im-CO_2H under basic conditions were not identified but contained very low percentages of C and N, both below 10 %, as was found when $RuCl_3 \cdot 3H_2O$ was reacted under basic conditions with Hpic (Section 5.2).

5.3.2 Synthesis and Characterization of $Ru(Im\text{-}CO_2)(Im\text{-}CO_2H)_2Cl_2 \cdot EtOH \cdot H_2O$ (33)

There are currently no literature examples of Ru complexes containing Im-CO_2H (Figure 5.7) or Im-CO_2^- as a ligand. The only such transition metal complexes reported are a pair of Mn clusters in which Im-CO_2^- chelates through a carboxylate-O and the imidazole-N(3).[17] There is, however, one reported Ru complex with imidazole 4,5-dicarboxylic acid,[18] where IR stretches for both bound $-COO^-$ and free –COOH are reported; these have proved useful in the formulation of $Ru(Im\text{-}CO_2)(Im\text{-}CO_2H)_2Cl_2 \cdot EtOH \cdot H_2O$ (**33**).

Unlike the reaction of $RuCl_3 \cdot 3H_2O$ with Hpic, the reaction with Im-CO_2H does not form a bimetallic complex. **33** is synthesized by refluxing Im-CO_2H and $RuCl_3 \cdot 3H_2O$ in a 3:1 ratio in EtOH (Figure 5.8). The IR data show two distinct types of carboxylates with ν_{asym} = 1718, 1706, and 1570 (Table 5.1). For $[Ru(PPh_3)_2(L\text{-}H)_2]$ (L-H_2 = imidazole 4,5-dicarboxylic acid) (Figure 5.9), ν_{asym} for the protonated carboxylic acid group was observed at 1720 cm^{-1} and for the bound carboxylate was observed at 1627 cm^{-1}.[18] This suggests that for **33,** the stretches at 1718 and 1706 cm^{-1} are for –COOH groups, and the stretch at 1577 cm^{-1} is for a bound $–COO^-$.

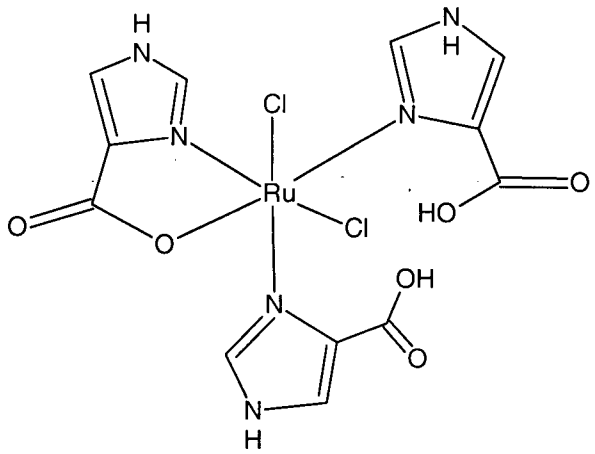

Figure 5.8 One possible isomer for the proposed structure for Ru(Im-CO_2)(Im-$CO_2H)_2Cl_2 \cdot EtOH \cdot H_2O$ (**33**) (solvent molecules not shown).

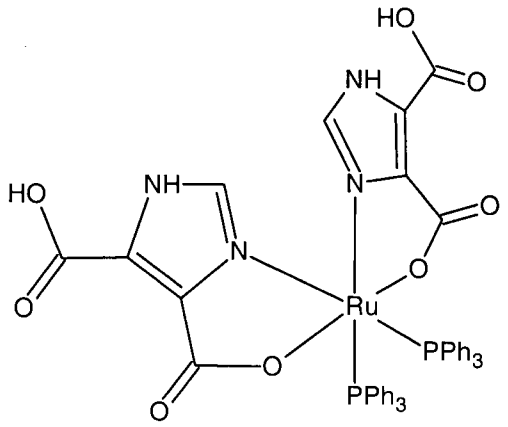

Figure 5.9 Molecular structure of $[Ru(PPh_3)_2(L\text{-}H)_2]$ (L-H_2 = imidazole 4,5-dicarboxylic acid).[18]

ESI-MS data (in MeOH) show a parent peak for **33** at 508 (Figure 5.10) with the same isotopic splitting pattern as that of a theoretically calculated spectrum (see Figure 5.4). In MeOH, the conductivity of **33** over 3h remained at 19-23 $\Omega^{-1}cm^2mol^{-1}$, consistent with a neutral species.[15,16]

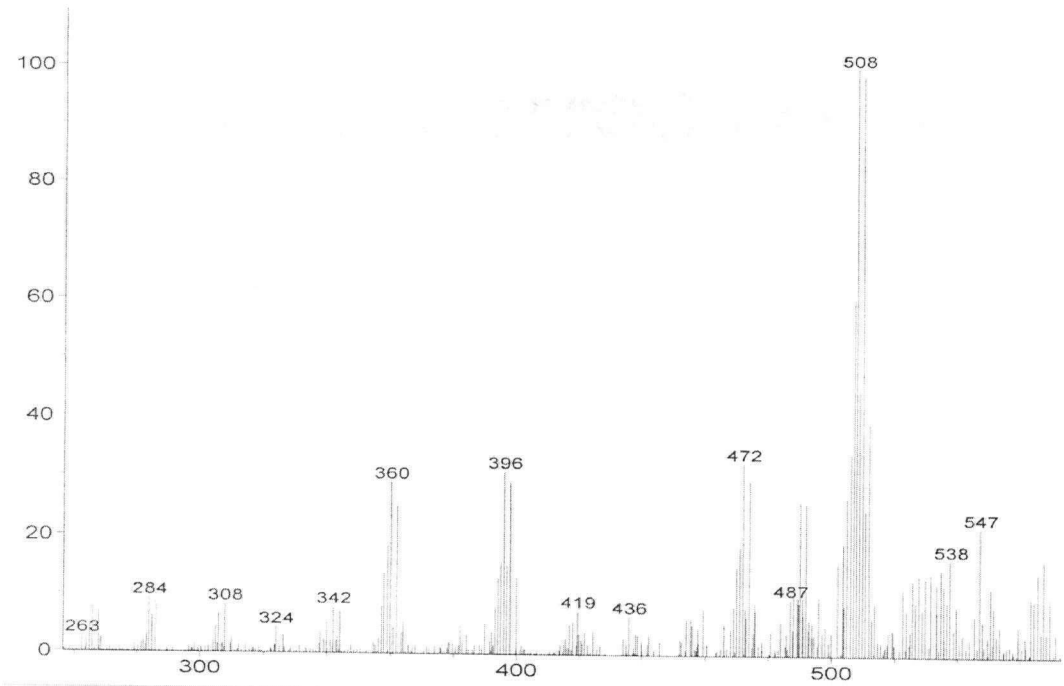

Figure 5.10 Mass spectrum of $Ru(Im\text{-}CO_2)(Im\text{-}CO_2H)_2Cl_2 \cdot EtOH \cdot H_2O$, showing M^+ at 508.

A more exact structural formulation for **33** cannot be given, but the elemental analysis requires EtOH and H_2O solvates. From the ^1H NMR spectrum in CD_3OD, both $Im\text{-}CO_2H$ ligands are likely in different chemical environments as three signals are observed for both the H(2) and H(5) protons of the $Im\text{-}CO_2H$ and $Im\text{-}CO_2$ ligands. Resonances for free EtOH are also observed in the ^1H NMR spectrum, while a strong IR band at 3467 cm^{-1} may show evidence for the water solvate.

5.4 Synthesis of Nitroimidazole and Nitrotriazole Carboxylic Acids

5.4.1 Synthesis of 3-Nitro-1,2,4-triazole-5-carboxylic Acid (HCANT)

The synthetic procedure for HCANT was modified from a general procedure published by Pevzner and coworkers for nitrating numerous aminotriazole compounds.[19,20] The precursor, 3-amino-1,2,4-triazole-5-carboxylic acid, was first synthesized using a reported procedure,[21] but was later purchased from Aldrich when it became available commercially in 2002. The nitration procedure used is an example of a Sandmeyer reaction.[22] The literature reports that the amino precursor is soluble in acetic acid; however this was found to be incorrect. In order to solubilize the amine-triazole, a higher H_2SO_4:CH_3COOH ratio was used for formation of the diazonium salt. The amino group is first converted to a diazonium salt, followed by the facile replacement of the $-N^+{\equiv}N$ group by NO_2^-. Caution must be taken in adding the diazonium salt solution to the $NaNO_2$ solution as rapid addition can lead to a violent reaction, producing a foam that erupts from the flask; dropwise addition with rapid stirring and gentle heating prevents this. The isolated solid was characterized by elemental analysis, mass spectrometry and IR spectroscopy.

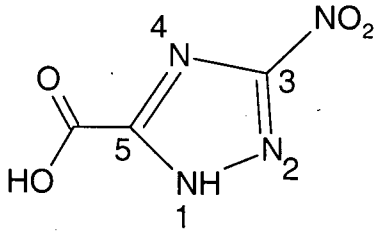

Figure 5.11 Molecular structure of HCANT.

5.4.2 Attempted Synthesis of 2-Nitroimidazole-4-carboxylic Acid

4-Hydroxymethyl-2-nitroimidazole was synthesized using a modified literature procedure to afford initially 4-hydroxymethyl-1-tritylimidazole, the imidazole precursor for the nitration step.[23] Davis and coworkers report the synthesis of this compound in 4 steps from imidazole-4,5-dicarboxylic acid. The first step, the synthesis of Im-CO_2H,

was omitted as this material was purchased (Aldrich). Then the methyl ester, rather than the reported ethyl ester, was synthesized and characterized by ^{1}H NMR and IR spectroscopies and mass spectrometry. As for the synthesis of H_2biim and H_2Me_2biim (Chapter 4), the trityl group was used to protect the imidazole-N(1) position, as this group is easily removed with dilute acid once the nitration at the C(2) position is complete.

The reported procedure for reducing the ester group used $LiAlH_4$,[23] but attempts to repeat this were unsuccessful. The $LiAlH_4$ decomposed rapidly during workup upon the addition of water, indicating that it was still active. Diisobutylaluminum hydride (Dibal-H), using two equivalents per ester, was subsequently used successfully for reduction of the ester group at r.t over 1 h, although the isolated yield of 4-hydroxymethyl-1-tritylimidazole was only 44 % compared to the reported yield, 86 %, using $LiAlH_4$.[23] This compound was also synthesized directly by treatment of 4-(hydroxymethyl)imidazole with trityl chloride. The availability and cost of 4-(hydroxymethyl)imidazole vary, but the relatively low yield from the ester reduction makes this second route economically viable.

The reported yield of 4-hydroxymethyl-2-nitroimidazole from 4-hydroxymethyl-1-tritylimidazole and *n*-propyl nitrate is 29 %;[23] however, two attempts to reproduce this reaction yielded only ~3 % of the desired product. When the same nitration procedure was used to synthesize 2-nitroimidazole from 1-tritylimidazole, the yield of 2-nitroimidazole obtained was 39 %, while the reported yield was 35-50 %.[23] This implies that there is no problem with the *n*-BuLi or *n*-propyl nitrate being used, or with the chromatographic set-up. The low yield of 4-hydroxymethyl-2-nitroimidazole prevented any attempt to oxidize it to 2-nitroimidazole-4-carboxylic acid. Either more work on optimizing the synthesis of 4-hydroxymethyl-2-nitroimidazole or a new synthetic route all together is needed in order to synthesize 2-nitroimidazole-4-carboxylic acid.

5.4.3 Attempted Synthesis of 2-Nitroimidazole-4,5-dicarboxylic Acid

As there is only one available position for substitution on the imidazole ring in imidazole-4,5-dicarboxylic acid, C(2), it was thought that introduction of a nitro group at this position might be facilitated by direct nitration using HNO_3 or a mixture of HNO_3 and H_2SO_4. Such a nitration might hopefully proceed in much higher yield than that

discussed for 4-hydroxymethyl-2-nitroimidazole in Section 5.4.2. The nitration of 4-nitroimidazole to form 2,4-dintroimidazole has been reported,[24] suggesting that nitration at this position is possible under certain conditions. Unfortunately, both imidazole-4,5-dicarboxylic acid and dimethyl imidazole-4,5-dicarboxylate did not react with HNO_3. After imidazole-4,5-dicarboxylic acid or the dimethyl ester was mixed with conc. HNO_3 for 12 h, and the mixtures neutralized with 5 M NaOH, only the unreacted imidazoles were collected by filtration.

The reported procedure using *n*-propyl nitrate[23] was then attempted with 4,5-bis(hydroxymethyl)-1-tritylimidazole; however, no nitrated species were observed and no products could be isolated from the reaction.

5.5 Attempted Reactions of HCANT with Ru Precursors

Reactions analogous to those discussed in Sections 5.2 and 5.3 with Hpic and Im-CO_2H were repeated using HCANT (Section 5.4.1) as a ligand. The reaction of three equivalents of HCANT with $K_3[RuCl_6]$ in H_2O gave a purple solution from which a purple solid was isolated. The MS showed a parent peak consistent with the formulation of $Ru(CANT)(HCANT)_2Cl_2$, analogous to that of **33** synthesized from $RuCl_3 \cdot 3H_2O$ (Section 5.3.2). In the IR spectrum, asymmetric C=O stretches were observed at 1677, 1665, and 1652 cm^{-1}, and there was also a nitro stretch at 1542 cm^{-1}.[25] An intense band at 1912 cm^{-1}, however, suggests that either a coordinated C≡O or N≡O may be formed during the reaction. Elemental analysis (Anal. Calcd for $C_9H_5N_{12}O_{12}Cl_2Ru$: C, 16.74; H, 0.78; N, 26.05. Found: C, 11.49; H, 3.04; N, 21.62) of this purple solid was low in both C and N but high in H for the proposed formulation, possibly suggesting the presence of considerable water; consistent with the presence of a broad, intense band at ~ 3400 cm^{-1} in the IR spectrum.

The reaction of HCANT with $Ru_2(acetate)_4Cl$ also gave a purple solution from which a purple solid was precipitated; its IR spectrum was the same as that mentioned above, except that the 1912 cm^{-1} band was now even more intense. ESI-MS (negative, MeOH) showed only one peak at 444 with a clear Ru splitting pattern, consistent with the formulation of $Ru(CANT)_2(NO)$; the stretch at 1912 cm^{-1} is in the range for N≡O bound to Ru(III).[26-28] The elemental analysis (Anal. Calcd for $C_6H_2N_9O_9Ru$: C, 16.18; H, 0.45;

N, 28.31. Found: C, 15.34; H, 2.56; N, 24.35) was also high in H and low in C and N for this proposed formulation.

Both reactions with HCANT gave products with reproducible IR spectra that differ only in the intensity of the 1912 cm^{-1} band. The elemental analyses for the isolated purple solids, however, were not reproducible, but were always low in C and N and high in H. Further study on these complexes is needed to determine their nature.

5.6 Experimental Procedures

5.6.1 3-Nitro-1,2,4-triazole-5-carboxylic Acid (HCANT)

This compound was synthesized by a modified literature procedure.[19,20] Sodium nitrite (1.10 g, 15.9 mmol) was added to 7 mL of H_2SO_4 at –5 °C, and to this was added glacial acetic acid (15 mL) and finely ground 3-amino-1,2,4-triazole-5-carboxylic acid (2.00 g, 15.6 mmol). The mixture was stirred at –5 °C for 10 min until most of the triazole had dissolved; H_2O (25 mL) was then added with the temperature kept below 0 °C. The resulting yellow solution was then added dropwise to a sodium nitrite solution (200 g $NaNO_2$ in 200 mL H_2O) at 50 °C. (If added too quickly, a foam of diazonium salts can form, causing the reaction to heat up out of control with contents erupting from the flask.) The green product solution was heated for 2 h at 50 °C, when the now colourless solution was extracted with EtOAc (4 x 50 mL), and the combined extracts were evaporated yielding the desired product. Yield: 1.41 g (57 %). IR (KBr pellet): ν 3416 (N-H, s), 3257 (O-H, m), 1710 (C=O, s), 1574 (NO_2, m), 1383 (NO_2, m), 1268 (m), 720 (m). ESI-MS: 159 (M^+). Anal. Calcd for $C_3H_2N_4O_4$: C, 22.78; H, 1.26; N, 35.43. Found: C, 22.52; H, 1.41; N, 35.40. The IR characterization data agree with those reported.[20]

5.6.2 Methyl imidazole-4-carboxylate

This compound was prepared by modifying a reported procedure used to synthesize the analogous ethyl ester.[23] To a suspension of imidazole-4-carboxylic acid (1.00 g, 8.92 mmol) in MeOH (20 mL) was added conc. H_2SO_4 (1.5 mL). The mixture was refluxed for 24 h, at which point the solid was completely dissolved and TLC

showed the absence of the carboxylic acid. The solution was then cooled to 0 °C and neutralized to pH 8 using 5 M NaOH. The solvent was removed under vacuum and the white residue redissolved in a minimal volume of boiling water. White crystals of the ester formed when the aqueous solution was cooled. After standing for 1 h, the mixture was filtered, and the crystals were washed with cold H_2O (1 x 5 mL). The solid was then dried under vacuum at r.t. for 24 h. Yield: 0.87 g (77 %). ^{1}H NMR (dmso-d_6): δ 7.74 (s, 1H, H_5-Im), 7.65 (s, 1H, H_2-Im), 2.51 (s, 3H, CH_3-Im). IR (KBr pellet): ν 3105 (N-H, s), 2976, 2846 (C-H, m), 1619 (C=O, m), 1363 (s), 1156 (m), 864 (m). FAB (+): 127 (M^+). Anal. Calcd for $C_5H_6N_2O_2$: C, 47.62; H, 4.76; N, 22.22. Found: C, 47.54; H, 4.85; N, 21.69.

5.6.3 Methyl 1-tritylimidazole-4-carboxylate

This compound was prepared by modifying a reported procedure used to synthesize the analogous ethyl ester.[23] To a solution of methyl imidazole-4-carboxylate (0.80 g, 6.3 mmol) in DMF (20 mL), under N_2, was added trityl chloride (1.77 g, 6.35 mmol), and the mixture was stirred at r.t. for 10 min until solution was complete. NEt_3 (0.98 mL, 7.0 mmol) was then added, and the mixture stirred for 16 h at r.t. The contents were then poured over ice, and the mixture left standing for 5 min. The cold mixture was then filtered and the precipitate was washed with H_2O (2 x 5 mL), and dried under vacuum at r.t. for 24 h. Yield: 2.01 g (86 %). ^{1}H NMR ($CDCl_3$): δ 7.65 (s, 1H, H_5-Im), 7.52 (s, 1H, H_2-Im), 7.03-7.36 (m, 15H, Ph_3C), 2.42 (s, 3H, CH_3-Im). FAB (+): 369 (M^+), 243 (CPh_3). Anal. Calcd for $C_{24}H_{20}N_2O_2$: C, 78.26; H, 5.43; N, 7.61. Found: C, 78.35; H, 5.56; N, 7.37.

5.6.4 4-Hydroxymethyl-1-tritylimidazole

Method A. This compound was prepared using a modified literature procedure.[23] To a solution of methyl 1-tritylimidazole-4-carboxylate (1.02 g, 2.72 mmol) in THF (15 mL) at r.t. under N_2 was added 5.50 mL of a 1.0 M diisobutylaluminum hydride (Dibal-H) solution in hexanes . The mixture was stirred for 1 h until the ester was no longer present by TLC. The mixture was then cooled to 0 °C and the following were slowly added in sequence: H_2O (0.8 mL) , 15 % aq. NaOH (1.0 mL), and H_2O (0.8 mL). The

mixture was then filtered, and the precipitate washed with THF (3 x 10 mL), and the filtrate and combined washings were then evaporated under vacuum. The residue was dissolved in CH_2Cl_2; this solution was washed with H_2O to remove any remaining inorganic salts and then the CH_2Cl_2 layer evaporated under vacuum. The white product was scraped from the flask and dried for an additional 24 h at r.t. under vacuum. Yield: 0.41 g (44 %).

Method B. To a solution of 4-(hydroxymethyl)imidazole (0.52 g, 5.3 mmol) in DMF (10 mL), under N_2, was added trityl chloride (1.48 g, 5.30 mmol). This mixture was stirred for 10 min at which time the solids had dissolved, and then NEt_3 (0.90 mL, 6.4 mmol) was added. This mixture was stirred for 16 h at r.t., then poured onto ice and left standing for 5 min. The resulting precipitate was collected, washed with H_2O (2 x 10 mL), and dried under vacuum at r.t. for 24 h. Yield: 1.53 g (85 %).

^{1}H NMR ($CDCl_3$): δ 7.39 (s, 1H, H_2-Im), 7.27-6.97 (m, 15H, CPh_3), 6.80 (s, 1H, H_5-Im), 4.62 (s, 2H, -CH_2OH). FAB (+): 341 (M^+), 243 (CPh_3). Anal. Calcd for $C_{23}H_{20}N_2O$: C, 81.18; H, 5.88; N, 8.24. Found: C, 81.24; H, 5.91; N, 7.87. The ^{1}H NMR data agree with those reported.[23]

5.6.5 4-Hydroxymethyl-2-nitroimidazole

This compound was prepared according to a literature procedure.[23] To a solution of 4-hydroxymethyl-1-tritylimidazole (0.99 g, 2.9 mmol) in THF (35 mL) under N_2 at 0 °C was added 4.05 mL (6.08 mmol) of a 1.5 M solution of *n*-BuLi in hexanes slowly over 1 min. The pale yellow solution, on being stirred for 2 h, became dark red and a white precipitate formed. *n*-Propyl nitrate (0.64 g, 6.1 mmol) was then added and gave immediately a dark brown mixture that was stirred for 1 h. The solution was then cooled to 0 °C, diluted with MeOH (40 mL), and then conc. HCl (5 mL) was added to remove the trityl group and to hydrolyze any remaining traces of nitrate esters. This mixture was stirred for 12 h, and then the solvent was removed under vacuum. The residue was triturated with 20 % aq. EtOH (10 mL) and then filtered. The filtrate was evaporated leaving a brown solid that was then chromatographed on silica gel (~ 80 g). The column was first eluted with EtOAc to remove impurities and then with 5 % MeOH in EtOAc to elute the desired product. The fractions were analyzed by TLC, and those containing the

product were combined and evaporated, and the resulting solid was dried at r.t. for 24 h. Yield: 12 mg (3 %). ^{1}H NMR (CD_3OD): δ 7.15 (s, 1H, H_5-Im), 4.50 (s, 2H, -CH_2OH). ESI-MS: 144 (M^+). The ^{1}H NMR data agree with those reported.[23]

5.6.6 Dimethyl imidazole-4,5-dicarboxylate

This compound was prepared according to a literature procedure.[29,30] To a suspension of imidazole-4,5-dicarboxylic acid (5.03 g, 32.2 mmol) in MeOH (80 mL) was added conc. H_2SO_4 (5 mL). The mixture was refluxed for 6 h when the solid had dissolved to give a colorless solution; TLC showed the absence of the dicarboxylic acid. The solution was then cooled at 0 °C and neutralized to pH 8 using 5 M NaOH. The solvent was removed under vacuum and the white residue redissolved in a minimal volume of boiling water. A white precipitate separated when the solution was cooled. The white precipitate was collected, washed with cold H_2O (1 x 5 mL), and dried under vacuum at r.t. for 24 h. Yield: 5.03 g (85 %). ^{1}H NMR (dmso–d_6): δ 7.89 (s, 1H, H_2-Im), 3.79 (s, 6H, -OCH_3). FAB (+): 185 (M^+). Anal. Calcd for $C_7H_8N_2O_4$: C, 45.65; H, 4.35; N, 15.22. Found: C, 45.42; H, 4.56; N, 15.01.

5.6.7 Dimethyl 1-tritylimidazole-4,5-dicarboxylate

This compound was prepared according to a literature procedure.[29] To a solution of dimethyl imidazole-4,5-dicarboxylate (4.02 g, 21.8 mmol) in DMF (40 mL) under N_2 was added trityl chloride (6.09 g, 21.9 mmol), and NEt_3 (3.05 mL, 21.9 mmol); the mixture was stirred at r.t. for 6 h when TLC revealed that none of the precursor dicarboxylate remained. The mixture was then poured over crushed ice and, after 10 min, was filtered; the white precipitate was collected, washed with H_2O (2 x 10 mL), and dried under vacuum at r.t. for 24 h. Yield: 6.61 g (71 %). ^{1}H NMR ($CDCl_3$): δ 7.55 (s, 1H, H_2-Im), 7.37-7.17 (m, 15H, CPh_3), 3.86 (s, 3H, -OCH_3), 3.17 (s, 3H, -OCH_3). FAB (+): 427 (M^+), 243 (CPh_3). Anal. Calcd for $C_{26}H_{22}N_2O_4$: C, 73.22; H, 5.19; N, 6.57. Found: C, 73.27; H, 5.23; N, 6.41.

5.6.8 4,5-Dihydroxymethyl-1-tritylimidazole

This compound was prepared according to a modified literature procedure.[29] To a solution of dimethyl 1-tritylimidazole-4,5-dicarboxylate (1.03 g, 2.41 mmol) in THF (20 mL) at r.t. under N_2 was added 10.5 mL of a 1.0 M Dibal-H solution in hexanes. The mixture was stirred for 4 h, when the TLC band for the dicarboxylate was no longer present. The mixture was cooled at 0 °C and to it was added in sequence: H_2O (1.5 mL), 15 % aq. NaOH (2 mL), and H_2O (1.5 mL). The mixture was then filtered and the precipitate washed with warm THF (3 x 10 mL). The combined filtrate and washings were evaporated under vacuum, and the residue was dissolved in CH_2Cl_2. This solution was filtered through Celite (~ 10 g) and the filtrate was evaporated. The resulting white solid was dried under vacuum at r.t. for 24 h. Yield: 0.42 g (44 %). ^{1}H NMR ($CDCl_3$): δ 7.67 (s, 1H, *H*$_2$-Im), 7.41-7.19 (m, 15H, CPh_3), 4.83 (s, 2H, -C*H*$_2$OH), 3.89 (s, 2H, -C*H*$_2$OH). FAB (+): 371 (M^+), 243 (CPh_3). Anal. Calcd for $C_{26}H_{22}N_2O_4$: C, 77.81; H, 5.99; N, 7.56. Found: C, 77.74; H, 5.91; N, 7.39.

5.6.9 Ru(pic)$_3$·H_2O (30)

Method A. This method was modified from a literature procedure.[3] Picolinic acid (0.14 g, 1.2 mmol) was added to a red solution of $K_3[RuCl_6]$ (Section 2.4.4) (0.17 g, 0.39 mmol) in 5 mL H_2O; this was heated at 60 °C for 5 h when a yellow precipitate slowly formed. The mixture was then cooled to r.t. before isolation of the solid by filtration; the solid was washed with MeOH (2 x 5 mL) and H_2O (1 x 5 mL) and dried under vacuum at 78 °C for 48 h. Yield: 0.11 g (58 %).

Method B. This method was performed as reported in the literature.[4] Hpic (0.096 g, 0.78 mmol) was added to a brown solution of $[Ru_2(CH_3COO)_4Cl]$ (0.062 g, 0.13 mmol) in water/MeOH, 1:1 (10 mL), and the mixture was refluxed for 8 h when a yellow precipitate formed. The reaction mixture was cooled to r.t. and the solid isolated by filtration, washed with H_2O (2 x 5 mL), and dried under vacuum at 78 °C for 24 h. Yield: 0.049 g (77 %).

IR (KBr pellet): ν 3443 (O-H, s), 1661 (C=O$_{asym}$, s), 1565 (m), 1315 (C=O$_{sym}$, m), 1280 (s), 1057(m). ESI-MS: 468 (M^+). Anal. Calcd for $C_{18}H_{12}N_3O_6Ru·H_2O$: C, 44.54; H, 2.89; N, 8.65. Found: C, 44.51; H, 2.74; N, 8.28. The IR data agree with those reported.[3,4]

5.6.10 $[Ru_2(pic)_4(EtOH)Cl]\cdot H_2O$ (31)

Hpic (0.072 g, 0.59 mmol) was added to a brown solution of $RuCl_3\cdot 3H_2O$ (0.051 g, 0.19 mmol) in 10 mL EtOH. This solution was refluxed for 6 h, the colour becoming red and finally bright orange. The solvent was reduced in volume to ~ 1 mL, when Et_2O (10 mL) was added to give an orange precipitate that was collected, washed with Et_2O (2 x 5 mL), and then dried under vacuum at 78 °C for 24 h. Yield: 0.066 g (86 %). ^1H NMR (D_2O): δ 8.76-7.92 (m, pic-H), 4.53 (br q, coordinated $HOCH_2CH_3$), 1.45 (br t, coordinated $HOCH_2CH_3$), 0.2, -5.1 (br s, pic-H). IR (KBr pellet): ν 3468 (O-H, s), 3124 (N-H, m), 1672 ($C=O_{asym}$, s), 1639 ($C=O_{asym}$, s), 1600 (m), 1456 (m), 1396 ($C=O_{sym}$, m), 1316 ($C=O_{sym}$, m), 1282 (m), 1147 (m), 856 (m), 759 (s), 691 (m). ESI-MS: 727 (M^+ - EtOH), 382 ($Ru(pic)_2Cl^+$), 346 ($Ru(pic)_2^+$). Λ_M (MeOH) = 112 $\Omega^{-1}cm^2mol^{-1}$. Anal. Calcd for $C_{26}H_{22}N_4O_9ClRu_2\cdot H_2O$: C, 39.52; H, 3.04; N, 7.09. Found: C, 39.38; H, 2.89; N, 6.94.

5.6.11 $Ru(Im\text{-}CO_2)_3\cdot 2H_2O$ (32)

Method A. Imidazole-4-carboxylic acid ($Im\text{-}CO_2H$) (0.094 g, 0.84 mmol) was added to a red solution of $K_3[RuCl_6]$ (0.12 g, 0.28 mmol) in H_2O (10 mL). The resulting red solution was refluxed for 6 h to afford a yellow precipitate that was collected at r.t., washed with MeOH (2 x 5 mL), and dried under vacuum at 78 °C for 48 h. Yield: 0.074 g (57 %).

Method B. $Im\text{-}CO_2H$ (0.092 g, 0.82 mmol) was added to a brown solution of $[Ru_2(CH_3COO)_4Cl]$ (0.065 g, 0.14 mmol) in water/MeOH, 1:1 (10 mL). The resulting brown solution was refluxed for 8 h to afford a yellow precipitate that was collected at r.t., washed with MeOH (2 x 5 mL), and dried under vacuum at 78 °C for 48 h. Yield: 0.043 g (67 %)

^1H NMR (dmso-d_6): δ 0.31, 0.09, -0.09 (s, H(5)-Im), -2.67, -13.55, -17.87 (s, H(2)-Im). IR (KBr pellet): ν 3423 (O-H, s), 3109 (N-H, br s), 1642 ($C=O_{asym}$, s), 1324 ($C=O_{sym}$, s), 1201 (m), 1090 (m), 1024 (m), 930 (m), 829 (m). ESI-MS: 435 (M^+). Anal. Calcd for $C_{12}H_9N_6O_6Ru\cdot 2H_2O$: C, 30.63; H, 2.77; N, 17.87. Found: C, 30.87; H, 2.58; N, 17.47.

5.6.12 $Ru(Im\text{-}CO_2)(Im\text{-}CO_2H)_2Cl_2 \cdot EtOH \cdot H_2O$ (33)

Im-CO_2H (0.084 g, 0.75 mmol) was added to a brown solution of $RuCl_3 \cdot 3H_2O$ (0.065 g, 0.25 mmol) in EtOH (10 mL). The resulting solution was refluxed for 4 h, when it had become yellow. The solvent was reduced in volume to ~2 mL and 15 mL of Et_2O was added to afford a yellow precipitate that was collected, washed with Et_2O (3 x 5 mL), and dried under vacuum at 78 °C for 24 h. Yield: 0.11 g (76 %). ^{1}H NMR (CD_3OD): δ 3.45 (q, $HOCH_2CH_3$), 1.12 (t, $HOCH_2CH_3$), -4.49, -7.20, -10.16 (s, H(5)-Im), -14.83, -16.75, -23.92 (br s, H(2)-Im). IR (KBr pellet): ν 3467 (O-H, br s), 3217 (O-H, m), 3149 (N-H, m), 1718 ($C{=}O_{asym}$, s), 1706 ($C{=}O_{asym}$, s), 1570 ($C{=}O_{asym}$, s), 1384 ($C{=}O_{sym}$, m), 1350 ($C{=}O_{sym}$, m), 1313 ($C{=}O_{sym}$, m), 1188 (m), 1089 (m). ESI-MS: 508 (M^+), 472 (M^+ - Cl), 396 (M^+ - Im-CO2H), 360 (M^+ - Im-CO2H – Cl). Λ_M (MeOH) = 19 $\Omega^{-1}cm^2mol^{-1}$. Anal. Calcd for $C_{12}H_{11}N_6O_6Cl_2Ru \cdot EtOH \cdot H_2O$: C, 29.42; H, 3.33; N, 14.71. Found: C, 29.36; H, 3.17; N, 14.44.

5.7 References

(1) Deacon, G.; Phillips, R. *Coord. Chem. Rev.* **1980**, *33*, 227.

(2) Nakamoto, K.; McCarthy, P. J. *Spectroscopy and Structure of Metal Chelate Compounds*; John Wiley & Sons, Inc.: New York, 1968.

(3) Ellis, R.; Quilligan, J.; Williams, N.; Yandell, J. *Aust. J. Chem.* **1989**, *42*, 1.

(4) Barral, M.; Jimenez-Aparicio, R.; Royer, E.; Saucedo, M.; Urbanos, F.; Gutierrez-Puebla, E.; Ruiz-Valero, C. *J. Chem. Soc. Dalton Trans.* **1991**, 1609.

(5) Ghatak, N.; Chakravarty, J.; Bhattacharya, S. *Polyhedron* **1995**, *14*, 3591.

(6) Kingry, K.; Royer, A.; Vincent, J. *J. Inorg. Biochem.* **1998**, *72*, 79.

(7) Cahtterjee, M.; Maji, M.; Ghosh, S.; Mak, T. *J. Chem. Soc., Dalton Trans.* **1998**, 3641.

(8) Chakov, N.; Collins, R.; Vincent, J. *Polyhedron* **1999**, *18*, 2891.

(9) Stearns, D. M.; Armstrong, W. H. *Inorg. Chem.* **1992**, *31*, 5178.

(10) Li, W.; Olmstead, M. M.; Miggins, D.; Fish, R. H. *Inorg. Chem.* **1996**, *35*, 51.

(11) Speetjens, J. K.; Collins, R. A.; Vincent, J. B.; Woski, S. A. *Chem. Res. Toxicol.* **1999**, *12*, 483.

(12) Anderson, R. A.; Bryden, N. A.; Polansky, M. M. *J. Am. Coll. Nutr.* **1997**, *16*, 273.

(13) Stephenson, T.; Wilkinson, G. *J. Inorg. Nucl. Chem.* **1966**, *28*, 2285.

(14) Martin, F. S. *J. Chem. Soc.* **1952**, 2682.

(15) Geary, W. J. *Coord. Chem. Rev.* **1971**, *7*, 81.

(16) Huheey, J. E. *Inorganic Chemistry: Principles of Structure and Reactivity, 3rd ed.*; Harper Collins Publishers: New York, 1983.

(17) Boskovic, C.; Folting, K.; Christou, G. *Polyhedron* **2000**, *19*, 2111.

(18) Sengupta, P.; Dinda, R.; Ghosh, S.; Sheldrick, W. *Polyhedron* **2001**, *20*, 3349.

(19) Tolstyakov, V. V.; Pevzner, M. S. *Russ. J. Org. Chem.* **1997**, *33*, 1803.

(20) Bagal, L. I.; Pevzner, M. S.; Frolov, A. N.; Sheludyakova, N. I. *Khim. Geterotsikl. Soedin. [English Translation]* **1970**, *2*, 240.

(21) Cipens, G. *Metody Poluch. Khim. Reaktivov Prep.* **1966**, *14*, 9.

(22) McMurry, J. *Organic Chemistry, 3rd ed.*; Brooks/Cole Publishing Co.: Pacific Grove, 1992.

(23) Davis, D. P.; Kirk, K. L.; Cohen, L. A. *J Heterocylic Chem.* **1982**, *19*, 253.

(24) Novikov, S. S.; Khmel'nitskii, L. I.; Lebedev, O. V.; Sevast'yanova, V. V.; Epishina, L. V. *Khim. Geterotsikl. Soedin. [English Translation]* **1970**, *6*, 465.

(25) Pavia, D. L.; Lampman, G. M.; Kriz, G. S. *Introduction to Spectroscopy*; Harcourt Brace College Publishers: Orlando, 1996.

(26) Nagao, H.; Hirano, T.; Tsuboya, N.; Shiota, S.; Mukaida, M.; Oi, T.; Yamasaki, M. *Inorg. Chem.* **2002**, *41*, 6267.

(27) Hirano, T.; Oi, T.; Nagao, H.; Morokuma, K. *Inorg. Chem.* **2003**, *42*, 6575.

(28) Serli, B.; Zangrando, E.; Gianferrara, T.; Yellowlees, L.; Alessio, E. *Coord. Chem. Rev.* **2003**, *245*, 73.

(29) Kavadias, G.; Luh, B.; Saintonge, R. *Can. J. Chem.* **1982**, *60*, 723.

(30) Vinogradova, N. B.; Kromov-Borisov, N. V. *Metody Poluch. Khim. Reactivov. Prep.* **1966**, *14*, 40.

Chapter 6

Antiproliferatory Activity of Ruthenium Complexes Using the MTT Assay

6.1 Introduction

For preliminary drug screening, tumour cell lines are used to test the antiproliferatory activity of compounds *in vitro*. Compounds then showing activity can be tested *in vivo* to determine if the *in vivo* and *in vitro* properties correlate. The MTT assay is a colourimetric assay commonly used as a screening process to examine the antiproliferatory activity of compounds over large concentration ranges.[1] The assay quantifies the extent of 3-(4,5-dimethylthiazol-2-yl)-2,5-diphenyltetrazolium bromide (MTT) reduction to formazan by mitochondrial dehydrogenase (Figure 6.1). In viable cells (Figure 6.2), MTT (yellow) is reduced to formazan (purple) which precipitates onto the surface of the wells. Dissolving the precipitate in DMSO gives a purple solution (Figure 6.3, details of the procedure are given in Section 6.3, as well as in a recent publication by our group[2]). The amount of formazan in each well is then measured spectrophotometrically to determine the number of viable cells in each well. The absorbance values at determined at each concentration are then divided by the absorbance values of the control and plotted vs. concentration. From these graphs, IC_{50} values can be

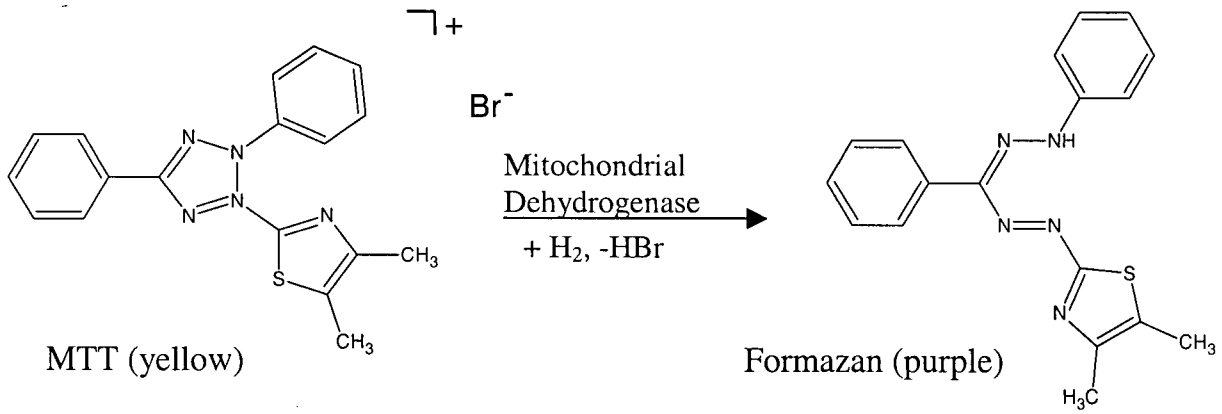

Figure 6.1 Mitochondrial reduction of MTT to Formazan.

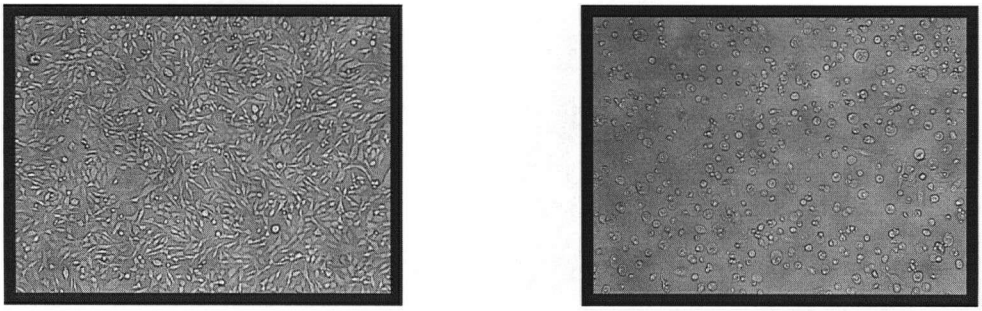

Figure 6.2 Pictures of cells on Day 5 of MTT assay before adding MTT in a control experiment with no complex (left), and in an experiment incubated for 69 h in 2 mM $Ru(ma)_3$ (right).

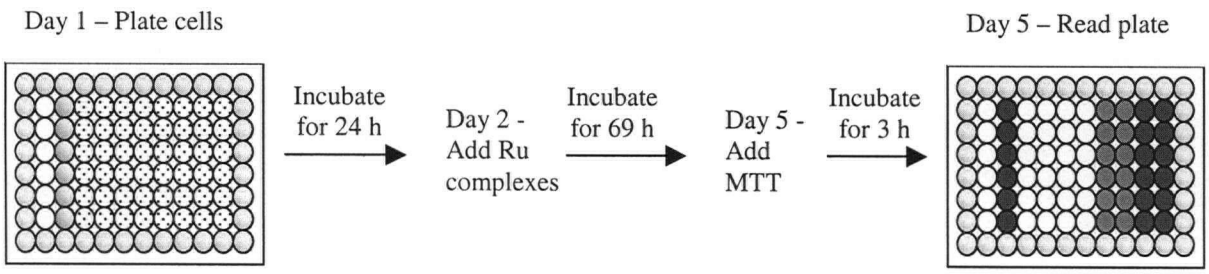

Figure 6.3 Outline of MTT assay from Day 1 - Day 5; see Section 6.3. The outer rows of wells are filled with water, and the inner wells with cells increasing in concentration of complex from right to left. The leftmost two columns are the blank (farthest left) and control (second from left). The intensity of the purple colour is proportional to the number of viable cells present (highest for the control and low concentration samples).

determined, the concentration at which the number of viable cells is 50 % that of the control.[3,4] Low IC_{50} values with respect, in particular, to that of cisplatin (40 μM for the MDA-MB-435S cell line under the reaction conditions described in this Section 6.3, Table 6.4), are desirable and suggest that the compound is having an antiproliferatory effect at low concentrations.[5] Complexes exhibiting high IC_{50} values may also have useful biological applications, particularly in the case of EF5 complexes (Table 6.3), which may be specific to hypoxic cells.[6] There is a need to develop useful imaging agents for hypoxia that should specifically target hypoxic cells while, at the same time, be

free of any cytotoxic effects that might also harm healthy cells (i.e. exhibit high IC_{50} values).[7]

The results of the MTT assay have been found generally to correlate well with *in vivo* studies as well as with other *in vitro* studies such as the dye exclusion assay.[8] Measurements of formazan absorption in MTT tests have been shown to correlate very well with the number of counted cells both using a Coulter counter[3] and using microscopic counting techniques.[9,10] Like all assays, however, results from the MTT assay vary between cell lines and, within a given cell line, results may vary from week to week (Section 6.4.2, ± 5 %) although this variation can often be difficult to distinguish from the natural distribution of the data.[11] For these reasons the MTT assay is only a preliminary assay. Positive results at this stage then lead to more detailed testing *in vitro* using more cell lines as well as *in vivo* studies.

Experience in the development of NAMI-A (Figure 1.8, Section 1.5.3.1) has led to a set of suggested guidelines for the testing of Ru complexes for anti-cancer properties. The Callerio Foundation, the group responsible for the development of NAMI-A, lists the MTT assay as the first step in a screening process recommended for determining whether a Ru complex may exhibit any antiproliferatory activity toward a given cancer cell line.[5]

6.2 General Experimental Procedures

6.2.1 Experimental Media, Solutions, and Materials

Leibovitz's L-15 medium with L-glutamine (L-15), Dubelco's modified essential medium (DMEM), fetal bovine serum (FBS), zinc bovine insulin, penicillin/streptomycin antibiotic, phosphate buffered saline solution 7.4 (PBS), and trypsin-EDTA (0.25 % trypsin in 1mM Na_4(EDTA)) were purchased from Gibco. 96-Well plates, T-25 and T-75 flasks were purchased from Falcon. MTT was purchased from Aldrich. The growth medium for the MDA-MB-435S cell line consisted of 500 mL L-15, 50 mL FBS, and 5.0 mg of insulin. The growth medium for the MDA435/LCC6-WT cell line consisted of 500 mL DMEM, 50 mL FBS, and 5,000 units of penicillin/streptomycin antibiotic. PBS, MTT and the growth medium were stored at 4 °C, while the trypsin-EDTA and FBS were stored at –20 °C. FBS was filter-sterilized through 0.1 μm filters before use.

6.2.2 Cell Preparation

Human breast cancer cells (MDA-MB-425S) were purchased from the American Type Tissue Culture Collection (ATCC), while MDA435/LCC6-WT cells[12,13] were kindly donated by Dr. K Skov of the BC Cancer Research Center. The MDA-MB-435S cells were maintained in L-15 medium in T-75 tissue culture flasks at 37 °C under air. The cells were transferred every 3-4 days to new flasks at a dilution factor of approximately 8. Before transfer, the medium was removed from the flask, and the cells were rinsed for 20 s with 2 mL trypsin-EDTA, which was then removed and 2 mL of fresh trypsin-EDTA were added to the flask. After 3-4 min the cells were observed to detach from the flask surface, and 8 mL of medium were added. The cells were then counted under a microscope using a hemacytometer (Hausser Scientific, 0.100 mm deep). 2 x 10^6 cells (typically in 2-3 mL of medium) were then transferred to a T-75 flask, and the suspension diluted to 20 mL with medium to yield a final density of 1 x 10^5 cells/mL.

For the MDA435/LCC6-WT cells, the cell preparation was the same as for the MDA-MB-435S cells using DMEM medium in place of L-15 medium (the preparation of the media is described in Section 6.2.1).

6.2.3 Preparation of Ru Complexes

The Ru complexes were weighed into glass vials and dissolved in PBS to make 1.5 mL of 4 mM stock solutions for each complex. These solutions were then sonicated and heated to 37 °C to ensure the complex was completely dissolved, and then filtered through 0.2 μm filters to remove any remaining particulates. From this stock solution, subsequent dilutions yielded the following final concentrations: 2, 1, 0.5, 0.2, 0.1, 0.05, 0.02, 0.01 mM (Section 6.3.2). Follow-up experiments for several compounds focused on a lower concentration range, and thus stock solutions of 0.400 mM were used instead and the dilutions were adjusted to test concentrations as low as 500 nM. For the complexes containing EF5 (**14**), $2NO_2$Im (**15**) and $3NO_2$tri (**17**), stock solutions of 4 mM could not be prepared because of poor complex solubilities in PBS. Instead 2 mM stock solutions of **15** and **17** were prepared in 20 % DMSO in PBS, while a 2 mM solution of **14** was prepared in 5 % DMSO in PBS. These three solutions were then heated to 50 °C

to ensure complete solubility of the complexes, filter sterilized while hot, and then cooled to room temperature before use.

6.2.4 Preparation of Ligand Precursor Solutions

Hma, HEma, DMSO and N-heterocyclic compounds (see Table 6.2) that acted as ligand precursors were tested over a concentration range from 5 to 0.02 mM. They were weighed into glass vials and dissolved in PBS to yield 1.5 mL of 10 mM stock solutions for each compound.

6.3 MTT Assay Procedure

6.3.1 Day 1 - Plating Cells

On day one of the MTT assay, cells were plated into 96-well plates. The medium was removed from a T-75 flask containing the cells, and 2 mL of trypsin-EDTA were then added. The flask was gently agitated to rinse the cells. The trypsin-EDTA was removed and an additional 2 mL were added to the flask which was then sealed for 3-4 min. After 3 min the cells were examined under a microscope to determine whether they were still adhering to the plastic flask or whether they had become detached. If the cells were still adhering, the flask was again gently shaken to assist in the removal of the cells from the flask wall. L-15 medium (8 mL) was then added to the flask. This suspension was thoroughly mixed by pipetting the mixture "up and down" several times. A 50 μL aliquot of the suspension were then removed and plated onto a hemacytometer to determine the cell count. Then the dilution factor needed to make a stock suspension of 1 x 10^5 cells/mL was calculated (5.4 mL of this suspension are required per plate), and 100 μL of this suspension were then added to each of the wells in columns 3-11 in rows B-G (Figure 6.4). Medium (100 μL) was added to the wells in column 2 rows B-G (blank). Water (200 μL) was then added to all the remaining wells to help prevent evaporation of the medium from the experimental wells. The plates were then placed into the incubator for 24 h.

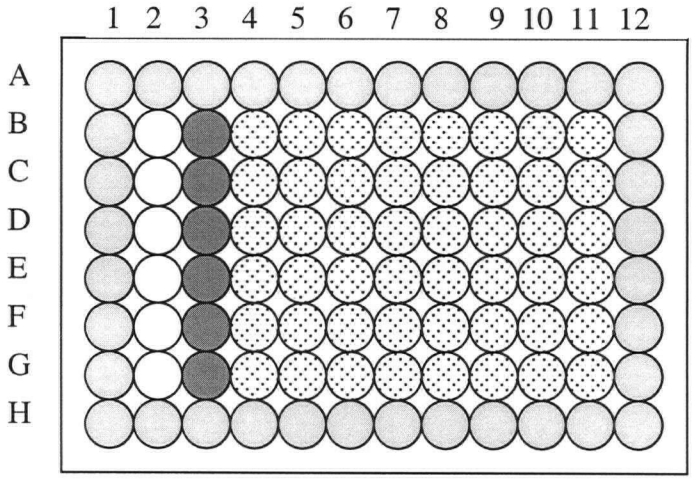

Figure 6.4 Experimental 96-well plate set-up showing the control column (dark grey), the blank (white), the wells with water (light grey) and those containing the complex solutions (speckled).

6.3.2 Day 2 – Addition of Ru Complexes and Ligand Precursors

The 96-well plates were removed from the incubator after 24 h. Stock solutions of Ru complexes were prepared as described in Section 6.2.3. Dilutions of such stock solutions were then prepared in 700 μL tubes using PBS (except for **14**, **15**, and **17,** see below), in order to yield eight 650 μL solutions spanning, when using a 4 stock solution, from 4 mM to 0.02 mM (Table 6.1). For those experiments in which a 0.4 mM stock solution was used, the concentrations of the corresponding diluted solutions were one order of magnitude less; in some cases different dilutions were used in order to test concentrations below 2 μM. The diluted solutions for all experiments were mixed using a multi-channel pipette and then 100 μL of each solution was pipetted into the wells in rows B-G and columns 2-11 (Figure 6.4). Only PBS (or PBS/DMSO in some cases, as discussed later below) was added to columns 2 and 3, as these two columns were the blank and control, respectively.

Solutions of **14**, **15**, and **17** were prepared as DMSO/PBS solutions and were thus subsequently diluted with the same solvent mixture used for their preparation (20 % DMSO for **15** and **17**, and 5 % DMSO for **14**) to ensure that any DMSO effect would be

minimized. In Section 3.3.3, it was observed that both **15** and **17** in DMSO dissociated ligands; however, the resulting solutions of these complexes in DMSO:PBS (1:1) were still tested using the MTT assay. The DMSO:PBS solvent mixtures were added to the control and blank to ensure that any DMSO effect would manifest itself in the control as well. The stock solutions of these three complexes were only 2 mM (see Section 6.2.3), and therefore the final concentrations of the diluted samples were half those shown in Table 6.1, which shows the final concentrations for samples diluted from a 4 mM stock solution.

Table 6.1 Dilution table for the addition of complexes using a 4 mM stock solution.[a] Solutions of 650 μL were made for each concentration of Ru complex, as well as those for the blank and the control.

Column	2	3	4	5	6	7	8	9	10	11
Concentration of complexes (μM)	0	0	4000	2000	1000	400	200	100	40	20
Vol. PBS (μL)	650	650	0	325	487.5	585	617.5	633.75	643.5	646.75
Vol. stock solution (μL)	0	0	650	325	162.5	65	32.5	16.25	6.5	3.25

[a] For some complexes different stock solution concentrations or different dilution factors were used to perform the assay (see Sections 6.2.3 and 6.2.4).

For the ligand precursors, 10 mM stock solutions were prepared in PBS, the samples then being diluted in PBS to final concentrations spanning 10 to 50 μM. The dilutions used were as for the Ru complexes (Table 6.1), with the final concentrations being 2.5 times greater than those shown, as 10 mM stock solutions were used instead of 4 mM ones.

6.3.3 Day 5 - Addition of MTT and Plate Reading

A modified version of a published procedure was used for the addition of MTT.[14] After incubation of the cell/complex mixture for 69 h, 50 μL of an MTT solution (2.5 mg/mL in PBS) were added to each of the wells in rows B-G, columns 2-11. The plates were then incubated for an additional 3 h, at which time the medium was removed from all the wells to leave purple formazan crystals. DMSO (150 μL) was then added to each

of the columns in rows B-G, columns 2-11, and the plates were then scanned at 570 nm on a Spectra Max 190 Elisa plate reader (Molecular Devices Co.) with a shake time set to 10 s before reading the plates (Figure 6.5). Values for the blank absorbance were averaged and automatically subtracted from those read for each well using Softmax Pro v2.2.1 software.

6.3.4 Data Analysis

For each compound, six replicates were performed at each of eight different concentrations. The absorbance of each well at 570 nm was determined. The values obtained were normalized by subtracting the average absorbance value for the 6 blank replicates from the value for each experimental and control well. At each concentration the average absorbance over the 6 replicates was determined and divided by the average value for the 6 control replicates to determine the percent cell viability at each concentration. Values presented in this chapter are the IC_{50} values determined by graphing the percent viability versus concentration, and for the complexes are the average value as determined from two or more experiments. For the free ligands, the IC_{50} values reported are those from a single experiment. With the MDA-MB-435S cell line, IC_{50} values were found to be reproducible within experimental uncertainty from week to week. Error bars are included on each graph and represent 2 standard deviations or a 95 % confidence limit.

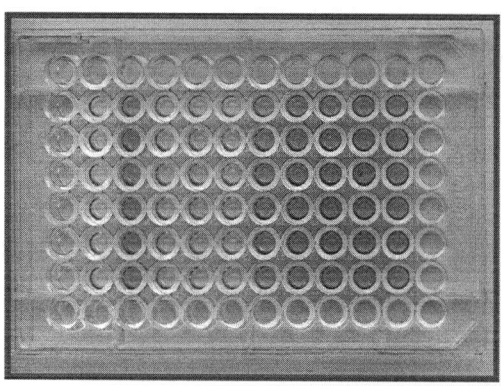

Figure 6.5 Image of plate after MTT treatment. The control is clearly seen as a purple column on the left, and the purple colours on the right clearly show the increase in cell viability at lower concentration.

6.4 Results and Discussion

6.4.1 Ligand Precursors

Table 6.2 shows the IC_{50} values for the ligand precursors used to form the Ru complexes that were tested. The only one of these compounds that showed significant activity was $2NO_2Im$, exhibiting an IC_{50} value of 50 μM. Only two other compounds exhibited IC_{50} values below 500 μM, EF5 and $3NO_2tri$, both N-heterocycles containing a

Table 6.2 IC_{50} values for the ligand precursors against MDA-MB-435S cells in L-15 medium after incubation at 37 °C for 69 h.

Compound[a]	IC_{50} (μM) (±10 %)
Hma	1000
HEma	900
Im	>5000
2MeIm	>5000
4MeIm	>5000
1MeIm	>5000
H_2Me_2biim	650
H_2biim	800
$2NO_2Im$	50
EF5	350
$3NO_2tri$	400
metro	>5000
Hpic	950
Im-CO_2H	4000
HCANT	1000
DMSO	>5000[b]

[a] See page xxii for compound abbreviations.
[b] Ref. 2.

nitro group. The lack of any significant activity of ma, Ema and most of the imidazoles (IC_{50} values are much higher than those observed for complexes containing these compounds as ligands, see Section 6.4.2) suggests that the lower IC_{50} values for the complexes are not a result of dissociated ligand inside the cell.

6.4.2 Ru Maltolato and Imidazole Complexes

In total, 23 complexes were screened using the MTT assay (Tables 6.3-6.6). Because of some variability in the assay from week to week resulting from changes in cell morphology over time, $Ru(ma)_3$ (**1**) and $[Ru(ma)_2(2MeIm)_2]CF_3SO_3$ (**10**) were used as standards to ensure consistency from week to week. These complexes were chosen as they exhibited activity in different concentration ranges (IC_{50} value for **1** is 140 μM and for **10** is 5 μM), and showed similar variability from week to week (e.g. if the IC_{50} value for **1** went up 5 %, so did the IC_{50} value for **10**; in general, weekly variability was < 5 % and thus values non-normalized values still fell within experimental error limits); in contrast, the activity of cisplatin, did not vary. Cisplatin was also tested and used as a control to help compare the results with those of other groups, who have used different cell lines but have used cisplatin as a standard.[15] The tests with the free ligands (Table 6.2) suggest that the intact complexes in solution likely give rise to the activity and not free ligand present as a result of ligand dissociation over the incubation period. Table 6.3 shows the IC_{50} values for the maltolato complexes that were tested. Only 3 complexes with nitro-substituted ligands were tested because of poor solubilities in PBS. In fact, at higher complex concentrations, the 570 nm absorbances for the complexes with EF5 (**14**), $2NO_2Im$ (**15**) and $3NO_2tri$ (**17**) increased as a result of metal-containing species precipitating from the reaction medium. This was confirmed by examining the cells under a microscope on day 5 of the MTT assay, before the addition of MTT. Under the microscope, blue solids for **15** and **17**, and a brown solid for **14**, were observed at concentrations of 500 μM and higher.

Against the MDA-MB-435S cell line, $[Ru(ma)_2(2MeIm)_2]CF_3SO_3$ (**10**) showed the lowest IC_{50} value of all the maltolato complexes tested (5 μM) (Figure 6.6); $[Ru(ma)_2(4MeIm)_2]CF_3SO_3 \cdot CH_2Cl_2$ (**6**) was also highly active (15 μM). The next most

Table 6.3 IC_{50} values for Ru-maltolato complexes against MDA-MB-435S cells in L-15 medium and against MDA435/LCC6-WT cells in DMEM after incubation at 37 °C for 69 h.[a]

Complex	IC_{50} (μM) MDA-MB-435S	IC_{50} (μM) MDA435/LCC6-WT
trans-$[Ru(ma)_2(2MeIm)_2]CF_3SO_3$ (**10**)	5	5
trans-$[Ru(ma)_2(4MeIm)_2]CF_3SO_3 \cdot CH_2Cl_2$ (**6**)	15	80
$[Ru(ma)_2(Im)_2]CF_3SO_3$ (**7**)	70	>2000
trans-$[Ru(ma)_2(1MeIm)_2]CF_3SO_3 \cdot CH_2Cl_2$ (**8**)	80	>2000
trans-$[Ru(ma)_2(metro)_2]CF_3SO_3$ (**4**)	80	>2000
trans-$[Ru(ma)_2(EtOH)_2]CF_3SO_3$ (**3**)	300	-
trans-$[Ru(ma)_2(EF5)_2]CF_3SO_3 \cdot EtOH$ (**14**)	>500	-
$[Ru(ma)_2(2NO_2Im)_2]CF_3SO_3$ (**15**)	25	90
$[Ru(ma)_2(3NO_2tri)_2]CF_3SO_3$ (**17**)	>500	-

[a] Error limits are ± 10 %.

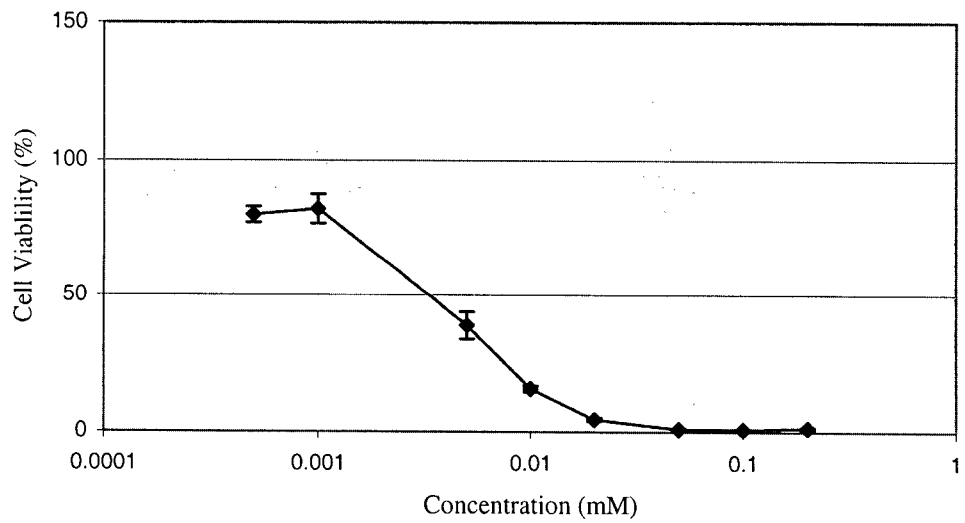

Figure 6.6 Cell viability vs. concentration for $[Ru(ma)_2(2MeIm)_2]CF_3SO_3$ (**10**), with error bars representing 95% confidence limit.

active imidazole complexes were the corresponding Im (**7**) and 1MeIm (**8**) species with IC_{50} values of 70 and 80 μM, respectively. These complexes (**6**, **7**, **8**, and **10**) showed no signs of ligand dissociation or reactivity in the PBS/medium solutions as judged by TLC analysis of the complex solutions after 5 days. This suggests that the intact complexes are responsible for the observed activity, and not a new complex resulting from partial ligand dissociation or displacement in the medium.

$[Ru(ma)_2(2NO_2Im)_2]CF_3SO_3$ (**15**) exhibited an IC_{50} value of 25 μM, half that of free $2NO_2Im$ (Tables 6.2 and 6.3), the activity likely resulting from the presence of free $2NO_2Im$, as TLC analysis of **15** dissolved in PBS:DMSO (1:1) showed a large band for this compound. The 25 μM IC_{50} value for **15** perhaps indicates that all of the $2NO_2Im$ is dissociating, thus exhibiting an IC_{50} value half that observed for the free ligand (25 μM complex is equiv. to 50 μM free ligand). If the $2NO_2Im$ is only partially dissociating in solution, the activity observed may be attributed to remaining undissociated Ru complex. The PBS/medium solution of the bis(EtOH) complex, **3**, changed colour from red to green over the 3 day incubation, likely as a result of displacement of the EtOH ligands; EtOH is readily displaced by water at room temperature but the aqua complex is also red in colour (Section 3.2.3). The green colour suggests components of the PBS/medium solution are coordinating to the Ru.

Some of the complexes listed in Table 6.3 were also tested against another cell line, MDA435/LCC6 –WT,[16] and the IC_{50} values differed from those observed against the MDA-MB-435S cell line for most of the complexes; **4**, **7**, and **8** exhibited IC_{50} values > 2 mM against the MDA435/LCC6-WT cell line, compared to values of 70 - 80 μM against the MDA-MB-435S cell line. Only the IC_{50} value for **10** was the same against both cell lines (5 μM).

$Ru(ma)_3$ (**1**) (Figure 6.7) and $Ru(Ema)_3$ (**2**) (Figure 6.8) gave IC_{50} values of 140 and 90 μM, respectively, against the MDA-MB-435S cell line (Table 6.4); the values agree with those reported earlier against this cell line under similar conditions (150 and 80 μM).[17] The increase in cell proliferation observed at lower concentration for **2** (at < 50 μM, Figure 6.8) was reproducible, suggesting that **2** has an advantageous effect on

cell proliferation at such concentrations as well as a deleterious one at higher concentrations.

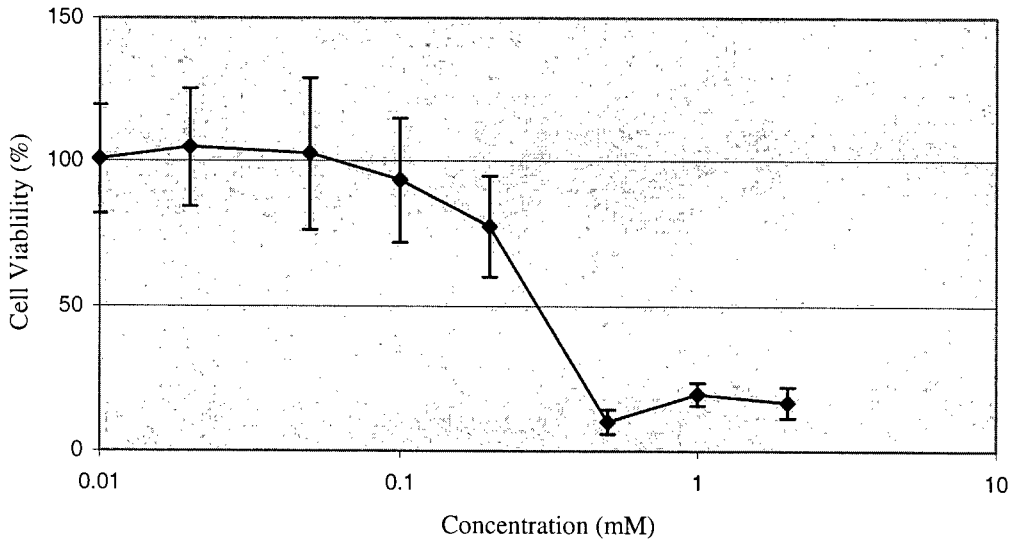

Figure 6.7 Cell viability vs. concentration for $Ru(ma)_3$ (**1**), with error bars representing 95% confidence limit.

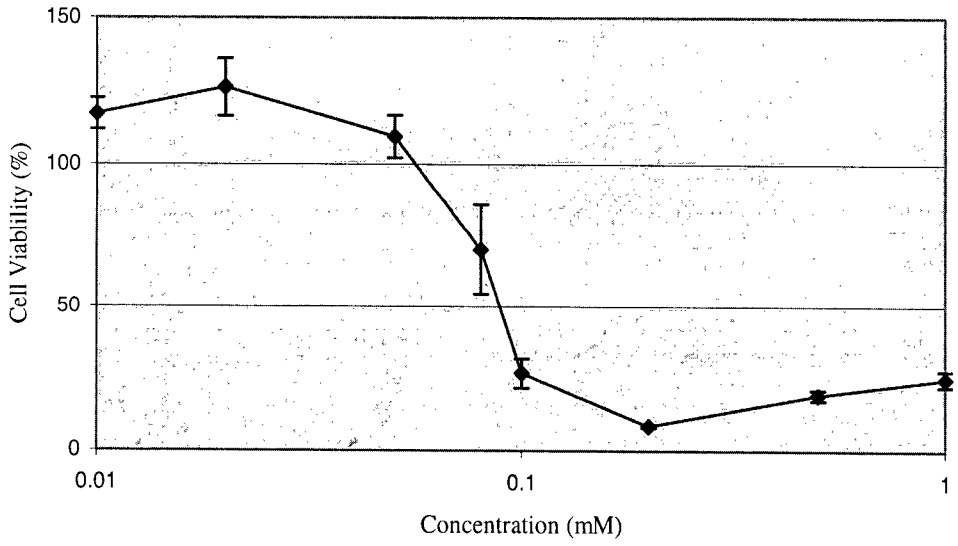

Figure 6.8 Cell viability vs. concentration for $Ru(Ema)_3$ (**2**), with error bars representing 95% confidence limit.

Table 6.4 IC_{50} values for cisplatin,[a] and three Ru complexes against MDA-MB-435S cells in L-15 medium after incubation at 37 °C for 69 h.[b] $Ru(ma)_3$ (**1**) and $Ru(Ema)_3$ (**2**) are precursors for the complexes in Tables 6.3 and 6.5, and $[RuCl(p\text{-cymene})]_2(\mu\text{-}Cl)_2$ is a precursor for biologically active Ru sulfoxide complexes.

Complex	IC_{50} (μM)
$Ru(ma)_3$ (**1**)	140
$Ru(Ema)_3$ (**2**)	90
Cisplatin	40
$[RuCl(p\text{-cymene})]_2(\mu\text{-}Cl)_2$	350

[a] Error limits are ± 5 % for cisplatin.
[b] Error limits are ± 10 % for the Ru complexes.

To determine if this trend of greater activity for Ema complexes (vs. ma species) was more general, Ema-4MeIm and -2MeIm derivatives were synthesized because **6** and **10** showed the lowest IC_{50} values of the ma complexes (Table 6.3). Again, the Ema systems exhibited lower IC_{50} values (Table 6.5): indeed, $[Ru(Ema)_2(2MeIm)_2]CF_3SO_3$ has an IC_{50} value of 500 nM (Figure 6.9), an order of magnitude lower than that of any other complex tested. It is unclear why the Ema derivatives exhibit IC_{50} values lower than those of the corresponding ma complexes, but this finding will be discussed further with other results given in Chapter 7.

Table 6.5 IC_{50} values for ethylmaltolato complexes against MDA-MB-435S cells in L-15 medium after incubation at 37 °C for 69 h.[a]

Complex	IC_{50} (μM)
$[Ru(Ema)_2(2MeIm)_2]CF_3SO_3$ (**13**)	0.5
$[Ru(Ema)_2(4MeIm)_2]CF_3SO_3$ (**12**)	5

[a] Error limits are ± 10 %.

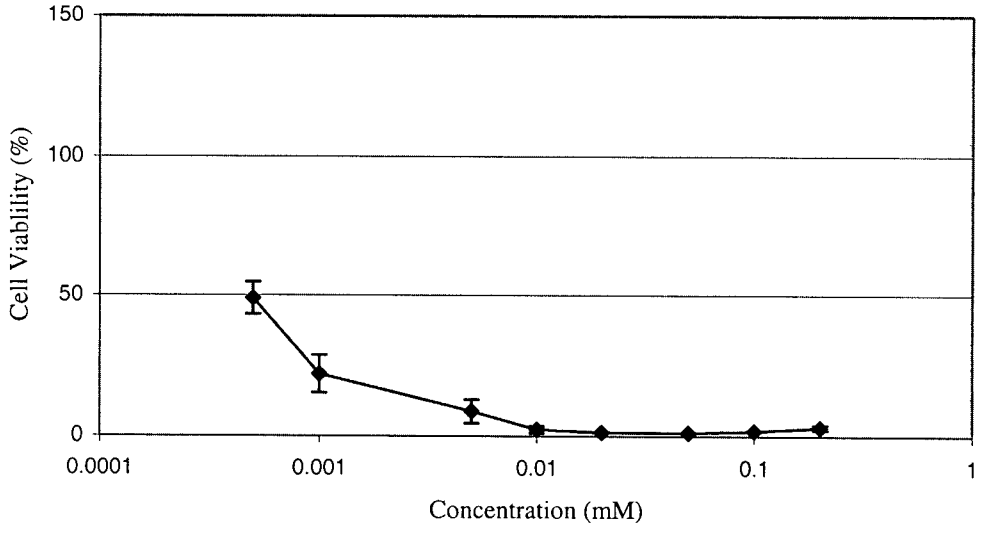

Figure 6.9 Cell viability vs. concentration for $[Ru(Ema)_2(2MeIm)_2]CF_3SO_3$ (**13**), with error bars representing 95% confidence limit.

Cisplatin was tested several times against the MDA-MB-435S cell line in order to provide a "known standard," and had an IC_{50} value of 40 μM (Figure 6.10, Table 6.4), while the value against the human ovarian cell line A2780 is reported as 0.5 μM,[15] eighty times lower. IC_{50} values are also reported for RuX(*p*-cymene)(N-N) complexes, where X = Cl or I and N-N = ethylenediamine or $(CH_3CN)_2$, against the A2780 cell line, some exhibiting IC_{50} values as low as 8 μM.[15] Previously in our group, Huxham *et al.* found that $[RuCl(p\text{-cymene})]_2$(μ-BESE) exhibited an IC_{50} value of 350 μM against the MDA-MB-435S breast cancer cell line.[18] As no one has reported on the biological activity of the precursor for these Ru-*p*-cymene complexes, $[Ru(p\text{-cymene})Cl_2]_2$, this dimer was tested against the MDA-MB-435S breast cancer cell line and its IC_{50} was also found to be 350 μM (Table 6.4). Per Ru atom, the IC_{50} values of both the starting dimer and $[RuCl(p\text{-cymene})]_2$(μ-BESE) are 700 μM; thus the presence of the chelated sulfoxide is not necessary to produce the observed activity for this complex.[18]

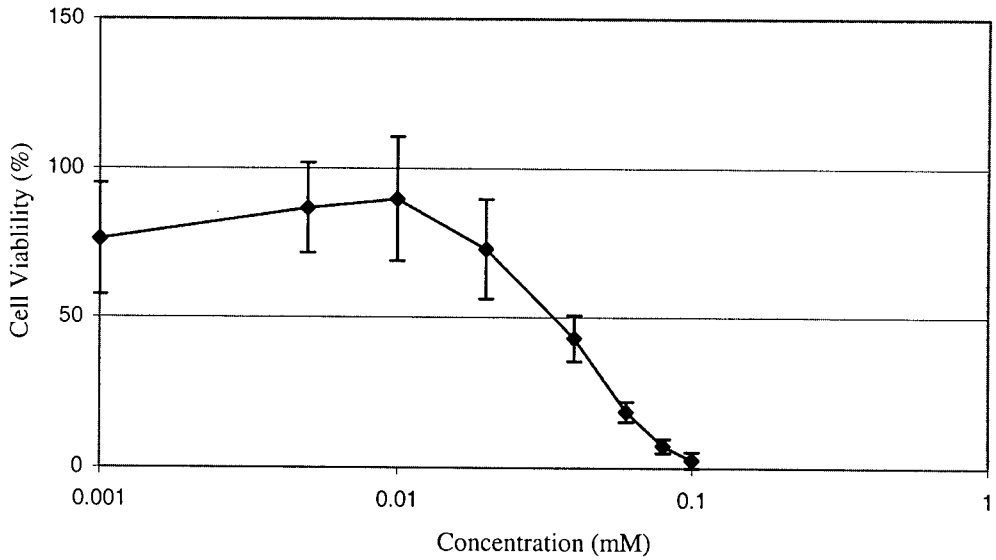

Figure 6.10 Cell viability vs. concentration for cisplatin, with error bars representing 95% confidence limit. This experiment was done over a shortened concentration range to produce more points near the IC_{50} value and improve the accuracy of the assay.

6.4.3 Ru 4,4'-Biimidazole Complexes

Complexes of 4,4'-biimidazoles were also tested using the MTT assay, including maltolato biimidazole complexes (Table 6.6). After a 2MeIm derivative was shown to exhibit the lowest IC_{50} value of a series of Ru-ma complexes (Table 6.3), 2,2'-dimethyl-4,4'-biimidazole (Me_2biim) was synthesized (Section 4.8) as well as 4,4'-biimidazole (biim) (Section 4.8), and a Ru ma complex of each was examined, as well as other complexes containing either of these two ligands.

The IC_{50} value for $[Ru(ma)_2(Me_2biim)]CF_3SO_3 \cdot 2H_2O$ (**25**) (Figure 6.11) is 15 μM, the same as for **6** (Table 6.3), while $[Ru(ma)_2(biim)]CF_3SO_3 \cdot 2H_2O$ (**24**) (Figure 6.12) exhibited an IC_{50} value of 50 μM. These two complexes exhibit activities different from those of the analogous bis(Im) (**7**, IC_{50} = 70 μM) and bis(2MeIm) (**10**, IC_{50} = 5 μM) complexes (Table 6.3). Two major differences that may account for this are the

Table 6.6 IC_{50} values[a] for biim and Me_2biim complexes against MDA-MB-435S cells in L-15 medium after incubation at 37 °C for 69 h; data for new Ru complexes containing picolinic acid (Hpic) or imidazole-4-carboxylic acid (Im-CO_2H) against the same cell line under the same conditions are also shown.

Complex	IC_{50} (μM)
$[Ru(ma)_2(biim)]CF_3SO_3 \cdot 2H_2O$ (**24**)	50
$[Ru(ma)_2(Me_2biim)]CF_3SO_3 \cdot 2H_2O$ (**25**)	15
$[Ru(biim)_3][CF_3SO_3]_2$ (**26**)	18
$[Ru(Me_2biim)_3][CF_3SO_3]_2$ (**27**)	36
$RuCl_2(DMSO)_2(biim)$ (**20**)	800
$RuCl_2(DMSO)_2(Me_2biim)$ (**22**)	400
$[Ru_2(pic)_4(EtOH)Cl] \cdot H_2O$ (**31**)	100
$Ru(Im\text{-}CO_2)(Im\text{-}CO_2H)_2Cl_2 \cdot H_2O \cdot EtOH$ (**33**)	400

[a] Error limits are ± 10 %.

geometric arrangement of the ligands (cis-ma for **24** and **25** vs. trans-ma for **7** and **10**) and the Ru(III/II) reduction potential in MeCN vs. SCE (–101 and –35 mV for **24** and **25**, respectively (Table 4.1), and -705 and –844 mV for **7** and **10**, respectively (Table 3.4)). Clarke *et al.* have suggested that the reduction of Ru(III) to Ru(II) may play an important role in the activation of Ru complexes inside the cell.[19,20] The low reduction potentials of **7** and **10** perhaps indicate that such a reduction is not relevant for these two complexes. **24** and **25**, however, have much more positive reduction potentials and might be reduced inside the cell.

The cis geometry of the biimidazole complexes **24** and **25** compared to the trans geometry of all the complexes listed in Table 6.3 (Section 6.4.2) may also play an important role. The orientation of ligands can be important for their biological activity as in the case of cisplatin: the trans-isomer (*trans*-$[PtCl_2(NH_3)_2]$) is completely inactive because it is unable to form the necessary intrastrand DNA crosslinks to prevent cell division.[21] **24** and **25** appear to remain intact throughout the experiment (as judged by TLC), at least outside the cells. From the experiments conducted, it could not be

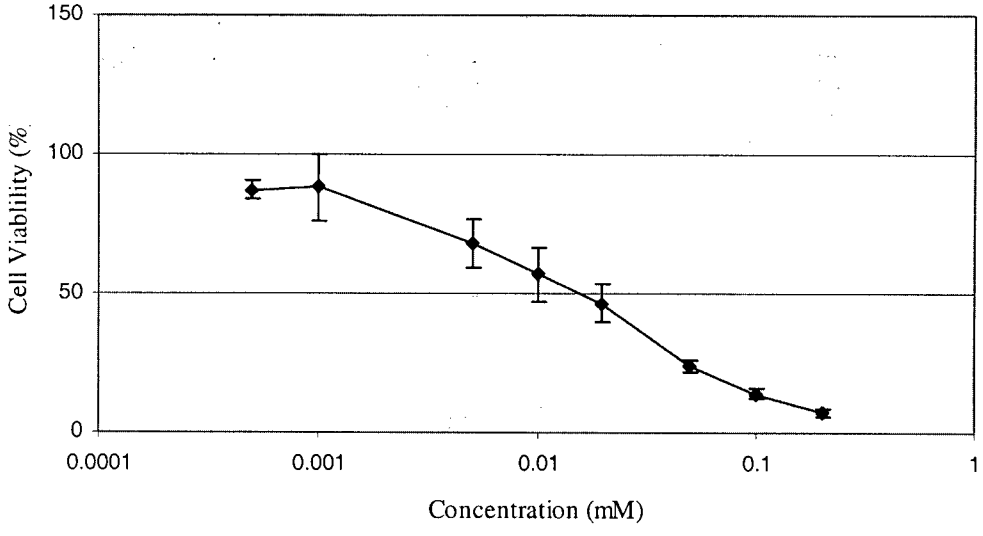

Figure 6.11 Cell viability vs. concentration for $[Ru(ma)_2(Me_2biim)]CF_3SO_3 \cdot 2H_2O$ (**25**), with error bars representing 95% confidence limit.

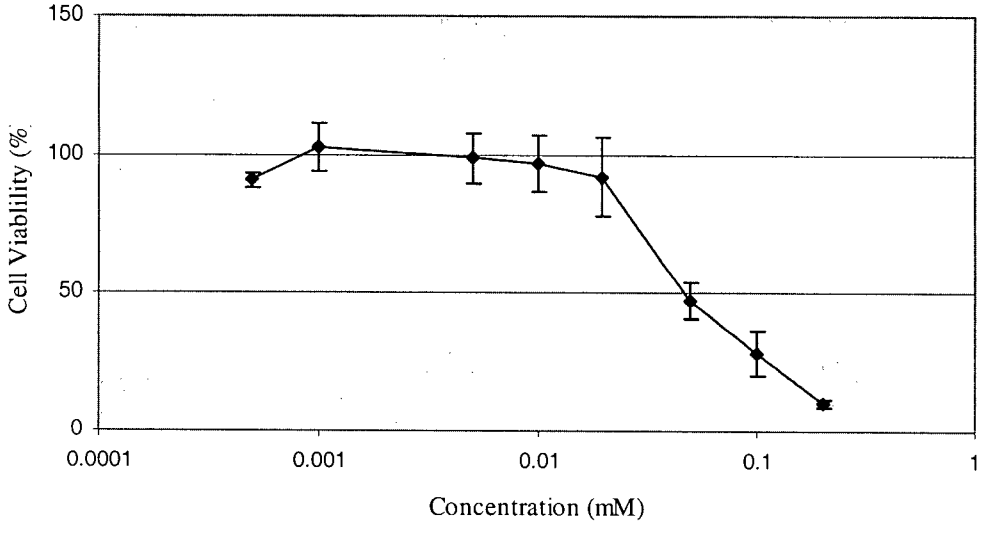

Figure 6.12 Cell viability vs. concentration for $[Ru(ma)_2(biim)]CF_3SO_3 \cdot 2H_2O$ (**24**), with error bars representing 95% confidence limit.

determined if an intra-cellular process might lead to any ligand dissociation. Even in the absence of vacant sites for binding components of intra-cellular molecules, the geometry of the ligands can still play a role in how the complexes interact with protein active sites: a transport protein, for example, may recognize only one of the cis- or trans-isomers.

Some Ru(II) complexes with biimidazoles were also tested (Table 6.6). The mixed biimidazole/DMSO complexes showed considerably less activity against this cell line than the Ru(III) complexes tested. Our group has reported on the activity of Ru(II)-maltolato sulfoxide complexes[2] and Ru(II)-acetylacetonato sulfoxide complexes[22] against the MDA-MB-435S cell line (data taken from Wu's M.Sc. thesis),[17] the lowest IC_{50} value being 190 μM for $Ru(Ema)_2(DMSO)_2$. $[Ru(Me_2biim)_3][CF_3SO_3]_2$ (**26**) and $[Ru(biim)_3][CF_3SO_3]_2$ (**27**) exhibit IC_{50} values of 36 and 18 μM, respectively (Figures 6.13 and 6.14), which indicates significant antiproliferatory activity in the absence of the ma ligand, these complexes are almost certainly acting through a different mechanism than that of the Ru(III) ma complexes. No MTT studies have been reported using $[Ru(Im)_6][CF_3SO_3]_2$ or other similar homoleptic imidazole complexes, so the effect of the

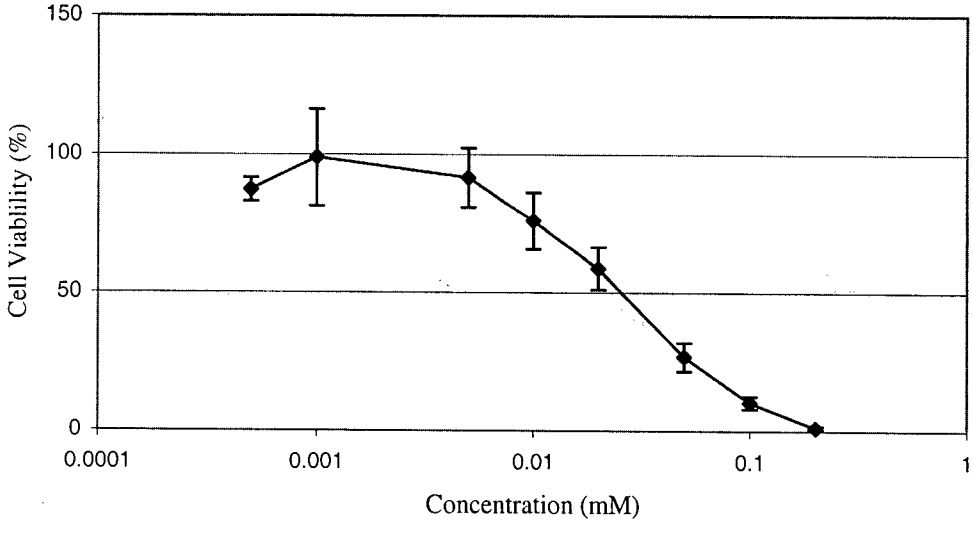

Figure 6.13 Cell viability vs. concentration for $[Ru(Me_2biim)_3][CF_3SO_3]_2$ (**27**), with error bars representing 95% confidence limit.

bidentate versus the corresponding monodentate ligands cannot be compared. Previous work in our group showed that incubation of SCCVII cells with $[Ru(Im)_6][CF_3SO_3]_2$ for 3 h did lead to some Ru uptake into the cells.[6] Further study of these Ru(II) systems is needed to arrive at a better understanding of their behaviour, and to determine what effect the biimidazoles produce with respect to complexes with monodentate imidazoles.

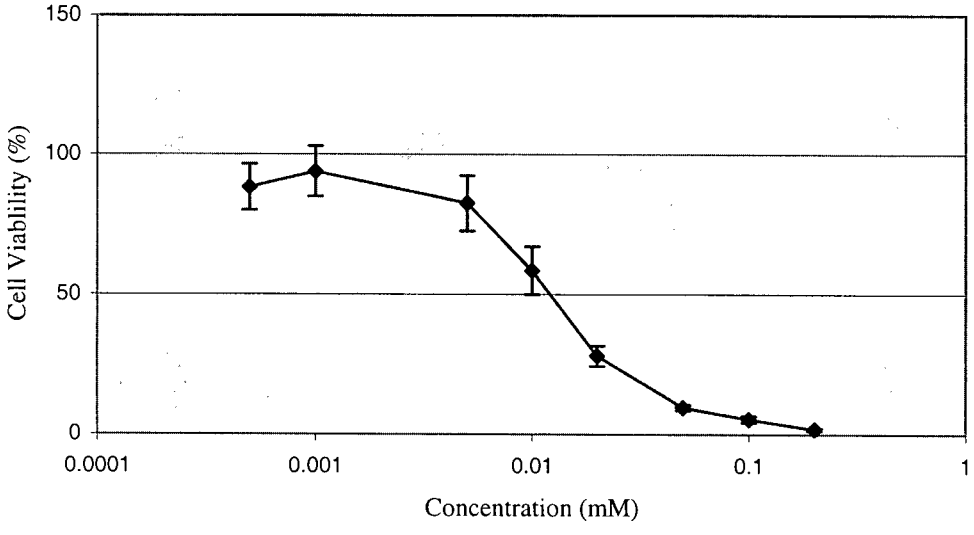

Figure 6.14 Cell viability vs. concentration for $[Ru(biim)_3][CF_3SO_3]_2$ (**26**), with error bars representing 95% confidence limit.

6.4.4 Ru Carboxylate complexes

A Ru(III) complex with imidazole-4-carboxylic acid (**32**), and a mixed valence Ru(III/II) bimetallic complex with picolinic acid (**31**) (Figure 6.15) were also tested using the MTT assay. Both exhibited higher IC_{50} values than did the imidazole maltolato complexes (Table 6.6); the IC_{50} value per Ru atom for the mixed valence species would be 200 μM. Further study of these two complexes is still warranted as they do show activity toward this cell line.

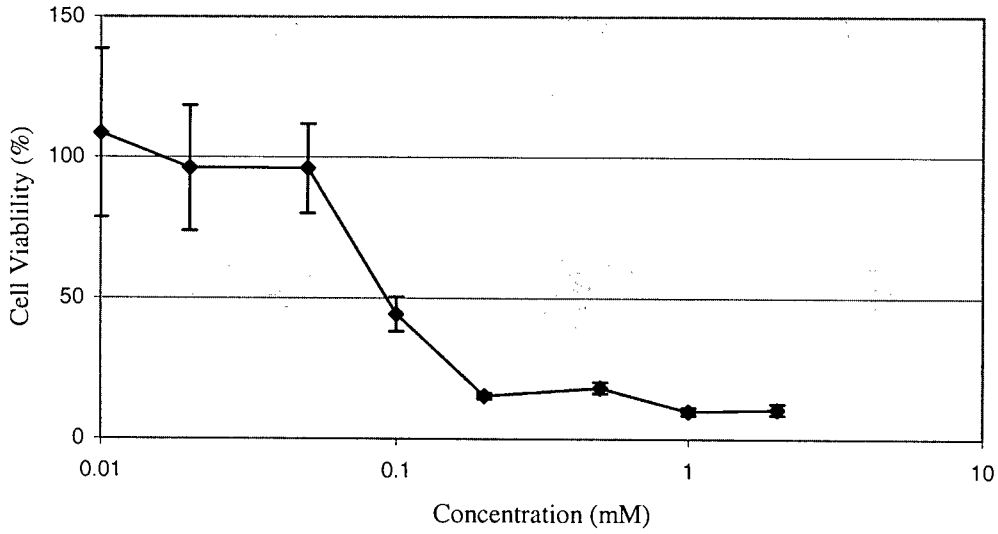

Figure 6.15 Cell viability vs. concentration for $[Ru_2(pic)_4(EtOH)Cl]\cdot H_2O$ (**31**), with error bars representing 95% confidence limit.

6.5 Summary

Direct comparison of the MTT assay data obtained here with those from other groups is difficult as results likely vary depending on the cell line used. However, by comparison with data for cisplatin, it is clear that a number of the Ru complexes show significant antiproliferatory activity and should be studied further to determine how they behave inside the cell. IC_{50} values reported for other Ru(III) complexes, as determined by MTT assays, include those for NAMI (Section 1.5.3.2) against the human colon cancer cell lines SW707 (195 μM) and SW948 (220 μM),[3] and that reported for a complex written as [H][Ru(1,2-dimethylimidazole)Cl_4] against SKW-3 cells(> 400 μM), a human T-lymphoma cell line.[4]

Ideally, the best way to gauge the activity of the new Ru complexes would be to test them simultaneously with NAMI-A, which is currently undergoing phase I clinical trials (Section 1.5.3.2), or other standards on the same cell line, and compare their activities. Performing these tests on the same cell lines and at the same time under the

same conditions would lead to a more comprehensive understanding of the effectiveness of the various complexes, and perhaps of their different levels of activity in different tumour models. Performing MTT assays on other cell lines, particularly cisplatin resistant cell lines, would also help determine the effectiveness of these new Ru complexes to arrest cell proliferation.

6.6 References

(1) Alley, M. C.; Scudiero, D. A.; Monks, A.; Hursey, M. L.; Czerwinski, M. J.; Fine, D. L.; Abbott, B. J.; Mayo, J. G.; Shoemaker, R. H.; Boyd, M. R. *Cancer Res.* **1988**, *48*, 589.

(2) Wu, A.; Kennedy, D.; Patrick, B. O.; James, B. R. *Inorg. Chem.* **2003**, *42*, 7579.

(3) Keppler, B. K.; Galeano, A.; Berger, M. R. *Drug Res.* **1992**, *42*, 821.

(4) Nikolova, A.; Ivanov, D.; Buyukliev, R.; Konstantinov, S.; Karaivanova, M. *Drug Res.* **2001**, *51*, 758.

(5) Sava, G.; Bergamo, A. *Int. J. Oncol.* **2000**, *17*, 353.

(6) Baird, I. R. *Fluorinated Nitroimidazoles and Their Complexes: Potential Hypoxia-Imaging Agents*, Ph. D. Dissertation, University of British Columbia: Vancouver, 1999.

(7) Hodgkiss, R. J. *Anti-Cancer Drug Des.* **1998**, *13*, 687.

(8) Carmichael, J.; DeGraff, W. G.; Gazdar, A. F.; Minna, J. D.; Mitchell, J. B. *Cancer Res.* **1987**, *47*, 936.

(9) Loosdrecht, A. A. V. d.; Beelen, R. H. J.; Ossenkoppele, G. J.; Broekhoven, M. G.; Langenhuijsen, M. M. A. C. *J. Immunol. Methods* **1994**, *174*, 311.

(10) Loosdrecht, A. A. V. d.; Nennie, E.; Ossenkoppele, G. J.; Beelen, R. H. J.; Langenhuijsen, M. M. A. C. *J. Immunol. Methods* **1991**, *141*, 15.

(11) Bellamy, W. T. *Drugs* **1992**, *44*, 690.

(12) Brinkley, B. R.; Beall, P. T.; Wible, L. J.; Mace, M. L.; Turner, D. S.; Cailleau, R. M. *Cancer Res.* **1980**, *40*, 3118.

(13) Siciliano, M. J.; Barker, P. E.; Cailleau, R. *Cancer Res.* **1979**, *39*, 919.

(14) Mosmann, T. *J. Immunol. Methods* **1983**, *65*, 55.

(15) Morris, R. E.; Arid, R. E.; Murdoch, P. S.; Chen, H.; Cummings, J.; Hughes, N. D.; Parsons, S.; Parkin, A.; Boyd, G.; Jodrell, D. I.; Sadler, P. J. *J. Med. Chem.* **2001**, *44*, 3616.

(16) Leonessa, F.; Green, D.; Licht, T.; Wright, A.; Wingate-Legette, K.; Lippman, J.; Gottesman, M. M.; Clarke, R. *Br. J. Cancer* **1996**, *73*, 154.

(17) Wu, A. *Synthesis and Characterization of Ruthenium Maltolato, Sulfoxide, and Nitroimidazole Complexes as Potential Anticancer Agents*, M. Sc. Dissertation, University of British Columbia: Vancouver, 2002.

(18) Huxham, L. A.; Cheu, E. L. S.; Patrick, B. O.; James, B. R. *Inorg. Chim. Acta* **2003**, *352*, 238.

(19) Clarke, M. J. *Coord. Chem. Rev.* **2002**, *232*, 69.

(20) Clarke, M. J.; Zhu, F.; Frasca, D. R. *Chem. Rev.* **1999**, *99*, 2511.

(21) Lippard, S. J.; Berg, J. M. *Principles of Bioinorganic Chemistry*; University Science Books: Mill Valley, 1994.

(22) Wu, A.; Kennedy, D.; Patrick, B. O.; James, B. R. *Inorg. Chem. Commun.* **2003**, *6*, 996.

Chapter 7

In Vitro Toxicity, Ru-Uptake and Ru-DNA Binding Studies of Ru Complexes, and Antibody Recognition Studies of a New Nitrotriazole in Chinese Hamster Ovarian (CHO) Cells

7.1 Introduction

A persistent problem in radiation therapy of cancerous tumours is that many tumours contain hypoxic regions that are resistant to radiation treatment. Rapid growth of tumours can lead to inadequate vasculature development and thus poor transport of oxygen to the tumour cells.[1] Typically an oxygen-gradient will be established with the innermost part of tumour being lowest in oxygen concentration (see Chapter 1, Figure 1.1); these oxygen depleted regions in which the cells are still viable, are called hypoxic regions, and their resistance to many treatments makes it important to identify these regions before a treatment is prescribed.[1]

Nitroimidazoles have been shown to accumulate in hypoxic cells, the nitro group being reduced inside the cell and the resulting reduced species then reacting with macromolecules to form adducts.[2] Quantification of the nitroimidazole content inside cells can help identify regions of hypoxia.[1] Through incorporation of radioactive atoms into the nitroimidazole, the localization of the radioactive species can be quantified using SPECT, PET, or MRI imaging.[1] Antigenic properties of the resulting adducts can also be used to quantify the levels of drug uptake by removing a tissue or cell sample and treating it with monoclonal antibodies. The concentration of bound antibodies can then be determined using fluorescence spectroscopy.[3,4]

There are literature examples of Ru complexes binding to DNA bases,[5-7] but in order to propose a mechanism of action involving DNA binding (as with cisplatin), one must first determine if the complex is in fact reaching the DNA *in vitro* and binding to it. It has also been suggested that some Ru complexes may act through extracellular mechanisms.[8] If so, then one would not expect to find correlation between the cellular uptake of Ru and the biological activity of the complex. The results of Ru-uptake and

DNA binding assays, discussed in this chapter, give information not only about hypoxia selectivity, but also about how and where the complexes might be interacting inside the cells. Furthermore, a lower plating efficiency of the cells after their incubation with a given complex for 3 h, an arbitrarily chosen time, compared with that of the control, indicates that the complex is having a cytotoxic or antiproliferatory effect on the cells over this period.

7.2 General Experimental

7.2.1 Materials, Media, and Prepared Solutions

Eagle's minimum essential medium powder (α-modification), and penicillin/streptomycin antibiotic were purchased from Gibco. Sterile tissue culture dishes (5 cm diameter), T-25 and T-75 flasks, and 15 and 50 mL Conical tubes were purchased from Falcon. Methylene blue was purchased from Aldrich. Other materials used in this chapter are listed in Section 6.2.1 (p 132). The media were prepared by the staff in the biological services laboratory in the UBC chemistry department. α-/- Medium was prepared by adding one packet of α-medium powder and 10,000 units of penicillin/streptomycin antibiotic to 1 L of doubly distilled (dd) H_2O, and stirring the resulting solution for 2 h at r.t. α+/- Medium was prepared by adding 10 % heat-inactivated fetal bovine serum (FBS) to α-/- medium buffered with 10 mM HEPES. α+/+ medium was prepared by adding 10 % FBS and $Na(HCO_3)$ (2 g/L) to α-/- medium and then adjusting the pH to 7.30 with 2 M NaOH. The media were then filter- sterilized and stored at 4 °C, while the trypsin-EDTA and FBS were stored at -20 °C.

Methylene blue solution was prepared by dissolving the solid (Aldrich) (200 mg) in 100 mL of ddH_2O; the resulting solution was filtered through a 0.1 μm filter to remove any undissolved solid and stored at 4 °C.

The following solutions were prepared exclusively for the monoclonal antibody binding assay (Section 7.3.4) with the assistance of staff at the BC Cancer Research Centre (BCCRC): PBS* was prepared by adding 0.25 % (v/v) 0.1 M Thimerosal (Aldrich) and 0.25 % (v/v) 1.0 M NaN_3 to the standard PBS solution. PBS^{tt} was prepared by adding 0.3 % Tween 20 (Aldrich) (v/v) to a PBS* solution. Ab Carrier, available

from BCCRC, consisted of 1.5 % bovine serum albumin (0.15 g) in PBS^{tt} (10 mL); as the bovine serum albumin is partially insoluble, the suspension was stirred at 37 °C for 1 h prior to use. Blocking solution was also available from BCCRC and consisted of 20 % skim milk and 5 % mouse serum added to the Ab Carrier mixture. Paraformaldehyde (pF) was prepared by boiling a solution of 100 μL of 1 M NaOH in 60 mL ddH_2O, and then adding this to a slurry of 4 g pF in 30 mL ddH_2O. The resulting colourless solution was cooled to 0 °C, when 10 mL of 10x PBS (available at BCCRC and having ten times the ionic strength of normal PBS) were added. This mixture was then filtered through a 0.22 μm sterile filter and to the filtrate was added 100 μL of 1 M HCl. pF was stored at 0 °C. The monoclonal antibody (MoAb), ELK3-51, was donated by Dr. C Koch (University of Pennsylvania) to BCCRC.

Atomic absorption spectroscopy (AAS) was performed by Celator Technologies on a Varian SpectrAA-300 Zeeman Atomic Absorption Spectrometer controlled by a Compaq Deskpro 386s computer. The instrument was calibrated using stock solutions of Ru from Aldrich, and a Ru hollow cathode lamp at a 10 mA current (λ_{max} = 349.9). A re-slope calibration was performed after every fifth sample to ensure that there was no significant shift in the background reference.

7.2.2 Cell Preparation

Chinese Hamster Ovarian (CHO) cells were donated by Dr. K. Skov at the BCCRC (Figure 7.1). After the cell culture was grown for three days, the cells were passaged and a frozen stock of cells was prepared (ten 1 mL vials containing 1 x 10^6 cells in medium with 5 % DMSO). The cells were maintained in T-75 tissue culture flasks in a 5 % CO_2 /air incubator from Forma Scientific in α+/+ media at 37 °C. The cells were transferred every 3-4 days using the procedure described in Section 6.2.2 for the MDA-MB-435S cell line, but using α+/+ medium instead of L-15 medium.

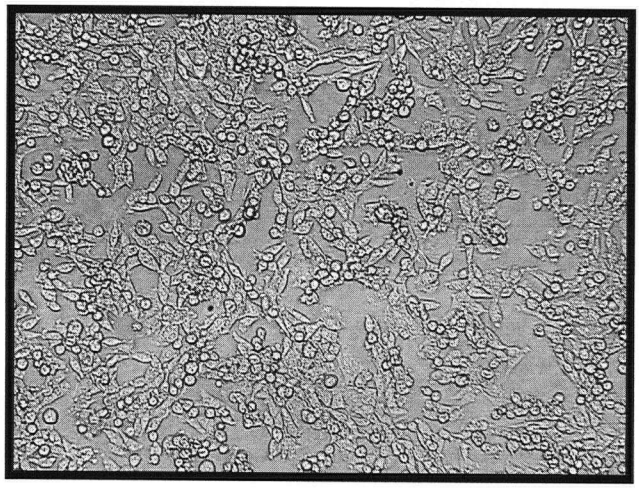

Figure 7.1 CHO cells in α+/+ medium (~10^6 cells/mL).

7.2.3 Stock Solutions of Ru Complexes

The Ru complexes were weighed into glass vials and dissolved in PBS to a concentration of 1.0 mM; 3.0 mL of stock solution were prepared for each complex. These solutions were then sonicated and heated to 37 °C to ensure the complex was completely dissolved, and then filter-sterilized through 0.2 μm filters, to remove an remaining particulates.

7.3 Hypoxia Selectivity Assays

7.3.1 Incubation of Complexes and Plating Efficiency

The hypoxia assays were performed at UBC in an innova 4300 incubator shaker (from New Brunswick Scientific) under a flow of N_2 or air, according to established protocols.[9] Centrifugation was performed on a Dynac Centrifuge. α+/- medium (8 mL) and Ru complex solution (1 mL) were added to 50 mL Falcon tubes. In most cases, two tubes were prepared for each complex, one for incubation under air, the other under N_2; however, some complex solutions were only tested under an air atmosphere (see Table 7.2, Section 7.4.2). The tubes were then placed in the incubator, attached to a gas line, shaken (150 rpm) at 37 °C for 1 h (Figure 7.2), and then removed from the incubator and

placed in a sterile hood. To each tube was then added 1 mL of a prepared cell suspension containing 3 x 10^6 cells/mL in α+/- medium. The tubes were then placed back in the incubator, reattached to the gas lines, and shaken (150 rpm) at 37 °C for 3 h. The suspensions were then transferred to 15 mL Falcon tubes and centrifuged (8 min at 800 rpm). The supernatant was removed, and the cells were resuspended in 5 mL of PBS to rinse them of any remaining Ru. The cell suspensions were centrifuged again (8 min at 800 rpm) and the supernatant removed. The pellets were then resuspended in 2 mL of PBS and the cell density of each suspension was determined by counting the cells under a microscope using a hemacytometer. A 10 μL aliquot of each cell suspension was then added to 5 mL of α+/- medium and the mixture vortexed to ensure that the diluted cell suspensions were homogeneous; 50 μL of each of these was then added to 5 mL of α+/+ medium in a 5 cm tissue culture dish. This was repeated 2 more times giving a total of 3 dishes for each sample. The tissue culture dishes were then placed in the 5 % CO_2 incubator for 7 days to allow colonies to form.

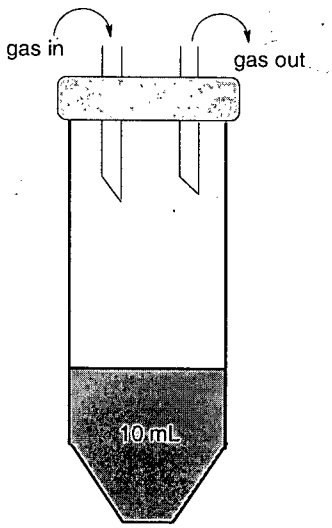

Figure 7.2 Conical tube set-up used for CHO experiments (gas = air or N_2).

The remaining 2 mL suspension in PBS and 5 mL suspension in α+/- medium were combined for each sample and centrifuged (8 min at 800 rpm). The cells in each flask were then resuspended in 2 mL of PBS. For those samples for which the DNA binding assay was performed, the suspensions were then divided in half, with 1 mL of the

cell suspension being used for the Ru-uptake assay (Section 7.3.2), and the other half for the DNA binding determination (Section 7.3.3). For those samples for which only the Ru-uptake assay was performed, the entire 2 mL suspension was used for the procedure. Alternately, for the Ru-free compounds, EF5 and triF5, only the monoclonal antibody binding assay was performed, the 2mL suspension being used to carry out the procedure described in Section 7.3.4.

After 7 days, the medium was removed from each dish and methylene blue solution was added (0.40 mL). The dishes were swirled to ensure the dye covered the entire surface of the dish and, after 10 min, the dishes were rinsed with water and the remaining colonies (Figure 7.3) were counted to determine the plating efficiency (PE), defined as the number of colonies counted for each sample divided by the number of cells plated 7 days earlier.

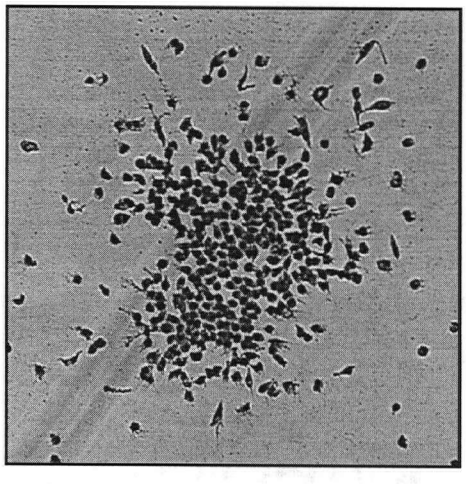

Figure 7.3 Colony of CHO cells after 7 days, following staining with methylene blue.

7.3.2 Ru-Uptake Determination

The final cell suspensions allotted for Ru-uptake determination (1 or 2 mL, see Section 7.3.1) were transferred to a fresh 15 mL Falcon tube and then centrifuged (10 min at 800 rpm). The supernatant was then removed and the tubes were placed with lids open in the shaker incubator (37 °C, 150 rpm) for 16 h to dry the cell pellets. Conc. HNO_3 (100 μL) was then added to each tube, which was then closed and left at r.t. for 24

h in order that the cell pellet be digested. Then, 250 μL of ddH_2O was added to dilute the acid, and the samples were then sent for AAS to determine the Ru content of each sample.

7.3.3 DNA Isolation

The DNA isolation was performed using a Wizard Genomic DNA Purification Kit from Promega. The 1 mL aliquots of the cell suspensions (see Section 7.3.1) were transferred to 1.5 mL microcentrifuge tubes and pelleted using centrifugation (15,000 x *g* for 10 s). The supernatant was then removed from each tube, leaving the cell pellet in ~50 μL of residual medium. PBS (200 μL) was then added to each pellet, and these mixtures were vortexed at high speed for 30 s to resuspend the cells. The cell suspensions were then centrifuged again (15,000 x *g* for 10 s). The supernatant was again discarded from each tube leaving the cell pellets in approximately 20 μL of liquid. Nuclei Lysis Solution (600 μL) (from the Kit) was then added to each cell pellet, and the mixtures gently "pipetted" until no visible clumps of cells remained. RNase (3 μL) Solution (from the Kit) was then added to each tube, and the samples were mixed. The cell mixtures were then incubated for 30 min at 37 °C to allow the cells to lyse. The tubes were then removed from the incubator and cooled to r.t. Protein Precipitation Solution (200 μL) (from the Kit) was then added to each tube, and the resulting mixtures were vortexed at high speed for 20 s and then cooled in an ice-bath for 5 min. The tubes were then centrifuged (15,000 x *g* for 4 min) causing the precipitated protein to form a white pellet at the bottom of each tube. The supernatant containing the DNA was then carefully removed and transferred to a clean 1.5 mL microcentrifuge tube containing 600 μL of isopropanol. The resulting solutions were then carefully mixed by inverting the tubes until white, thread-like strands of DNA became visible. The tubes were then centrifuged (15,000 x *g* for 1 min) to pellet the DNA. The supernatant was then removed and 600 μL of 70 % aq. EtOH was added. The tube was inverted several times to wash the DNA. The tubes were again centrifuged at 15,000 x *g* for 1 min to pellet the DNA and the EtOH was aspirated with a pipette leaving only the DNA pellet. The tubes were then left open and inverted over a paper towel to air dry the pellet for 30 min. Finally, 100 μL of DNA Rehydration Solution (from the Kit) was added to each tube and the

sealed tubes were then heated at 65 °C for 1 h. The tubes containing the rehydrated DNA were then stored at 4 °C until the amount of isolated DNA from each sample was determined by UV-Vis spectroscopy (Section 7.3.3.1) and the amount of associated Ru by AAS .

The amount of DNA in each sample was determined by measuring the optical density, and then employing Equation 7.1. The absorption of a DNA suspension was recorded at both 260 and 280 nm on a Perkin Elmer Lambda 2 UV/VIS spectrometer in a 1 cm optical cell. The ratio of the absorptions at 260 and 280 nm provides a check on the DNA purity: values > 1.7 are considered to be good,[10] and for all the samples, this ratio was between 1.71 and 1.85. The rehydrated DNA samples were diluted from 30 to 800 μL, a dilution factor of 26.67, before the absorbances at 260 and 280 nm were recorded.

$$A\ (OD) \times D \times 50\ (ng\ mL^{-1}\ OD^{-1}) \times (0.100\ mL) = \mu g\ DNA \quad (Eq.\ 7.1)$$

A = absorption at 260 nm, D = dilution factor, 0.100 mL is the total sample volume and 50 is a constant.

7.3.4 Monoclonal Antibody Binding Assay

This assay was performed at the BCCRC with the assistance of Haibo Zhou. The two compounds tested, EF5 and triF5, were incubated with CHO cells using the procedure described in Section 7.3.1 for the incubation of complexes. The 2 mL cell suspensions from the EF5 and triF5 experiments were then centrifuged (8 min at 800 rpm) and the supernatant, removed from each using a 1000 μL micropipettor, was discarded. pF (3 mL) was then added dropwise to each tube as it was vortexed at medium speed. The tubes were then inverted continuously for 1 h at 4 °C. After 1 h, the cells were centrifuged (8 min at 800 rpm) and washed twice with PBS* (by addition of 5 mL of PBS*, centrifugation for 8 min at 800 rpm and then removal of the supernatant). After the second wash, the cells were resuspended in 1 mL PBS* and then transferred to Eppendorf tubes. These were then centrifuged (8 min at 800 rpm), their supernatant removed, and 100 μL of blocking solution was added to each tube (blocking solution prevents the antibody from binding molecules other than the intended target inside the cell). The tubes were then inverted for 5 h at 4 °C. Then 1 mL of PBS* was added to each Eppendorf tube, and these were shaken gently to mix the suspensions. The mixtures

were then centrifuged (8 min at 1200 rpm) and the supernatant removed; 100 μL of a MoAb solution was then added (the ELK3-51 antibody was conjugated to a Cy3 fluorescent label[11] (Figure 7.4) to make detection of the antibody possible, and the MoAb solution contained a 20:1 mixture of Ab Carrier:MoAb). The resulting suspensions were then covered with Al foil and rotated overnight at 4 °C (12 h). (Note: all work with the MoAb was done in a dark-room as the intensity of the fluorescence of the MoAb decreases if the antibody is exposed to light). The samples were then centrifuged (8 min

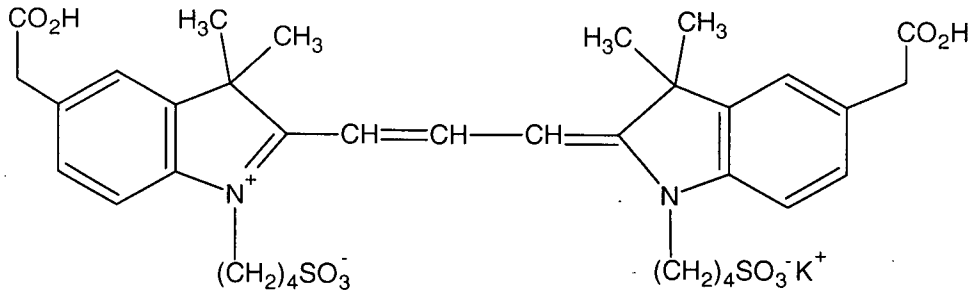

Figure 7.4 Structure of the fluorescent dye, Cy3, used to label the ELK3-51 MoAb.

at 1200 rpm) and the supernatant containing the MoAb solution was removed. PBS^{tt} was then added to each tube and the resulting mixtures gently vortexed to resuspend the pellet. The tubes were then rotated for 40 min at 4 °C, centrifuged (8 min at 1200 rpm), and the supernatant discarded. This procedure was repeated two more times. After the last wash with PBS^{tt}, the samples were resuspended in 400 μL of PBS^{tt}. These suspensions were diluted with 2 mL of 1 % pF and then submitted for analysis at BCCRC by flow cytometry. The final suspensions were stored at 4 °C for 1-2 weeks before the analyses were performed.

The concentration of MoAb adducts and thus the concentration of EF5 or triF5 in a given sample was measured by a technician at BCCRC on a Coulter Epics Elite fluorescence-activated cell-sorter, with a Coherent Inova 90 Ar laser. Detection of the MoAb adducts is facilitated by the Cy3 label on the MoAb. The sample is passed through the laser using an ultrasonic vibrator to split the sample into droplets; only drops

containing a single cell were analyzed. The laser was set to 510 nm for the excitation wavelength, and the emission was detected between 580-590 nm. For each sample, the fluorescence of 10,000 cells was measured.

7.4 Results and Discussion

7.4.1 Plating Efficiency of CHO Cells

The toxicity of several compounds (Table 7.1) was investigated under hypoxic (under N_2) and oxic (under air) conditions by determining the plating efficiency (PE) of the cells after a 3 h incubation period in media usually containing 100 μM of the compound; $[Ru(ma)_2(EF5)_2]CF_3SO_3 \cdot EtOH$ (**14**) was tested at 48 μM because of a solubility limitation. The procedure for this experiment is outlined in Section 7.3.1. The plating efficiency was determined by counting the colonies for of the 3 replicates for each sample, and then dividing by the number of cells plated 7 days earlier after the 3 h incubation with the complex.

The PE data (Table 7.1) are the average of two experiments, each having a plating efficiency determined by averaging the number of colonies in the 3 replicates. For the controls, the values are the average of six experiments, as a control was performed each time a complex or ligand was tested, and only 5 complexes could be tested at once. The error in the PE of the controls is only ± 4 % because there are more experiments within the average value, and the variation of the PE values for the controls was less than those for the complexes. Several of the complexes do exhibit a small cytotoxic effect; however, there is no significant hypoxia selectivity observed for the PE of any of the complexes. The two nitro-heterocycles, EF5 and triF5, showed no toxicity at all. Repeating these experiments might be valuable as a greater number of trials would decrease the error limits. The experiments could also be lengthened or monitored over time to determine how the amount of complex in the cells varies with time. The use of a Coulter counter (not available in the UBC chemistry department) might help reduce the errors as counting cells on the hemacytometer was not very accurate for this particular assay. Clumping of cells was a major problem, both in the counting of cells, and the fact

that cell clumps form large cell masses (Figure 7.5) and not individual countable colonies.

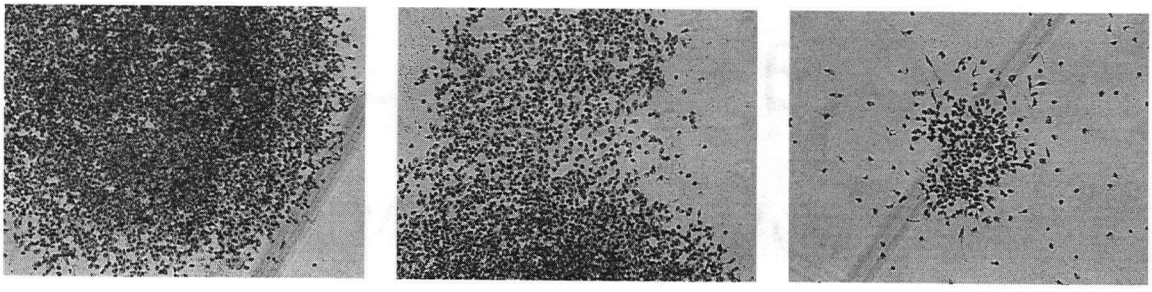

A B C

Figure 7.5 Large cell colony formations resulting from clumped cells (A and B) compared with a colony grown from a single cell over the same time period, C.

Our group has previously synthesized and tested similar Ru-acac-imidazole and -nitroimidazole complexes in SCCVII cells, and also found no hypoxia selective toxicity.[12]

There may be several reasons why the PEs of complexes active in the MTT assay (with IC_{50} values well below 100 μM, see Section 6.4) do not show any significant toxicity in this PE assay. A different cell line was used here than that for the MTT assay (CHO vs. MDA-MB-435S) because of past experience at BCCRC in which CHO cells were known to provide a good model for testing hypoxia. This PE assay also differs in that the incubation is only 3 h compared with 69 h for the MTT assay, and the complexes may not accumulate quickly enough to have a significant effect on the cells. The cells are also plated in media in which no complex is present. If the complexes are able to diffuse out through the cell membrane, then an equilibrium between complex inside and outside the cell may be important; removing the extracellular complex may drive the complex outside of the cell. This sort of mechanism is not unreasonable, as there is no evidence to suggest that the complex decomposes inside the cell, and no intracellular targets have yet been established to suggest that, once the complex is taken up, it is 'trapped' inside the cell.

Table 7.1 Plating efficiency[a] of CHO cells after a 3 h incubation period under both aerobic and anaerobic conditions with several Ru(III) complexes at 100 μM.

Compound	PE-oxic	PE-hypoxic
Control	69[b]	66[b]
$Ru(ma)_3$ (**1**)	42	35
$Ru(Ema)_3$ (**2**)	41	32
$[Ru(ma)_2(metro)_2]CF_3SO_3$ (**4**)	36	48
$[Ru(ma)_2(2MeIm)_2]CF_3SO_3$ (**10**)	72	58
$[Ru(ma)_2(4MeIm)_2]CF_3SO_3 \cdot CH_2Cl_2$ (**6**)	50	48
$[Ru(ma)_2(1MeIm)_2]CF_3SO_3 \cdot CH_2Cl_2$ (**8**)	48	62
$[Ru(ma)_2(EF5)_2]CF_3SO_3 \cdot EtOH$ (**14**)	72[c]	65[c]
$[Ru(Ema)_2(2MeIm)_2]CF_3SO_3$ (**13**)	43	45
$[Ru(Ema)_2(4MeIm)_2]CF_3SO_3$ (**12**)	35	35
$Ru(Im\text{-}CO_2)(Im\text{-}CO_2H)_2Cl_2 \cdot EtOH \cdot H_2O$ (**32**)	32	39
EF5	68	66
triF5	65	62

[a] Error limits are ± 12 %.
[b] The error for these values is only ± 4 %.
[c] The final concentration of $[Ru(ma)_2(EF5)_2]CF_3SO_3 \cdot EtOH$ was 48 μM due to poor solubility.

7.4.2 Ru-Uptake

The uptake of Ru into CHO cells was determined in order to help understand how the Ru(III) complexes that showed low IC_{50} values (Chapter 6) might be acting *in vitro*. Sava and Bergamo[8] have suggested that some Ru complexes may bind extracellular components in order to produce cytotoxic or antiproliferatory effects, while others may act with intracellular components such as proteins or DNA to produce a biological effect. In the former case, one would expect low levels of Ru to be taken up into the cells. In the latter case, the level of activity might be dependent on the amount of complex in the cell.

The data (Table 7.2) show that the complexes containing the Ema ligands (**2**, **12** and **13**) are taken up more readily into the cells than the corresponding ma complexes (**1**, **6**, and **10**), and the former group also exhibit lower IC_{50} values in MDA-MB-435S cells than the latter group (Section 6.4.2). This suggests a link between the Ru-uptake and antiproliferatory activity for these complexes. Conversely, the Ru-uptake for $[Ru(ma)_2(2MeIm)_2]CF_3SO_3$ (**10**) and $[Ru(ma)_2(1MeIm)_2]CF_3SO_3 \cdot CH_2Cl_2$ (**8**) under both oxic and hypoxic conditions are exactly the same for each complex, whereas the corresponding IC_{50} values are 5 and 70 μM, respectively (Section 6.4.2). These findings imply that the nature of the imidazole ligand is important for the biological effect; as the free imidazoles (2MeIm and 1MeIm) alone produce no significant cytotoxic effect (Section 6.4.1), at least one of the imidazole ligands must remain bound *in vitro* in order for the Ru complexes to produce their biological effects.

CHO cells incubated with $[Ru(ma)_2(EF5)_2]CF_3SO_3 \cdot EtOH$ (**14**) showed the highest level of Ru-uptake, suggesting that this complex is taken up more readily than analogous imidazole- and nitroimidazole-maltolato complexes; **14**, however, exhibits no significant antiproliferatory activity (Section 6.4.2), nor does this complex accumulate selectively in hypoxic cells as does free EF5 (Section 7.4.4). Indeed, none of the complexes tested under both oxic and hypoxic conditions shows any hypoxia selectivity (Table 7.2). The Ru-uptake values reported for **14** (Table 7.2) are for a 3 h incubation at 48 μM as determined by AAS after the complex solution had been filtered. Other workers have noted a linear correlation between Ru-uptake vs. concentration at concentrations below 100 μM in MEM (minimum essential medium),[13] suggesting that at 100 μM, the values listed in Table 7.2 for **14** would be 169 and 152 ng $Ru/10^6$ cells under oxic and hypoxic conditions, respectively.

For the biimidazole complexes, the Ru-uptake values for $[Ru(ma)_2(biim)]CF_3SO_3 \cdot 2H_2O$ (**24**) and $[Ru(ma)_2(Mebiim)]CF_3SO_3 \cdot 2H_2O$ (**25**) are very similar, as are the values for $[Ru(biim)_3][CF_3SO_3]_2$ (**26**) and $[Ru(Mebiim)_3][CF_3SO_3]_2$ (**27**). Nevertheless, the complexes with perhaps higher uptake (**25** and **26**) do have lower IC_{50} values (15 and 10 μM, respectively) than do **24** and **27** (50 and 25 μM, respectively). Further experiments that might help determine if these differences are real or not will be noted in Chapter 8.

Table 7.2 Uptake of Ru by CHO[a] cells after a 3 h incubation period under both aerobic and anaerobic conditions with several Ru complexes at 100 μM.

Compound	Oxic - Ru ($ng/10^6$ cells)	Hypoxic - Ru ($ng/10^6$ cells)	IC_{50} values[c] (μM)
Control	1.0	0.5	-
$Ru(ma)_3$ (**1**)	15.3	16.7	140
$Ru(Ema)_3$ (**2**)	42.3	36.5	90
$[Ru(ma)_2(metro)_2]CF_3SO_3$ (**4**)	14.9	15.2	80
$[Ru(ma)_2(2MeIm)_2]CF_3SO_3$ (**10**)	14.3	16.5	5
$[Ru(ma)_2(4MeIm)_2]CF_3SO_3 \cdot CH_2Cl_2$ (**6**)	27.0	21.0	15
$[Ru(ma)_2(1MeIm)_2]CF_3SO_3 \cdot CH_2Cl_2$ (**8**)	14.1	17.2	80
$[Ru(ma)_2(Im)_2]CF_3SO_3$ (**7**)	16.7	19.6	70
$[Ru(ma)_2(EF5)_2]CF_3SO_3 \cdot EtOH$ (**14**)	81.3[b]	72.8[b]	>500
$[Ru(ma)(1MeIm)_4]CF_3SO_3$ (**9**)	13.3	-	-
$[Ru(ma)_2(biim)]CF_3SO_3 \cdot 2H_2O$ (**24**)	12.7	-	50
$[Ru(ma)_2(Me_2biim)]CF_3SO_3 \cdot 2H_2O$ (**25**)	18.0	-	15
$[Ru(biim)_3][CF_3SO_3]_2$ (**26**)	26.0	-	18
$[Ru(Me_2biim)_3][CF_3SO_3]_2$ (**27**)	20.0	-	36
$Ru(Im\text{-}CO_2)(Im\text{-}CO_2H)_2Cl_2 \cdot EtOH \cdot H_2O$ (**32**)	15.4	24.3	400
$[Ru(Ema)_2(2MeIm)_2]CF_3SO_3$ (**13**)	67.2	82.0	0.5
$[Ru(Ema)_2(4MeIm)_2]CF_3SO_3$ (**12**)	79.5	94.1	5

[a] Error limits are ± 5 $ng/10^6$ cells.

[b] The final concentration of $[Ru(ma)_2(EF5)_2]CF_3SO_3 \cdot EtOH$ was 48 μM due to poor solubility.

[c] Data from Tables 6.3-6.6 (p. 138, 141, and 144) using the MDA-MB-435S cell line.

Recently, Frausin *et al.* have examined the Ru-uptake of NAMI-A in KB cells (human nasopharynx cancer cells), and concluded that the complex enters the cell both by passive diffusion across the membrane and by active transport.[14] Over 4 h, at both 4 and 37 °C, the complex only accumulated in the cells at the higher temperature, the Ru-uptake increasing when the experiment was performed in PBS instead of MEM; this was thought

to result from competition for transport sites in the membrane with other components present in MEM. When the concentration was varied between 10 and 1000 μM, the percent of Ru taken into the cell remained constant in MEM, while in PBS, the percent of Ru-uptake from the total present in solution decreased as the concentration increased.[14]

Ru-uptake data have also been reported for the dimeric Ru complexes $[RuCl_4(DMSO)]_2(\mu\text{-L})$, where L = pyrazine, pyrimidine, 4,4'-bipyridine as well as other substituted pyridine ligands;[13] these were also tested against KB cells, and uptake values were similar to those found for NAMI-A in the same cell.

Further experiments examining the Ru-uptake of the complexes discussed in this section might help to understand how the complexes act *in vitro*. Use of the MDA-MB-435S cell line used for the MTT assay (Chapter 6) instead of CHO cells would allow a more direct comparison to be made between the Ru-uptake values (Table 7.2) and IC_{50} values (Section 6.4.1, Table 6.6).

7.4.3 Ru-DNA Binding

DNA was isolated from cells after a 3 h incubation with a selected Ru(III) complex in order to determine if it was interacting with DNA. With the exception of $[Ru(ma)_2(EF5)_2]CF_3SO_3 \cdot EtOH$ (**14**), none of the other complexes tested (**1**, **2**, **4**, **6**, **8**, **10**) exhibited any DNA binding (Table 7.3). **14** exhibits some hypoxia selectivity for binding DNA: 5.9 and 10.5 ng Ru/mg DNA at 48 μM for oxic and hypoxic conditions, respectively. Previous studies in our group with $[Ru(acac)_2(EF5)_2]CF_3SO_3$ in SCCVII cells[12] showed that, after a 3 h incubation, the amount of bound Ru was 9.6 and 11.1 ng Ru/mg DNA for oxic and hypoxic conditions, respectively. These values are calculated here for 48 μM complex solutions, assuming that there is a linear correlation between Ru-DNA binding and Ru concentration, as poor solubility of $[Ru(acac)_2(EF5)_2]CF_3SO_3$ limited its testing to a concentration of 22 μM.[12] Such an assumption has been made for the Ru-uptake of NAMI-A at low concentrations.[13] This complex also exhibited a 4-fold increase in fluorescence over that of free EF5 in the MoAb assay,[12] suggesting that the complex facilitates the accumulation of EF5 inside the cell to a greater concentration

Table 7.3 Amount of Ru[a] associated with DNA isolated from CHO cells after a 3 h incubation period under both aerobic and anaerobic conditions with several Ru(III) complexes at 100 μM.

Compound	Oxic Ru (ng/mg DNA) (± 3 ng/mg)	Hypoxic Ru (ng/mg DNA) (± 3 ng/mg)
Control	0	0
1, 2, 4, 6, 8, 10	0	0
$[Ru(ma)_2(EF5)_2]CF_3SO_3$·EtOH (**14**)	5.9[b]	10.5[b]

[a] Error limits are ± 3 ng/mg, AA detection limit ~ 1 ng/mg DNA.
[b] The final concentration of **14** was 48 μM due to poor solubility.

than when EF5 acts alone. The higher level of Ru-DNA binding for $[Ru(acac)_2(EF5)_2]CF_3SO_3$ suggests that, in the cell, the EF5 is being released from the complex and replaced by donor ligands of DNA. The same may be true for **14,** and thus further study, in particular the MoAb binding assay, is needed on this complex. The DNA binding assay should also be repeated using the MDA-MB-435S cell line so that a more accurate correlation can be made between the DNA-binding results and the IC_{50} values from the MTT assay (Chapter 6).

For the other complexes, their method of action inside the cell does not include DNA binding; thus further experiments are needed to locate other potential targets for these complexes *in vitro*. In Section 7.4.5, a preliminary study will be discussed with L-cysteine potential intracellular target.

7.4.4 The Monoclonal Antibody Binding Assay

This assay was performed using only EF5 (Section 3.6.2) and the corresponding fluorinated nitrotriazole derivative, triF5 (Section 3.6.3). For triF5, detection of the MoAb adducts was carried out using flow cytometry and, as in the case of earlier work on EF5,[12] triF5 accumulates preferentially in hypoxic cells (Figure 7.4). However, the mean fluorescence for the triF5 MoAb adducts was considerably less than that observed

for the EF5 MoAb adducts: at 100 μM, the signal for EF5 adducts are up to 7 times greater than that for triF5 adducts. More important is that the ratio of the hypoxic:oxic signals for triF5 is much less than that of EF5; in a search for new hypoxia imaging agents, this ratio determines the effectiveness of the compound to detect specifically hypoxic cells with low levels of background fluorescence in normal tissue.

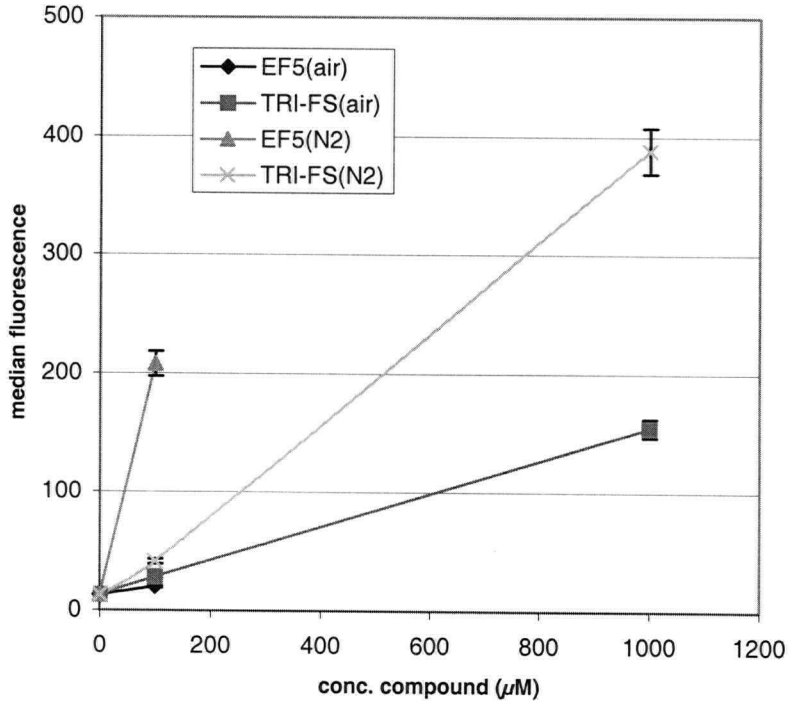

Figure 7.6 Median fluorescence intensity of CHO cells incubated with EF5 or triF5 under N_2 or air and then treated with the ELK3-51/Cy3 antibody.

7.4.5 Reaction of $[Ru(ma)_2(2MeIm)_2]CF_3SO_3$ (10) with L-cysteine

An *in situ*, r.t. reaction of $[Ru(ma)_2(2MeIm)_2]CF_3SO_3$ (**10**, Section 3.7.9) in D_2O (~ 10^{-3} M) under air with 1 equivalent of L-cysteine (Figure 7.7) was followed by ^1H NMR spectroscopy. After 24 h, the initial intensities of the proton resonances for **10** were unchanged, and there were no new paramagnetic or diamagnetic signals, showing that **10** was still intact. The resonances for L-cysteine (δ 3.92 (-C*H*-), 3.08 (-CH_2-)) had decreased in intensity by ~ 50 %, and new resonances for L-cystine (δ 4.13 (-C*H*-), 3.32

(-CH_2-)) were present in about equal intensity as those for L-cysteine. In a control with only L-cysteine in D_2O, only trace amounts of L-cystine were present after 24 h. **10** is apparently catalyzing the aerial solution oxidation of L-cysteine.

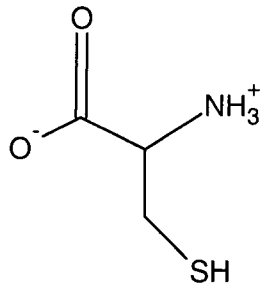

Figure 7.7 Molecular structure of L-cysteine

The ^{1}H NMR spectrum **10** in D_2O in air remained unchanged for up to 48 h. For the L-cysteine sample at this time, the resonances for L-cystine were more intense than at 24 h, but still only ~ 10 % of the L-cysteine had been oxidized. In the spectrum of the 1:1, **10**:L-cysteine system, there were no longer any resonances for L-cysteine present; and the only paramagnetic signals observed were those for **10**, although a trace of 2-methylimidazole was now present in solution. No signals could be seen for either free or diamagnetically bound maltolato, showing that none of the initial Ru(III) had been reduced to Ru(II). At the concentrations used, the signals for **10** are weak and difficult to resolve (minimum 150 scans, Section 3.3.2) and it is possible that trace amounts of other Ru(III) species might be present. The integration of the 2-methylimidazole signals with respect to those of L-cystine suggests that ~ 0.05 equivalents of 2-methylimdiazole have dissociated, leaving 95 % of intact **10**. From this it can be concluded that the complex is catalytically oxidizing the cysteine to cystine in air. Repeating the reaction under Ar could give evidence for a reduced species.

TLC analysis after 48 h of solutions of **10**, and **10** with L-cysteine, revealed the same band as a sample of **10** which had just been dissolved. All three samples also gave a brown spot (R_f = 0) that was less intense for the freshly prepared sample. No new bands for reduced species or newly formed complexes were observed.

Glutathione (a tripeptide containing a cysteine) can reduce certain Ru(III) species *in situ*,[15] while reaction with glutathione is also the primary means by which cisplatin is deactivated *in vivo*.[16] The stability of **10** in the presence of L-cysteine suggests that this complex is not being reduced *in situ* to a biologically active Ru(II) species, and an intact or only partially substituted Ru(III) species is likely responsible for the antiproliferatory activity observed and not a species from which both imidazole ligands have been dissociated.

Further experiments monitoring the reaction of glutathione with **10** and other Ru(III) complexes listed in Table 7.2 are needed to help determine more definitively the fate of the complex inside cells.

7.5 References

(1) Hodgkiss, R. J. *Anti-Cancer Drug Des.* **1998**, *13*, 687.

(2) Wardman, P. *Environ. Health Perspect.* **1985**, *64*, 309.

(3) Matthews, J.; Adomat, H.; Farrell, N.; King, P.; Koch, C.; Lord, E.; Palcic, B.; Poulin, N.; Sangulin, J.; Skov, K. *Br. J. Cancer* **1996**, *74*, S200.

(4) Koch, C. J.; Evans, S. M.; Lord, E. M. *Br. J. Cancer* **1995**, *72*, 869.

(5) McNamara, M.; Clarke, M. J. *Inorg. Chim. Acta* **1992**, *195*, 175.

(6) Hotze, A. C. G.; Broekhuisen, M. E. T.; Velders, A. H.; Kooijman, H.; Spek, A. L.; Haasnoot, J. G.; Reedijk, J. *J. Chem. Soc., Dalton Trans.* **2002**, 2809.

(7) Hotze, A. C. G.; Broekhuisen, M. E. T.; Velders, A. H.; Van der Schilden, K.; Haasnoot, J. G.; Reeijk, J. *Eur. J. Inorg. Chem.* **2002**, 369.

(8) Sava, G.; Bergamo, A. *Int. J. Oncol.* **2000**, *17*, 353.

(9) Moore, B. A.; Palcic, B.; Skarsgard, L. D. *Radiat. Res.* **1976**, *67*, 459.

(10) Ausubel, F. M.; Brent, R.; Kingston, R. E.; Moore, D. D.; Seidman, J. G.; Smith, J. A.; Struhl, K. *Short Protocols in Molecular Biology 2nd ed.*; John Wiley and Sons: New York, 1992.

(11) Southwick, P. L.; Ernst, L. A.; Tauriello, E. W.; Parker, S. R.; Mujumdar, R. B.; Mujumdar, S. R.; Clever, H. A.; Waggoner, A. S. *Cytometry* **1990**, *11*, 418.

(12) Baird, I. R. *Fluorinated Nitroimidazoles and Their Complexes: Potential Hypoxia-Imaging Agents*, Ph. D. Dissertation, University of British Columbia: Vancouver, 1999.

(13) Bergamo, A.; Stocco, G.; Gava, B.; Cocchietto, M.; Alessio, E.; Serli, B.; Iengo, E.; Sava, G. *J. Pharmacol. Exp. Ther.* **2003**, *305*, 725.

(14) Frausin, F.; Cocchietto, M.; Bergamo, A.; Scarcia, V.; Furlani, A.; Sava, G. *Cancer Chemother. Pharmacol.* **2002**, *50*, 405.

(15) Clarke, M. J. *Coord. Chem. Rev.* **2002**, *232*, 69.

(16) Hall, M. D.; Hambley, T. W. *Coord. Chem. Rev.* **2002**, *232*, 49.

Chapter 8

Conclusions, and Direction of Future Work

8.1 Conclusions

Several new Ru(III)-ma imidazole and –ma nitroimidazole complexes have been synthesized and tested for biological activity; selected, corresponding Ema complexes were also synthesized and tested (Chapter 3). The ^{1}H NMR spectra of the paramagnetic Ru(III)-ma imidazole complexes were used to determine their purity and molecular structure. In the ^{1}H NMR spectra of **6**, **8** and **10**, single resonances for the ma-Me protons were assigned to the trans-ma, trans-imidazole isomer, and X-ray crystallography confirmed such a structure for **8** and **10**. Similarly, in the ^{1}H NMR spectra of the Ema complexes **11** – **13**, single resonances for the -CH_2- groups were also assigned to trans-isomers, which was demonstrated for **11** by X-ray analysis. Ru(III)-ma complexes of nitroimidazoles in which the N(1) proton was not substituted (EF5 and metro are both 1-substituted nitroimidazoles) were not soluble (without decomposition) in any solvent tested and were not obtained in high purity.

Ema complexes were taken up more readily into CHO cells than their ma analogues (Chapter 7), and this higher uptake corresponded with lower observed IC_{50} values (Chapter 6). Within the series of Ru-ma complexes, $[Ru(ma)_2(2MeIm)_2]CF_3SO_3$ (**10**) exhibited the lowest IC_{50} value (5 μM), while the corresponding Ema complex, $[Ru(Ema)_2(2MeIm)_2]CF_3SO_3$ (**13**), exhibited the lowest IC_{50} value of all complexes tested, 500 nM. Differences in IC_{50} values that resulted from changes in the imidazole ligand did not correlate with changes in Ru-uptake. $[Ru(ma)_2(EF5)_2]CF_3SO_3 \cdot EtOH$ (**14**) exhibited the highest Ru-uptake of all the complexes tested (Chapter 7), and was the only complex to exhibit DNA binding, which increased by ~ 50 % under hypoxic conditions. Despite its high uptake and DNA binding values, this complex did not exhibit any noticeable antiproliferatory activity up to a concentration of 500 μM (Chapter 6).

Of several new complexes synthesized using 4,4'-biimidazole ligands (Chapter 4), four Ru(II) and two Ru(III) species exhibited low IC_{50} values and warrant further investigation (Chapter 6). The biimidazole complexes vary in charge, oxidation state, and ancillary ligands, making it unclear what biological mechanism is operating, although more than one mechanism is likely involved judging by the similar activity of the different complexes. The findings suggest that known Ru complexes of other bidentate N-donor ligands such as 2,2'-bipyridine or 2,2'-biimidazole might also exhibit similar activity.

A triazole derivative of EF5 (triF5) was developed and tested for hypoxic selectivity, but was less specific for hypoxia than EF5; triF5 may utilize different metabolic pathways than EF5 or may be less able to bind the fluorescent antibodies used for detection.

Finally, some new Ru carboxylate complexes were synthesized and tested for biological activity (Chapter 5). In particular, a new bimetallic complex with picolinate (**31**) and a monomeric complex with Im-CO_2H (**33**) were studied. Preliminary reactions with a 3-nitro-1,2,4-triazole-5-carboxylic acid were also performed.

8.2 New Complexes to Synthesize and Test

Ru(III)-ma complexes with nitroimidazole and nitrotriazole ligands containing an N(1)-H group were not soluble in any solvent except DMSO in which they decomposed. Methylation at the N(1) position of $2NO_2Im$, $4NO_2Im$ or $3NO_2tri$ might provide ligands that form stable Ru-ma complexes with higher solubilities, allowing for easier characterization and biological testing.

The high activity (low IC_{50} values) of several of the complexes containing biim and Me_2biim suggests that they should be studied in greater detail. Similar complexes with other N-donor ligands are known, but have not been tested for antiproliferatory activity or other biological activity. In particular, $[Ru(2,2'\text{-biimidazole})_3][PF_6]$,[1,2] $[Ru(imidazole)_6][CF_3SO_3]_2$[3] and $[Ru(2,2'\text{-bipyridine})_3][PF_6]_2$[1,2] could be tested alongside $[Ru(4,4'\text{-biimidazole})_3][CF_3SO_3]_2$ (**26**) to determine the effect of (a) changing from a monodentate imidazole to a chelating biimidazole, (b) changing the connectivity of the

biimidazole, and (c) changing the ring structure from imidazole to pyridine. Results from such comparisons could then give insight into the effect of the imidazole group, and could lead to new complexes with maltolato and other ancillary ligands (e.g. $[Ru(ma)_2(2,2'\text{-biimidazole})]CF_3SO_3$).

As noted in Chapter 7, complexes of Ema tend to be taken up more readily into cells than the corresponding ma complexes, and so the synthesis of the Ema derivative of $[Ru(ma)_2(EF5)_2]CF_3SO_3 \cdot EtOH$ (**14**) might lead to improved uptake in cells and higher levels of DNA binding.

New ma-complexes could be synthesized using some of the carboxylate ligands discussed (Chapter 5), for example, $[Ru(ma)_2(HCANT)_2]CF_3SO_3$ or $Ru(ma)_2(CANT)$ containing nitro-N-heterocycles. Similar-type complexes may also be possible with Hpic and Im-CO_2H ligands. The incorporation of the nitro and carboxylate groups within the N-heterocyclic ligand may significantly affect the biological properties.

Isopropylmaltol and *n*-butylmaltol are known[4] and the corresponding tris-(maltolato)complexes with Ru could be prepared and tested. Pyridinones, in which the O in the ma ring has been substituted by a N-R group, might also be useful ligands to try. A member of our group has synthesized Ru(3-hydroxy-1,2-dimethyl-4-pyronate)$_3$, although attempts to incorporate some ancillary imidazole ligands has yet to yield positive results.[5]

8.3 New Directions for Hypoxia Markers

The high level of cellular uptake and selective DNA binding of $[Ru(ma)_2(EF5)_2]CF_3SO_3 \cdot EtOH$ (**14**) suggest that this complex is worth further investigation as a hypoxic marker. Previously in our group, Baird reported on the activity of $[Ru(acac)_2(EF5)_2]CF_3SO_3$ that showed a degree of Ru uptake into SCCVII cells similar to that found for **14** in CHO cells, but exhibited no selectivity toward hypoxic cells in the DNA binding assay.[6] This complex did, however, show a 75-fold increase in fluorescence in hypoxic cells over that observed in normal cells in the monoclonal antibody binding assay, and levels of fluorescence that were 4 times greater than those

for the free ligand alone (free EF5 itself also showed a 75-fold selectivity for hypoxic cells).[6] From these results it can be inferred that $[Ru(acac)_2(EF5)_2]CF_3SO_3$ is taken up by all cells equally, and once inside the cell the EF5 is released; the EF5 is then able to diffuse back out of the normal cells. This would account for the non-specific DNA binding and cellular uptake values for Ru, and the selective accumulation for EF5 in hypoxic cells. The complex may be taken up by cells more readily than the free ligand, thus resulting in the 4-fold increase in fluorescence. Further tests with $[Ru(acac)_2(EF5)_2]CF_3SO_3$ were not pursued because of its poor water-solubility. $[Ru(ma)_2(EF5)_2]CF_3SO_3 \cdot EtOH$ (**14**) is more water-soluble than the acac analogue and, unlike $[Ru(acac)_2(EF5)_2]CF_3SO_3$, shows selectivity for DNA binding in hypoxic cells. Results from the antibody binding assay with **14** might show that it is a viable candidate for further testing as a hypoxia imaging agent. The ELK3-51 antibody used to quantify EF5 was supplied by BCCRC; however, to continue this work, a new source for this antibody is needed.

8.4 Future Biotests

The higher cellular uptake of Ema complexes may mean that they can more readily diffuse across cell membranes. Lipophilicity studies would help determine if the complexes are entering the cell through passive diffusion or via an activated transport mechanism. The synthesis of complexes with isopropyl and n-butyl derivatives of ma would be useful in determining the effect of the ma-substituents on cellular uptake.

The Ru-uptake and Ru-DNA binding assays should be repeated using MDA-MB-435S cells. The CHO cells were used to mimic a hypoxic environment, but as only **14** exhibited any hypoxia selectivity, the other complexes should be tested on the same cell line used for the MTT assay in order to make more accurate correlations between cell uptake and antiproliferatory activity. In addition, complexes could be tested against other cancer cell lines to see if the activity is specific for the MDA-MB-435S cell line or if the effect of the complexes is more general. In particular, tumour cell lines resistant to cisplatin should be used to determine if these Ru-ma complexes are active against such tumour models *in vitro*.

As only **14** interacted with DNA *in vitro*, other tests are needed to determine what type of interaction the complexes experience inside the cell and how the complexes enter the cell. The latter can be tested by performing the Ru-uptake assay (see Section 7.3.2) using PBS in place of growth medium. For some other Ru complexes,[7] the uptake of Ru has been found higher in PBS because components in the growth medium compete with the complex for active transport sites. In PBS, this competition for transport proteins is removed and the concentration of complex inside the cell increases. No increase in Ru-uptake in PBS might suggest that the complex is entering the cell via passive diffusion.

To determine the ultimate fate of the complexes inside the cell, it would be helpful to first run a gel on a protein extraction from control MDA-MB-435S cells, and then on a protein extraction of cells that have been incubated with $[Ru(Ema)_2(2MeIm)_2]CF_3SO_3$ (**13**, lowest IC_{50} value, Section 6.4.2). Differences in the protein expression between the two extractions may indicate how and where inside the cell the complex is interacting. Proteins that are either over- or under-expressed in the cells incubated with **13** could then be isolated from the gel, and identified by comparison of their amino acid composition with on-line library data. Gradient centrifugation could then be used to separate and isolate various components of the cell in which the identified proteins are known to be present.

Another experiment that could be performed to determine the cellular distribution of Ru is a micro-SRIXE study (Synchrotron Radiation-Induced X-ray Emission). This experiment can be used to detect the cellular distribution of elements, down to ppm levels.[8] This technique has not been reported for detecting Ru, but has been employed to detect Pt, Zn, K, Cu, and Ca distributions inside cells.[8,9]

8.5 References

(1) Goulle, V.; Thummel, R. *Inorg. Chem.* **1990**, *29*, 1767.

(2) Rillema, D. P.; Sahai, R.; Matthews, P.; Edwards, A. K.; Shaver, R. J.; Morgan, L. *Inorg. Chem.* **1990**, *29*, 167.

(3) Bastos, C. M.; Gordon, K. A.; Ocain, T. D. *Bioorg. Med. Chem. Lett.* **1998**, *8*, 147.

(4) Thompson, K. H.; Liboiron, B. D.; Sun, Y.; Bellman, K. D. D.; Setyawati, I. A.; Patrick, B. O.; Karunaratne, V.; Rawji, G.; Wheeler, J.; Sutton, K.; Bhanot, S.; Cassidy, C.; Mcneill, J. H.; Yuen, V. G.; Orvig, C. *J. Biol. Inorg. Chem.* **2003**, *8*, 66.

(5) Wu, A. **2003**, Unpublished Results.

(6) Baird, I. R. *Fluorinated Nitroimidazoles and Their Complexes: Potential Hypoxia-Imaging Agents*, Ph. D. Dissertation, University of British Columbia: Vancouver, 1999.

(7) Frausin, F.; Cocchietto, M.; Bergamo, A.; Scarcia, V.; Furlani, A.; Sava, G. *Cancer Chemother. Pharmacol.* **2002**, *50*, 405.

(8) Hall, M. D.; Hambley, T. W. *Coord. Chem. Rev.* **2002**, *232*, 49.

(9) Hall, M. D.; Dillon, C. T.; Zhang, M.; Beale, P.; Cai, Z.; Lai, B.; Stampfl, A. P. J.; Hambley, T. W. *J. Biol. Inorg. Chem.* **2003**.

Appendix A1

Experimental Details for the X-ray Crystallographic Study of *mer*-Ru(ma)$_3$ (1)

Empirical formula	C_{18} H_{15} O_9 Ru
Formula weight	476.37
Temperature	173(2) K
Wavelength	0.71069 A
Crystal system, space group	triclinic, Pbca
Unit cell dimensions	a = 17.017(3) A alpha = 90 deg. b = 11.6860(8) A beta = 90 deg. c = 18.6414(14) A gamma = 90 deg.
Volume	3707.0(7) A^3
Z, Calculated density	8, 1.707 Mg/m^3
Absorption coefficient	0.895 mm^-1
F(000)	1912
Theta range for data collection	3.04 to 27.93 deg.
Limiting indices	-15<=h<=19, -9<=k<=13, -22<=l<=19
Reflections collected / unique	3820 / 3820 [R(int) = 0.0000]
Completeness to theta = 27.93	85.9 %
Refinement method	Full-matrix least-squares on F^2
Data / restraints / parameters	3820 / 0 / 291
Goodness-of-fit on F^2	0.716
Final R indices [I>2sigma(I)]	R1 = 0.0380, wR2 = 0.0889
R indices (all data)	R1 = 0.0879, wR2 = 0.1042
Largest diff. peak and hole	0.478 and -0.663 e.A^-3

Table A1.1 Atomic Coordinates (x 10^4) and U(eq)

	x	y	z	U(eq)
Ru(1)	1313(1)	2225(1)	2180(1)	42(1)
O(1)	617(2)	1430(3)	2882(2)	58(1)
O(2)	463(2)	3462(3)	2239(2)	51(1)
O(3)	-1205(2)	2475(3)	3643(2)	71(1)
O(4)	1986(2)	2913(3)	2940(2)	64(1)
O(5)	2165(2)	977(2)	2197(2)	48(1)
O(6)	3843(2)	1901(4)	3619(2)	77(1)
O(7)	1915(2)	3098(3)	1416(2)	64(1)
O(8)	755(2)	1562(4)	1298(2)	67(1)
C(1)	-7(3)	2093(4)	3042(2)	47(1)
C(2)	-569(4)	1787(4)	3524(3)	60(1)
C(3)	-1272(4)	3484(5)	3290(3)	75(2)
C(4)	-744(3)	3840(4)	2827(3)	61(1)
C(5)	-79(3)	3164(4)	2680(3)	46(1)
C(6)	-574(4)	706(5)	3943(3)	91(2)
C(7)	2621(3)	2261(4)	3047(2)	51(1)
C(8)	3207(4)	2571(5)	3515(3)	69(2)
C(9)	3905(4)	914(6)	3248(3)	73(2)
C(10)	3364(3)	549(4)	2781(3)	60(1)
C(11)	2698(3)	1218(4)	2652(3)	45(1)
C(12)	3232(5)	3660(6)	3931(4)	111(3)
C(13A)	971(8)	1925(11)	740(4)	49(4)
C(14A)	645(7)	1575(10)	93(6)	81(5)
O(9A)	911(8)	2045(11)	-548(4)	140(6)
C(15A)	1502(8)	2866(10)	-540(4)	101(8)
C(16A)	1828(7)	3216(10)	107(5)	76(5)
C(17A)	1562(7)	2746(11)	748(4)	52(4)
C(18A)	63(16)	817(17)	-13(10)	208(12)
C(13B)	1730(6)	3008(9)	861(3)	45(4)
C(14B)	2061(4)	3621(7)	298(3)	84(6)
O(9B)	1774(5)	3483(10)	-395(3)	108(4)
C(15B)	1156(7)	2734(12)	-525(4)	138(12)
C(16B)	825(7)	2121(11)	39(5)	109(7)
C(17B)	1112(7)	2259(10)	731(5)	70(6)
C(18B)	2651(6)	4381(10)	257(5)	100(5)

Table A1.2 Bond Lengths (Å)

Ru(1)-O(4)	1.990(3)
Ru(1)-O(1)	1.993(3)
Ru(1)-O(7)	2.030(3)
Ru(1)-O(2)	2.049(3)
Ru(1)-O(8)	2.052(3)
Ru(1)-O(5)	2.056(3)
O(1)-C(1)	1.347(5)
O(2)-C(5)	1.284(5)
O(3)-C(3)	1.355(7)
O(3)-C(2)	1.366(6)
O(4)-C(7)	1.337(6)
O(5)-C(11)	1.273(5)
O(6)-C(9)	1.349(7)
O(6)-C(8)	1.351(7)
O(7)-C(17A)	1.443(8)
O(8)-C(13A)	1.181(7)
C(1)-C(2)	1.361(6)
C(1)-C(5)	1.427(7)
C(2)-C(6)	1.485(7)
C(3)-C(4)	1.313(7)
C(3)-H(3)	0.9500
C(4)-C(5)	1.408(7)
C(4)-H(4)	0.9500
C(6)-H(6A)	0.9800
C(6)-H(6B)	0.9800
C(6)-H(6C)	0.9800
C(7)-C(8)	1.373(7)
C(7)-C(11)	1.430(7)
C(8)-C(12)	1.491(8)
C(9)-C(10)	1.338(8)
C(9)-H(9)	0.9500
C(10)-C(11)	1.397(7)
C(10)-H(10)	0.9500
C(12)-H(12A)	0.9800
C(12)-H(12B)	0.9800
C(12)-H(12C)	0.9800
C(13A)-C(14A)	1.3900
C(13A)-C(17A)	1.3900
C(14A)-O(9A)	1.3900
C(14A)-C(18A)	1.34(2)
O(9A)-C(15A)	1.3900
C(15A)-C(16A)	1.3900
C(15A)-H(15A)	0.9500
C(16A)-C(17A)	1.3900
C(16A)-H(16A)	0.9500
C(18A)-H(18A)	0.9800
C(18A)-H(18B)	0.9800
C(18A)-H(18C)	0.9800
C(13B)-C(14B)	1.3900
C(13B)-C(17B)	1.3900
C(14B)-C(18B)	1.3433
C(14B)-O(9B)	1.3900

Table A1.2 Bond Lengths (Å) (contd.)

O(9B)-C(15B)	1.3900
C(15B)-C(16B)	1.3900
C(15B)-H(15B)	0.9500
C(16B)-C(17B)	1.3900
C(16B)-H(16B)	0.9500
C(18B)-H(18D)	0.9800
C(18B)-H(18E)	0.9800
C(18B)-H(18F)	0.9800

Table A1.3 Bond Angles (°)

O(4)-Ru(1)-O(1)	93.61(15)
O(4)-Ru(1)-O(7)	90.39(16)
O(1)-Ru(1)-O(7)	173.84(15)
O(4)-Ru(1)-O(2)	94.80(14)
O(1)-Ru(1)-O(2)	82.78(13)
O(7)-Ru(1)-O(2)	92.22(14)
O(4)-Ru(1)-O(8)	171.62(16)
O(1)-Ru(1)-O(8)	94.30(16)
O(7)-Ru(1)-O(8)	81.97(16)
O(2)-Ru(1)-O(8)	88.96(14)
O(4)-Ru(1)-O(5)	82.56(13)
O(1)-Ru(1)-O(5)	94.48(13)
O(7)-Ru(1)-O(5)	90.68(13)
O(2)-Ru(1)-O(5)	176.09(12)
O(8)-Ru(1)-O(5)	94.05(14)
C(1)-O(1)-Ru(1)	110.2(3)
C(5)-O(2)-Ru(1)	110.4(3)
C(3)-O(3)-C(2)	120.0(4)
C(7)-O(4)-Ru(1)	109.9(3)
C(11)-O(5)-Ru(1)	110.8(3)
C(9)-O(6)-C(8)	119.0(5)
C(17A)-O(7)-Ru(1)	104.6(4)
C(13A)-O(8)-Ru(1)	115.2(6)
O(1)-C(1)-C(2)	123.4(5)
O(1)-C(1)-C(5)	117.8(4)
C(2)-C(1)-C(5)	118.8(5)
C(1)-C(2)-O(3)	120.7(5)
C(1)-C(2)-C(6)	125.1(5)
O(3)-C(2)-C(6)	114.3(5)
C(4)-C(3)-O(3)	122.6(6)
C(4)-C(3)-H(3)	118.7
O(3)-C(3)-H(3)	118.7
C(3)-C(4)-C(5)	119.9(5)
C(3)-C(4)-H(4)	120.0
C(5)-C(4)-H(4)	120.0
O(2)-C(5)-C(4)	123.3(5)
O(2)-C(5)-C(1)	118.6(4)
C(4)-C(5)-C(1)	118.1(5)
O(4)-C(7)-C(8)	122.1(5)
O(4)-C(7)-C(11)	118.9(4)
C(8)-C(7)-C(11)	119.0(5)
O(6)-C(8)-C(7)	121.4(5)
O(6)-C(8)-C(12)	113.4(5)
C(7)-C(8)-C(12)	125.2(6)
C(10)-C(9)-O(6)	123.5(5)
C(10)-C(9)-H(9)	118.2
O(6)-C(9)-H(9)	118.2
C(9)-C(10)-C(11)	119.5(5)
C(9)-C(10)-H(10)	120.3
C(11)-C(10)-H(10)	120.3
O(5)-C(11)-C(10)	124.7(5)
O(5)-C(11)-C(7)	117.7(4)
C(10)-C(11)-C(7)	117.6(5)

Table A1.3 Bond Angles (°) (contd.)

O(8)-C(13A)-C(14A)	122.3(8)
O(8)-C(13A)-C(17A)	117.6(8)
C(14A)-C(13A)-C(17A)	120.0
O(9A)-C(14A)-C(13A)	120.0
O(9A)-C(14A)-C(18A)	112.0(11)
C(13A)-C(14A)-C(18A)	128.0(11)
C(14A)-O(9A)-C(15A)	120.0
C(16A)-C(15A)-O(9A)	120.0
C(16A)-C(15A)-H(15A)	120.0
O(9A)-C(15A)-H(15A)	120.0
C(15A)-C(16A)-C(17A)	120.0
C(15A)-C(16A)-H(16A)	120.0
C(17A)-C(16A)-H(16A)	120.0
C(16A)-C(17A)-C(13A)	120.0
C(16A)-C(17A)-O(7)	119.5(6)
C(13A)-C(17A)-O(7)	120.5(6)
C(14A)-C(18A)-H(18A)	109.6
C(14A)-C(18A)-H(18B)	109.4
H(18A)-C(18A)-H(18B)	109.5
C(14A)-C(18A)-H(18C)	109.5
H(18A)-C(18A)-H(18C)	109.5
H(18B)-C(18A)-H(18C)	109.5
C(14B)-C(13B)-C(17B)	120.0
C(18B)-C(14B)-C(13B)	133.3
C(18B)-C(14B)-O(9B)	106.7
C(13B)-C(14B)-O(9B)	120.0
C(15B)-O(9B)-C(14B)	120.0
O(9B)-C(15B)-C(16B)	120.0
O(9B)-C(15B)-H(15B)	120.0
C(16B)-C(15B)-H(15B)	120.0
C(17B)-C(16B)-C(15B)	120.0
C(17B)-C(16B)-H(16B)	120.0
C(15B)-C(16B)-H(16B)	120.0
C(16B)-C(17B)-C(13B)	120.0
C(14B)-C(18B)-H(18D)	109.5
C(14B)-C(18B)-H(18E)	109.5
H(18D)-C(18B)-H(18E)	109.5
C(14B)-C(18B)-H(18F)	109.5
H(18D)-C(18B)-H(18F)	109.5
H(18E)-C(18B)-H(18F)	109.5

Appendix A2

Experimental Details for the X-ray Crystallographic Study of *trans*-$[Ru(ma)_2(1MeIm)_2]CF_3SO_3 \cdot CH_2Cl_2$ (8)

Empirical formula	C22 H24 Cl2 F3 N4 O9 Ru S
Formula weight	749.48
Temperature	173(2) K
Wavelength	0.71069 A
Crystal system, space group	triclinic, $P\bar{1}$ (#2)
Unit cell dimensions	a = 9.1784(8) A alpha = 64.082(14) deg. b = 12.9918(3) A beta = 78.771(19) deg. c = 13.6855(3) A gamma = 85.95(2) deg.
Volume	1439.48(13) A^3
Z, Calculated density	2, 1.729 Mg/m^3
Absorption coefficient	0.878 mm^-1
F(000)	754
Crystal size	0.20 x 0.10 x 0.02 mm
Theta range for data collection	2.26 to 27.09 deg.
Index ranges	-11<=h<=11, -16<=k<=15, -17<=l<=16
Reflections collected / unique	5707 / 5707 [R(int) = 0.0000]
Completeness to 2theta = 27.09	90.1%
Refinement method	Full-matrix least-squares on F^2
Data / restraints / parameters	5707 / 69 / 421
Goodness-of-fit on F^2	0.981
Final R indices [I>2sigma(I)]	R1 = 0.0595, wR2 = 0.1345
R indices (all data)	R1 = 0.1147, wR2 = 0.1563
Largest diff. peak and hole	1.049 and -0.802 e.A^-3

Table A2.1 Atomic Coordinates (x 10^4) and U(eq)

	x	y	z	U(eq)	occ
Ru(1)	5000	0	5000	19(1)	
Ru(2)	10000	0	10000	18(1)	
S(1)	9026(5)	4518(3)	3007(3)	26(1)	0.75(1)
F(1)	10758(7)	4699(5)	4233(5)	57(2)	0.75(1)
F(2)	11914(7)	4882(7)	2637(5)	85(3)	0.75(1)
F(3)	11150(15)	3212(6)	3913(6)	76(3)	0.75(1)
O(1)	5196(5)	1665(4)	3926(3)	24(1)	
O(2)	3911(5)	669(4)	6062(3)	25(1)	
O(3)	4180(5)	4123(4)	4473(4)	32(1)	
O(4)	8197(5)	-159(4)	9440(3)	23(1)	
O(5)	10494(5)	1328(4)	8437(3)	22(1)	
O(6)	6831(5)	1922(4)	7050(4)	33(1)	
O(7)	7969(7)	4017(6)	4012(4)	41(2)	0.75(1)
O(8)	8934(8)	5736(4)	2420(5)	53(3)	0.75(1)
O(9)	9201(10)	3918(6)	2330(6)	66(3)	0.75(1)
N(1)	6937(5)	94(4)	5503(4)	20(1)	
N(2)	8785(7)	-383(6)	6426(6)	42(2)	
N(3)	8868(6)	1176(4)	10499(4)	21(1)	
N(4)	8113(7)	2796(5)	10536(5)	31(1)	
C(1)	3987(7)	1754(6)	5584(5)	26(2)	
C(2)	3435(7)	2474(6)	6123(6)	26(2)	
C(3)	3548(8)	3602(6)	5551(6)	31(2)	
C(4)	4711(7)	3486(6)	3905(6)	27(2)	
C(5)	4672(7)	2322(5)	4450(5)	22(1)	
C(6)	5298(8)	4162(6)	2728(5)	35(2)	
C(7)	7919(8)	997(7)	5072(6)	36(2)	
C(8)	9067(8)	709(7)	5658(7)	43(2)	
C(9)	7484(8)	-740(7)	6324(6)	34(2)	
C(10)	9727(10)	-1048(9)	7208(7)	60(3)	
C(11)	9351(7)	1546(6)	7972(5)	23(1)	
C(12)	9212(8)	2532(6)	6994(5)	29(2)	
C(13)	7948(8)	2666(6)	6586(5)	34(2)	
C(14)	6880(8)	965(6)	7995(5)	28(2)	
C(15)	8097(8)	752(5)	8496(5)	24(2)	
C(16)	5539(8)	211(6)	8396(6)	36(2)	
C(17)	7808(7)	957(6)	11418(5)	25(1)	
C(18)	7342(8)	1938(6)	11456(6)	32(2)	
C(19)	9017(7)	2311(5)	9972(5)	24(1)	
C(20)	7956(11)	4024(6)	10208(7)	48(2)	
C(21)	10784(9)	4318(6)	3454(5)	53(3)	0.75(1)
C(22)	6780(7)	7270(2)	538(15)	55(3)	0.85(1)
Cl(1)	4844(3)	7263(2)	926(3)	59(1)	0.85(1)
Cl(2)	7311(6)	6875(4)	-551(3)	95(2)	0.85(1)
S(1B)	9132(16)	4364(12)	2980(11)	26(1)	0.25(1)
O(7B)	8370(3)	4541(19)	3909(14)	41(2)	0.25(1)
O(8B)	9260(3)	5354(15)	1943(13)	53(3)	0.25(1)
O(9B)	8730(3)	3332(14)	2959(19)	66(3)	0.25(1)

Table A2.1 Atomic Coordinates (x 10^4) and U(eq) (contd.)

C(21B)	10960(17)	4050(18)	3315(17)	53(3)	0.25(1)
F(1B)	11890(2)	3805(17)	2559(14)	57(2)	0.25(1)
F(2B)	11600(2)	4910(2)	3380(2)	85(3)	0.25(1)
F(3B)	10920(5)	3130(2)	4292(17)	76(3)	0.25(1)
C(22B)	6989(19)	7130(13)	460(8)	55(3)	0.15(1)
Cl(1B)	5460(2)	7304(14)	1370(14)	59(1)	0.15(1)
Cl(2B)	6440(4)	6790(2)	-510(2)	95(2)	0.15(1)

Table A2.2 Bond Lengths (Å)

Ru(1)-O(1)	2.012(4)
Ru(1)-O(1)#1	2.012(4)
Ru(1)-N(1)	2.057(5)
Ru(1)-N(1)#1	2.057(5)
Ru(1)-O(2)	2.072(4)
Ru(1)-O(2)#1	2.072(4)
Ru(2)-O(4)#2	2.012(4)
Ru(2)-O(4)	2.012(4)
Ru(2)-O(5)	2.065(4)
Ru(2)-O(5)#2	2.065(4)
Ru(2)-N(3)#2	2.072(5)
Ru(2)-N(3)	2.072(5)
S(1)-O(7)	1.429(4)
S(1)-O(9)	1.431(4)
S(1)-O(8)	1.432(4)
S(1)-C(21)	1.797(8)
F(1)-C(21)	1.354(4)
F(2)-C(21)	1.342(5)
F(3)-C(21)	1.341(5)
O(1)-C(5)	1.348(8)
O(2)-C(1)	1.269(8)
O(3)-C(3)	1.349(8)
O(3)-C(4)	1.373(8)
O(4)-C(15)	1.332(7)
O(5)-C(11)	1.283(7)
O(6)-C(13)	1.319(8)
O(6)-C(14)	1.352(7)
N(1)-C(9)	1.329(8)
N(1)-C(7)	1.369(8)
N(2)-C(8)	1.351(10)
N(2)-C(9)	1.364(9)
N(2)-C(10)	1.444(9)
N(3)-C(19)	1.331(8)
N(3)-C(17)	1.364(8)
N(4)-C(19)	1.335(8)
N(4)-C(18)	1.366(8)
N(4)-C(20)	1.461(9)
C(1)-C(5)	1.425(9)
C(1)-C(2)	1.438(9)
C(2)-C(3)	1.326(9)
C(2)-H(2)	0.9500
C(3)-H(3)	0.9500
C(4)-C(5)	1.363(9)
C(4)-C(6)	1.466(9)
C(6)-H(6A)	0.9800
C(6)-H(6B)	0.9800
C(6)-H(6C)	0.9800
C(7)-C(8)	1.380(10)
C(7)-H(7)	0.9500
C(8)-H(8)	0.9500
C(9)-H(9)	0.9500
C(10)-H(10A)	0.9800
C(10)-H(10B)	0.9800

Table A2.2 Bond Lengths (Å) (contd.)

C(10)-H(10C)	0.9800
C(11)-C(12)	1.412(8)
C(11)-C(15)	1.450(9)
C(12)-C(13)	1.351(9)
C(12)-H(12)	0.9500
C(13)-H(13)	0.9500
C(14)-C(15)	1.372(9)
C(14)-C(16)	1.487(9)
C(16)-H(16A)	0.9800
C(16)-H(16B)	0.9800
C(16)-H(16C)	0.9800
C(17)-C(18)	1.334(9)
C(17)-H(17)	0.9500
C(18)-H(18)	0.9500
C(19)-H(19)	0.9500
C(20)-H(20A)	0.9800
C(20)-H(20B)	0.9800
C(20)-H(20C)	0.9800
C(22)-Cl(2)	1.751(6)
C(22)-Cl(1)	1.752(6)
C(22)-H(22A)	0.9900
C(22)-H(22B)	0.9900
S(1B)-O(9B)	1.429(5)
S(1B)-O(7B)	1.430(5)
S(1B)-O(8B)	1.430(5)
S(1B)-C(21B)	1.797(9)
C(21B)-F(3B)	1.343(5)
C(21B)-F(2B)	1.343(5)
C(21B)-F(1B)	1.343(5)
C(22B)-Cl(2B)	1.751(7)
C(22B)-Cl(1B)	1.752(7)
C(22B)-H(22C)	0.9900
C(22B)-H(22D)	0.9900

Table A2.3 Bond Angles (°)

O(1)-Ru(1)-O(1)#1	180.0
O(1)-Ru(1)-N(1)	90.94(19)
O(1)#1-Ru(1)-N(1)	89.06(19)
O(1)-Ru(1)-N(1)#1	89.06(19)
O(1)#1-Ru(1)-N(1)#1	90.94(19)
N(1)-Ru(1)-N(1)#1	180.0
O(1)-Ru(1)-O(2)	82.04(17)
O(1)#1-Ru(1)-O(2)	97.96(17)
N(1)-Ru(1)-O(2)	88.15(19)
N(1)#1-Ru(1)-O(2)	91.85(19)
O(1)-Ru(1)-O(2)#1	97.96(17)
O(1)#1-Ru(1)-O(2)#1	82.04(17)
N(1)-Ru(1)-O(2)#1	91.85(19)
N(1)#1-Ru(1)-O(2)#1	88.15(19)
O(2)-Ru(1)-O(2)#1	180.0
O(4)#2-Ru(2)-O(4)	179.999(1)
O(4)#2-Ru(2)-O(5)	97.77(16)
O(4)-Ru(2)-O(5)	82.23(16)
O(4)#2-Ru(2)-O(5)#2	82.23(16)
O(4)-Ru(2)-O(5)#2	97.77(16)
O(5)-Ru(2)-O(5)#2	180.000(1)
O(4)#2-Ru(2)-N(3)#2	88.92(18)
O(4)-Ru(2)-N(3)#2	91.08(18)
O(5)-Ru(2)-N(3)#2	92.77(19)
O(5)#2-Ru(2)-N(3)#2	87.23(19)
O(4)#2-Ru(2)-N(3)	91.08(18)
O(4)-Ru(2)-N(3)	88.92(18)
O(5)-Ru(2)-N(3)	87.23(19)
O(5)#2-Ru(2)-N(3)	92.77(19)
N(3)#2-Ru(2)-N(3)	180.000(1)
O(7)-S(1)-O(9)	114.9(3)
O(7)-S(1)-O(8)	114.5(3)
O(9)-S(1)-O(8)	114.7(3)
O(7)-S(1)-C(21)	104.1(4)
O(9)-S(1)-C(21)	102.9(4)
O(8)-S(1)-C(21)	103.6(4)
C(5)-O(1)-Ru(1)	110.2(4)
C(1)-O(2)-Ru(1)	110.1(4)
C(3)-O(3)-C(4)	120.3(5)
C(15)-O(4)-Ru(2)	109.9(4)
C(11)-O(5)-Ru(2)	109.7(4)
C(13)-O(6)-C(14)	121.1(5)
C(9)-N(1)-C(7)	106.4(6)
C(9)-N(1)-Ru(1)	125.6(5)
C(7)-N(1)-Ru(1)	128.0(5)
C(8)-N(2)-C(9)	108.5(6)
C(8)-N(2)-C(10)	125.0(7)
C(9)-N(2)-C(10)	126.5(8)
C(19)-N(3)-C(17)	105.8(5)
C(19)-N(3)-Ru(2)	126.7(4)
C(17)-N(3)-Ru(2)	127.6(4)
C(19)-N(4)-C(18)	107.6(6)

Table A2.3 Bond Angles (°) (contd.)

C(19)-N(4)-C(20)	125.9(6)
C(18)-N(4)-C(20)	126.5(6)
O(2)-C(1)-C(5)	119.7(6)
O(2)-C(1)-C(2)	123.9(6)
C(5)-C(1)-C(2)	116.4(6)
C(3)-C(2)-C(1)	119.5(6)
C(3)-C(2)-H(2)	120.2
C(1)-C(2)-H(2)	120.2
C(2)-C(3)-O(3)	123.1(7)
C(2)-C(3)-H(3)	118.4
O(3)-C(3)-H(3)	118.4
C(5)-C(4)-O(3)	119.7(6)
C(5)-C(4)-C(6)	125.7(6)
O(3)-C(4)-C(6)	114.6(6)
O(1)-C(5)-C(4)	121.6(6)
O(1)-C(5)-C(1)	117.5(6)
C(4)-C(5)-C(1)	120.8(6)
N(1)-C(7)-C(8)	109.4(7)
N(1)-C(7)-H(7)	125.3
C(8)-C(7)-H(7)	125.3
N(2)-C(8)-C(7)	105.8(6)
N(2)-C(8)-H(8)	127.1
C(7)-C(8)-H(8)	127.1
N(1)-C(9)-N(2)	109.8(7)
N(1)-C(9)-H(9)	125.1
N(2)-C(9)-H(9)	125.1
O(5)-C(11)-C(12)	124.2(6)
O(5)-C(11)-C(15)	118.4(6)
C(12)-C(11)-C(15)	117.4(6)
C(13)-C(12)-C(11)	118.6(6)
C(13)-C(12)-H(12)	120.7
C(11)-C(12)-H(12)	120.7
O(6)-C(13)-C(12)	123.5(6)
O(6)-C(13)-H(13)	118.2
C(12)-C(13)-H(13)	118.2
O(6)-C(14)-C(15)	120.4(6)
O(6)-C(14)-C(16)	114.1(6)
C(15)-C(14)-C(16)	125.5(6)
O(4)-C(15)-C(14)	123.3(6)
O(4)-C(15)-C(11)	117.8(6)
C(14)-C(15)-C(11)	118.9(6)
C(18)-C(17)-N(3)	109.9(6)
C(18)-C(17)-H(17)	125.0
N(3)-C(17)-H(17)	125.0
C(17)-C(18)-N(4)	106.5(6)
C(17)-C(18)-H(18)	126.8
N(4)-C(18)-H(18)	126.8
N(3)-C(19)-N(4)	110.2(6)
N(3)-C(19)-H(19)	124.9
N(4)-C(19)-H(19)	124.9
F(3)-C(21)-F(2)	107.4(5)
F(3)-C(21)-F(1)	106.1(5)
F(2)-C(21)-F(1)	106.0(5)

Table A2.3 Bond Angles (°) (contd.)

F(3)-C(21)-S(1)	112.2(7)
F(2)-C(21)-S(1)	113.4(6)
F(1)-C(21)-S(1)	111.3(6)
Cl(2)-C(22)-Cl(1)	111.8(6)
Cl(2)-C(22)-H(22A)	109.3
Cl(1)-C(22)-H(22A)	109.3
Cl(2)-C(22)-H(22B)	109.3
Cl(1)-C(22)-H(22B)	109.3
H(22A)-C(22)-H(22B)	107.9
O(9B)-S(1B)-O(7B)	114.9(5)
O(9B)-S(1B)-O(8B)	114.8(4)
O(7B)-S(1B)-O(8B)	114.8(5)
O(9B)-S(1B)-C(21B)	102.2(15)
O(7B)-S(1B)-C(21B)	100.5(13)
O(8B)-S(1B)-C(21B)	107.3(14)
F(3B)-C(21B)-F(2B)	106.8(6)
F(3B)-C(21B)-F(1B)	106.9(6)
F(2B)-C(21B)-F(1B)	106.8(6)
F(3B)-C(21B)-S(1B)	111(2)
F(2B)-C(21B)-S(1B)	113.8(16)
F(1B)-C(21B)-S(1B)	111.4(16)
Cl(2B)-C(22B)-Cl(1B)	111.8(7)
Cl(2B)-C(22B)-H(22C)	109.2
Cl(1B)-C(22B)-H(22C)	109.2
Cl(2B)-C(22B)-H(22D)	109.2
Cl(1B)-C(22B)-H(22D)	109.2
H(22C)-C(22B)-H(22D)	107.9

Appendix A3

Experimental Details for the X-ray Crystallographic Study of *trans*-[Ru(ma)$_2$(2MeIm)$_2$]CF_3SO_3 (10)

Empirical formula	C21 H22 F3 N4 O9 S Ru
Formula weight	664.55
Temperature	173.2 K
Wavelength	0.7107 A
Crystal system, space group	Triclinic, P -1
Unit cell dimensions	a = 8.9512(6) A alpha = 94.908(5) deg. b = 9.2949(7) A beta = 93.453(5) deg. c = 15.817(1) A gamma = 93.059(4) deg.
Volume	1306.5(2) A^3
Z, Calculated density	2, 1.689 Mg/m^3
Absorption coefficient	0.758 mm^-1
F(000)	670.00
Crystal size	0.20 x 0.15 x 0.15 mm
Theta range for data collection	2.20 to 27.86 deg.
Limiting indices	-9<=h<=11, -11<=k<=11, -18<=l<=19
Reflections collected / unique	11677 / 5269 [R(int) = 0.04146]
Absorption correction	Semi-empirical from equivalents
Max. and min. transmission	1.000 and 0.8142
Refinement method	Full-matrix least-squares on F^2
Data / restraints / parameters	5269 / 0 / 363
Goodness-of-fit on F^2	0.951
Final R indices [I>2sigma(I)]	R1 = 0.032, wR2 = 0.040
R indices (all data)	R1 = 0.0603, wR2 = 0.0896
Largest diff. peak and hole	0.78 and -0.83 e.A^-3

Table A3.1 Atomic Coordinates (x 10^4) and U(eq)

	x	y	z	U(eq)
Ru(1)	0	0	10000	18(1)
Ru(2)	0	0	5000	22(1)
S(1)	4642(1)	-5654(1)	7488(1)	32(1)
F(1)	4116(3)	-5039(3)	9080(1)	49(1)
F(2)	2821(3)	-6863(3)	8472(2)	60(1)
F(3)	2271(3)	-4732(3)	8209(2)	79(1)
O(1)	1420(2)	76(2)	9069(1)	22(1)
O(2)	1689(2)	-1099(2)	10555(1)	22(1)
O(3)	4980(2)	-1557(2)	8936(1)	28(1)
O(4)	-1508(2)	-1640(3)	5101(1)	30(1)
O(5)	1351(2)	-1242(2)	5705(1)	28(1)
O(6)	-968(4)	-4971(3)	6049(2)	66(1)
O(7)	3753(3)	-6381(3)	6790(2)	47(1)
O(8)	5118(4)	-4179(3)	7411(2)	61(1)
O(9)	5824(3)	-6447(4)	7847(2)	62(1)
N(1)	-897(2)	-1979(3)	9428(2)	21(1)
N(2)	-2018(3)	-3709(3)	8576(2)	30(1)
N(3)	651(3)	-1038(3)	3892(2)	24(1)
N(4)	1931(3)	-1996(3)	2883(2)	33(1)
C(1)	2623(3)	-659(3)	9255(2)	21(1)
C(2)	2755(3)	-1239(3)	10056(2)	20(1)
C(3)	4085(3)	-1929(3)	10275(2)	25(1)
C(4)	5134(3)	-2042(4)	9713(2)	30(1)
C(5)	3723(3)	-870(3)	8700(2)	25(1)
C(6)	3724(4)	-422(4)	7826(2)	37(1)
C(7)	-986(3)	-3226(4)	9844(2)	26(1)
C(8)	-1699(4)	-4304(4)	9325(2)	32(1)
C(9)	-1537(3)	-2311(3)	8650(2)	24(1)
C(10)	-1682(4)	-1349(4)	7949(2)	37(1)
C(11)	-863(4)	-2664(4)	5515(2)	28(1)
C(12)	656(4)	-2424(4)	5825(2)	30(1)
C(13)	1310(5)	-3566(4)	6245(3)	48(1)
C(14)	514(5)	-4754(5)	6321(3)	68(2)
C(15)	-1656(4)	-3926(4)	5643(3)	44(1)
C(16)	-3251(4)	-4292(5)	5380(3)	54(1)
C(17)	-333(4)	-1540(4)	3211(2)	29(1)
C(18)	452(4)	-2128(4)	2584(2)	38(1)
C(19)	2025(4)	-1337(4)	3671(2)	29(1)
C(20)	3465(4)	-992(5)	4185(3)	48(1)
C(21)	3396(4)	-5551(4)	8355(2)	35(1)
H(3)	4230	-2314	10830	30
H(4)	6059	-2500	9872	36
H(6A)	2692	-297	7614	44
H(6B)	4161	-1166	7457	44
H(6C)	4318	495	7829	44
H(7)	-591	-3313	10428	31
H(8)	-1937	-5299	9454	38
H(10C)	-682	-1034	7792	45
H(10A)	-2222	-502	8138	45

Table A3.1 Atomic Coordinates (x 10^4) and U(eq) (contd.)

H(10B)	-2238	-1878	7455	45
H(13)	2355	-3452	6475	57
H(14)	1002	-5536	6588	81
H(16C)	-3781	-4572	5870	65
H(16A)	-3330	-5098	4934	65
H(16B)	-3700	-3449	5160	65
H(17)	-1424	-1478	3189	35
H(18)	49	-2563	2025	46
H(20B)	4271	-1478	3904	58
H(20C)	3381	-1326	4752	58
H(20A)	3693	56	4237	58
H(21)	-2460(40)	-4110(40)	8220(20)	31(9)
H(22)	2630(50)	-2340(50)	2630(30)	60(10)

Table A3.2 Bond Lengths (Å)

Ru(1)-O(1)	2.006(2)
Ru(1)-O(1)#1	2.006(2)
Ru(1)-O(2)	2.063(2)
Ru(1)-O(2)#1	2.063(2)
Ru(1)-N(1)	2.078(2)
Ru(1)-N(1)#1	2.078(2)
Ru(2)-O(4)	2.005(2)
Ru(2)-O(4)#2	2.005(2)
Ru(2)-O(5)	2.061(2)
Ru(2)-O(5)#2	2.061(2)
Ru(2)-N(3)	2.058(2)
Ru(2)-N(3)#2	2.058(2)
S(1)-O(7)	1.421(2)
S(1)-O(8)	1.431(3)
S(1)-O(9)	1.438(3)
S(1)-C(21)	1.818(4)
F(1)-C(21)	1.320(4)
F(2)-C(21)	1.330(4)
F(3)-C(21)	1.316(4)
O(1)-C(1)	1.338(3)
O(2)-C(2)	1.279(3)
O(3)-C(4)	1.346(4)
O(3)-C(5)	1.371(4)
O(4)-C(11)	1.337(4)
O(5)-C(12)	1.268(4)
O(6)-C(14)	1.369(5)
O(6)-C(15)	1.364(5)
N(1)-C(7)	1.383(4)
N(1)-C(9)	1.329(4)
N(2)-C(8)	1.371(5)
N(2)-C(9)	1.340(4)
N(2)-H(21)	0.72(3)
N(3)-C(17)	1.382(4)
N(3)-C(19)	1.335(4)
N(4)-C(18)	1.374(4)
N(4)-C(19)	1.337(4)
N(4)-H(22)	0.82(4)
C(1)-C(2)	1.419(4)
C(1)-C(5)	1.369(4)
C(2)-C(3)	1.421(4)
C(3)-C(4)	1.334(4)
C(3)-H(3)	0.98
C(4)-H(4)	0.98
C(5)-C(6)	1.477(5)
C(6)-H(6A)	0.98
C(6)-H(6B)	0.98
C(6)-H(6C)	0.98
C(7)-C(8)	1.346(5)
C(7)-H(7)	0.98
C(8)-H(8)	0.98
C(9)-C(10)	1.487(5)
C(10)-H(10C)	0.98

Table A3.2 Bond Lengths (Å) (contd.)

C(10)-H(10A)	0.98
C(10)-H(10B)	0.98
C(11)-C(12)	1.417(4)
C(11)-C(15)	1.375(5)
C(12)-C(13)	1.433(5)
C(13)-C(14)	1.300(6)
C(13)-H(13)	0.98
C(14)-H(14)	0.98
C(15)-C(16)	1.476(5)
C(16)-H(16C)	0.98
C(16)-H(16A)	0.98
C(16)-H(16B)	0.98
C(17)-C(18)	1.344(5)
C(17)-H(17)	0.98
C(18)-H(18)	0.98
C(19)-C(20)	1.486(5)
C(20)-H(20B)	0.98
C(20)-H(20C)	0.98
C(20)-H(20A)	0.98

Table A3.3 Bond Angles (°)

O1-Ru1-O2	82.32(7)
O1-Ru1-N1	88.88(9)
O1-Ru1-O1_a	180.00
O1-Ru1-O2_a	97.68(7)
O1-Ru1-N1_a	91.12(9)
O2-Ru1-N1	87.87(8)
O1_a-Ru1-O2	97.68(7)
O2-Ru1-O2_a	180.00
O2-Ru1-N1_a	92.13(8)
O1_a-Ru1-N1	91.12(9)
O2_a-Ru1-N1	92.13(8)
N1-Ru1-N1_a	180.00
O1_a-Ru1-O2_a	82.32(7)
O1_a-Ru1-N1_a	88.88(9)
O2_a-Ru1-N1_a	87.87(8)
O4-Ru2-N3	89.74(9)
O4-Ru2-O4_b	180.00
O4-Ru2-O5_b	97.81(8)
O4-Ru2-N3_b	90.26(9)
O5-Ru2-N3	90.41(9)
O4_b-Ru2-O5	97.81(8)
O5-Ru2-O5_b	180.00
O5-Ru2-N3_b	89.59(9)
O4_b-Ru2-N3	90.26(9)
O5_b-Ru2-N3	89.59(9)
N3-Ru2-N3_b	180.00
O4_b-Ru2-O5_b	82.19(8)
O4_b-Ru2-N3_b	89.74(9)
C2-C1-C5	119.2(3)
O2-C2-C1	118.9(2)
O2-C2-C3	122.8(3)
C1-C2-C3	118.3(3)
C9-C10-H10A	109.47
H10B-C10-H10C	109.48
H10A-C10-H10C	109.50
O4-C11-C12	118.8(3)
C12-C11-C15	120.4(3)
O4-C11-C15	120.8(3)
C11-C12-C13	116.8(3)
O5-C12-C13	124.4(3)
O5-C12-C11	118.8(3)
N1-C9-C10	127.5(3)
N1-C9-N2	108.6(3)
C2-C3-H3	120.58
C4-C3-H3	120.55
C11-C15-C16	125.9(4)
O6-C15-C11	119.9(3)
N3-C17-C18	108.8(3)
N4-C18-C17	106.3(3)
N4-C19-C20	123.5(3)
N3-C19-C20	127.4(3)
N3-C19-N4	109.1(3)
C12-C13-H13	120.07
C14-C13-H13	120.07
C13-C14-H14	118.20
O6-C14-H14	118.27
C15-C16-H16A	109.42
C15-C16-H16C	109.52

Table A3.3 Bond Angles (°) (contd.)

C19-C20-H20B	109.45
C19-C20-H20C	109.51
H20A-C20-H20B	109.44
H20A-C20-H20C	109.47
S1-C21-F1	111.6(3)
S1-C21-F2	110.3(3)
S1-C21-F3	112.3(2)
F1-C21-F2	106.7(3)
F1-C21-F3	108.1(3)
F2-C21-F3	107.6(3)
O5_b-Ru2-N3_b	90.41(9)
O4-Ru2-O5	82.19(8)
O9-S1-C21	100.75(17)
O8-S1-O9	112.0(2)
O8-S1-C21	104.11(18)
O7-S1-C21	104.53(17)
O7-S1-O8	116.70(18)
O7-S1-O9	116.25(19)
Ru1-O1-C1	109.94(16)
Ru1-O2-C2	110.10(16)
C4-O3-C5	120.2(2)
Ru2-O4-C11	109.63(19)
Ru2-O5-C12	110.43(19)
C14-O6-C15	119.4(3)
C7-N1-C9	106.8(3)
Ru1-N1-C9	129.7(2)
Ru1-N1-C7	123.5(2)
C8-N2-C9	109.8(3)
C8-N2-H21	122(3)
C9-N2-H21	128(3)
Ru2-N3-C19	129.3(2)
C17-N3-C19	106.9(3)
Ru2-N3-C17	123.7(2)
C18-N4-C19	108.8(3)
C18-N4-H22	125(3)
C19-N4-H22	126(3)
O1-C1-C5	122.2(3)
O1-C1-C2	118.5(2)
H10A-C10-H10B	109.48
C9-C10-H10C	109.44
C9-C10-H10B	109.45
C2-C3-C4	118.9(3)
O3-C4-C3	123.0(3)
O3-C5-C1	120.3(3)
C1-C5-C6	126.4(3)
O3-C5-C6	113.3(2)
N1-C7-C8	109.6(3)
N2-C8-C7	105.1(3)
N2-C9-C10	123.8(3)
O5-C12-C11	118.8(3)
C12-C13-C14	119.9(4)
O6-C14-C13	123.5(4)
O6-C15-C16	114.2(3)
O3-C4-H4	118.47
C3-C4-H4	118.54
H6A-C6-H6C	109.45
C5-C6-H6A	109.38
H6B-C6-H6C	109.54
H6A-C6-H6B	109.55

Table A3.3 Bond Angles (°) (contd.)

C5-C6-H6C	109.45
C5-C6-H6B	109.46
N1-C7-H7	125.22
C8-C7-H7	125.16
C7-C8-H8	127.47
N2-C8-H8	127.40
H16A-C16-H16B	109.44
C15-C16-H16B	109.47
H16B-C16-H16C	109.45
H16A-C16-H16C	109.53
N3-C17-H17	125.57
C18-C17-H17	125.62
N4-C18-H18	126.87
C17-C18-H18	126.80
H20B-C20-H20C	109.50
C19-C20-H20A	109.46

Appendix A4

Experimental Details for the X-ray Crystallographic Study of *trans*-[Ru(Ema)$_2$(metro)$_2$]CF_3SO_3 (11)

Empirical formula	C28 H34 F3 N6 O16 Ru S
Formula weight	900.74
Temperature	173(2) K
Wavelength	0.71069 A
Crystal system, space group	Triclinic, P-1
Unit cell dimensions	a = 11.0867(12) A alpha = 105.636(4) deg. b = 12.5113(14) A beta = 97.737(3) deg. c = 13.8897(15) A gamma = 99.838(4) deg.
Volume	1794.6(3) A^3
Z, Calculated density	2, 1.667 Mg/m^3
Absorption coefficient	0.591 mm^-1
F(000)	918
Crystal size	0.25 x 0.20 x 0.15 mm
Theta range for data collection	2.66 to 27.87 deg.
Index ranges	-12<=h<=14, -16<=k<=14, -17<=l<=15
Reflections collected / unique	7380 / 7380 [R(int) = 0.0000]
Completeness to 2theta = 27.87	86.2%
Absorption correction	Semi-empirical from equivalents
Max. and min. transmission	1.0000 and 0.7654
Refinement method	Full-matrix least-squares on F^2
Data / restraints / parameters	7380 / 37 / 545
Goodness-of-fit on F^2	0.969
Final R indices [I>2sigma(I)]	R1 = 0.0501, wR2 = 0.1190
R indices (all data)	R1 = 0.0855, wR2 = 0.1322
Largest diff. peak and hole	1.155 and -0.963 e.A^-3

Table A4.1 Atomic Coordinates (x 10^4) and U(eq)

	x	y	z	U(eq)
Ru(1)	0	0	0	16(1)
Ru(2)	0	0	5000	21(1)
O(1)	1772(3)	234(2)	816(2)	24(1)
O(2)	953(3)	628(2)	-931(2)	25(1)
O(3)	4252(3)	1826(3)	-497(3)	37(1)
O(4)	562(3)	3497(3)	3807(2)	40(1)
O(5)	-365(3)	4673(2)	3271(2)	38(1)
O(6)	-3001(4)	3428(3)	369(3)	41(1)
O(7)	933(3)	79(2)	3827(2)	30(1)
O(8)	1358(3)	1372(2)	5750(2)	27(1)
O(9)	3256(3)	3162(3)	4631(3)	44(1)
O(10)	-2814(3)	1258(3)	1833(2)	44(1)
O(11)	-3177(4)	2832(3)	2737(3)	44(1)
O(12)	-3952(5)	2798(4)	5640(4)	80(2)
O(13)	-4835(4)	696(3)	3094(3)	58(1)
N(1)	-114(3)	1627(2)	788(2)	19(1)
N(2)	-467(3)	3364(2)	1241(3)	22(1)
N(3)	58(3)	3800(3)	3119(3)	27(1)
N(4)	-1020(3)	1080(3)	4540(3)	23(1)
N(5)	-1928(3)	2512(3)	4506(3)	21(1)
N(6)	-2741(4)	1977(3)	2648(3)	30(1)
C(1)	2590(4)	690(3)	392(3)	25(1)
C(2)	2179(4)	950(3)	-511(3)	26(1)
C(3)	3022(5)	1557(4)	-908(4)	32(1)
C(4)	4659(5)	1515(4)	318(4)	41(1)
C(5)	3907(4)	972(4)	782(4)	33(1)
C(6)	2705(6)	2029(5)	-1747(4)	50(1)
C(7)	-462(4)	2458(3)	440(3)	23(1)
C(8)	-82(4)	3085(3)	2110(3)	22(1)
C(9)	127(4)	2028(3)	1825(3)	20(1)
C(10)	-742(5)	2395(4)	-641(3)	36(1)
C(11)	-832(4)	4415(3)	1126(4)	30(1)
C(12)	-2205(5)	4364(4)	1170(4)	36(1)
C(13)	1727(4)	1028(4)	4063(3)	29(1)
C(14)	1924(4)	1756(3)	5078(3)	26(1)
C(15)	2674(4)	2820(4)	5333(4)	36(1)
C(16)	3118(5)	2447(5)	3687(5)	49(1)
C(17)	2411(5)	1396(4)	3368(4)	39(1)
C(18)	2930(6)	3694(4)	6324(4)	51(2)
C(19)	-1275(4)	2035(3)	5114(3)	22(1)
C(20)	-2081(4)	1807(3)	3520(3)	23(1)
C(21)	-1509(4)	942(3)	3550(3)	23(1)
C(22)	-883(5)	2515(4)	6237(3)	34(1)
C(23)	-2319(4)	3601(3)	4878(3)	26(1)
C(24)	-3676(5)	3411(4)	4957(4)	43(1)
C(25)	-4232(6)	-506(6)	4029(6)	68(2)
C(26)	-5054(5)	-227(4)	3241(4)	42(1)
C(27)	-6167(6)	-1106(5)	2626(6)	72(2)
S(1B)	-2670(4)	5263(5)	8491(3)	24(1)

Table A4.1 Atomic Coordinates (x 10^4) and U(eq) (contd.) (x 10^4)

O(14B)	-2128(18)	6309(8)	9217(8)	73(6)
O(15B)	-2277(15)	4335(8)	8714(9)	32(4)
O(16B)	-2676(18)	5259(11)	7482(6)	53(5)
C(28B)	-4271(9)	5087(11)	8590(10)	41(5)
F(1B)	-4889(18)	5736(16)	8253(17)	77(6)
F(2B)	-4365(16)	5306(13)	9533(10)	59(4)
F(3B)	-4900(15)	4068(11)	8129(12)	70(5)
S(1A)	-2885(2)	4690(2)	8165(3)	72(1)
O(14A)	-2102(7)	4904(11)	9111(5)	228(9)
O(15A)	-2266(5)	4828(5)	7379(4)	73(2)
O(16A)	-3889(7)	3760(5)	7905(7)	246(9)
C(28A)	-3649(5)	5850(5)	8411(5)	64(3)
F(1A)	-2847(6)	6796(4)	8595(7)	138(4)
F(2A)	-4467(7)	5789(7)	7634(8)	140(4)
F(3A)	-4296(7)	5878(7)	9119(7)	142(4)
O(6B)	-2280(3)	5560(2)	1270(2)	66(9)

Table A4.2 Bond Lengths (Å)

Ru(1)-O(2)#1	1.998(3)
Ru(1)-O(2)	1.998(3)
Ru(1)-O(1)	2.051(3)
Ru(1)-O(1)#1	2.051(3)
Ru(1)-N(1)#1	2.080(3)
Ru(1)-N(1)	2.080(3)
Ru(2)-O(8)#2	2.007(3)
Ru(2)-O(8)	2.007(3)
Ru(2)-O(7)#2	2.060(3)
Ru(2)-O(7)	2.060(3)
Ru(2)-N(4)	2.075(3)
Ru(2)-N(4)#2	2.075(3)
O(1)-C(1)	1.280(5)
O(2)-C(2)	1.350(5)
O(3)-C(4)	1.340(6)
O(3)-C(3)	1.353(6)
O(4)-N(3)	1.221(5)
O(5)-N(3)	1.240(4)
O(6)-C(12)	1.438(6)
O(7)-C(13)	1.283(5)
O(8)-C(14)	1.339(5)
O(9)-C(16)	1.345(7)
O(9)-C(15)	1.360(6)
O(10)-N(6)	1.225(5)
O(11)-N(6)	1.231(4)
O(12)-C(24)	1.404(7)
O(13)-C(26)	1.216(6)
N(1)-C(7)	1.350(5)
N(1)-C(9)	1.363(5)
N(2)-C(7)	1.358(5)
N(2)-C(8)	1.378(5)
N(2)-C(11)	1.481(5)
N(3)-C(8)	1.417(5)
N(4)-C(19)	1.345(5)
N(4)-C(21)	1.362(5)
N(5)-C(19)	1.360(5)
N(5)-C(20)	1.384(5)
N(5)-C(23)	1.481(5)
N(6)-C(20)	1.414(5)
C(1)-C(2)	1.416(6)
C(1)-C(5)	1.434(6)
C(2)-C(3)	1.369(6)
C(3)-C(6)	1.471(7)
C(4)-C(5)	1.327(7)
C(7)-C(10)	1.469(6)
C(8)-C(9)	1.344(5)
C(11)-C(12)	1.523(6)
C(13)-C(14)	1.422(6)
C(13)-C(17)	1.426(7)
C(14)-C(15)	1.370(6)
C(15)-C(18)	1.466(7)
C(16)-C(17)	1.334(8)
C(19)-C(22)	1.485(6)

Table A4.2 Bond Lengths (Å) (contd.)

C(20)-C(21)	1.352(5)
C(23)-C(24)	1.505(6)
C(25)-C(26)	1.483(8)
C(26)-C(27)	1.486(8)
S(1B)-O(14B)	1.396(5)
S(1B)-O(16B)	1.399(5)
S(1B)-O(15B)	1.402(5)
S(1B)-C(28B)	1.779(8)
C(28B)-F(2B)	1.286(6)
C(28B)-F(1B)	1.287(6)
C(28B)-F(3B)	1.287(6)
S(1A)-O(16A)	1.395(5)
S(1A)-O(15A)	1.399(4)
S(1A)-O(14A)	1.406(5)
S(1A)-C(28A)	1.781(7)
C(28A)-F(2A)	1.289(5)
C(28A)-F(3A)	1.290(5)
C(28A)-F(1A)	1.293(5)

Table A4.3 Bond Angles (°)

O(2)#1-Ru(1)-O(2)	180.0
O(2)#1-Ru(1)-O(1)	97.86(12)
O(2)-Ru(1)-O(1)	82.14(12)
O(2)#1-Ru(1)-O(1)#1	82.14(12)
O(2)-Ru(1)-O(1)#1	97.86(12)
O(1)-Ru(1)-O(1)#1	180.0
O(2)#1-Ru(1)-N(1)#1	90.01(12)
O(2)-Ru(1)-N(1)#1	89.99(12)
O(1)-Ru(1)-N(1)#1	89.12(11)
O(1)#1-Ru(1)-N(1)#1	90.88(11)
O(2)#1-Ru(1)-N(1)	89.99(12)
O(2)-Ru(1)-N(1)	90.01(12)
O(1)-Ru(1)-N(1)	90.88(11)
O(1)#1-Ru(1)-N(1)	89.12(11)
N(1)#1-Ru(1)-N(1)	180.0
O(8)#2-Ru(2)-O(8)	180.0
O(8)#2-Ru(2)-O(7)#2	81.48(12)
O(8)-Ru(2)-O(7)#2	98.52(12)
O(8)#2-Ru(2)-O(7)	98.52(12)
O(8)-Ru(2)-O(7)	81.48(12)
O(7)#2-Ru(2)-O(7)	180.0
O(8)#2-Ru(2)-N(4)	91.92(12)
O(8)-Ru(2)-N(4)	88.07(12)
O(7)#2-Ru(2)-N(4)	93.18(13)
O(7)-Ru(2)-N(4)	86.82(13)
O(8)#2-Ru(2)-N(4)#2	88.07(12)
O(8)-Ru(2)-N(4)#2	91.93(12)
O(7)#2-Ru(2)-N(4)#2	86.82(13)
O(7)-Ru(2)-N(4)#2	93.18(13)
N(4)-Ru(2)-N(4)#2	179.999(1)
C(1)-O(1)-Ru(1)	110.7(3)
C(2)-O(2)-Ru(1)	109.7(3)
C(4)-O(3)-C(3)	120.1(4)
C(13)-O(7)-Ru(2)	110.6(3)
C(14)-O(8)-Ru(2)	109.3(2)
C(16)-O(9)-C(15)	120.1(4)
C(7)-N(1)-C(9)	107.0(3)
C(7)-N(1)-Ru(1)	130.1(3)
C(9)-N(1)-Ru(1)	122.8(3)
C(7)-N(2)-C(8)	106.6(3)
C(7)-N(2)-C(11)	123.4(4)
C(8)-N(2)-C(11)	130.0(3)
O(4)-N(3)-O(5)	123.0(3)
O(4)-N(3)-C(8)	117.5(3)
O(5)-N(3)-C(8)	119.4(4)
C(19)-N(4)-C(21)	107.9(3)
C(19)-N(4)-Ru(2)	130.6(3)
C(21)-N(4)-Ru(2)	122.0(3)
C(19)-N(5)-C(23)	124.2(3)
C(20)-N(5)-C(23)	129.5(3)
O(10)-N(6)-O(11)	123.8(4)
O(10)-N(6)-C(20)	116.6(3)

Table A4.3 Bond Angles (°) (contd.)

O(11)-N(6)-C(20)	119.6(4)
O(1)-C(1)-C(2)	118.6(4)
O(1)-C(1)-C(5)	124.2(4)
C(2)-C(1)-C(5)	117.3(4)
O(2)-C(2)-C(3)	122.1(4)
O(2)-C(2)-C(1)	118.5(4)
C(3)-C(2)-C(1)	119.3(4)
O(3)-C(3)-C(2)	120.8(4)
O(3)-C(3)-C(6)	113.9(4)
C(2)-C(3)-C(6)	125.2(5)
C(5)-C(4)-O(3)	123.3(5)
C(4)-C(5)-C(1)	118.8(5)
N(1)-C(7)-N(2)	109.5(4)
N(1)-C(7)-C(10)	124.6(3)
N(2)-C(7)-C(10)	125.9(4)
C(9)-C(8)-N(2)	108.0(3)
C(9)-C(8)-N(3)	126.8(4)
N(2)-C(8)-N(3)	125.2(3)
C(8)-C(9)-N(1)	108.9(4)
N(2)-C(11)-C(12)	111.0(3)
O(6)-C(12)-C(11)	111.9(4)
O(7)-C(13)-C(14)	117.6(4)
O(7)-C(13)-C(17)	124.0(4)
C(14)-C(13)-C(17)	118.4(4)
O(8)-C(14)-C(15)	122.4(4)
O(8)-C(14)-C(13)	118.3(4)
C(15)-C(14)-C(13)	119.3(4)
O(9)-C(15)-C(14)	120.3(4)
O(9)-C(15)-C(18)	113.2(4)
C(14)-C(15)-C(18)	126.5(5)
C(17)-C(16)-O(9)	124.0(5)
C(16)-C(17)-C(13)	117.7(5)
N(4)-C(19)-N(5)	109.5(3)
N(4)-C(19)-C(22)	125.5(4)
N(5)-C(19)-C(22)	125.0(3)
C(21)-C(20)-N(5)	108.2(3)
C(21)-C(20)-N(6)	127.0(4)
N(5)-C(20)-N(6)	124.8(3)
C(20)-C(21)-N(4)	108.2(3)
N(5)-C(23)-C(24)	111.6(3)
O(12)-C(24)-C(23)	112.7(4)
O(13)-C(26)-C(25)	121.5(5)
O(13)-C(26)-C(27)	120.1(5)
C(25)-C(26)-C(27)	118.4(5)
O(14B)-S(1B)-O(16B)	114.6(5)
O(14B)-S(1B)-O(15B)	114.2(5)
O(16B)-S(1B)-O(15B)	113.6(5)
O(14B)-S(1B)-C(28B)	102.9(10)
O(16B)-S(1B)-C(28B)	104.0(10)
O(15B)-S(1B)-C(28B)	105.9(9)
F(2B)-C(28B)-F(1B)	104.4(15)
F(2B)-C(28B)-F(3B)	107.5(14)
F(1B)-C(28B)-F(3B)	105.2(14)

Table A4.3 Bond Angles (°) (contd.)

F(2B)-C(28B)-S(1B)	109.6(11)
F(1B)-C(28B)-S(1B)	116.9(13)
F(3B)-C(28B)-S(1B)	112.7(11)
O(16A)-S(1A)-O(15A)	116.0(3)
O(16A)-S(1A)-O(14A)	115.8(3)
O(15A)-S(1A)-O(14A)	114.8(3)
O(16A)-S(1A)-C(28A)	101.7(4)
O(15A)-S(1A)-C(28A)	103.7(4)
O(14A)-S(1A)-C(28A)	101.6(6)
F(2A)-C(28A)-F(3A)	102.9(8)
F(2A)-C(28A)-F(1A)	106.3(7)
F(3A)-C(28A)-F(1A)	111.6(7)
F(2A)-C(28A)-S(1A)	111.8(5)
F(3A)-C(28A)-S(1A)	114.0(5)
F(1A)-C(28A)-S(1A)	109.9(5)

Appendix A5

Experimental Details for the X-ray Crystallographic Study of 1,1'-Bis(triphenylmethyl)-4,4'-biimidazole

Empirical formula	$C_{22.5}\ H_{18}\ N_2\ Cl$	
Formula weight	$M = 351.84\ g\ mol^{-1}$	
Crystal system	monoclinic	
Space group	C 2/c (No. 15)	
Unit cell dimensions	a = 14.7825(4) Å	$\alpha = 90.000\ °$
	b = 13.3779(2) Å	$\beta = 93.2370(10)°$
	c = 18.3481(4) Å	$\gamma = 90.000\ °$
Volume	3622.71(14) $Å^3$	
Z	Z = 8	
Density (calculated)	$\rho = 1.290\ g\ cm^{-3}$	
F(000)	1472	
Diffractometer	Four circle diffractometer Siemens Smart	
Mo Kα Radiation	λ = 0.71073 Å	
Linear absorptions coefficient	μ (Mo Kα) 0.218 mm^{-1}	
Data collection range	$4.10 \leq 2\theta \leq 45$	
Index ranges	$-21 \leq h \leq 20, -17 \leq k \leq 19, -24 \leq l \leq 26$	
Temperature	293 K	
Programs	SHELX86, SHELX93	
Crystal dimension	0.60 x 0.53 x 0.14 mm^3	
Transmission coefficient T_{Max} /T_{Min}	0.9766 / 0.5171	
Reflections collected	13577	
Independent reflections	4158 [$R_{(int)} = 0.0850$]	
Refinement (on F^2)	Full matrix least squares	
Reflections observed	n = 4146	
No. of parameters refined	p = 299	
Largest peak/hole	0.467 and -0.824 e.$Å^{-3}$	
$GOF=S=[\Sigma[w(F_o^2 - F_c^2)]^2 \mid (n-p)]^{1/2}$	1.028	
$R=\Sigma\tau F_o\sigma - \sigma F_c\tau \mid \Sigma\sigma F_o\sigma$	0.0719 [$F_o>4\sigma(F_o)$], 0.1437 (all data)	
$wR_2=[\Sigma[w(F_o^2 - F_c^2)^2] \mid \Sigma[w(F_o^2)]^2]^{1/2}$	0.1714 [$F_o>4\sigma(F_o)$], 0.2071 (all data)	

Table A5.1 Atomic Coordinates (x 10^4) and U(eq)

Atom	x/a	y/b	z/c	$U_{(eq)}$
C(1)	0.3200(5)	0.0119(4)	0.6032(2)	0.0053(1)
N(1)	0.3134(1)	0.4566(2)	0.0296(1)	0.0036(1)
N(2)	0.4522(2)	0.4127(2)	0.0678(1)	0.0045(1)
C(1)	0.4571(2)	0.4828(2)	0.0125(1)	0.0038(1)
C(2)	0.3722(2)	0.5090(2)	- 0.0114(2)	0.0042(1)
C(3)	0.3663(2)	0.4004(2)	0.0760(2)	0.0041(1)
C(4)	0.2137(2)	0.4739(2)	0.0265(1)	0.0033(1)
C(5)	0.1668(2)	0.3915(2)	0.0695(2)	0.0036(1)
C(6)	0.1064(2)	0.3239(2)	0.0363(2)	0.0042(1)
C(7)	0.0607(3)	0.2554(3)	0.0765(2)	0.0058(1)
C(8)	0.0752(3)	0.2518(3)	0.1509(2)	0.0065(1)
C(9)	0.1352(3)	0.3168(3)	0.1850(2)	0.0060(1)
C(10)	0.1794(2)	0.3874(3)	0.1451(2)	0.0047(1)
C(11)	0.1822(2)	0.4706(2)	- 0.0552(1)	0.0035(1)
C(12)	0.1197(2)	0.5361(2)	- 0.0864(2)	0.0040(1)
C(13)	0.0898(2)	0.5258(3)	- 0.1594(2)	0.0052(1)
C(14)	0.1222(2)	0.4507(3)	- 0.2013(2)	0.0056(1)
C(15)	0.1858(2)	0.3863(3)	- 0.1711(2)	0.0056(1)
C(16)	0.2156(2)	0.3952(3)	-0.0987(2)	0.0048(1)
C(17)	0.1941(2)	0.5749(2)	0.0632(1)	0.0037(1)
C(18)	0.1054(2)	0.5981(3)	0.0780(2)	0.0046(1)
C(19)	0.0839(3)	0.6869(3)	0.1110(2)	0.0058(1)
C(20)	0.1509(3)	0.7535(3)	0.1302(2)	0.0066(1)
C(21)	0.2388(3)	0.7314(3)	0.1181(2)	0.0070(1)
C(22)	0.2608(2)	0.6429(3)	0.0846(2)	0.0054(1)
C(23)	0.0	-0.0597(5)	0.2500	0.0080(2)
Cl(1)	0.0981(1)	0.0092(1)	0.2445(1)	0.0126(1)

Table A5.2 Bond Lengths (Å)

bond	length	bond	length
N(1)-C(3)	1.351(3)	C(11)-C(12)	1.374(4)
N(1)-C(2)	1.374(4)	C(11)-C(16)	1.394(4)
N(1)-C(4)	1.491(3)	C(12)-C(13)	1.393(4)
N(2)-C(3)	1.297(4)	C(13)-C(14)	1.367(5)
N(2)-C(1)	1.387(4)	C(14)-C(15)	1.369(5)
C(1)-C(2)	1.353(4)	C(15)-C(16)	1.381(4)
C(1)-C(1)#1	1.448(5)	C(17)-C(22)	1.382(4)
C(4)-C(17)	1.544(4)	C(17)-C(18)	1.390(4)
C(4)-C(5)	1.542(4)	C(18)-C(19)	1.378(5)
C(4)-C(11)	1.545(4)	C(19)-C(20)	1.364(6)
C(5)-C(6)	1.387(4)	C(20)-C(21)	1.363(6)
C(5)-C(10)	1.391(4)	C(21)-C(22)	1.381(5)
C(6)-C(7)	1.378(5)		
C(7)-C(8)	1.371(5)	C(23)-Cl(1)#2	1.726(4)
C(8)-C(9)	1.369(6)	C(23)-Cl(1)	1.726(4)
C(9)-C(10)	1.381(5)		

Table A5.3 Bond Angles (°) (contd.)

Atom	angle	Atom	angle
C(3)-N(1)-C(2)	105.6(2)	C(12)-C(11)-C(16)	118.3(3)
C(3)-N(1)-C(4)	130.3(2)	C(12)-C(11)-C(4)	123.1(3)
C(2)-N(1)-C(4)	123.7(2)	C(16)-C(11)-C(4)	118.6(2)
C(3)-N(2)-C(1)	105.2(2)	C(11)-C(12)-C(13)	120.5(3)
C(2)-C(1)-N(2)	109.1(3)	C(14)-C(13)-C(12)	120.7(3)
C(2)-C(1)-C(1)#1	128.8(4)	C(13)-C(14)-C(15)	119.4(3)
N(2)-C(1)-C(1)#1	122.1(3)	C(14)-C(15)-C(16)	120.5(3)
C(1)-C(2)-N(1)	107.0(3)	C(15)-C(16)-C(11)	120.7(3)
N(2)-C(3)-N(1)	113.1(3)	C(22)-C(17)-C(18)	117.5(3)
N(1)-C(4)-C(17)	109.1(2)	C(22)-C(17)-C(4)	123.5(3)
N(1)-C(4)-C(5)	110.0(2)	C(18)-C(17)-C(4)	118.9(3)
C(17)-C(4)-C(5)	107.6(2)	C(19)-C(18)-C(17)	121.5(3)
N(1)-C(4)-C(11)	106.0(2)	C(20)-C(19)-C(18)	119.7(4)
C(17)-C(4)-C(11)	113.2(2)	C(21)-C(20)-C(19)	120.1(4)
C(5)-C(4)-C(11)	110.9(2)	C(20)-C(21)-C(22)	120.6(4)
C(6)-C(5)-C(10)	117.3(3)	C(21)-C(22)-C(17)	120.6(4)
C(6)-C(5)-C(4)	122.6(2)		
C(10)-C(5)-C(4)	120.0(3)	Cl(1)#2-C(23)-Cl(1)	115.4(4)
C(7)-C(6)-C(5)	121.5(3)		
C(8)-C(7)-C(6)	120.1(4)		
C(9)-C(8)-C(7)	119.6(4)		
C(8)-C(9)-C(10)	120.4(4)		
C(9)-C(10)-C(5)	121.0(4)		